Loudspeaker Cabinet Diffraction

Tore Skogberg

Acoustical Technology

Ørsted●DTU – 2006

Abstract

Sound output from a loudspeaker system is seriously affected by the presence of the cabinet due to diffraction of the propagating waves at the edge of the cabinet. The study introduces a model for diffraction and compares the results to measurements. The model is refined to include high-order diffraction components and is compared to an existing diffraction model. Diffraction theory from the optical field is reviewed and used to determine the diffracted signal.

1 Introduction

This document targets the problem of diffraction of the sound waves around a loudspeaker cabinet and presents different methods to solve the problem.

1.1 The author

My background is somewhat different from my fellow student due to the twenty-plus years of professional experience within the electronics industry where my main concerns have been the design of analogue and digital circuits, programming, documentation and hardware prototyping.

I decided in 2004 to quit my present employment and assign for the "+2" two-year education programme at DTU thus upgrading my *Bachelor of Science in Electronics Engineering* (Danish: *Akademiingeniør, Elektronik*) to *Master of Science in Acoustical Engineering* (Danish: *Civilingeniør, Akustik*) for which the current document represents my final project.

I am married to Hanne, who I met at a musical course related to our common interest, which is renaissance and baroque music.

1.2 The idea

High-fidelity sound reproduction and electronic musical instruments have been the two most important factors for selecting the area of electronics engineering and I have built countless amplifiers and loudspeakers for testing various ideas. My interest was however put on wait while I was occupied within the electronics industry but was restored to life during the present study at DTU where two 3-week courses have been devoted to loudspeaker cross-over filters and the study of resonances within an ancient musical instrument.

Sound diffraction has been a mystery to me for years. Popular magazines and links on the Internet address the subject now and then but most of the articles are considering loudspeaker cabinet diffraction as an *illness* that can be *cured* using an electrical filter raising the bass; but this seemed to be far too easy an explanation, which made my curious. Hence, I decided to do my final project studying loudspeaker cabinet diffraction.

Initial reading showed that the direct sound from the loudspeaker was followed by an echo and that the delay was related directly to the distance from the loudspeaker to the edge of the cabinet. Hence, the idea originated representing loudspeaker cabinet diffraction as a reflection from the edge of the cabinet and this study occupies the first part of this document.

Diffraction is a well-known problem within the optical field so I studied the subject and found the theory usable for the study of loudspeaker cabinet diffraction. Hence, the second part of this document, which deals with the wavelet model.

1.3 What is diffraction

A common assumption within architectural acoustics is that waves propagate through straight lines (rays) and that large and rigid surfaces block propagation of the wave thus creating a sound shadow behind the obstruction. According to this theory there should be silence behind a wall but sound waves do reach to the listener within the shadow zone; and this is due to *diffraction* of the wave front close to the edge of the obstruction.
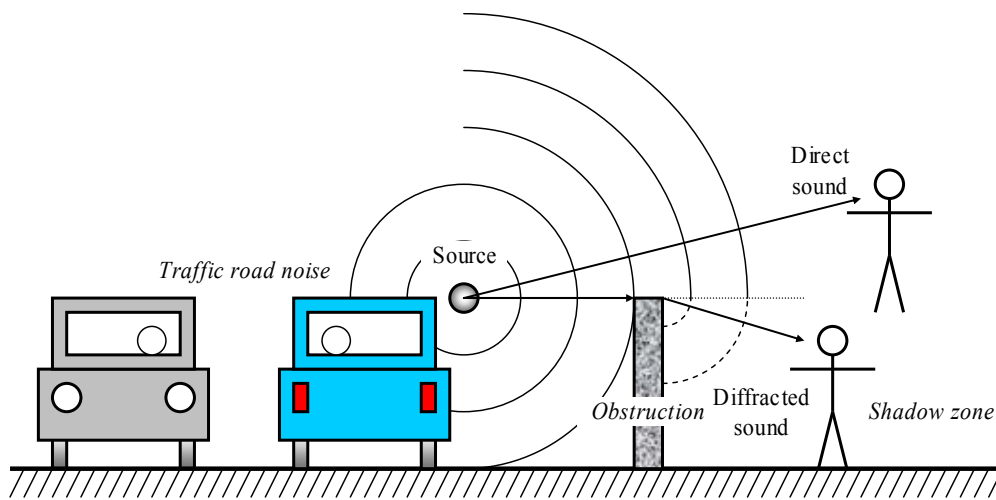
Figure 1 – An every-day situation with noise from a motor vehicle reaches the uppermost listener directly. The lowermost listener cannot see the source but he receives anyway noise from the road through diffraction at the upper edge of the obstruction.

A definition is offered by J. R. Wright: "Diffraction is the change in direction of propagating of a wave front due to the presence of an obstacle or discontinuities (with no change of velocity)". Diffraction is occasionally confused by refraction, which is the change is direction due to a change within the velocity usually caused by a change of medium.
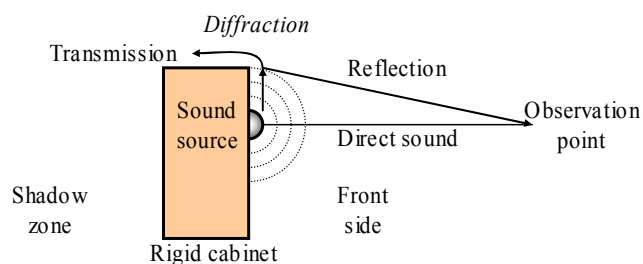
Figure 2 – The sound travels directly to the observation point from the sound source but the signal is also diffracted at the edge and travels to the observation point through another path causing interference when the signals are added.

Sound output from a loudspeaker reaches a discontinuity at the cabinet edge where it is being diffracted thus *transmitting* sound power into the shadow zone behind the loudspeaker and *reflecting* sound power back into the front side where it interferes with the direct sound. The objective of this study is creating models for the diffraction caused by the edges of a conventional loudspeaker cabinet.

1.4 The document

H. F. Olson studied diffraction from loudspeaker cabinets back in the 1950'ies and several papers have been printed in professional magazines, such as the journal from the Audio Engineering Society, and have been an inspiration for the current project. However, the basic idea was to study the effect of diffraction from loudspeaker cabinets and testing my own ideas and thus not just reproducing the findings of other authors. I do refer to selected works but the major part of the study is my responsibility and when this is not the case, I add the name of the reference along with the page number in parenthesis.

Some basic knowledge of acoustics is required for this study and I found it valuable to explain this fundamental theory using my own words; partly to ease referencing within the document and partly to structure my mind. The theory is introduced in the *Acoustics* chapter, which presents the wave equation and the concept of impedance, defines the point source model to be used throughout the study and finally touches upon the hearing threshold needed for discriminating between audibility and inaudibility.

Simulations are be related to measurements to confirm the theory using a set-up constructed within the large anechoic chamber at DTU and the result is presented in the *Measurements* chapter and is used for comparison to model predictions. A small test run was conducted in my home and is also reported.

Initially were three models considered; the *edge diffraction model*, which introduced the author to the field of diffraction; an *analytical model* where the wave equation should have been solved but this project was cancelled; and finally the *wavelet model*, which is based upon results from the optical field.

The *edge diffraction model* has its origin from reading of popular magazines covering high-fidelity sound reproduction, and is the author's introduction to the subject. The model is based upon a common approach within the popular literature regarding diffraction as reflection from the edge of the cabinet thus interfering with the direct sound at the receiving point. The idea of edge reflection is supported by other authors but a reflection-based theory has not been found in the available literature, which is focussing on the wavelet theory and the reciprocity principle, so I am "left alone" within this chapter and cannot disclaim the responsibility. An equation is derived to determine the sound pressure in the front side of the baffle as well as within the shadow zone and is enhanced into a numerical model with fairly good experimental results for the on-axis response but the model fails off-axis for large angles. The chapter ends with a brief study of the *distributed edge diffraction model* by Urban et al.

The *analytical model* originated from the mathematical course Partial Differential Equations, where a solution method based upon the integral transformations showed that the wave equation could be solved despite the presence of a discontinuity within one of the coordinates. This solution would have been a nice complement to the present study, but the required mathematical skills were unfortunately not within reach of the author so this model could not be finished and the subject was terminated to save valuable time for the remaining part of the study. Some of the fragments are presented in the appendix but come without a conclusion.

The *wavelet model* is based upon material from textbooks within the field of optics where diffraction is one of the limiting factors for the obtainable resolution and was expected an important part of the study. The wave front is modelled through infinitesimal point sources,

wavelets, which are integrated at the observation point into the received frequency response. The optical field is typically operating with narrow frequency ranges and short wavelengths thus enabling the use of simplifications whereas the frequency range within the acoustical field covers several decades and the wavelengths are very long so the theory must be adjusted to fit the objective. The theory is separated into two sections concerns the far-field approximations and the near-field approximations and the results are combined in a final section. Partial results are the derivation of the radiation pattern for a loudspeaker in an infinite baffle, which is a nice way of verifying the usefulness of the wavelet model and a model for the frequency response of diffraction using an infinite edge.

All frequency responses are calculated and plotted using the MATLAB tool, which is an efficient programming language for mathematical problems. The major software routines are documented within a *Software* chapter and a final *Appendix* contains miscellaneous mathematical background materials.

This project was scheduled to last five months, which is the minimum length for the master project at DUT and corresponds to 30 ECTS points. According to my log I have used some 750 hours of work for the project, most of which was spent working at home.

1.5 Acknowledgements

I would like to thank my supervisor *Finn Agerkvinst*, for discussions, help, advices and first of all patience; I prefer to work alone and thank you for accepting this.

I want to thank *Finn Jacobsen* for discussions on radiation impedance and for the comments during the mid-term presentation; *Ove Skovgaard* for help attacking the wave equation and *Jørgen Rasmusen* for assistance with the test equipment.

2 Acoustics

A collection of acoustical background material is presented in this chapter for use throughout the document. The chapter presents a brief derivation of the wave equation, which is followed by the solutions for the plane wave and the spherical wave. The concept of impedance is presented and used for derivation of the spherical point source. Using the loudspeaker as a point source is discussed and the reciprocity principle is introduced to simplify the set-up of the measurement.

2.1 The wave equation

In this section the physical principles of Newton's second law, the gas law and the laws of conservation of mass are combined into the three-dimensional wave equation. The derivation is based upon Beranek (pages 16-24).

2.1.1 The equation of motion

A small "box" of air (Figure 3) is situated in a medium where the sound pressure p changes along the x-axis at a ratio of $\partial p/\partial x$. The vector representation of the change, i.e. the gradient of the sound pressure along the axes of a rectangular coordinate system, is:

$$\bar{e}_x \frac{\partial p}{\partial x} + \bar{e}_y \frac{\partial p}{\partial y} + \bar{e}_z \frac{\partial p}{\partial z} = \mathrm{grad}(p)$$

The gradient of the pressure is a force that accelerates the box of air. The pressure gradient in the x direction is the gradient $\partial p/\partial x$ multiplied by distance Δx, as $(\partial p/\partial x)\Delta x$, and the resulting force on the box of air is the pressure gradient multiplied by the area it is working against, i.e. the area $\Delta y\Delta z$. The box will be accelerated in the direction from higher to lower pressure so the resulting force becomes $-(\partial p/\partial x)\Delta x\Delta y\Delta z$ along the x-axis. The product $\Delta x\Delta y\Delta z$ represents a volume of air, ΔV, so the general expression of the force acting on the box becomes:

$$F = -\left[\bar{e}_x \left(\frac{\partial p}{\partial x}\Delta x \right)\Delta y\Delta z + \bar{e}_y \left(\frac{\partial p}{\partial y}\Delta y \right)\Delta x\Delta z + \bar{e}_z \left(\frac{\partial p}{\partial z}\Delta z \right)\Delta x\Delta y \right] = -\Delta V \,\mathrm{grad}(p)$$

Newton's second law of motion states that force equals mass times acceleration. Mass is the density of the medium ρ multiplied by the volume ΔV, and acceleration is the time-derivative of the velocity vector u, so $F = \rho\Delta V\partial u/\partial t$. Hence, the force per volume is $F/\Delta V = \rho\partial u/\partial t$, and since $F/\Delta V = -\mathrm{grad}(p)$, according to the previous equation, it follows that:

$$\mathrm{grad}(p) = -\rho \frac{\partial u}{\partial t} \qquad\qquad 1$$

This is the equation of motion and it relates sound pressure to particle velocity.

2.1.2 The gas law

Whenever a portion of gas is compressed rapidly, its temperature increases, and when it is expanded rapidly, its temperature drops. This is according to the gas law, $PV = RT$, which relates pressure P and volume V to the absolute temperature T with R being the gas constant.

At any one point in an alternating sound field, the temperature rises and falls relative to the ambient temperature. At points separated by one-half wavelength, the fluctuations will be 180° out of phase with each other. The question arises: is there sufficient time during one-half

an alteration in the temperature for an exchange of heat to take place? It has been established, that under normal atmospheric conditions the speed of travel of a thermal diffusion wave is about 0.5 m/s at audible frequencies. The time for one-half an alteration at 1 kHz is 0.5 ms, and within this time, the thermal wave travels 0.25 mm, which is very small compared with one-half wavelength of 170 mm. It appears safe to conclude, that there is negligible heat exchange in the wave, so the compression and expansion of air can be considered adiabatic within the audible frequency range.
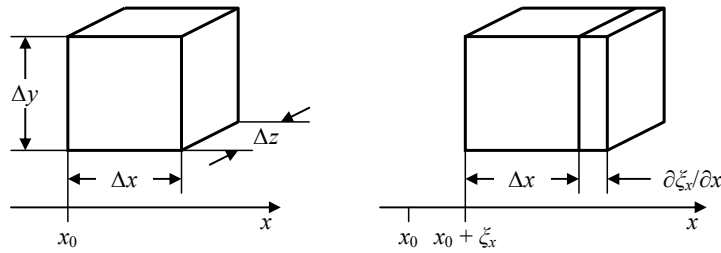
Figure 3 – Left: A small box of air is situated in a medium in which the sound pressure increases by the gradient of p. Right: Change in volume of the box with change in position.

For adiabatic expansions, the relation between the total pressure P and the volume V is as follows, where γ is specified for gases with diatomic molecules, such as air (consisting of the diatomic molecules H_2 hydrogen, N_2 nitrogen and O_2 oxygen) and c is a constant:

$$PV^\gamma = c, \quad \gamma = 1.4$$

Both variables are function of V, and the derivative with respect to V must be zero since the speed of sound is constant:

$$\frac{\partial}{\partial V}\left\{PV^\gamma\right\} = 0 \quad \Rightarrow \quad \frac{\partial P}{\partial V}V^\gamma + \gamma PV^{\gamma-1} = 0 \quad \Rightarrow \quad \frac{\partial P}{P} = -\gamma\frac{\partial V}{V}$$

The instantaneous pressure can be represented by $P = P_0 + p$, where P_0 is the static pressure (approximately 10^5 Pa) and p is an incremental pressure, referenced as the *sound pressure*, with a typical value far below 200 Pa (140 dB SPL); so $p \ll P_0$. The instantaneous volume can be represented similarly by $V = V_0 + v$. The derivatives can be simplified by using the incremental variables to the following relation between pressure and volume:

$$\frac{p}{P_0} = -\gamma\frac{v}{V_0}$$

The time-derivative of the pressure and volume becomes:

$$\frac{1}{P_0}\frac{\partial p}{\partial t} = -\gamma\frac{1}{V_0}\frac{\partial v}{\partial t} \qquad\qquad 2$$

The change in incremental sound pressure causes a change in incremental volume.

2.1.3 Continuity equation

Mass cannot disappear and cannot be generated; this is the basis of the continuity principle. The change in incremental volume depends only on the divergence of the vector displacement if the mass within the box remains constant. This means, that unless the air particles adjacent to any given side of the box move at the same velocity as the side of the box itself, some will cross into or out of the box and the mass will change.

For the box moved distance ξ_x along the *x*-axis, the distance is changed $\partial\xi_x/\partial x$. The net change in volume becomes:

$$v = V_0\left(\frac{\partial\xi_x}{\partial x} + \frac{\partial\xi_y}{\partial y} + \frac{\partial\xi_z}{\partial z}\right) = V_0\,\mathrm{div}(\xi)$$

Differentiating with respect to time and observing that the time-derivative of ξ is velocity, yields the continuity equation:

$$\frac{\partial v}{\partial t} = V_0\,\mathrm{div}\left(\frac{\partial\xi}{\partial t}\right) = V_0\,\mathrm{div}(u) \qquad\qquad 3$$

This equation states the change in incremental volume given by the particle velocity vector.

2.1.4 The wave equation

Combining equations 2 and 3 eliminates the time-derivative of the incremental volume $\partial v/\partial t$:

$$\frac{\partial v}{\partial t} = -\frac{V_0}{\gamma P_0}\frac{\partial p}{\partial t} = V_0\,\mathrm{div}(u) \quad\Rightarrow\quad \frac{\partial p}{\partial t} = -\gamma P_0 V_0\,\mathrm{div}(u)$$

Differentiating with respect to time gives:

$$\frac{\partial^2 p}{\partial t^2} = -\gamma P_0\,\mathrm{div}\left(\frac{\partial u}{\partial t}\right) \quad\Rightarrow\quad \mathrm{div}\left(\frac{\partial u}{\partial t}\right) = -\frac{1}{\gamma P}\frac{\partial^2 p}{\partial t^2}$$

An expression for div($\partial u/\partial t$) can be found by taking the divergent of equation 1:

$$\mathrm{div}(\mathrm{grad}(p)) = -\rho\,\mathrm{div}\left(\frac{\partial u}{\partial t}\right) \quad\Rightarrow\quad \mathrm{div}\left(\frac{\partial u}{\partial t}\right) = -\frac{1}{\rho}\mathrm{div}(\mathrm{grad}(p))$$

Eliminating the $\partial u/\partial t$ term yields the wave equation as shown below using an alternative notation of the vector operators, where ∇ is the gradient operator of *p* and $\nabla\bullet$ is the divergent operator, so $\nabla\bullet\nabla p$ represents the divergent of the gradient of *p*, and this is most often written as $\nabla^2 p$; which is the Laplace operator (Westergren, 248):

$$\mathrm{div}(\mathrm{grad}(p)) = \nabla\bullet\nabla p = \nabla^2 p = \frac{\rho}{\gamma P_0}\frac{\partial^2 p}{\partial t^2}$$

The Laplace operator is defined for several coordinate systems of which only the rectangular and spherical coordinate systems will be considered here. The coefficient $\rho/\gamma P_0$ represents the square of the speed of sound. Hence, the wave equation:

$$\nabla^2 p = \frac{1}{c^2}\frac{\partial^2 p}{\partial t^2}, \quad c = \sqrt{\frac{\gamma P_0}{\rho}} \qquad\qquad 4$$

The equation could equally well use the particle velocity as the dependent variable, substituting *u* for *p* in the above equation, or the dependent variable could be the particle displacement ξ or the incremental increase in mass density ρ; this assumes that there is no rotation in the medium (Beranek, 24).

Using the following values: $\gamma = 1.4$, $P_0 = 1000$ hPa and $\rho = 1.18$ kg/m^3, the speed of sound becomes 345 m/s. The value decreases for very low frequencies where the process is no

longer adiabatic ($\gamma < 1.4$), and it is related to the static pressure (P_0), which may vary in the range from 960 to 1070 hPa, and also to the mass density of air (ρ), which is depending upon the static pressure and the geographic location on the earth. These variations should be allowed for – so the speed of sound is somewhere between 340 and 355 m/s. However, a single value will be used for the calculations within this document:

$$c = 345 \,\text{m/s} \qquad\qquad 5$$

The Laplace operator will be referenced using two coordinate systems, the *rectangular* coordinate system, using x,y,z where the coordinates are defined within the infinite range from $-\infty$ to ∞, and the *spherical* coordinate system using radius r, defined from zero to ∞, the observation angle θ, defined from zero to π, and the rotation angle φ, defined from zero to 2π.
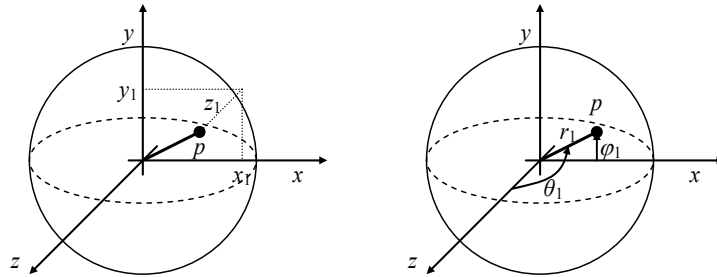
Figure 4 – A point on the spherical sphere represented by the rectangular coordinate system $p(x_1,y_1,z_1)$, and the spherical coordinate system $p(r_1,\theta_1,\varphi_1)$.

The Laplace operator is defined as follows for rectangular coordinate system (Asmar, 196):

$$\nabla^2 p = \frac{\partial^2 p}{\partial x^2} + \frac{\partial^2 p}{\partial y^2} + \frac{\partial^2 p}{\partial z^2}, \quad p = p(x,y,z,t) \qquad 6$$

The Laplace operator will be simplified into one coordinate only in this document where the pressure is assumed constant to changes in variables y and z so the derivatives in these directions become zero since the derivative of a constant is zero.

The spherical coordinate system will be used for most of the analytical work with the Laplace operator defined as follows (Asmar, 197):

$$\nabla^2 p = \frac{\partial^2 p}{\partial r^2} + \frac{2}{r}\frac{\partial p}{\partial r} + \frac{1}{r^2}\left[\frac{\partial^2 p}{\partial \theta^2} + \cot(\theta)\frac{\partial p}{\partial \theta} + \csc^2(\theta)\frac{\partial^2 p}{\partial \varphi^2}\right], \quad p = p(r,\theta,\varphi,t) \qquad 7$$

All calculations will assume rotational symmetry around the main axe so the rotation angle φ will not be referenced in this document and the last term becomes zero. The observation angle θ will be ignored within the initial analysis but will be referenced for the more serious work.

2.2 Linearity

The superposition principle will be used for the addition of individual solutions to the wave equation thus assuming linearity. This means that the assumption from section 2.1.2; that the sound pressure is small compared to the static pressure, must be fulfilled with a good margin. The static pressure is approximately 10^5 Pa and the sound pressure is rarely above 200 Pa, which corresponds to 140 dB SPL re. 20 µPa, so the acoustical systems to be analysed will be assumed linear.

2.3 Harmonic oscillation

Most measurements within acoustics are performed after a short delay to ensure that the initial transient has decayed to zero. The initial transient is related to switching the excitation signal. A change within the set-up of the test system creates a discontinuity within the signal, which generates a broadband noise signal that interferes with the wanted signal. The delay gives the initial transient time to decay toward zero and a delay of a couple of seconds is commonly satisfactory. In the analytical work is the assumption used to simplify the equations by removing the inhomogeneous term from the differential equation. The prize to pay is that the history from $t = 0$ and up to the time of observation has been lost.

A harmonic oscillation is represented by the complex exponential, which can be regarded as a unit vector rotating within the complex plane, with the angular speed $\omega = 2\pi f$, where f is frequency (Hz). The expected solution to the wave equation is thus of the following form, where $p(\bar{r})$ is the sound pressure at the position pointed to by the vector:

$$p(\bar{r},t) = p(\bar{r})\exp(i\omega t) \qquad\qquad 8$$

The simplification corresponds to excitation with sinusoidal signal, but any waveform can be included into the analysis using the Fourier series expansion of periodic signals. This will not be brought further since it is not required within the analysis work to follow.

The First the time-derivative of the sound pressure becomes:

$$\frac{\partial^2 p(\bar{r},t)}{\partial t^2} = -\omega^2 p(\bar{r})\exp(i\omega t)$$

The spatial derivative of the sound pressure becomes:

$$\nabla^2 p(\bar{r},t) = \nabla^2 p(\bar{r})\exp(i\omega t)$$

Inserting these expressions into equation 4 generates the following simplified wave equation, where the time dependency can be removed:

$$\nabla^2 p(\bar{r})\exp(i\omega t) + \frac{\omega^2}{c^2} p(\bar{r})\exp(i\omega t) = 0$$

The resulting equation, shown below, introduces a new parameter, k, the angular wave number, which will be discussed below.

$$\nabla^2 p(\bar{r}) + k^2 p(\bar{r}) = 0, \quad k = \frac{\omega}{c} = \frac{2\pi}{\lambda} \qquad\qquad 9$$

This equation is known as the *Helmholtz equation* and it is the basic equation for the analysis work within this document.

The dimension of the angular wave number k is reciprocal distance (m^{-1}) and the angular wave number appears typically together with a distance thus creating a compact expression for frequency and distance. The parameter ka represents frequency through k and distance through a. It should be noted that $2\pi a$ represents the circumference of a disk with radius a and ka relates this circumference to wavelength. For $ka = 1$ is the circumference identical to the wavelength. For $ka < 1$ is the disk acoustically small; i.e. the radius is less than $1/2\pi$ of the wavelength and for $ka > 1$ is the disk acoustically large. A loudspeaker with $a = 50$ mm is comparable to wavelength at 1.1 kHz and cannot be assumed small for higher frequencies.

2.4 Plane wave

Plane waves are rarely encountered in real life, but sound waves may be regarded as locally plane at large distance from the source. The waves within narrow tubes and ducts can be considered plane when the dimensions are small, i.e. the diameter is less than one-sixth of the wavelength (Beranek, 29).
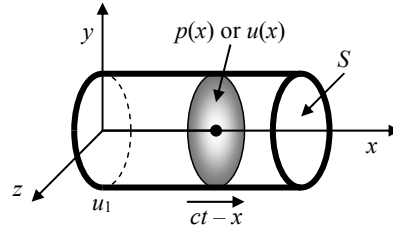
Figure 5 – A cylindrical tube with sufficiently small diameter allows only plane propagating waves thus simplifying the problem to one dimension.

Using x as the independent variable, the Laplace operator of equation 6 simplifies to $\partial/\partial x$, and the one-dimensional wave equation becomes:

$$\frac{\partial^2 p}{\partial x^2} + k^2 p = 0, \quad p = p(x)\exp(i\omega t) \tag{10}$$

A good starting point is assuming a trial function based upon the exponential function, since it is not changed by the differentiation process, with exception of a constant scaling factor. Constant p_1 in the trial function below is defined by the problem at hand and μ is an unknown constant. The trial function is differentiated two times into $\mu^2 p(x)$, and after insertion into equation 10, the problem boils down to a second-order equation for determination of μ.

$$p(x) = p_1 \exp(\mu x) \quad \Rightarrow \quad \mu^2 p(x) + k^2 p(x) = 0 \quad \Rightarrow \quad \mu = \pm ik$$

There are two solutions, since the wave equation is of second order, and the complete solution is a superposition of the solutions since the problem is linear.

$$p(x,t) = \left[p_+ \exp(-ikx) + p_- \exp(ikx) \right] \exp(i\omega t) \tag{11}$$

Constants p_+ and p_- are defined by the boundary conditions.

Combining the exponential functions for position and time, the equation can also be written in the form of D'Alembert (Asmar, 126):

$$p(x,t) = p_+ \exp(ik(ct - x)) + p_- \exp(ik(ct + x)) \tag{12}$$

The solution can thus be separated into two components; an outgoing wave with amplitude p_+ and a backward-travelling wave with amplitude p_-. The waves travel at the speed of sound, since the $ct \pm x$ terms are constant for increasing or decreasing x at the speed of sound.

The particle velocity u can be determined using equation 1:

$$\frac{\partial p(x,t)}{\partial x} = -\rho \frac{\partial u(x,t)}{\partial t} \quad \Rightarrow \quad u(x,t) = -\frac{1}{\rho} \int \frac{\partial p(x,t)}{\partial x} dt$$

Inserting the expression from equation 11, the particle velocity for the plane wave becomes:

$$u(x,t) = \frac{1}{\rho c}\left[p_+ \exp(-ikx) - p_- \exp(ikx)\right]\exp(i\omega t)$$

13

Note the change in sign for the backward-travelling wave. The outgoing wave is in-phase with the sound pressure but the backward-travelling wave is not.

2.5 Spherical wave

Spherical waves are met in real life as the sound field at low frequencies from a loudspeaker without reflecting boundaries and most sources are spherical at large distance. The spherical Laplace operator is defined as follows (Asmar, 270):

$$\nabla^2 p = \frac{\partial^2 p}{\partial r^2} + \frac{2}{r}\frac{\partial p}{\partial r} + \frac{1}{r^2}\left[\frac{\partial^2 p}{\partial \theta^2} + \cot(\theta)\frac{\partial p}{\partial \theta} + \frac{1}{\sin^2(\theta)}\frac{\partial^2 p}{\partial \varphi^2}\right], \quad p = p(r,\theta,\varphi)$$

14

It will be assumed that the problem is independent upon φ so the derivative of the sound pressure with respect to φ becomes zero; the problem must as a consequence be symmetrical around the radius. It is further assumed that the sound pressure is independent upon θ, so the derivative of p with respect to θ to also becomes zero; this requires that the dimensions are small compared to wavelength, which can be regarded fulfilled when the circumference of the wave front is less than the wave length, $kr < 1$. This requires that:

$$kr < 1 \quad \Rightarrow \quad f < \frac{c}{2\pi r}$$

15

For $r = 0.1$ m is the upper limit 550 Hz. The sound pressure is determined solely by radius and the simplified spherical wave equation becomes:

$$\frac{\partial^2 p}{\partial r^2} + \frac{2}{r}\frac{\partial p}{\partial r} + k^2 p = 0, \quad p = p(r)\exp(i\omega t)$$

16

The sound pressure p, can be substituted with the particle velocity u, the volume velocity q, the particle displacement ξ or the incremental increase in mass density ρ (Beranek, 24).
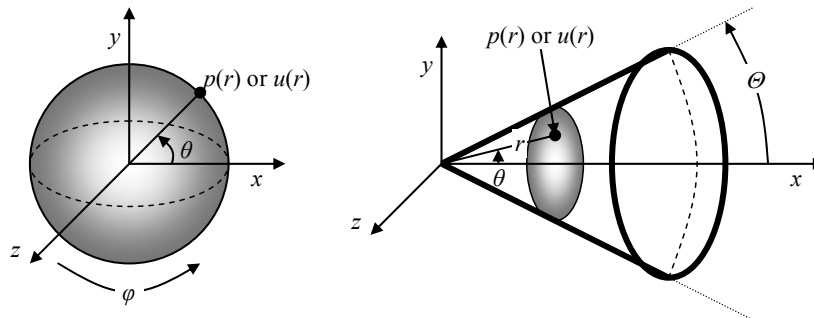
Figure 6 – Left: A spherical sound source radiates equally well in any direction and is described by radius r, ignoring θ and φ. Right: A conical horn with opening angle Θ ≤ 90° and sufficiently small diameter allows only spherical propagating waves.

The equation can be solved by a change of variable from p to rp, since this transforms the problem into the wave equation for the plane wave, where the solution is known. The change of variable results in the following representation of the derivative:

$$\frac{\partial^2 \{rp\}}{\partial r^2} = \frac{\partial}{\partial r}\left\{\frac{\partial\{rp\}}{\partial r}\right\} = \frac{\partial}{\partial r}\left\{p + r\frac{\partial p}{\partial r}\right\} = 2\frac{\partial p}{\partial r} + r\frac{\partial^2 p}{\partial r^2}$$

Multiplying the wave equation for the plane wave (equation 10) by r and using the above substitution, the equation for the spherical wave becomes:

$$r\left(\frac{\partial^2 p}{\partial r^2} + \frac{2}{r}\frac{\partial p}{\partial r} + k^2 p\right) = 0 \quad \Rightarrow \quad \frac{\partial^2 rp}{\partial r^2} + k^2 rp = 0$$

The solution in equation 11 can be used with p substituted by rp as the dependent variable and x substituted by r as the independent variable:

$$rp(r,t) = \left[p_+ \exp(-ikr) + p_- \exp(ikr)\right]\exp(i\omega t)$$

Hence, the solution to the spherical wave equation:

$$p(r,t) = \frac{1}{r}\left[p_+ \exp(-ikr) + p_- \exp(ikr)\right]\exp(i\omega t) \qquad 17$$

A reflected spherical wave is indeed possible using a spherical and concentric reflector but this is not common; hence $p_- = 0$ is often assumed.

The sound pressure from a spherical source without reflections ($p_- = 0$) is:

$$p(r,t) = \frac{1}{r} p_+ \exp(-ikr)\exp(i\omega t) \qquad 18$$

The sound pressure is inversely proportional to distance; the *inverse distance law*. The law holds for real loudspeakers when the observation point is at large distance compared to the size of the loudspeaker and assuming freedom from any reflecting surfaces. The particle velocity for the spherical source is determined using equation 1:

$$\frac{\partial p(r,t)}{\partial r} = -\rho\frac{\partial u(r,t)}{\partial t} \quad \Rightarrow \quad u(r,t) = -\frac{1}{\rho}\int\frac{\partial p(r,t)}{\partial r}dt$$

Inserting the expression for $p(r,t)$ from equation 17, differentiating with respect to radius and integrating with respect to time, generates the following expression for the particle velocity:

$$u(r,t) = \frac{1}{r\rho c}\left[\left(\frac{1+ikr}{ikr}\right)p_+ \exp(-ikr) - \left(\frac{1-ikr}{ikr}\right)p_- \exp(ikr)\right]\exp(i\omega t) \qquad 19$$

Note the change of sign of the backward-travelling wave around the frequency where $kr = 1$. At low frequency or short distance ($kr < 1$) is the velocity proportional to the inverse distance squared and the signal is 90° delayed compared to the sound pressure.

$$u(r,t) \xrightarrow[kr \to 0]{} \frac{1}{ikr^2\rho c}\left[p_+ \exp(-ikr) - p_- \exp(ikr)\right]\exp(i\omega t)$$

At high frequency or long distance ($kr > 1$) is the velocity proportional to the inverse distance and in-phase with the sound pressure.

$$u(r,t)\xrightarrow[kr\to\infty]{}\frac{1}{r\rho c}\left[p_+\exp(-ikr)+p_-\exp(ikr)\right]\exp(i\omega t)$$

The particle velocity for a progressive spherical wave without reflection ($p_- = 0$) is:

$$u(r,t)=\frac{p_+}{r\rho c}\frac{1+ikr}{ikr}\exp(-ikr)\exp(i\omega t) \qquad 20$$

This equation will be considered defining the spherical sound source but it will be required to introduce the volume velocity and the impedance first.

2.6 Volume velocity

Sound pressure and particle velocity are important variable within acoustics but the particle velocity is not commonly encountered in real lift; it is more useful to refer to the volume velocity q, since this is directly related to the physical sound source.
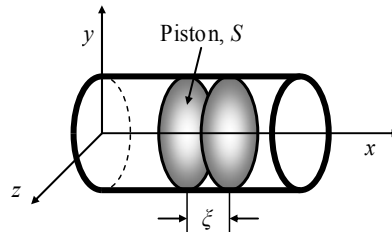
Figure 7 – A plane wave of area SD is moved distance ξ thus moving a volume of SDξ.

Consider the plane piston within the tube of Figure 7. The cross-sectional area of the plane piston is S and when it is moved distance ξ along the positive direction of the x-axis, it displaces the volume $S\xi$ of air. The velocity of the change is $d\xi/dt$, which is the particle velocity u, so the volume velocity becomes:

$$q = S\frac{d\xi}{dt} = Su \qquad 21$$

The volume velocity applies directly to loudspeakers as the cross-sectional area of the diaphragm multiplied by the velocity of the diaphragm.

2.7 Impedance

Acoustics operates with two basic variables, sound pressure p and volume velocity q, which corresponds to the voltage e and current i within an electrical circuit. In electrical circuit theory is the *electrical impedance Z_E* of a circuit defined as the proportionality constant between voltage e and current i for the circuit: $e = Z_E i$, so the impedance is characteristic for the circuit and can be measured by driving a current through the circuit and measure the voltage across the circuit. The reverse relation defined by $i = Y_E e$ is the *admittance* (or mobility) so admittance is the reciprocal of impedance: $Y_E = 1/Z_E$.

Acoustic circuits are described through the *specific impedance*, which is characterising the medium (air), and the *acoustical impedance Z_A*, which is characterising the acoustical circuit. The impedances are related to each other by the cross-sectional area that the particles are passing through.

The *specific impedance* is the complex ratio of the sound pressure at a point of an acoustic medium or mechanical device to the particle velocity at that point (Beranek, 11):

$$Z_S = \frac{p}{u} = S Z_A \qquad\qquad 22$$

The unit is Ns/m^3 and the value is $Z_S = \rho c$ for the plane wave in air, with the value 407 Ns/m^3 at standard air pressure of 10^5 Pa and 22°C temperature (Beranek, 36). The value is also reported to 413 Ns/m^3 at 101.3 kPa and 20°C (Jacobsen, 11).

The *acoustic impedance* at a given surface is the complex ratio of the sound pressure averaged over the surface to the volume velocity through it. The surface may be either a hypothetical surface in an acoustic medium or the moving surface of a mechanical device (Beranek, 11):

$$Z_A = \frac{p}{q} = \frac{p}{Su} = \frac{Z_S}{S} \qquad\qquad 23$$

The unit is Ns/m^5. The direction of the volume velocity or the particle velocity must be in the positive direction of the independent variable.
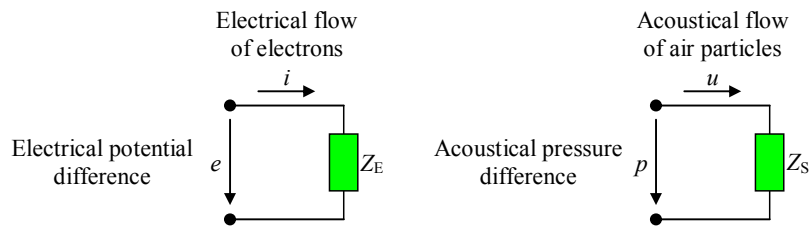
Figure 8 – Electrical and acoustic impedances are defined similarly through Ohm's law. For an acoustical circuit is the sound pressure given by the particle velocity or (alternatively the volume velocity) and the impedance of the acoustical circuit.

2.7.1 Plane wave – propagation

For a progressive plane wave travelling in the *x*-direction ($p_- = 0$), the sound pressure and particle velocity are determined from equations 11 and 13:

$$p(x,t) = p_+ \exp(-ikx)\exp(i\omega t)$$

$$u(x,t) = \frac{p_+}{\rho c} \exp(-ikx)\exp(i\omega t)$$

Inserting the expressions into the above definition, the specific impedance for the progressing plane wave within a tube becomes:

$$Z_S = \rho c \qquad\qquad 24$$

The acoustic impedance for a circuit with cross-sectional area *S* becomes:

$$Z_A = \frac{\rho c}{S} \qquad\qquad 25$$

The equation is valid for tubes and ducts with a cross-sectional dimension, which is small compared to wavelength, in order to guarantee plane waves. The acoustic impedance is high for narrow tubes and ducts.

2.7.2 Plane wave – Reflection

Consider the cylindrical tube of cross-sectional area S shown in Figure 9. A plane wave is assumed propagating to the right toward the end of the cylinder at $z = L$, where an acoustical impedance Z_{AT} is terminating the tube. The acoustic impedance is unknown for the moment and will be considered later. The wave will be partially reflected, thus introducing a backward-travelling wave within the tube, and partially transmitted into the surrounding medium where the energy is lost.
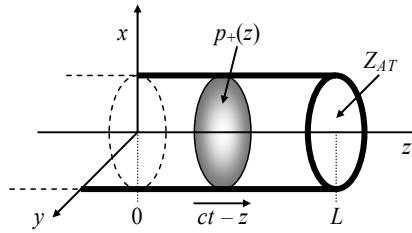
Figure 9 – Plane wave within a semi-infinite cylindrical tube, which is terminated at the open end by known acoustical impedance.

The wave equation for the tube is characterised by an incident wave p_+ travelling to the right, and a reflected wave p_-, which is due to the reflection at the terminated end and is travelling to the left. From equations 11 and 12, the sound pressure and particle velocity becomes:

$$p(z,t) = \left[p_+ \exp(-ikz) + p_- \exp(ikz) \right] \exp(i\omega t)$$

$$u(z,t) = \frac{1}{\rho c} \left[p_+ \exp(-ikz) - p_- \exp(ikz) \right] \exp(i\omega t)$$

A reflection coefficient R is defined as the ratio between the sound pressures of the reflected wave and the incident wave.

$$R = \frac{p_-}{p_+} \qquad\qquad 26$$

Determining an expression for the reflection coefficient starts by calculating the acoustical impedance of the plane wave, which is the sound pressure divided by the volume velocity:

$$Z_{AP}(z) = \frac{p(z,t)}{Su(z,t)} = \frac{\rho c}{S} \frac{\exp(-ikz) + R \cdot \exp(ikz)}{\exp(-ikz) - R \cdot \exp(ikz)} = \frac{\rho c}{S} \frac{1 + R \cdot \exp(2ikz)}{1 - R \cdot \exp(2ikz)}$$

At the termination of the tube ($z = L$) is the boundary condition $Z_{AP}(L) = Z_{AT}$, which gives:

$$Z_{AT} = \frac{\rho c}{S} \frac{1 + R \cdot \exp(2ikL)}{1 - R \cdot \exp(2ikL)}$$

Solving for the reflection coefficient:

$$R = \frac{Z_{AT} - \dfrac{\rho c}{S}}{Z_{AT} + \dfrac{\rho c}{S}} \exp(-2ikL) \xrightarrow[L \to 0]{} R = \frac{Z_{AT} - \dfrac{\rho c}{S}}{Z_{AT} + \dfrac{\rho c}{S}} \qquad\qquad 27$$

The exponential becomes unity for $L = 0$, corresponding to the termination impedance Z_{AT} being located at $x = 0$. The exponential becomes a delay for $L > 0$; i.e. the time required for

the incident wave moving from 0 to L plus the time required for the reflected wave moving from L back to 0. The delay term is related to the position of the termination but not to the termination itself and will thus be ignored for the current analysis.

No reflection is encountered for Z_{AT} equal to the impedance of the tube $\rho c/S$ since $R = 0$ with this condition. A rigid termination, such as a closed end, causes the terminating impedance to approach infinity so the reflection coefficient becomes $R = 1$, so the reflected wave is of the same amplitude and phase as the incident wave. With an open end, the termination impedance approaches zero since there can be no pressure build-up at the open end (pressure relief), and the reflection coefficient becomes $R = -1$, so the reflected wave is of same amplitude but opposite phase as the incident wave. The latter situation is representative for the baffle but the open-end value does not apply directly.

The amount of transmitted signal T can be calculated by writing the expressions for the section before the discontinuity ($z < L$) where the equation contains an incident and a reflected wave and for the section after the discontinuity ($z > L$) where the equation contains only one propagating wave:

$$p(z,t) = p_+\left[\exp(-ikz) + R \cdot \exp(ikz)\right]\exp(i\omega t), \quad z < L$$
$$p(z,t) = p_+ T \cdot \exp(-ikz)\exp(i\omega t), \quad z > L$$

The sound pressure at the two sides of the discontinuity must be the same, so:

$$p(L,t) = \exp(-ikL) + R \cdot \exp(ikL) = T \cdot \exp(-ikL)$$

Solving for T, we get:

$$T = 1 + R \cdot \exp(2ikL)$$

Assigning the point of discontinuity to $L = 0$, the relation becomes:

$$T = 1 + R \qquad\qquad 28$$

This equation will be referenced for the signal transmitted into the shadow zone. The equation applies to the spherical wave as well.

2.7.3 Spherical wave

For a progressive spherical wave travelling in the r-direction ($p_- = 0$), the sound pressure and particle velocity are given by equation 17 and 19 to:

$$p(r,t) = \frac{p_+}{r}\exp(-ikr)\exp(i\omega t)$$
$$u(r,t) = \frac{p_+}{r\rho c}\frac{1 + ikr}{ikr}\exp(-ikr)\exp(i\omega t)$$

The specific impedance at distance r for the progressive spherical wave becomes:

$$Z_S(r) = \rho c\frac{ikr}{1 + ikr} \qquad\qquad 29$$

The acoustic impedance at distance r for the progressive spherical wave becomes:

$$Z_A(r) = \frac{\rho c}{S} \frac{ikr}{1+ikr}$$

30

The acoustic impedance of the spherical wave differs from the plane wave by the frequency and distance dependent term kr. The impedance is almost purely imaginary and proportional to frequency at short distances ($kr < 1$), which corresponds to a moving mass. The impedance becomes almost real and approaches the specific impedance of the plane wave at sufficiently large distance or frequency ($kr > 1$), which corresponds to a loss (resistance).

2.8 Spherical source

A spherical sound source is radiating equally well in any direction and can be described as a pulsating balloon, which is creating local modulations of the air pressure and these alternating high/low pressure regions propagates away from the balloon at the speed of sound.
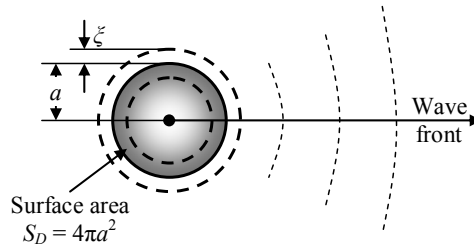
Figure 10 – A spherical sound source with radius a and displacement ξ.

The volume velocity q of the source will be used deriving an expression of the sound pressure from the spherical source. The sound pressure at distance r for a progressive spherical sound wave without reflections ($p_- = 0$) was given by equation 18:

$$p(r) = \frac{p_+}{r} \exp(-ikr)$$

Coefficient p_+ can be determined using the acoustic impedance Z_A from equation 30 to define the sound pressure $p(a)$ at the surface of the sphere using the volume velocity. From the definition of the acoustic impedance (equation 23):

$$p(a) = Z_A q = \frac{\rho c}{S} \frac{ika}{1+ika} q$$

Solving for p_+ at $r = a$:

$$p_+ = \frac{ap(a)}{\exp(-ika)} = \frac{a}{\exp(-ika)} \frac{\rho c}{S} \frac{ika}{1+ika} q$$

Inserting the expression for the surface area ($S = 4\pi a^2$) we finally determine the amplitude of the outward propagating wave for a sphere of radius a:

$$p_+ = \frac{ik\rho c}{4\pi}\frac{q}{1+ika}\exp(ika) \qquad\qquad 31$$

Hence, the sound pressure at distance r from the centre of a pulsating sphere with radius a:

$$p(r) = \frac{ik\rho c}{4\pi r}\frac{q}{1+ika}\exp(-ik(r-a)) \qquad\qquad 32$$

It is interesting to note that the amplitude of the sound pressure becomes independent of the frequency for $ka > 1$, so a relative large pulsating sphere with constant volume velocity would be an ideal loudspeaker. The cross-over frequency is $f = c/2\pi a$, so $a = 50$ mm would be useful from 1.1 kHz and upward. As will be shown later, the electro-dynamic loudspeaker becomes almost frequency-independent within a range by compensating the frequency proportionality by an opposing relation due to the mechanical construction. For the source radius approaching zero the expression becomes the sound pressure at distance r from a point source with volume velocity q.

$$\boxed{p(r) = \frac{ik\rho c}{4\pi r}\exp(-ikr)q \qquad\qquad 33}$$

The sound pressure is proportional to frequency and inversely proportional to distance. Note that the sound pressure is approaching infinite for r approaching zero. Combining equation 20 and 31 the particle velocity in the direction of propagation becomes:

$$u(r) = \frac{1}{r\rho c}\frac{ik\rho c}{4\pi}\frac{q}{1+ika}\exp(ika)\frac{1+ikr}{ikr}\exp(-ikr)$$

For the source radius approaching zero the expression becomes the sound pressure at distance r from a point source with volume velocity q.

$$\boxed{u(r) = \frac{ik}{4\pi r}\frac{1+ikr}{ikr}\exp(-ikr)q \qquad\qquad 34}$$

The near-field term affects amplitude and phase. At short distance or low frequencies is the particle velocity in-phase with the source but the amplitude is reduced by distance squared:

$$u(r) \xrightarrow[kr\ll 1]{} \frac{1}{4\pi r^2}\exp(-ikr)q$$

At large distance or high frequencies is the particle velocity 90° in advance of the source and the amplitude is inversely proportional to distance:

$$u(r) \xrightarrow[kr\gg 1]{} \frac{ik}{4\pi r}\exp(-ikr)q$$

2.8.1 Infinite surface

For a point source located close to an infinitely large and rigid surface the sound directed through the surface will be reflected back into the half-plane in front of the surface. This corresponds to a mirror source placed behind an imaginary surface.
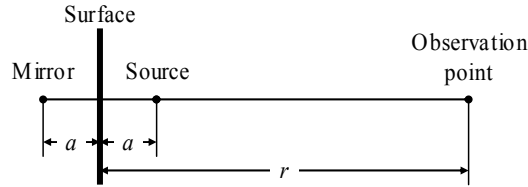
Figure 11 – A spherical sound source above a rigid surface.

The output becomes the addition of the direct sound, which is travelling the distance $r - a$, and the reflected sound, which is travelling the distance $r + a$:

$$p(r) = \frac{ik\rho c}{4\pi(r+a)} q \exp(-ik(r+a)) + \frac{ik\rho c}{4\pi(r-a)} q \exp(-ik(r-a))$$

For a source located very close to the surface, a is approaching zero:

$$p(r) = \frac{ik\rho c}{2\pi r} q \exp(-ikr) \qquad\qquad 35$$

Hence, the sound pressure from a point source located close to a large surface becomes two times the sound pressure of a spherical source but radiation is restricted to the half space in front of the surface.

For $a > 0$, the addition of both the direct and delayed signals causes interference. Assuming that $a \ll r$ allows for a simplification since the difference in amplitude becomes minimal and the distance can be approximated by r for both the direct and reflected signal.

$$p(r) = \frac{ik\rho c}{4\pi r} q [\exp(-ik(r+a)) + \exp(-ik(r-a))]$$

$$= \frac{ik\rho c}{2\pi r} q \exp(-ikr)\cos(ka)$$

Destructive interference occurs at $\cos(ka) = 0$, i.e. $ka = n\pi/2$, where n is odd ($f = nc/4a$) and constructive interference occurs at $\cos(ka) = \pm1$, i.e. $ka = n\pi$ ($f = nc/2a$). For $a = 50$ mm, the first dip occurs at 1.7 kHz, the first peak at 3.4 kHz and so forth. A loudspeaker located close to a surface will behave as a baffled loudspeaker at sufficiently low frequencies.

2.8.2 Radiation impedance

The sound pressure from a pulsating sphere with radius a is given by equation 32 with $r = a$, and the acoustical impedance as seen from the sphere can be calculated using equation 23:

$$Z_A = \frac{p(a)}{q} = \frac{i\omega\rho}{4\pi a}\frac{1}{1+ika} \qquad 36$$

It will be valuable deriving a circuit model of this impedance, which is a model consisting of resistive and reactive components.
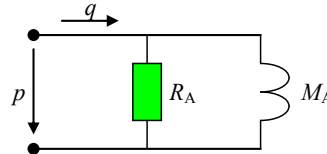
Figure 12 – Acoustic equivalent of the loading upon the spherical source. The impedance is defined by the mass for low frequencies (ka < 1) and by the resistor for high frequencies. The limiting frequency is f = c/2πa, which is 550 Hz for a = 100 mm (8 inch bass loudspeaker) and 5.5 kHz for a = 10 mm (1 inch dome loudspeaker). The loudspeaker can be considered small for ka < 1 where the radiation is approximately spherical.

The components of the model will appear to be in parallel, so the expression is most easily derived using the admittance (Leach, 34):

$$Y_A = \frac{1}{Z_A} = \frac{4\pi a(1+ika)}{i\omega\rho} = \frac{4\pi a}{i\omega\rho} + \frac{4ik\pi a^2}{i\omega\rho} = \frac{4\pi a}{i\omega\rho} + \frac{4\pi a^2}{\rho c} = \frac{1}{R_A} + \frac{1}{i\omega M_A}$$

The impedance of a resistor is independent upon frequency ($Z_R = R_A$) and the impedance of a mass is imaginary and proportional to frequency ($Z_M = i\omega M_A$), so the acoustical resistance and acoustical mass, seen by the pulsating sphere of radius a, are:

$$R_A = \frac{\rho c}{4\pi a^2} = 0.080\frac{\rho c}{a^2}, \quad M_A = \frac{\rho}{4\pi a} = 0.080\frac{\rho}{a} \qquad 37$$

For a = 50 mm is the acoustical radiation resistance R_A = 13 10³ Nsm⁻⁵ and the acoustical mass of the air close to the pulsating sphere is M_A = 1.9 kgm⁻⁴.

For comparison, the radiation impedance for <u>one side</u> of a piston of radius a, which is placed in an infinite baffle is (Leach, 44):

$$R_A = \frac{128\rho c}{9\pi^3 a^2} = 0.46\frac{\rho c}{a^2}, \quad M_A = \frac{8\rho}{3\pi^2 a} = 0.038\frac{\rho}{a} \qquad 38$$

The piston is loaded on both sides so the resulting mass term becomes approximately equal.

2.8.3 Loudspeaker

An electro dynamic loudspeaker within a closed cabinet (Figure 13, left) is a low-frequency approximation to the spherical sound source and it offers in addition a frequency-independent sound pressure within a relatively large frequency range. The on-axis response of a typical loudspeaker is flat throughout some five octaves from the mechanical resonance frequency to $ka = 1$ where the loudspeaker becomes directive and the cabinet will also affect the radiation. The sound pressure at distance r will be estimated using the diaphragm velocity u, which can be derived from the mechanical properties of the loudspeaker and the electrical stimulus.
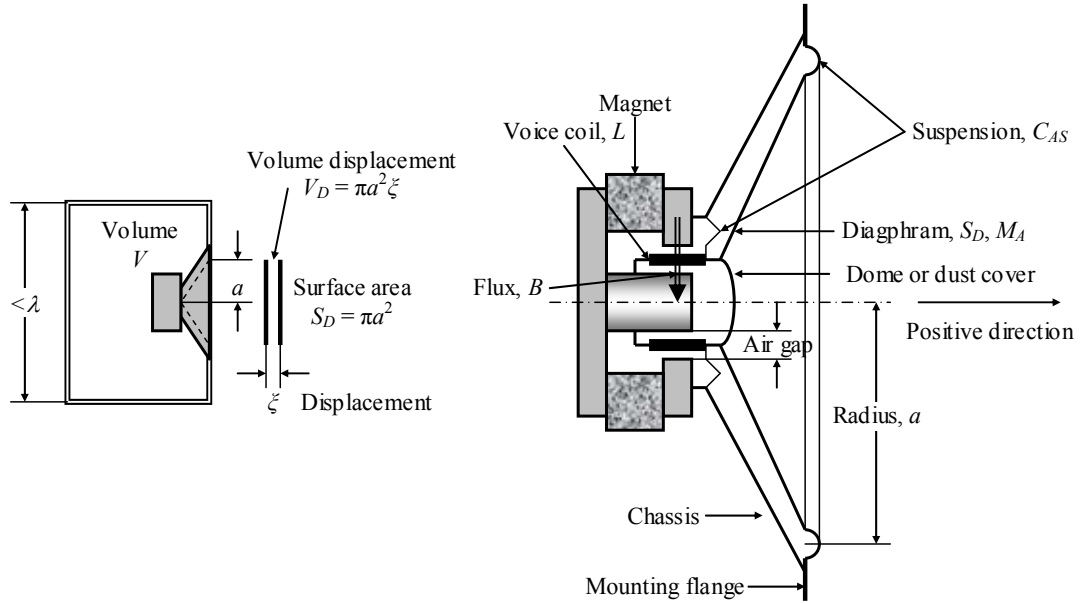
Figure 13 – A loudspeaker in closed cabinet may model the spherical source for wavelengths longer than the largest dimension of the cabinet (left). The principle of the electro-dynamic loudspeaker is shown for a conventional bass/medium loudspeaker (right).

A voice coil with the effective length of wire L is located within a magnetic flux B with the current I flowing through the coil causing a force on the voice coil expressed by the product BLI. The current is approximately equal to the applied voltage E_G from the voltage generator divided by the resistance R_E of the voice coil. Assuming harmonic excitation with amplitude E_G and oscillation frequency $\omega = 2\pi f$, the force becomes:

$$F = BLI = BL\frac{E_G \exp(i\omega t)}{R_E} \qquad\qquad 39$$

The force accelerates the total mechanical mass M_M of the voice coil, diaphragm and air loading according to Newton's second law of motion, where du/dt represents acceleration.

$$F = M_M \frac{du}{dt} \quad\Rightarrow\quad \frac{du}{dt} = \frac{F}{M_M} = \frac{BLE_G \exp(i\omega t)}{M_M R_E} \qquad\qquad 40$$

Diaphragm velocity u is determined by integration and the integration constant is set to zero avoiding movement of the voice coil without an applied voltage.

$$u = \int \frac{BLE_G \exp(i\omega t)}{M_M R_E} dt = \frac{BLE_G \exp(i\omega t)}{i\omega M_M R_E} \qquad\qquad 41$$

The volume velocity is $q = S_D u$ and insertion into equation 33 enables removal of $i\omega$ so the amplitude of the sound pressure becomes $\rho/4\pi r$ multiplied by the volume velocity and by the delay term, which gives the following expression of the sound pressure at distance r from the electro-dynamic loudspeaker:

$$p(r) = \frac{\rho}{4\pi r}\frac{S_D BL}{M_M R_E}\exp(-ikr)E_G \qquad\qquad 42$$

The equation holds for frequencies where the moving system is *mass controlled* and the diaphragm can be considered small compared to wavelength. The loudspeaker is mass

controlled for frequencies above the resonance frequency f_0, where the velocity is determined by acceleration of the moving mass (as opposed to lower frequencies where the velocity is determined by the compliance of the suspension; the sound pressure is then reduced below the resonance frequency by 12 dB/octave). The radiation from the loudspeaker is proportional to frequency for $ka < 2$ (Beranek, 118) so the loudspeaker can be considered small up to $ka = 1$.

Examples are shown below for four arbitrarily selected loudspeakers ranging from 4 to 10 in.

<u>4 inch device</u> (*Peerless BC11SG49-08*): $S_D = 5.8 \ 10^{-3}$ m^2, $BL = 4.9$ N/A, $M_M = 5$ g, $R_E = 5.5$ Ω. For $E_G = 2.83$ V is $p = 0.275$ Pa at 1 m, which is 83 dB SPL. Specified to 87 dB.

<u>6 inch device</u> (*Peerless BC18WG49-08*): $S_D = 13.8 \ 10^{-3}$ m^2, $BL = 5.0$ N/A, $M_M = 10$ g, $R_E = 5.7$ Ω. For $E_G = 2.83$ V is $p = 0.39$ Pa at 1 m, which is 86 dB SPL. Specified to 87 dB.

<u>8 inch device</u> (*ScanSpeak 21W/8554-00*): $S_D = 22 \ 10^{-3}$ m^2, $BL = 8.0$ N/A, $M_M = 20.5$ g, $R_E = 5.5$ Ω. For $E_G = 2.83$ V is $p = 0.41$ Pa at 1 m, which is 86 dB SPL. Specified to 90 dB.

<u>10 inch device</u> (*ScanSpeak 25W/8565-01*): $S_D = 33 \ 10^{-3}$ m^2, $BL = 9.3$ N/A, $M_M = 47$ g, $R_E = 5.5$ Ω. For $E_G = 2.83$ V is $p = 0.32$ Pa at 1 m, which is 84 dB SPL. Specified to 88 dB.

Note that $S_D BL / M_M R_E$ is almost constant for the example speakers with an average value around 1.3 Pa.m/V so the typical loudspeaker delivers 0.35 Pa (85 dB) at 1 m distance and 2.83 V of input voltage corresponding to 1 W of input power to 8 Ω nominal impedance.

The formulas below are from Beranek (35, 222) with some simplifications.

$$f_0 = \frac{1}{2\pi\sqrt{M_A C_A}}, \quad C_A = \frac{C_{AS} C_{AB}}{C_{AS} + C_{AB}}, \quad C_{AB} = \frac{V_B}{\rho c^2} \quad \text{and} \quad f_1 = \frac{c}{2\pi a} \qquad 43$$

The resonance frequency is defined by the total acoustical mass $M_A = M_M/S_D^2$, where M_M is the mechanical mass of voice coil and diaphragm, and S_D the cross-sectional area of the diaphragm. The total acoustical compliance is $C_A = C_M S_D^2$, where C_A includes the suspension compliance C_{MS} and the compliance of the confirmed air C_{AB} within the box with volume V_B. The suspension can be ignored for loudspeakers within small boxes where C_{AB} becomes very small; hence, $C_A \approx C_{AB}$.

The loudspeaker approximates a spherical sound source for $ka < 0.5$ with the sound pressure reduced 2 dB from 0° (on-axis) to 180° (rear side of the cabinet) and the loudspeaker is useful up to $ka = 1$ with less than 5 dB drop at 180°. At $ka = 2$ is the sound pressure dropped 10 dB at 180° (Beranek, 104). The figures are reported for a piston at the end of an infinite tube and can be used for loudspeakers mounted in cabinets with only slightly larger dimensions than the diameter of the loudspeaker (Beranek, 103). The conclusion is that the loudspeaker should point toward the test set-up for the best amplitude response.

2.9 Hearing thresholds

A study of diffraction effects cannot be conducted on its own without at least some minimum reference to audibility since a corrective action will not be required for inaudible effects. It is the objective of this short section defining a threshold limit for discriminating between significant levels and insignificant levels. The hearing thresholds will be introduced and the effect of discrimination will be lightly touched upon.

The sound pressure level (SPL) of the sound pressure p is defined as 20 log10(p/p_{REF}) where the reference threshold level p_{REF} is defined as 20 μPa; this level is 0 dB SPL and represents the limit for a normal-hearing person around 1 kHz; it is the *absolute threshold of hearing* (Moore, 10). Normal conversation is typically conducted at 70 dB and live rock music may reach the *threshold of pain* at 120 dB (Moore, 11).

The audible frequency range is from 20 Hz to 15 kHz for young people and at sound pressure levels around 70 dB SPL but signals below 100 Hz become inaudible below 25 dB SPL and the upper limit is reduced at increasing age. The most "linear" range for the human ear is from 400 Hz to 6 kHz where the "response" is within ±5 dB of the level at 1 kHz (Moore, 56). The current study uses the frequency range from 60 Hz to 10 kHz for the majority of the study thus applying to most normal listening situations.

2.9.1 Level discrimination

The ability to discriminate between different levels is around 0.5 dB for wideband noise, which holds from about 20 dB SPL to 100 dB SPL (Weber's law), but the discrimination is improved at high sound levels for pure tones; this is called the "near miss" to Weber's law (Moore, 139). A subjective impression of doubling the loudness is obtained for 10 dB of increase (Steven's law), which holds from 20 dB SPL and up (Moore, 132). We can thus conclude that changes below 0.5 dB are inaudible and that changes above 10 dB are indeed audible.

The change in level ΔL is assumed *significant* if it is larger than the below limit:

$$\Delta L = 5\,\text{dB}, \quad 60\,\text{Hz K } 10\,\text{kHz} \qquad\qquad 44$$

This is not a scientifically supported hearing threshold; it is *defined* by the author for use within the present study. Hence, a frequency response with less than 5 dB from the lowest dip to the highest peak is defined as *good* while a response with larger deviations than this is *bad*. As will be seen from the results to follow is the effect of a loudspeaker baffle an amplitude change of some 10 dB around 300 Hz so this is *bad* and the loudspeaker system needs some kind of correction, such as changing the design of the cabinet or inclusion of electrical correction of the frequency response, while the model that can copy the actual response to within the above limit is a *good* model regardless of the "quality" of the actual response. For symmetrical deviations around an average level the above limit corresponds to ±2.5 dB for discrimination between good or bad.

2.9.2 Frequency discrimination

The ability to discriminate between different signals is complex but can to a certain degree be described through the equivalent rectangular bandwidth (ERB), which represents a frequency-detection model for the ear and brain. The ERB is related to frequency through the following equation where ERB is output in hertz for frequency input in hertz (Moore, 73):

$$ERB = 24.7 + 0.108 \times f$$

The narrowest ERB is found for low frequencies (36 Hz at 100 Hz) and the bandwidth become approximately proportional to frequency well above 250 Hz. Bandwidth-limited signals of constant energy (which in this context is the same as constant power) become louder if the bandwidth exceeds one ERB than if its bandwidth is less than one ERB (Moore, 135). Two sounds spaced in the frequency domain are captured as individual sounds if the frequency spacing is larger than 1.25 times the ERB at the frequency range of interest and the sounds are combined into an amplitude modulated sound is the spacing is less than the ERB measure (Moore, 85).

The ERB is 130 Hz for frequencies around 1 kHz so the least detectable frequency difference is 16 %, which corresponds to two or three semi-tones on the musical scale so notes separated more than this are detected as individual tones while notes separated less are captured as an

amplitude modulated tone, known as "beating". The ERB is 35 Hz around 100 Hz so 44 % difference is required for signal detection at low frequencies. This means that music does not contain chords (i.e. notes sounding together) with notes placed close together in the bass region since they cannot be heard individually. For harmonically related tones, i.e. the partials of a complex signal repeating at a fixed frequency, are we able to detect 5 to 8 partials (Moore, 84), which indicates a limit between 25 % (partials 4 to 5) and 15 % (partials 7 to 8) and is in good agreement with the bandwidth given by the ERB.

The change in frequency *ΔF* is assumed *significant* if it is larger than the below limit:

$$\Delta F = 15\%, \quad 60\,\text{Hz K } 10\,\text{kHz} \qquad\qquad 45$$

This means that a peak around 1 kHz and of 5 dB height will be considered inaudible if the bandwidth is less than 150 Hz, i.e. if the signal is within one ERB.

The problem of discrimination is much more complex for real music where a loud sound may suppress the audibility of weaker sounds in the neighbourhood of the loud signal; an effect called "masking", which is described in literature both in the frequency domain and in the time domain. Masking can suppress a weak signal is at higher frequency than a loud signal; an effect used within the popular MP3 encoding scheme to avoid coding of inaudible sounds thus saving bits for transmission or storage onto media. It is not easy to specify a limit for audibility since masking is very complex and depends upon much more than just level differences.

This concludes this non-scientific discussion on audibility. The above limits will not be quoted later on but will be implied when the performance of the models are being judged.

3 Measurements

This chapter introduces the set-up used for the measurements presented within this study and displays the results. It is the objective of the study addressing the effect of the baffle alone thus not including the effects related to the physical size of the loudspeaker so the test set-up was arranged to represent the loudspeaker by a point source.

Figure 14 – The measurement set-up showing the baffle and probe microphone (left) and the source loudspeaker (right).

A real loudspeaker is far from being an approximation to a point source; a bass loudspeaker is comparable to wavelength around 500 Hz and even a dome tweeter is acoustically large at the highest part of the audible range. The reciprocity principle was addressed to allow swapping of loudspeaker and microphone, thus using the small size of the microphone as a test probe to substitute the loudspeaker.

3.1 Reciprocity

Linear circuit theory states relations between voltage and current for two-port representation of a passive electrical network, such as the one shown to the left in Figure 15. The circuit is fully described through the currents I_1 and I_2 flowing into the ports and voltages E_1 and E_2 across the ports. The network can be represented by a range of mathematical models with or without controlled sources, such as the *pi-circuit* often used for high-frequency analysis, the *h parameter* model, which is popular within semiconductor theory, the *z* or *y parameter* models used for network analysis, and the *T-model*, which is shown to the right in the figure below.
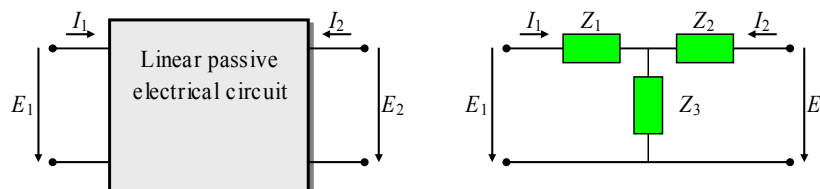
Figure 15 – Left: A linear and passive electrical two-port network with an input port (E₁, I₁) and an output port (E₂, I₂). Right: Representation of the two-port using the T-network.

Assuming that the current I_2 is driven into port 2 with port 1 open ($I_1 = 0$), then the port 1 voltage E_1 becomes $Z_3 I_2$ since no current is flowing through Z_1 and the voltage across Z_2 is of no consequence. Similarly for the current I_1 driven into port 1 with port 2 open ($I_2 = 0$), the

voltage E_2 becomes Z_3I_1. Since impedance Z_3 is the same for both expressions we have the following expression for the reciprocity principle:

$$\left. \begin{array}{l} E_1 = Z_3 I_2 \quad \text{for } I_1 = 0 \\ E_2 = Z_3 I_1 \quad \text{for } I_2 = 0 \end{array} \right\} \quad \Rightarrow \quad \frac{E_1}{I_2} = \frac{E_2}{I_1} \qquad\qquad 46$$

Forcing current I into one port produce the voltage $E = Z_3I$ across the other port.

It does not matter which port is which; the ports can be interchanged for any linear and passive network. This is the core of the reciprocity principle but the idea must be broadened for the use within acoustics where signals are transmitted through a medium.

The impedances of Figure 15 may represent any combination of resistance, capacitance and inductance, as well as controlled sources, $I(E)$ and $E(I)$, so any network can be represented except networks with nonreciprocal components, such as the *gyrator* and *negative impedance converter*. The gyrator is encountered for microwave systems and sometimes also as a mathematical model when combining electrical and mechanical systems and the negative impedance converter is used for electrical filters. Avoiding these pitfalls, interconnection of systems with different analogies is allowed so the reciprocity principle holds for acoustical transducers with electrical terminals and communication through a medium (air, water), such as microphones and loudspeakers (Beranek, 377).
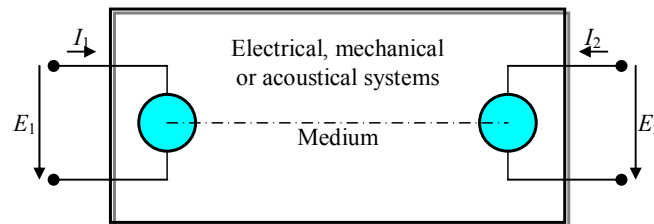
Figure 16 – A system with a two transducers connected through a medium, such as air. The transfer function of the system remains the same if ports 1 and 2 are interchanged.

An extension of the reciprocity principle includes the directivity of a transducer and proves that the directivity is the same whether it is being used as a microphone or loudspeaker. Consider Figure 17, where one of the transducers can be rotated in a plane.
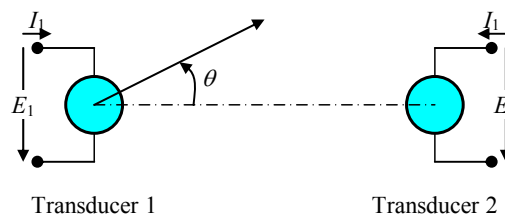
Figure 17 – Two transducers where one can be rotated. The transfer function becomes function of the rotation angle but not the signal direction between the transducers.

If the open-circuit output voltage from transducer 2 varies as $f_2(\theta)$ when transducer 1 is rotated, then its output voltage is $E_2f_2(\theta)$ when current I_1 is applied to the terminals of transducer 1. Similarly, if the output voltage of transducer 1 varies as $f_1(\theta)$ when it is rotated, then its output voltage is $E_1f_1(\theta)$ when current I_2 is applied to transducer 2.

$$\frac{E_1 f_1(\theta)}{I_2} = \frac{E_2 f_2(\theta)}{I_1} \quad \Rightarrow \quad f_1(\theta) = \frac{E_2}{I_1}\frac{I_2}{E_1} f_2(\theta)$$

For $\theta = 0$ is $f_1(\theta) = f_2(\theta) = 1$ and the equation becomes $E_2/I_1 = E_1/I_2$. Thus, in general:

$$f_1(\theta) = f_2(\theta) \qquad\qquad 47$$

The directivity pattern for transducer 1 is the same when used as transmitter (f_2) as it is when used as receiver (f_1). The consequence of the analysis is that the loudspeaker and microphone can be interchanged without changing the transfer function (Beranek, 379).
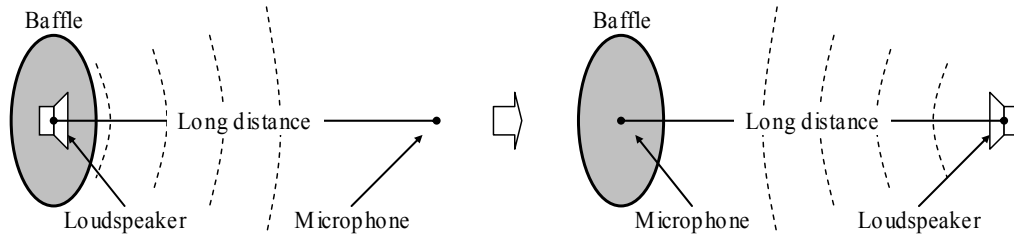
Figure 18 – The small size of the microphone improves the high-frequency response so an interchange of microphone and loudspeaker reduces the influence due to the physical size of the loudspeaker.

3.2 Set-up

Using the reciprocity principle the loudspeaker and microphone are interchanged and the term *test position* will be introduced to avoid confusion between the loudspeaker position on the baffle and the loudspeaker used for testing.

➢ The *test position* is the point at the surface of the baffle where the tip of the probe microphone will be located during the measurement. The test position represents the corresponding position for a real loudspeaker on a cabinet front baffle.

Full reciprocity is not required in the current application since the microphone will not be used as a loudspeaker, so the requirement of a linear and passive transducer can be neglected without invalidating the reciprocity assumptions; it is thus possible using a microphone of the electret-condenser type. Such a microphone with 6 mm capsule diameter is acoustically small to 18 kHz ($ka = 1$) and can easily be moved to study the effect of changing the test position. A conventional loudspeaker will be used at large distance from the baffle since the only requirement is that the wave front is approximating locally plane waves at the baffle and any loudspeaker satisfies this requirement at sufficiently large distance.
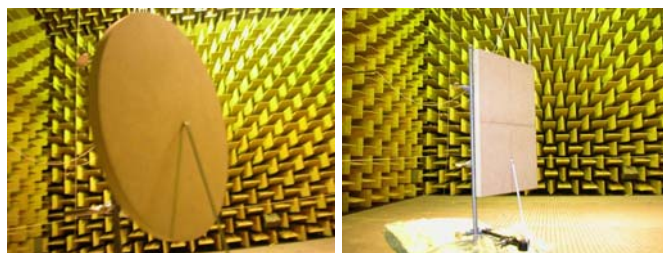
Figure 19 – The baffles to be measured, the circular baffle with 0.34 m diameter (left) and the rectangular baffle measuring 0.20 m by 0,34 m (right).

Two baffles were analysed, a *circular baffle*, which is the simplest one to analyse from a theoretical point of view and thus a very important shape for verification or rejection of the theories, and a *rectangular baffle*, which is the most important shape from a manufacturing point of view since a vast majority of commercially available cabinets are rectangular.

All measurements were performed within the large anechoic room at Ørsted●DTU, and some time was spent on finding a location without disturbing reflections. The anechoic room includes a computer-controlled turntable used for polar measurements on loudspeaker systems but this was not used for the current project so the set-up was arranged to radiate away from this turntable. The door to the anechoic chamber was not closed while the measurements were performed so reflections from the opening were reduced by using large distance to the door.

The loudspeaker was located at large distance from the baffle to avoid loudspeaker near field effects and minimising the sensitivity to change in angles for signals coming from different points on the baffle. The term "large" is here defined as larger than the circumference of the baffle, which is 1.1 m for both baffles. The measurements were performed at 1.3 m for both baffles and were at a later time later repeated at 1.4 m for the circular baffle. The set-up is shown below with the baffle to the left and the loudspeaker (representing the observation point) to the right. The baffle was fixated to a small turntable for manual change of the angle between baffle and loudspeaker. One bat of 50 mm Rockwool was applied to damp reflections from the turntable.
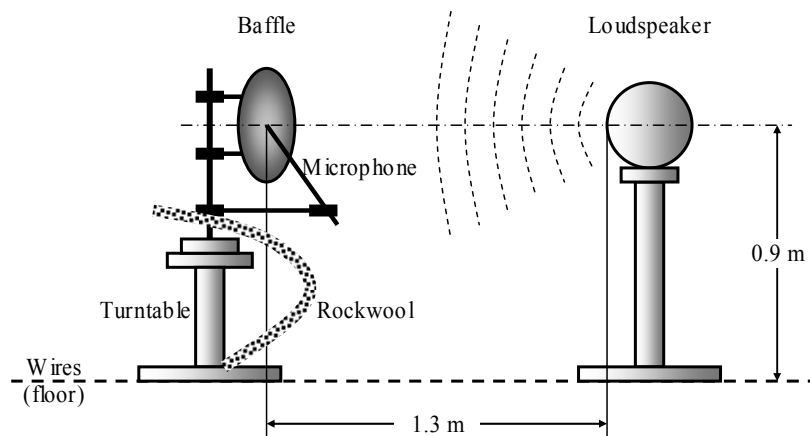
Figure 20 – The set-up with the baffle and microphone at a turntable and the loudspeaker at fixed height above the floating floor.

Two measurements are required for each plot of amplitude response, one with the baffle and another without the baffle; the latter serving as the free-field reference for the measurement. The reference spectrum was subtracted from the measured spectrum, which corresponds to a normalisation of the measured pressure-response to the reference, and it produces unity (0 dB) when there is no change in the sound pressure, such as for low frequencies where the baffle is small compared to wavelength. This may be formally written as shown below where p_{TEST} is the measured pressure-response for the test object, p_{FF} is the free-field pressure-response and p_{REF} is the usual 0 dB reference level of 20 μPa, which is included here to avoid taking the logarithm to a physical quantity.

$$20\log\left(\frac{p_{TEST}}{p_{FF}}\right) = 20\log\left(\frac{p_{TEST}/p_{REF}}{p_{FF}/p_{REF}}\right) = 20\log\left(\frac{p_{TEST}}{p_{REF}}\right) - 20\log\left(\frac{p_{FF}}{p_{REF}}\right)$$

Differences between measurements enable one to focus on the changes of the response to an alteration of the set-up such as a change in the test point where the microphone is placed or new angling of the baffle. The set-up is very sensitive to changes since the spectres are subtracted for every frequency bin, so the resulting plot consists of 6400 differences separated horizontally by 2 Hz.

Phase was not considered in this study, but each individual spectrum of the measurement and reference will be sensitive to changes in phase. The wavelength is about 25 mm at the upper frequency limit (12.8 kHz) so changes must be smaller than 12 mm for less than 180° change at the upper frequency limit and this is not easily achieved. The test set-up was standing upon a grid of steel wires so the set-up was changed by the additional weight of the test conductor while preparing the next measurement and this load was not present while measuring.
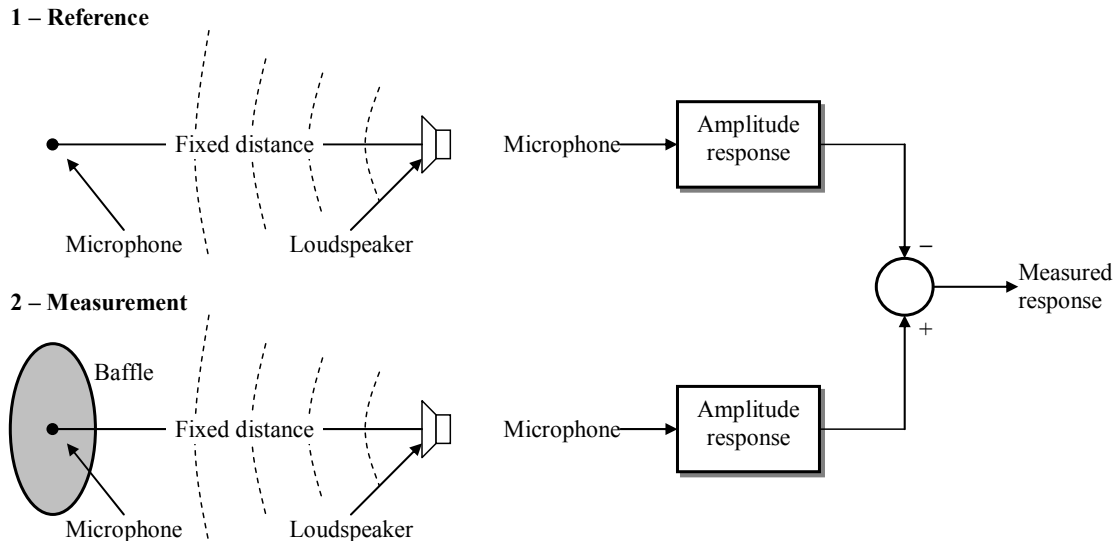
Figure 21 – The amplitude response is measured as the difference between the measured amplitude response with baffle (bottom) and a reference response without baffle (top).

In addition to this may the set-up be accompanied by changes in reflection from the set-up itself due to the change of the set-up while turning the baffle, which moves the frequency of interfering peaks and dips. The difference between spectra may thus show up as large change in amplitude although it is the frequency of a peak or dip, which has changed.

3.3 Test equipment

All measurements used the Brüel & Kjær PULSE test equipment, which is shown to the left in the picture below. The PULSE hardware is housed within a small module (shown to the right of the first picture) and contains the sound generator for output to the loudspeaker, two microphone inputs and the software for calculation of complex spectra in real time and for connection to the computer, a personal computer running Microsoft Windows and the PULSE software.

Figure 22 – The personal computer and the PULSE equipment used for measurement of the spectra (left); and the power amplifiers and active cross-over network with power supply, which were located within the anechoic room (right) .

The set-up is sketched below and is centred on the PULSE system, which generates the test signal (random noise with a bandwidth of 12.8 kHz) for output to the loudspeaker through an active cross-over and two power amplifiers. Input from the microphone was fed through a battery power supply (discussed below) to the PULSE system on input channel 2 for correlation with the output signal from the PULSE system, which was fed back from the output to input channel 1.
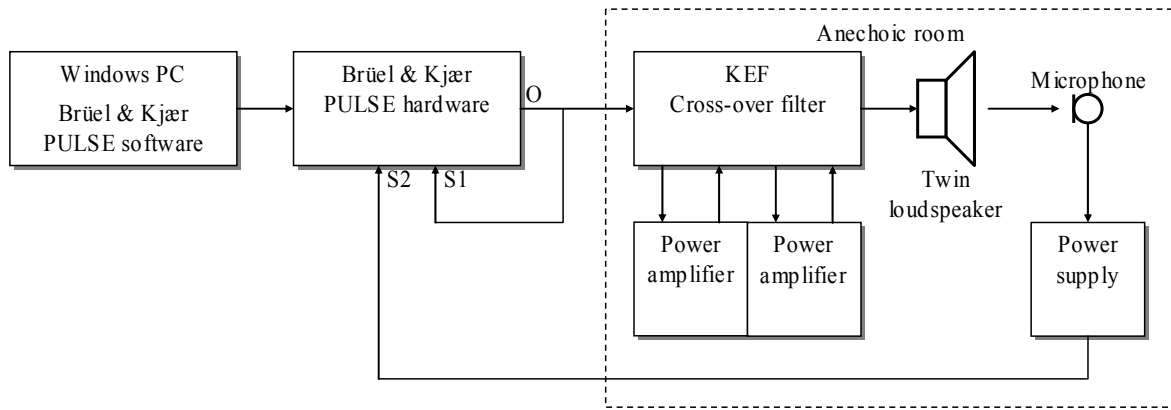
Figure 23 – The PULSE equipment generates the test signal, which is amplified and fed to the source loudspeaker, and the signal from the microphone is fed back to the PULSE equipment for calculation of the amplitude response.

A relative strong 50 Hz signal (mains hum) was seen in the recorded spectra but this affected only the low-frequency range below the range of interest and did not cause problems with the FFT – so it was ignored. The cause of the hum was not traced.

3.3.1 Loudspeaker

The signal is output through a KEF loudspeaker system housed within a ball-like cabinet for reduction of cabinet diffraction. The loudspeaker contains two concentrically mounted units; a bass unit for the low-frequency range and a treble unit for the high-frequency range. The loudspeaker was found to be directional so it will be oriented with the axis pointing toward the test set-up.

Using the simplified loudspeaker model of section 2.8.3 the resonance frequency of the loudspeaker within the closed cabinet was calculated to the approximate value of 60 Hz, according to the calculation below.

> The outer diameter of the cabinet was 300 mm so the internal radius was assumed to 145 mm and the internal volume becomes $V_B = (4/3)\pi r^3 = 12$ dm^3. The acoustical compliance of the confirmed air becomes $V_B/\rho c^2 = 91\ 10^{-9}$ m^5/N. The bass loudspeaker was fitted with rubber suspension so the compliance of the suspension can be ignored since it is much softer than the acoustical compliance of the confirmed air. The bass loudspeaker diameter was 100 mm so the cross-sectional area of the diaphragm is around $S_D = \pi r^2 = 7.8\ 10^{-3}$ m^2 and assuming a moving mass of some $M_M = 5\ 10^{-3}$ kg the acoustical mass becomes $M_A = M_M/S_D^2 = 82$ kg/m^4 and the estimated resonance frequency within the closed cabinet becomes $f_0 = 1/2\pi\sqrt{M_A C_B} = 60$ Hz.

It indicates that the loudspeaker should be a fairly good low-frequency reproducer despite the relatively small cabinet so it is expected adequate for the current study. The directivity at the high-frequency end was however rather marked as will be shown in the measurements to follow.

3.3.2 Power amplifier

Individual power amplifiers were used for the bass and treble channels with a layout shown in the drawing below. The amplifier is based upon an integrated power IC LM1875, which is capable of outputting 30 W into 4 Ω, but the power supply was only ±16 V thus limiting the output to 10 W for loudspeaker protection in case of an error during the set-up of the PULSE system. The frequency is downward limited to 3 Hz by the input DC blocking capacitor and to 5 Hz by the feedback circuitry (both frequencies at the –3 dB point) and upward limited by the power bandwidth of the chip, which is specified to 70 kHz without further information. Hence, the power amplifier is not the limiting factor for the frequency response. The linear gain was 21 times according to the schematic diagram and a linear potentiometer could be used to lower the gain.
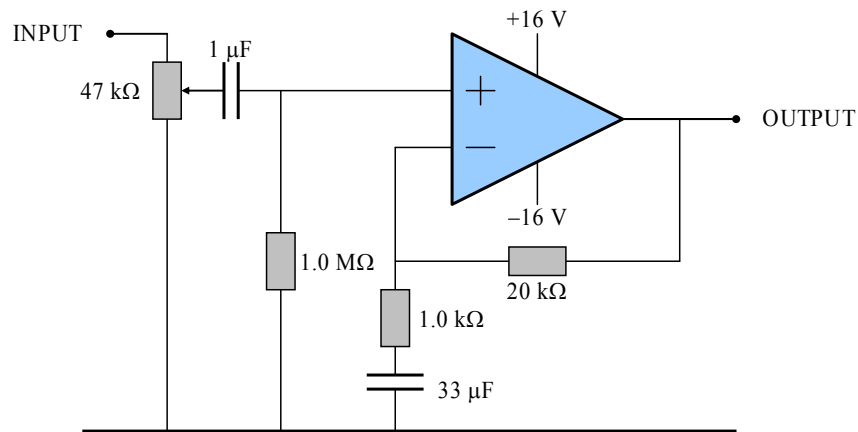
Figure 24 – The basic layout of the power amplifier, which can deliver 10 W into 8 Ω load. Details, such as bypass capacitors, Zobel network and power supply, have been omitted.

Distortion was specified at <0.05 % for <20 W (using ±25 V supply) and the equivalent input noise was specified to 3 μV/√Hz so the wideband output noise level was 7 mV RMS taking the linear gain into account. The input signal was 200 mV RMS from the PULSE test system so the output level was 4.2 V RMS corresponding to 2.2 W into 8 Ω. The signal/noise ratio at the output was 55 dB so the noise should not cause problems.

3.3.3 Microphone

The microphone used for the measurements, Panasonic MCE-2000, is a low-cost capacitor microphone with "build-in" polarisation voltage and a FET-buffer to reduce the output impedance. The microphone was preferred due to its size; it is tiny, the diameter is 6 mm and it is 5 mm long, which is small even to the highest frequency within the audible range.

Figure 25 – The microphone was glued to a thin rod and a screened wire soldered to the terminals and battery-powering was used to reduce noise injection from mains hum.

The microphone was glued to the end of a knitting needle, which is a metal rod some 2.5 mm thick and 350 mm long, and the connection cable, which is of the same diameter, was also glued to the rod thus forming a slim construction. The microphone does not need to be a precision measurement microphone; the prime characteristic is the size, the sensitivity is not important and the amplitude characteristic will be measured during the initial phase. The available data for the microphone is shown below.

Table 1 – Data sheet for the Panasonic MCE-2000 microphone with key parameters shown.

Parameter	Specification
Frequency range	20 … 20.000 Hz, ±2 dB
Sensitivity at 1 kHz	6 mV/Pa, ±4 dB
Signal/noise ratio	>58 dB
Temperature range	0 … 40 °C
Supply (via resistor)	1,5 … 10 V @ 0,5 mA

Data was obtained from http://www.shop3000.de/product_info.php/products_id/1671.

Noise is assumed expressed relative to 94 dB SPL so the specified noise floor is at 36 dB SPL (around 6 µV RMS), which is rather optimistic even if A-weighting is assumed; these cheap microphones are known as being rather noisy. Anyway, the average test level will be significantly higher than the noise floor – around 80 dB SPL was planned – and the analyser will use Fourier transformation with narrow bandwidth and averaging to suppress the noise.

The capsule was purchased in 1998 from Monacor Danmark A/S.

3.3.4 Microphone supply

Power to the FET-buffer within the microphone is supplied externally from a battery within a screened cabinet, which also carries some additional components as shown in Figure 26. The microphone is attached to the box through a jack plug and the power is interrupted when the jack is removed. Output to the PULSE equipment is supplied through standard BNC.
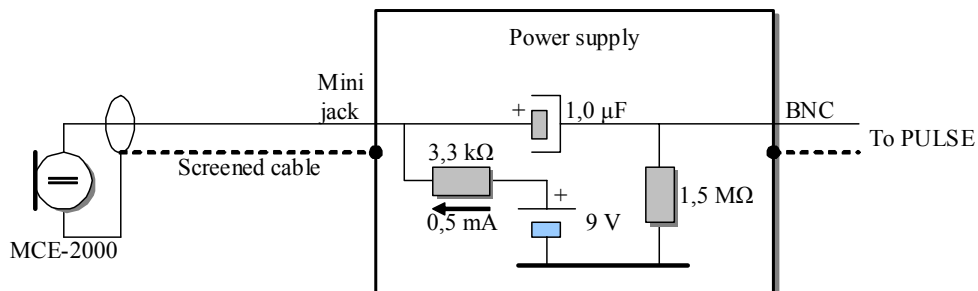
Figure 26 – The FET-buffer is supplied from a 9 V battery through a resistor. The capacitor blocks for DC and a resistor keeps the output referenced to zero. The voltage across the microphone was measured to 8.4 V with 9.2 V across the battery, so the current consumption was 240 µA and the peak output becomes limited at ±0.8 V, which corresponds to 0.6 V RMS for sine wave signal and somewhat lesser for random noise.

It is the source loudspeaker and the microphone capsule that limits the obtainable frequency range since the electrical interface is inactive within the audible frequency range.

The low-frequency response is limited downward by the capacitor but the knee frequency will never be higher than 80 Hz at –3 dB even with a shorted output. With the assumed 1 MΩ loading

from the PULSE test equipment will the lower frequency limit be 0.3 Hz. The high-frequency response is upward limited by the capacity of the connection cables used (some 100 pF/m) and by the input capacitance of the PULSE equipment. Using 20 m cable between microphone and test equipment loading becomes 2 nF, which corresponds to a knee frequency of 40 kHz assuming an output resistance of 2 kΩ from the microphone.

3.3.5 Sound pressure

The output signal from the microphone is specified to by its sensitivity, which indicates that the microphone is expected to output 6 mV signal for 1 Pa of sound pressure, corresponding to 94 dB SPL (using 20 µPa as the 0 dB reference). The sound pressure during testing was planned at minimum 80 dB SPL so the expected signal should exceed 1 mV RMS, which leaves some 40 dB of distance to the noise level. According to the PULSE *Level Meter*, the signal level was around –40 dB relative to the maximum input setting of 0.7 V RMS, which is signal of 7 mV RMS, so the actual sound pressure level was some 95 dB SPL.

With 2.2 W of input power and 1.3 m distance, the loudspeaker sensitivity can be calculated to 90 dB at 1 W input power and 1 m distance. This seems to be a reasonable figure but it was unfortunately not possible to verify the value.

3.3.6 Frequency response

An initial measurement of the amplitude response of the set-up without the baffle is shown to the left in Figure 27 using 1.0 m of distance between loudspeaker and microphone. The treble loudspeaker is obviously too loud so the high-frequency amplifier was turned down to 50 % of full level resulting in the amplitude response shown to the right, which is more level but an amplitude dip of almost 15 dB is observed at 2 kHz.
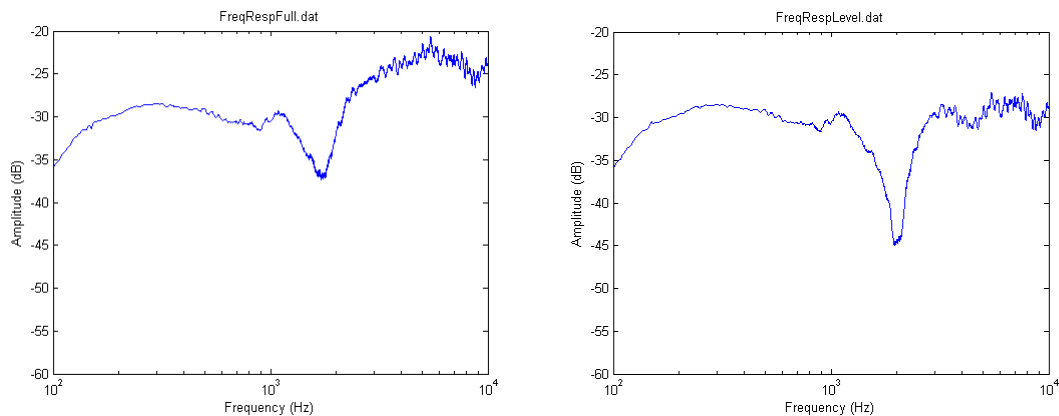
Figure 27 – Left: Raw amplitude response for the loudspeaker and microphone at 1.0 m distance. Right: Treble amplifier reduced to the 50 % setting.

Two-way loudspeakers are commonly using a cross-over frequency in the range from 2 kHz to 5 kHz dependent upon the high-frequency response of the bass unit and the low-frequency capability of the treble unit so the notch could represent problems at cross-over. The set-up was arranged to measure the bass and treble channels individually and the cut-off slopes were found to ±30 dB/octave, which is quite steep; it requires five poles within the transfer characteristic and at least three of these must be within the electronic circuitry.

As is shown in the figures below, the –3 dB frequencies was found at different values for the loudspeakers; 1.5 kHz for the bass unit and 2.5 kHz for the treble unit, which could be an

attempt to level amplitude peaking due to increased directivity or diaphragm break-up for the bass unit; however, this is assumptions.
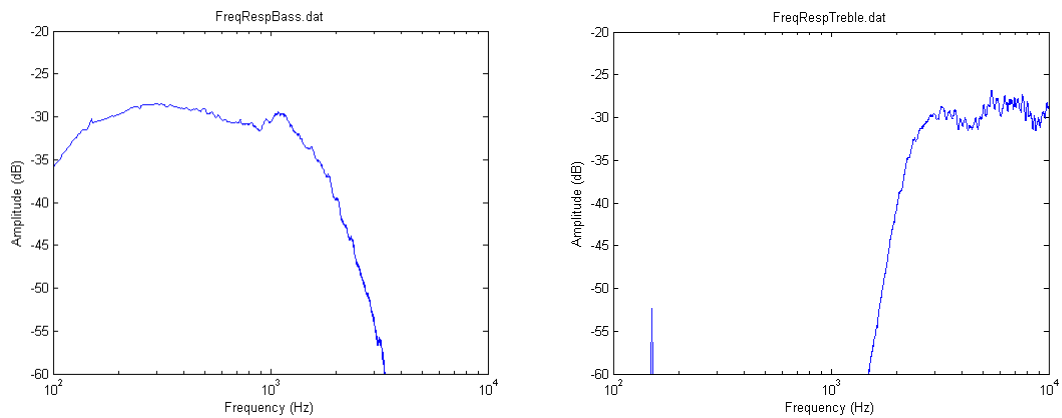
Figure 28 – Amplitude response for the bass loudspeaker channel (left) and for the treble loudspeaker channel (right).

The loudspeaker was tilted some 10° backward due to the mechanical support, which was not attempted corrected but since the loudspeaker position was kept unchanged during all measurements it was considered of minor importance. The directivity was measured at a later time and found supportive for this assumption.

An unintended phase difference between the bass and treble units at cross-over could be a problem since a half wavelength at 2 kHz is 85 mm, which is comparable to the size of the loudspeaker construction, so the response with the treble unit inverted is shown below (the treble unit was inverted by swapping the white and blue plugs). This reduced the depth of the notch to a more manageable level around –6 dB and the resultant amplitude response is shown below as the blue curve. Note the changed ordinate axis.
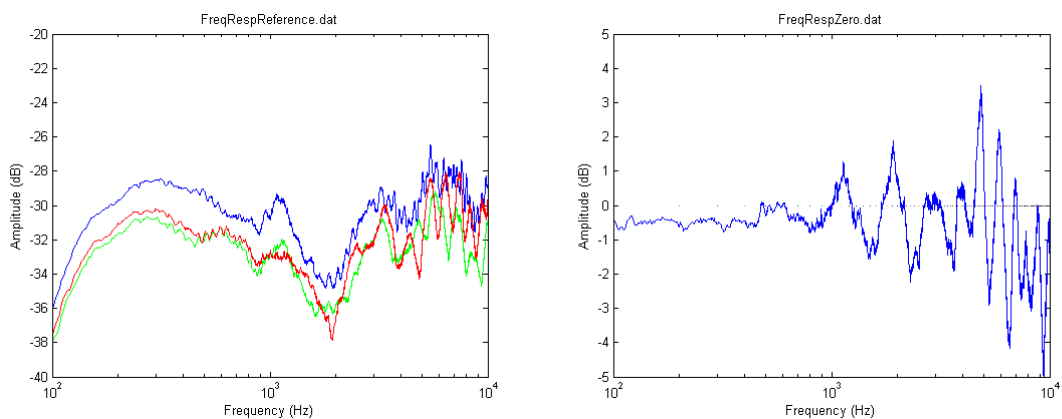
Figure 29 – Amplitude response of the set-up with treble loudspeaker attenuated 50 % and phase inverted using a measuring distance of 1.0 m (blue). The measurements were repeated with damping material added and measuring distance increased to 1.3 m (green) and again a later time with the same set-up (red). The difference between green and red curves shown in the right picture illustrates the uncertainty.

The measurement was reproduced with the microphone pointing directly toward the loudspeaker and the distance was increased from 1.0 m to 1.3 m, which was to be used during the measurements to follow (green and red curves). A reduction in amplitude of –2.2 dB was expected due to the increase in distance and this is seen to apply. The difference between the

two last measurements is shown to the right to display the uncertainty associated with the set-up. The uncertainty reaches some ±5 dB toward the high-frequency, which is quite much so the set-up was reproduced two weeks later in order to improve the accuracy of the most important measurements using the circular baffle. The microphone was pushed into the hole in the centre of the baffle and tape was applied to seal the narrow slit between the microphone and the baffle. The distance was fixed at 1.41 m, which was measured for each change of set-up, and assumed to be within ±0.01 m for all subsequent measurements but the previously mentioned uncertainty due to the floor of steel wires still applies.

A series of measurements were executed and the initial position with the microphone without baffle was repeated several times creating a total of four free-field measurements, where the average of the measurements is shown below. This forms the reference for the measurements within this study.
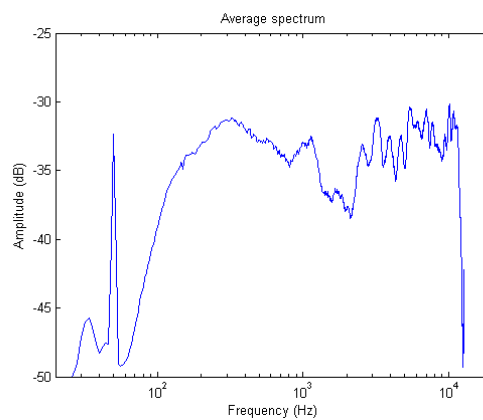
Figure 30 – Free-field 0 dB reference spectrum as the average of four measurements using 1.41 m distance. The peak at 50 Hz is mains hum and the steep cut-off above 12.8 kHz is due to the PULSE test system.

The response is within ±3 dB from 120 Hz to 12 kHz allowing for a couple of peaks above the upper limit and is sufficiently flat for the present study where only *changes* from the free-field response are of concern. The peaks and dips affect the precision only due to the risk of non-linear behaviour at high level and noise at low level so the sound pressure level was arranged to be within the upper limit set by the amplifier and loudspeaker and the lower limit set by the microphone and PULSE system.

Each measurement was output from the PULSE test system as an ASCII text file with 6401 lines carrying (1) the line number from 0 to 6400, (2) the frequency from 0 Hz to 12800 Hz in 2 Hz steps, (3) the real value of the recorded sound pressure *re(f)* and (4) the imaginary value of the sound pressure *im(f)*. The file also carried some 50 lines of information for the set-up but these lines were deleted and the files saved using the DAT-extension.

Each file was read into a MATLAB program and converted into a magnitude spectrum *m(f)*:

$$m(f) = \sqrt{re^2(f) + im^2(f)}$$

The average of the four measurements was computed and converted to decibels:

$$m(f) = 20\log_{10}\left[\frac{m_1(f) + m_2(f) + m_3(f) + m_4(f)}{4}\right]$$

It was found unnecessarily to include the reference pressure (p_{REF}) since it would be removed again when the spectrum is subtracted from the test spectrum. Each of the four measurements was related to the average spectrum to determine the difference and the result is shown below. As can be seen, the data are within ±2 dB throughout the frequency range, which is an improvement to the previous measurement. The labels with "Initial" and "Source" refer to the hand-written documentation from the laboratory test.
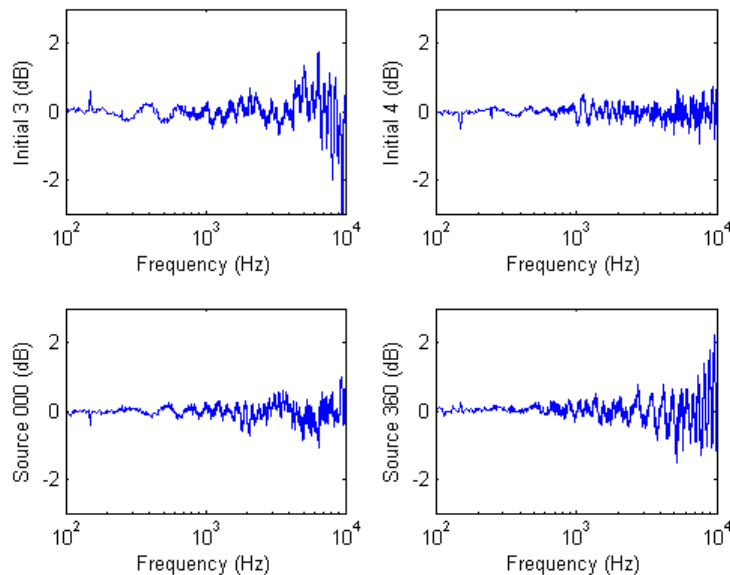
Figure 31 – Difference between each of the individual measurements and the average spectrum.

An amplitude response measurement using a calibrated microphone has not been conducted since the present work does not depend upon absolute values and precision in the sub-decibel level is not required. The interest is within this study focused on the change in amplitude response versus a change within the set-up and the accuracy of the change this is primarily related to the linearity of the transducer devices, which are assumed to be ideal transducers. However, the linearity of the microphone – or the complete test set-up – has not been verified; they have simply been assumed to be sufficiently linear for the present study.

The directivity of the source loudspeaker was measured and the result is shown below with the measurements normalised to the on-axis measurement of Figure 30 so the 0° response should ideally be a straight line at 0 dB (the blue curve). All measurements were performed using 1.41 m distance measured from the front cover of the loudspeaker to the tip of the microphone.

All curves should ideally start from 0 dB, which is obviously not the case; the difference is approximately 1 dB at low frequencies corresponding to some 10 % of change in amplitude. This cannot be due alone to uncertainty within the distance measurement since this would require a variation of 0.14 m, and the distance was measured to within one centimetre for each measurement. Although some uncertainty may be due to the steel wires it is unlikely that the set-up is the sole source to error; it is more likely that at least some of the variation is due to the loudspeaker system.
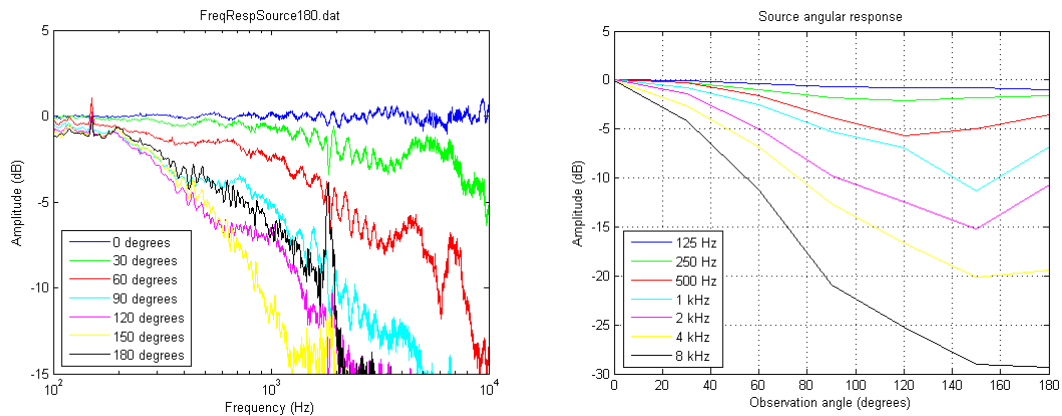
Figure 32 – Frequency response of the source loudspeaker from 0° or on-axis to 180°, which is with the loudspeaker pointing away from the measurement microphone.

There is no visual effect related to the cross-over frequency, although the output is weak around 3.5 kHz, so this part of the system seems to work very well in this respect. All measurements in this document were conducted with the treble loudspeaker unit inverted and its power amplifier turned 6 dB down as described previously.

It is obvious that the source loudspeaker is directive and must point directly toward the baffle. It was chosen to point toward the centre of the baffle so that ±170 mm of variation (the height of the baffles were 340 mm) leads to less than ±10° of uncertainty, which indicates an uncertainty level of ±1 dB except at upper frequency extreme.

3.3.7 Microphone alignment

Measurements with the circular baffle were performed with the microphone pointing toward the loudspeaker through a hole in the centre of the circular baffle and the sensitivity to the microphone not being flush with the front of the baffle was measured with the microphone moved ±5 mm relative to the surface of the baffle.
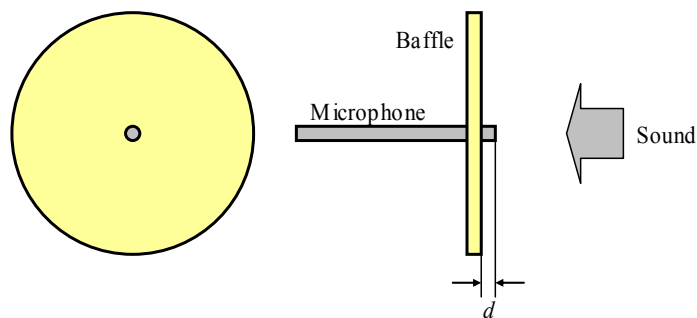
Figure 33 – Set-up for studying the effect of varying the distance from the peak of the microphone to the surface of the baffle.

The result is shown below and is within ±1 dB below 5 kHz although larger effect is seen at higher frequencies. The 5 mm deep hole in front of the microphone (left figure below) corresponds roughly to a quarter-wave resonator at 17 kHz, so the increase in amplitude is expected related to the resonance. The ripples are spaced by approximately 1 kHz and are expected representing reflections from the edge of the baffle since the baffle radius was selected to equate one half wavelength at 1 kHz.
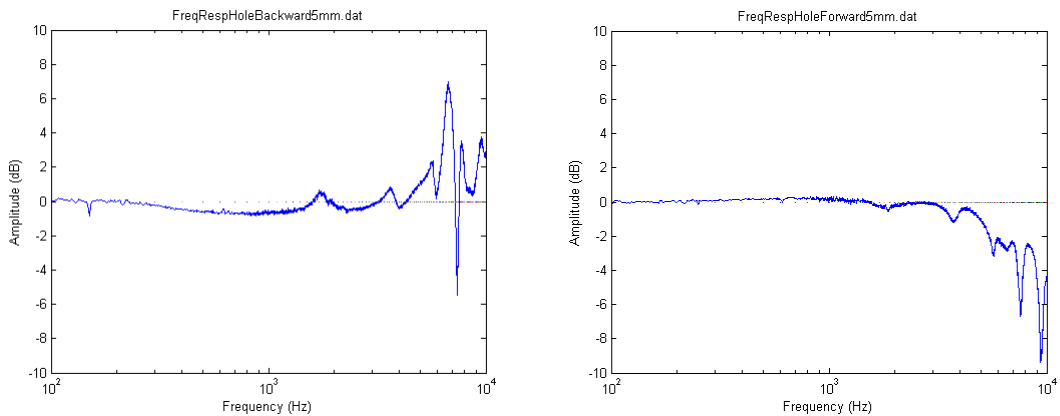
Figure 34 – Amplitude response change with the microphone 5 mm behind the surface of the baffle (left) or 5 mm in front of the surface of the baffle (right).

In general is the treble increased when the microphone is dragged backward and decreased by the microphone is pushed forward. The important frequency range up to 4 kHz is almost not affected by the misalignment but the effect becomes very significant at higher frequencies. The microphone was placed flush with the baffle to maximum ±1 mm of uncertainty so the measurements are not expected to be seriously affected by the unavoidable misalignment.

Measurements were also conducted with the microphone located at the front side in order to ease movement of the test point. This should produce the same result as measurement with the microphone pointing toward the loudspeaker through a hole in the centre of the baffle but this was unfortunately not the case as the following measurement shows so the set-up was avoided for measurements with the microphone at the centre of the circular baffle.
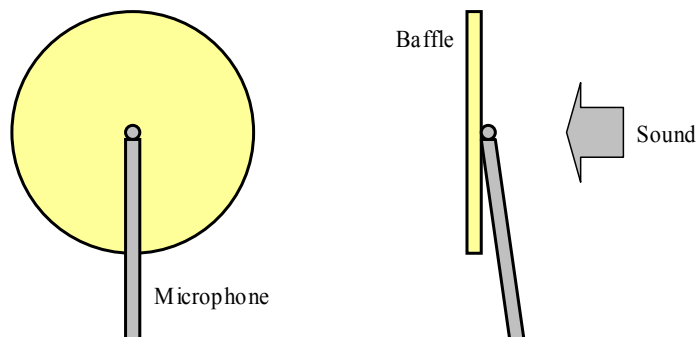
Figure 35 – Set-up for studying the effect of monitoring the sound pressure with microphone located at the front side of the baffle.

The figure below shows the difference between a measurement with the microphone pointing to the test point at the front side of the baffle and with the microphone pointing toward the loudspeaker through a hole in the centre of the baffle. The difference is within ±1 dB for frequencies below 500 Hz, within ±2 dB up to 4 kHz and within ±5 dB at higher frequencies. The conclusion is that the measurements are equivalent up to approximately 4 kHz and that higher frequencies are inaccurate.
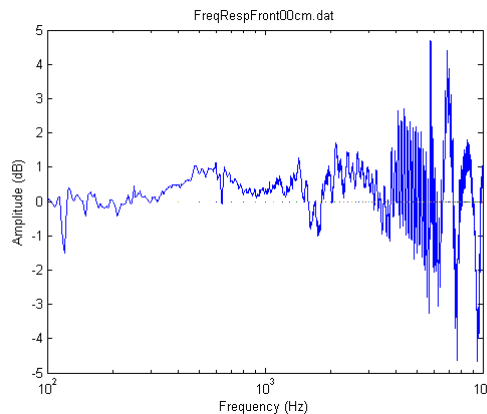
Figure 36 – Difference between measurement with the microphone at the front side of the baffle and the microphone pointing through a hole in the baffle.

The hole in the baffle was closed during the measurement using a wooden plug pushed into the hole and tape for sealing of leakage.

3.4 Circular baffle

The amplitude response for the circular baffle with radius $R = 170$ mm is detailed in this section for different observation angles and for the test point being offset from the centre of the baffle. The measurements are assembled from two test runs using different measurement distances, which affect the measurement of source offsetting and rectangular baffle.

3.4.1 Response to change in observation angle

The sound pressure was measured at the centre of the baffle for angles from 0° (on-axis) to 180° (rear side) in 30° increments with the microphone pushed through a hole at the centre of the baffle. The reference was free-field so 0 dB corresponds to the sound pressure from a point source without baffle and this level is approached toward the low-frequency end.

Low frequencies are not affected by the baffle but the high-frequency response is greatly influenced by the baffle, which is seen as the 10 dB increase in level from 500 Hz to 1 kHz and the ripple at higher frequencies. The cross-over frequency due to the baffle is 400 Hz, which is in reasonable agreement with the estimated value for $kB = 1$, which is 320 Hz for the circular baffle with 170 mm radius.

Middle frequencies are characterised by the ripple caused by the baffle. The expected peak frequency of 1 kHz is due to the half wavelength delay due to baffle radius where the direct and diffracted signals combine constructively and the dip at 2 kHz is due to the delay of a full wavelength causing destructive interference. Changing the axis to 30° reduces the amplitude of peaks dips and the measurement at 90° represents the signal at the border between front side and rear side, which is fairly unaffected for frequencies below 4 kHz; higher frequencies cannot be trusted although the sudden reduction is amplitude above 6 kHz is so large that it could be correct.

A final plot is included where selected frequencies from 125 Hz to 8 kHz are reported versus the observation angle using the 0° measurement as 0 dB reference. The plot shows large changes in the frequency response even for a change of 30° in the observation angle so the sound quality from such a baffle is varying much with the observation angle.

Loudspeaker Cabinet Diffraction
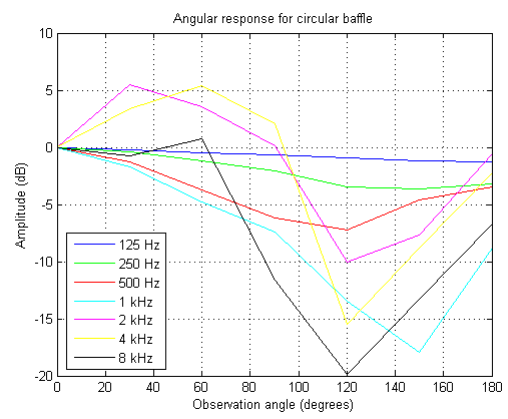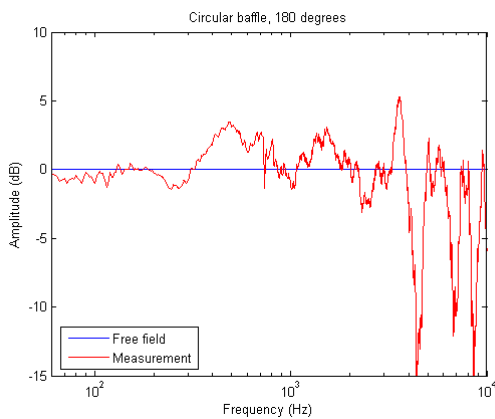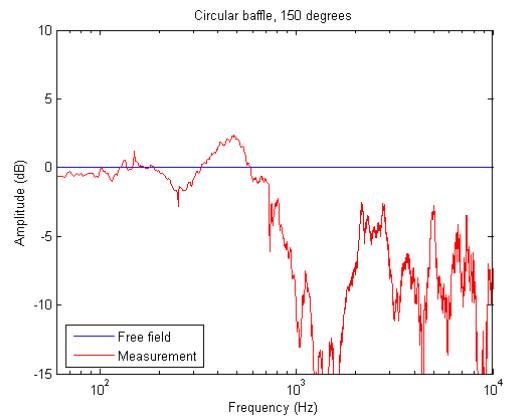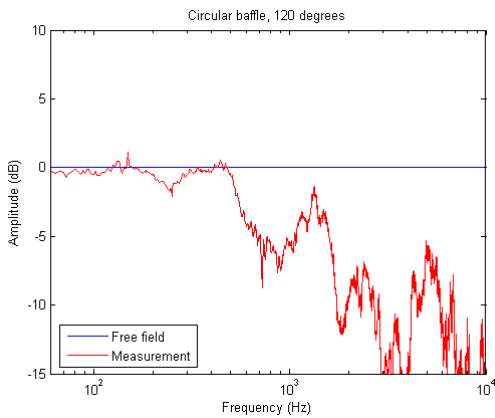
Figure 37 – Amplitude response for the circular baffle from 0° to 180° observation angle.

3.4.2 Response to change in loudspeaker position

Offsetting the test point from the centre of the circular baffle is studied within this section with the microphone pointing toward the test point from the front of the baffle.
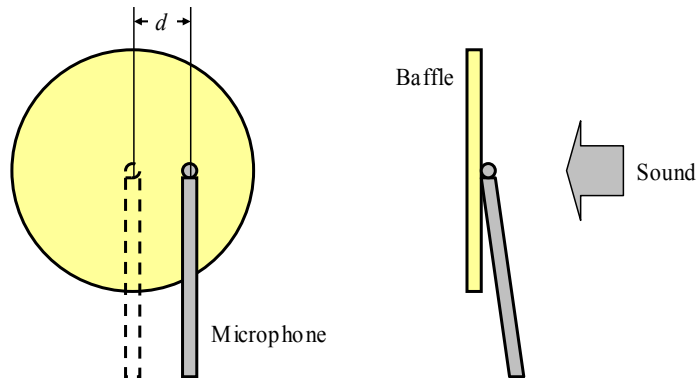
Figure 38 – Set-up for studying the effect of monitoring the sound pressure with microphone located at the front side of the baffle.

Measurements were performed at r_0 = 1.30 m but the 0 dB reference for free-field are related the distance r_0 = 1.41 m so the monitored level is increased according to the inverse distance law and the reported values must therefore be reduced by the following value.

$$\Delta L = 20\log_{10}\left(\frac{1/r_{TEST}}{1/r_{REF}}\right)dB = 20\log_{10}\left(\frac{r_{REF}}{r_{TEST}}\right)dB = 20\log_{10}\left(\frac{1.41\,m}{1.30\,m}\right)dB = 0.71\,dB \qquad 48$$

The result of offsetting the source from the centre is shown below using 3 cm step size. The first step removes most of the ripple caused by the symmetrical case with a circular baffle and a test point at the centre although the dip at 2 kHz is left virtually unaffected.
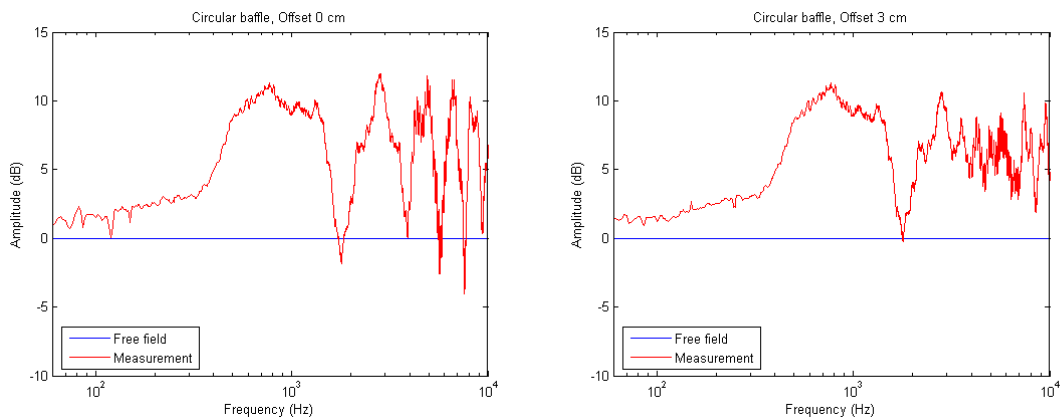
Figure 39 – Amplitude response for the circular baffle with the test point moved 0 or 3 cm from centre, where the latter corresponds to 20 % of radius.

The following steps remove the dip at 2 kHz and the result for an offset around 50 % of the baffle radius produces a quite acceptable result for the high-frequency region.
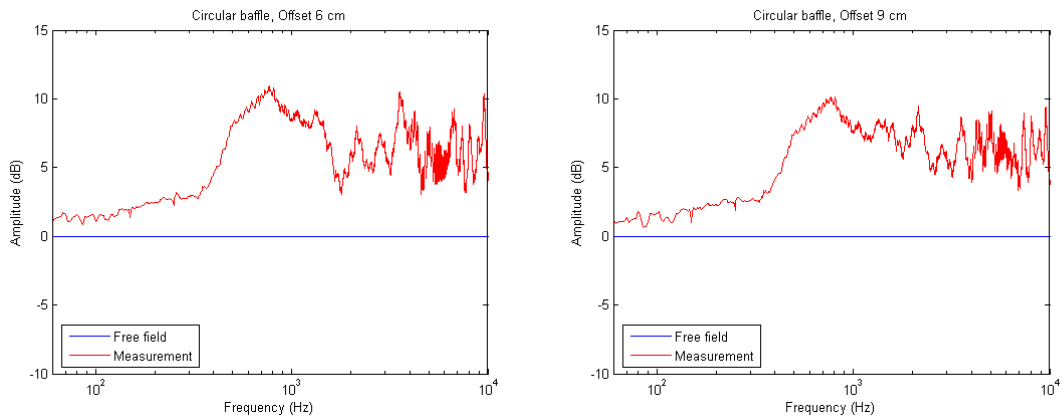
Figure 40 – Amplitude response for the circular baffle with the test point moved 6 or 9 cm from centre, which corresponds to 35 % and 50 % of radius.
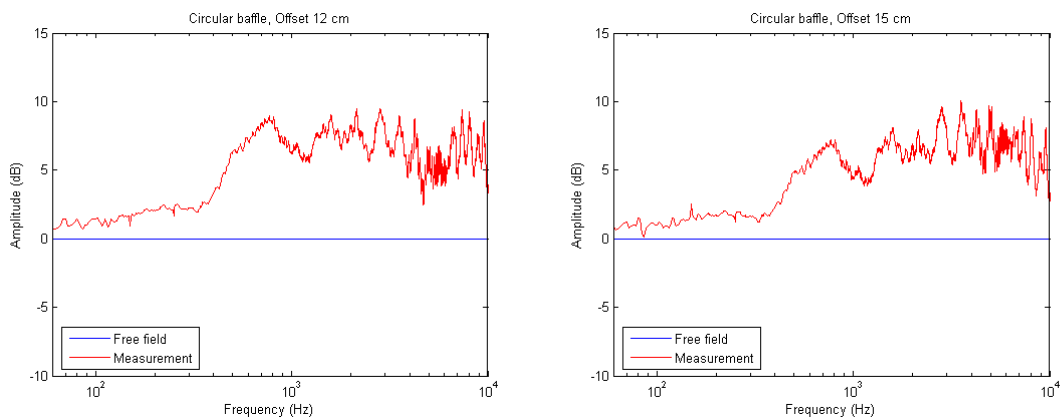
Figure 41 – Amplitude response for the circular baffle with the test point moved 12 or 15 cm from centre which corresponds to 70 % and 90 % of radius.

The measurements below are for the test point moved *outside* the baffle, so they represent the effect of locating a loudspeaker in the proximity of a larger surface. However, the effect is a minimal increase at middle frequencies for the loudspeaker just outside the baffle and nothing significant for the loudspeaker at 1.5 times radius. The 8 cm distance corresponds to one-quarter of a wavelength at 1 kHz thus showing the effect of *small* and *large* distance.
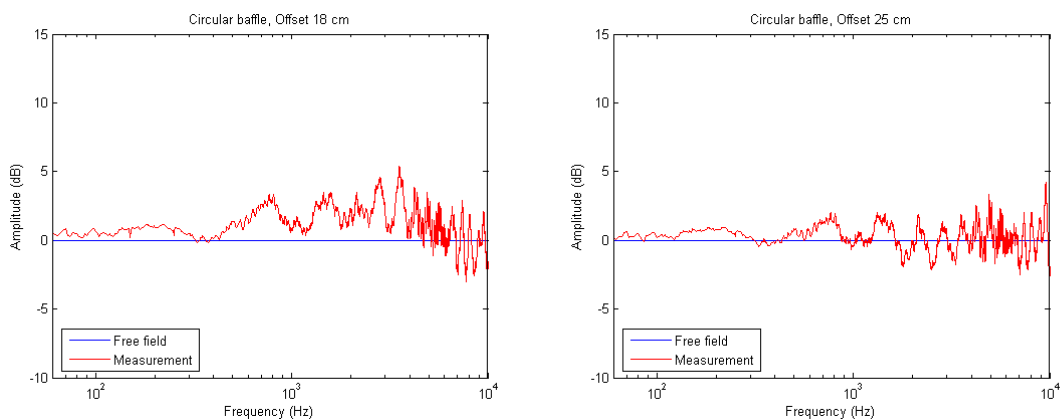
Figure 42 – Amplitude response for the circular baffle with the test point moved 1 or 8 cm outside the edge.

3.5 Rectangular baffle

The amplitude response was measured for a rectangular baffle 200 mm wide by 340 mm high. The basic behaviour is much the same as the response for a circular baffle; the level is increased from 0 dB at low frequencies to around 10 dB at 1 kHz where the large dimension equates one wavelength. However, the high-frequency response is less ragged since the phase of the reflected signal is blurred by the different path lengths between the test point and the edge of the baffle.

3.5.1 Response to change in observation angle

Measurement distance was $d_0 = 1.30$ m for the on-axis measurement and the response will be related to the free-field reference using $r_0 = 1.41$ m so the monitored level is increased and this must be compensated for 0 dB at the low frequency end. The set-up was not arranged for constant distance between source and baffle during the change in observation angle and this must be corrected too.
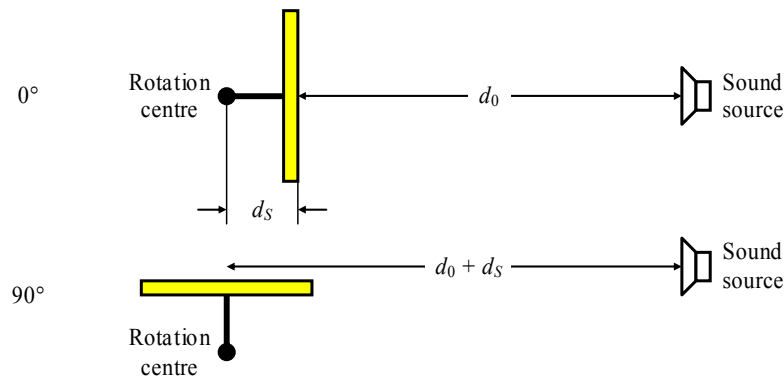
Figure 43 – The change in observation distance during change of observation angle.

The baffle was positioned at the small distance $d_S = 0.15$ m from the centre of rotation and the source loudspeaker was not moved during the test sequence so the distance between source and microphone was changed during the test sequence from $d_0 = 1.30$ m to $d_{180} = 1.60$ m. Assuming a circular relation the actual distance from the tip of the microphone at the test point to the source was:

$$d(\theta) = d_0 + d_S - d_S \cos(\theta)$$

Assuming that the sound pressure is inversely proportional to distance and changing the reference distance to r_0, the measured level will appear increased by:

$$\Delta L = 20\log_{10}\left(\frac{r_0}{d(\theta)}\right) \text{dB} = 20\log_{10}\left(\frac{r_0}{d_0 + d_S(1-\cos(\theta))}\right) \text{dB}$$

The figures become: 0.71 dB at 0°, 0.57 dB at 30°, 0.22 dB at 60°, –0.24 dB at 90°, –0.68 dB at 120°, –0.99 dB at 150° and –1.10 dB at 180°. These figures are subtracted from the measurements to level the measurement to the selected measurement distance.

The result is shown in the figures below and shows an increase of the front-side amplitude of approximately the same level and frequency range as was seen for the circular baffle although the high-frequency range is less ragged due to the blurring of the transient response. The final plot shows the relative behaviour for change in observation angle with the 0° measurement as

0 dB reference. The result is an improvement compared to the circular baffle since the first 30° change in the observation angle does not significantly change the frequency response.
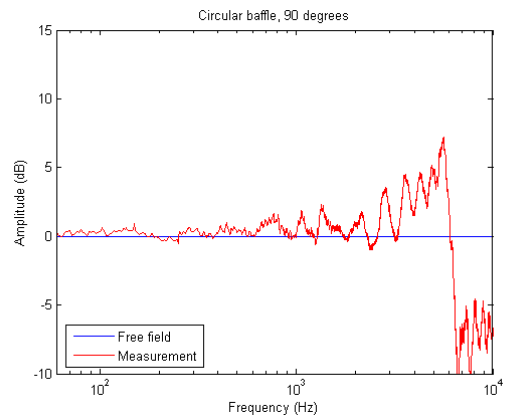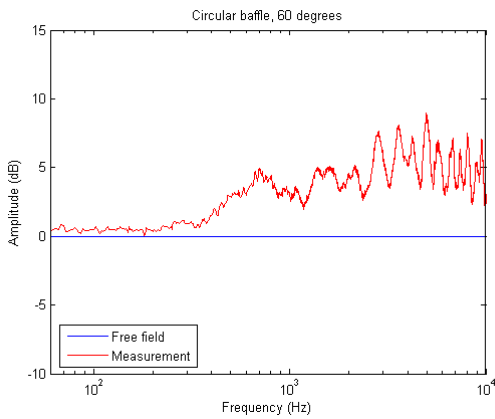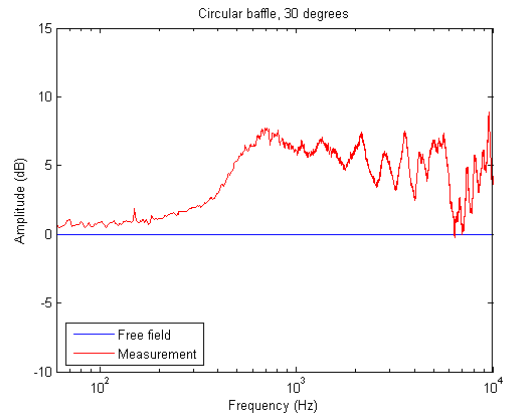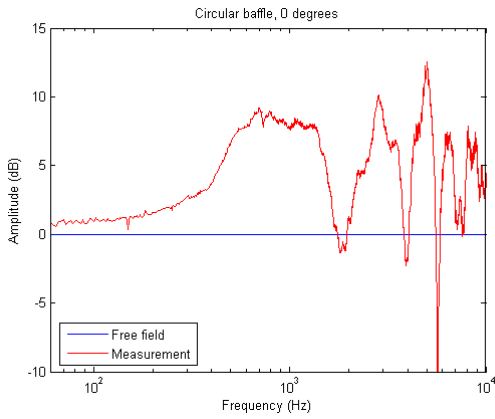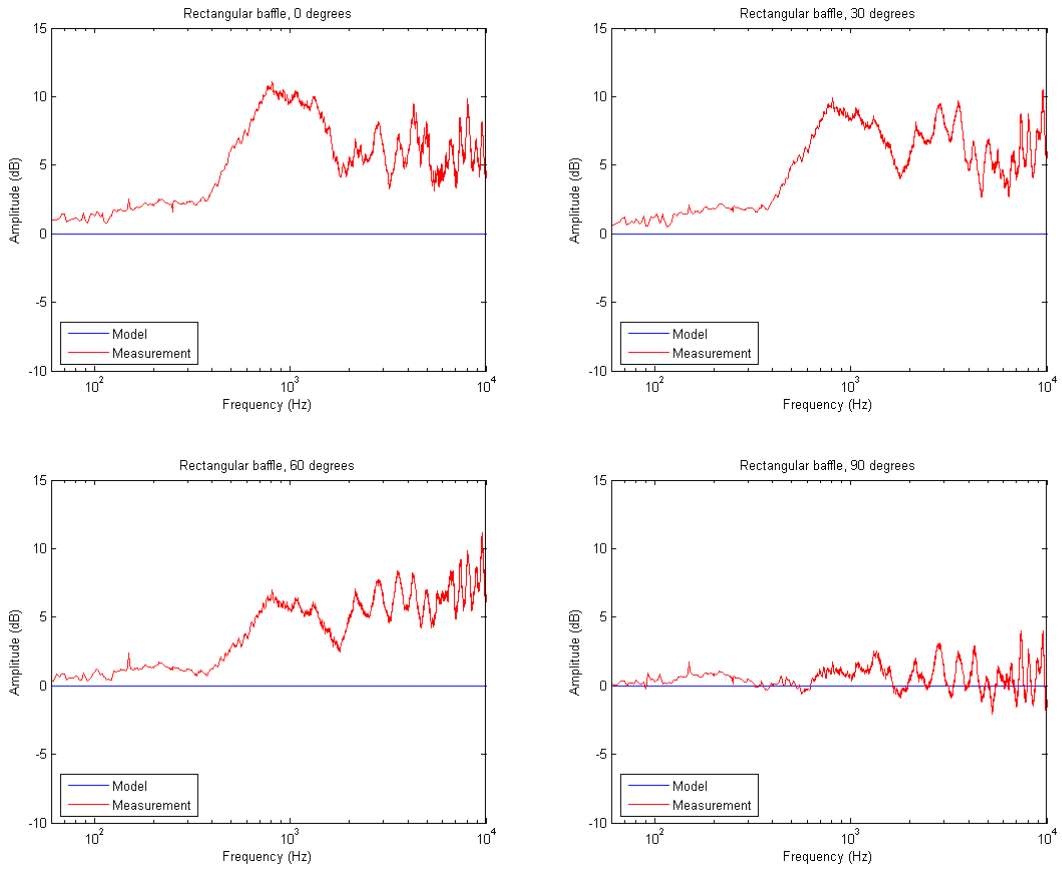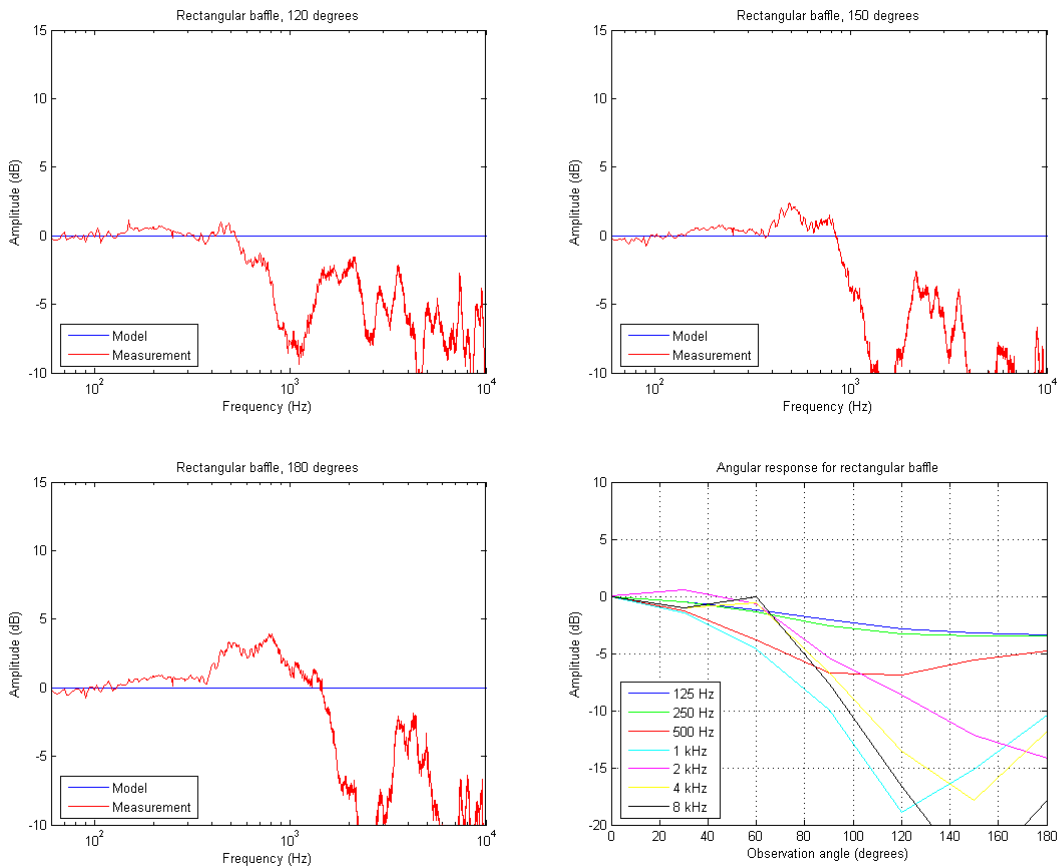
Figure 44 – Amplitude response for the rectangular baffle at 0° to 180° observation angle.

3.5.2   Response to change in loudspeaker position

Three test point positions was selected to represent typical loudspeaker designs and the results is primarily a change of the level around 2 to 5 kHz, which can be important for the design of a cross-over network for a typical two-way loudspeaker.
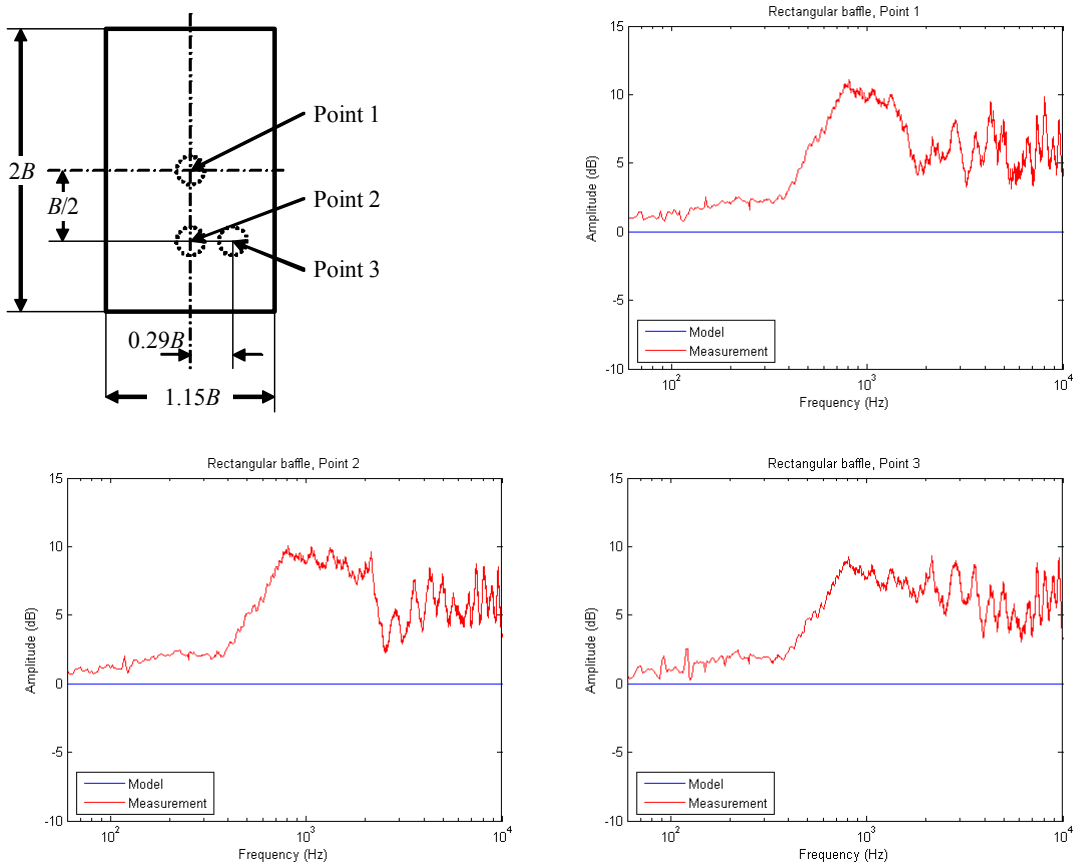
Figure 45 – Definition of the positions for the test points and amplitude response for the rectangular baffle measured at test point 1, 2 and 3.

The centre position is the most symmetrical but phase blurring reduces the ripple amplitude although the range around 1 kHz is pronounced. A typical two-way loudspeaker system may use a cross-over frequency around 2 kHz, which is at the frequency where a bass loudspeaker at position 1 will be attenuated some 5 dB due to the baffle thus complicating the design of the cross-over network. Small loudspeaker boxes may locate the loudspeaker at position 2, which is a small improvement since the attenuation is moved up in frequency but the attenuation within the dip around 2.5 kHz is slightly increased. A treble loudspeaker may be located at position 3, which levels the range from below 1 kHz and up and is thus giving the loudspeaker good support below the cross-over frequency.

3.6 Semi-infinite baffle

A series of measurements were conducted in order to validate the diffraction theory for a semi-infinite baffle. The set-up was build at the author's home and a "low-noise" ventilation fan was used as the sound source giving a nice broadband noise of sufficient level to be useful for the measurement. The fan was positioned on a table with the axe 0.9 m above the floor and the microphone was at the same height. The fan blade radius was 85 mm.

Figure 46 – Measurement set-up for the frequency response with an infinite edge using a fan as sound source. The baffle was located vertically and horizontally to test for the influence of the diffraction around the baffle ends.

A semi-infinite baffle was not available so a 3 mm plate with measure 0.52 m by 0.90 m was used to block the sound from the fan. Sound will unavoidably diffract around the sides of the baffle so short measurement distances were used to reduce the level from the far edges and two orientations of the plate were used. The upper edge was aligned with the line-of-sight between fan and microphone with 0.25 m from fan to plate and 0.50 m from plate to microphone. The additional distance through a reflection from the floor was 1.1 m so the half-wavelength frequency becomes 160 Hz where the first dip in the frequency response could be expected for some of the measurements but interference was not observed.

Figure 47 – A rear-view showing the other side of the set-up. The remote fan was not in use and the doors were shut to keep noise low. The measurement equipment consisted of a home-build instrument with preamplifier, third-octave filter and true RMS rectifier.

A voltmeter with build-in pre-amplifier and filter was designed 1982 by the author and served for the present measurements for third-octave measurements from 16 Hz to 20 kHz. The filter section included a second-order resonance filter tuned to the bandwidth required for third-octave filtering; the RMS rectifier was designed to measure correctly for both sine wave and noise signals and all readings used 0.5 s integration time. A LED display outputs the current gain selection to avoid misreading of range and the data was input to MATLAB for plotting.

Measurements are to be used for verification of the far-field and near-field diffraction theories from the wavelet model chapter where two different models are considered; one using a source of plane waves (the Fraunhofer far-field approximation) and another using a spherical source (the Fresnel near-field approximation). The outputs from the models are comparable, as will be shown in the chapter, so one common measurement set-up was considered sufficient. The basic idea for the test is to monitor the reduction in sound pressure from one case to another as shown in the figure below.
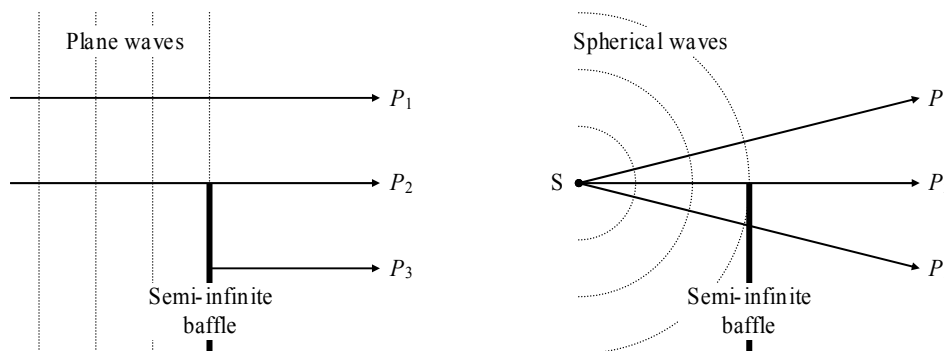
Figure 48 – An infinite edge is blocking part of the sound at the observation point.

Three measurement cases are to be considered.

- In the *first case* is the obstruction not present, so the radiation propagates unobstructed from the source to the observer where it creates the sound pressure P_1; this is the 0 dB reference for the two following measurements.

- In the *second case* is the obstruction arranged to remove precisely 50 % of the radiation from the source. This was accomplished by levelling the upper edge of the baffle with the line-of-sight from source to observer where the rotational axe was used as the fan position. Since half the radiation is removed the sound pressure is expected reduced to half its unobstructed level, i.e. $P_2 = P_1/2$. This relation is postulated in the chapter and is thus to be verified.

- In the *third case* is the obstruction brought further up thus removing the direct signal so the observer reaches only signals that are diffracted at the upper edge. The residual signal P_3 is the interfering signal without direct signal and can be used for verification of the ripple amplitude – but this was not possible to measure with the set-up.

The raw results are plotted below.

The uppermost curve (dash-dotted blue line) represents the output from the fan measured without baffle. This was the most problematic of all measurements since the level changed slowly so four recordings were averaged (other measurements are averaged through two recordings). The dotted black curve was included for comparison to a first-order slope thus showing that the "frequency response" of the fan was –6 dB/octave. The noise floor was measured with the fan switched off (hence the "Silence" label) and the baffle removed and is also averaged from four measurements although this was not required since measurements were much alike. The lower limit of 25 dB SPL is due to noise input from the environment as well as internal noise from the microphone capsule and noise from the input attenuator and pre-amplifier stage. The difference between the blue and magenta curves represents the available headroom since the measurements will be squeezed in between these curves.
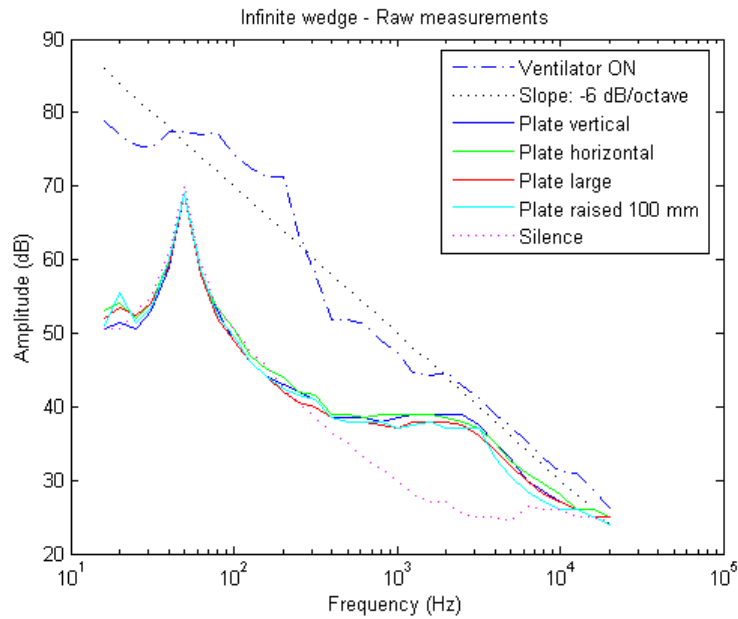
Figure 49 – Raw measurements with the top curve as the fan signal and the doted line for comparison. The next curves represent two orientations of the small plate, one large plate and the small plate raised 100 mm above the line of sight for increased blocking. The bottom curve is the background noise with fans off.

The measurements are indistinguishable from the noise floor below 200 Hz so the lower range was ignored in the following plot, which shows the difference between the top curve and the measurements with the baffle present. The reference, shown as the horizontal line at 0 dB, represents the signal without baffle and the noise floor is shown as the dotted magenta line. The signal-to-noise is around 10 dB for the important middle part of the range, which is just about acceptable for a conclusion.
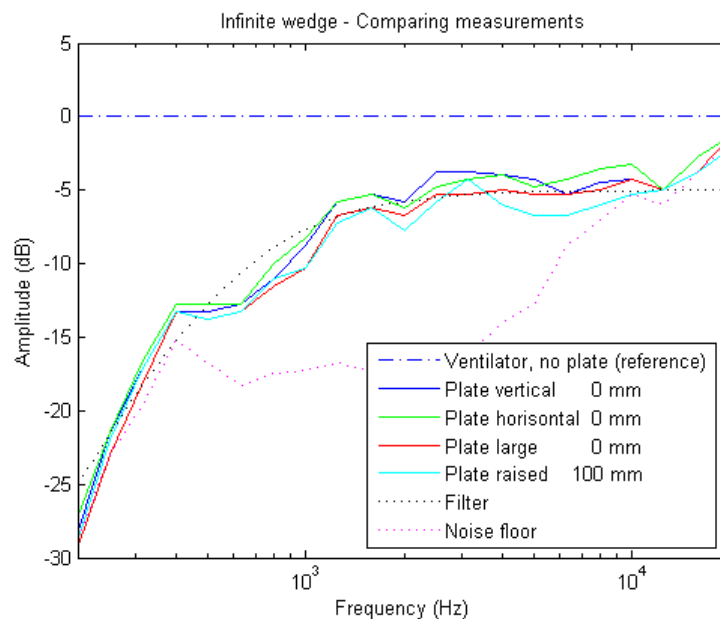
Figure 50 – Measurements with the baffle shows a dependency on frequency below 1 kHz and approximately constant levels around –5 dB for higher frequencies. The plate alignment is reported relative to the line-of-sight between fan and microphone.

Two plate orientations were used with the upper edge at the line-of-sight between fan and microphone. The blue curve represents the baffle standing on the floor thus blocking sound from the lower half of the fan for diffraction measurement but an additional contribution from the left and right sides are of course unavoidable. The baffle was rotated to horizontal position to see if this changed anything; the left and right sides are further away from the fan but the sound may now travel through the lower side as well. There is barely a change from the blue curve to the green curve. A large plate was constructed from several smaller plates to a 1.50 m wide and 0.90 m high construction and the result is shown as the red curve. An improvement of 1 to 2 dB was observed within the range from 600 Hz to 6 kHz compared to the blue and green curves.

The smaller horizontal baffle was lifted 100 mm above the line-of-sight thus blocking for most of the fan and the result is shown as the cyan curve. The level is reduced above 3 kHz with up to 3 dB compared to the horizontal baffle at 0 mm (green curve).

Comments:

1. The low-frequency level is attenuated significantly by the presence of the baffle, which was surprising since the baffle is small compared to wavelength ($ka = 1$ for a baffle "radius" of $a = 0.25$ m at 250 Hz) so the signal was expected to propagate with minimum attenuation at the lowest frequencies. The result may be an effect related to the near-field since the distances to source and microphone were small related to wavelength. An interesting point is that the theory for the semi-infinite baffle does indeed introduce a low-frequency cut-off although with a lower knee-frequency.

2. The mid-frequency range from 1 to 10 kHz is approaching a constant level at –5 dB compared to the reference without the baffle. The expected –6 dB is probably not reached due to additional sound sources from diffraction around the sides and it is also possible that the sound pressure is increased between source and plate from sound build-up in analogy to the pressure increase known from microphones (Leach, 64-66).

3. The high-frequency level above approximately 6 kHz is less than 6 dB from the background noise and details can be expected masked by the noise. However, the response with the 100 mm raised baffle is obstructing the direct sound and the increase in attenuation may reflect the obstruction of the direct sound.

A second-order high-pass filter with 600 Hz cut-off at –6 dB $Q = 0.5$ was plotted solely for comparison (dotted black curve) and shows that the measured responses are complex; this can be seen from the plateau around 600 Hz, from the increasing slope at lower frequencies and the weak indications of ripples with peak frequencies at 400 Hz, 1.5 kHz and 2.5 kHz. However, the noise level is relatively high and this may as well be the reason.

Conclusions:

1. The measurement will be accepted as supporting the $P_2 = P_1/2$ postulate.

2. The discrimination between large and semi-infinite baffle is of minor importance, which allows the model for the semi-infinite baffle being used for a finite baffle such as the loudspeaker cabinet boundary.

This concludes the measurement section.

4 Edge diffraction model

This chapter introduces the model and compares the results to the measurements. The model is not derived from existing models although ideas were discovered and incorporated during the progress. The origin to the model is shortly discussed below.

4.1 Background

It all started by the simple assumption that diffraction was some kind of reflection from the cabinet boundary. The wave front is at the edge changing from propagation within the half space in front of the baffle into full space at some distance from the cabinet. The associated change in impedance is a discontinuity that must split the propagating wave into a reflected wave and a transmitted wave so it should be possible simulating diffraction using the theory of reflection. The sound pressure on the front side could thus be modelled as the direct signal plus the reflected signal and the sound pressure on the rear side could be modelled through the transmitted signal. An edge diffraction model was born.
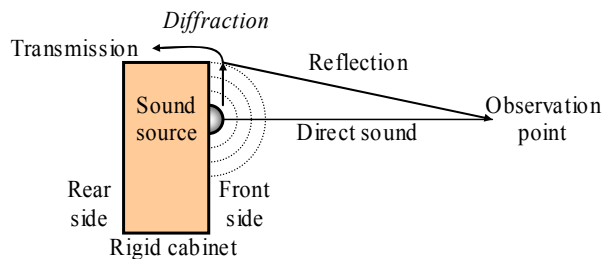
Figure 51 – Graphical presentation of diffraction. The observation point at the front side receives direct signal from the loudspeaker unit as well as a reflection due to the diffraction at the cabinet edge while the shadow zone receives a transmitted signal.

A consequence of the reflection theory is that the model must include a *reflection coefficient*, which proved the first obstacle to attack since the reflection coefficient could be related to such different subjects as the wedge angle, the observation angle and frequency. The values found in the literature were contradicting, as will be shown below, so an expression for the reflection coefficient was derived and the value calculated to –0.60 (see section 4.5.1). Using this value, the frequency response was calculated and found in agreement with measurement.
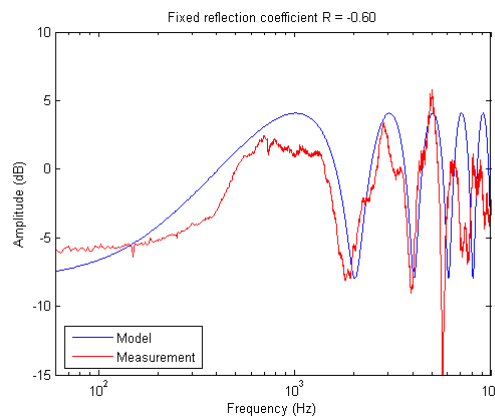
Figure 52 – On-axis frequency response for a circular baffle with the source at the centre.

However, the value of the reflection coefficient remained a mystery for quite some time until the results from literature were fully understood. A review of the literature is reported below.

Bews & Hawksford (1986) quoted Lord Rayleigh (1878) for the sound pressure P_E at the edge of the cabinet due to the sound pressure $P_{fs,r}$ of an undisturbed point source at distance r. The level is defined from the cabinet wedge γ, according to their Eq. (1):

$$P_E = \left(\frac{4\pi}{4\pi - \gamma} \right) P_{fs,r}$$

49

The sound pressure becomes $2P_{fs,r}$ for an infinite baffle ($\gamma = 2\pi$), and at the edge of a boxlike cabinet ($\gamma = \pi$) is the sound pressure reduced to $1.33P_{fs,r}$; the difference is -0.67 so the reflection coefficient becomes -0.33 since the direct sound is $2P_{fs,r}$. For a thin baffle ($\gamma = 0$) is the sound pressure $1.00P_{fs,r}$ so the level of the diffracted component becomes $\underline{-0.50}$.

Vanderkooy (1991) measured the impulse response from a circular baffle using a tweeter and found that the diffracted signal is inverting at the front side and non-inverting on the rear side. His thin-baffle model is $-1/2\cos(\chi/2)$ for the diffracted signal where χ is the angle between source and observer (Urban, 1045). The on-axis value is $\underline{-0.71}$ at far field and approaches infinity at the shadow boundary; "this is unphysical" according to Vanderkooy (p. 926).
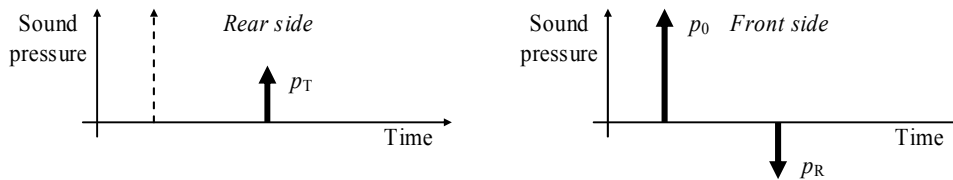
Figure 53 – Impulse response from a loudspeaker cabinet due to edge diffraction.

Wright (1996) used Finite Element Analysis with a circular disk for calculation of an impulse response. The reported level of the direct signal was 362 units of "half-space magnitude" and his figure 2a reports the diffracted signal level to -210 units with a relative level of $\underline{-0.58}$.

Urban et al. (2004) introduced a model based on a solution to the wave equation where the level of the diffracted component was at $\underline{-0.50}$ in the forward direction.

The author decided to measure the impulse response using a circular baffle and the result is shown below. The diffraction component is delayed 0.5 ms due to baffle radius of 0.17 m. The amplitude starts off from almost unity and the diffraction component level is $\underline{-0.77}$
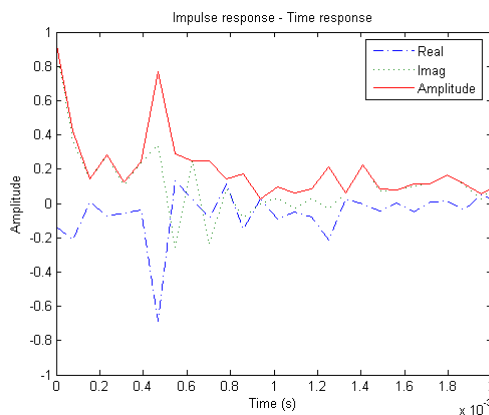
Figure 54 – Frequency and time responses for circular baffle measured on-axis.

As will become apparent later (see section 4.9.5) is an optimal value for the reflection coefficient between -0.5 and -0.6 for the best fit to measurements.

4.2 Introduction

A model will be developed for description of the effect of loudspeaker cabinet diffraction and the model will be divided into separate expressions for the front side and rear side to reflect the different sign of the diffracted component. The model will further be divided into two separate parts where the first part is an analytical approach, which leads to simple expressions using standard functions, and the second part is a computer model improving the accuracy of the model.
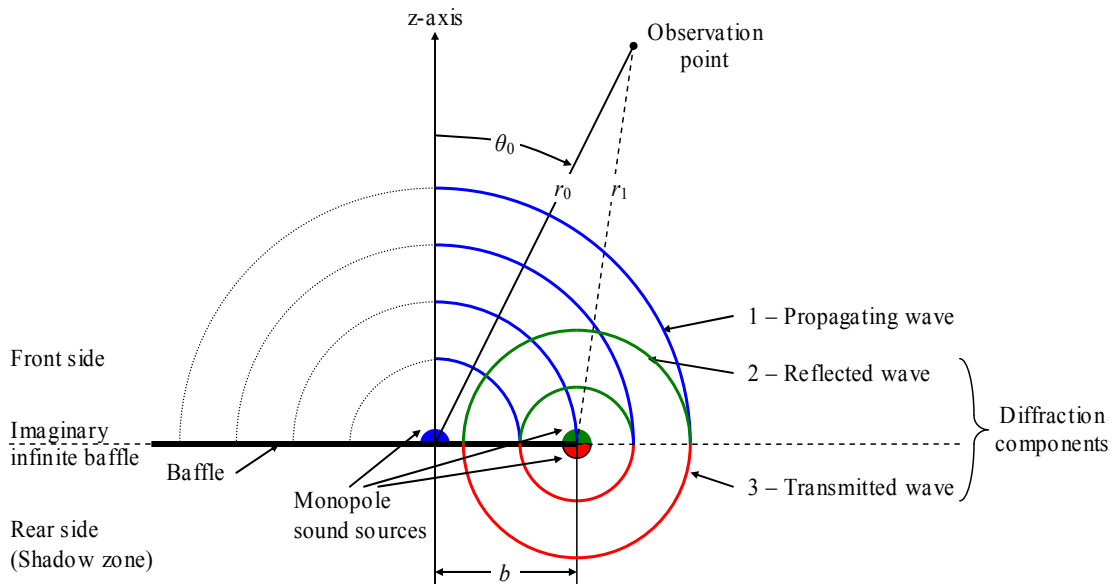
Figure 55 – Graphical presentation of diffraction model. The propagating wave (1) is partially reflected into the front side of the baffle (2) and transmitted into the rear side (3).

A spherical wave front is propagating from the monopole sound source within the half-space in front of the baffle. The wave is diffracted at the edge of the baffle and this diffraction will be modelled through three waveforms each propagating in half-spaces. The direct sound (1) is assumed to continue within the half-space in front of the baffle as if the baffle was of infinite extent. The diffraction sound from the edge is represented by two waves, a *reflected* wave (2) radiated into the half-space in front of the baffle and a *transmitted* wave (3) radiated into the half-space on the rear side.

At the front side is the resultant sound pressure represented by the combination of the direct and reflected waves while the sound pressure at the rear side is represented by the transmitted wave alone. Introducing the *reflection coefficient* with label R, the basic relations for the sound pressure at the front and rear sides of the baffle become:

$$p_F = p_0 + Rp_1$$
$$p_R = (1 + R)p_1$$

50

A derivation will show that the reflection coefficient is around –0.60 at low frequencies, which is 20 % below the previously measured value. The level of the signal transmitted into the rear side is represented by the transmission coefficient $T = 1 + R$, according to equation 28, so this signal is approximately 0.40 times the level of the direct signal so the baffle is attenuating the signal in the shadow zone by 8 dB. Using this model the problem boils down to estimating the diffracted sound pressure p_1, which is the main objective of this study.

It is obvious that a wave front cannot change its sign at the border between the front and rear sides as this would correspond to a singularity without physical ground, but this is a diffraction *model* and the discontinuity was introduced to simplify derivation since all waves are radiated into half-space. The model does thus not apply to monitoring at the edge, i.e. for an observation angle of 90° since this is at the border between two models.

The model is somewhat analogous to the *Geometric Theory of Diffraction* presented by Bews & Hawksford (1986), although their model was restricted to ±10° from on-axis and without discussion of the rear side radiation; also, their model was presented without comparison to measurements. There are also similarities to the model of Urban, et al. (2004) although their edge sources are dipoles with continuous definition from 0° to 180°.

4.3 Direct sound

A model is shown in the figure below and consists of a sound source radiating into the front side of the cabinet and the wave front travels through distance r_0 to the observation point as if the monopole sound source was located at the front of a large (infinite) baffle; this sound pressure will be designated p_0. The direct sound from a point source within the proximity of an infinite baffle and at distance r_0, is given by equation 35. The definition of the sound source for the direct signal is:

$$p_0 = p(r_0) = \frac{ik\rho cq}{2\pi r_0} \exp(-ikr_0)$$

51

In this equation is frequency represented through the angular wave number $k = 2\pi f/c$ and the medium is represented by the characteristic impedance ρc. The strength of the point source is characterised by its volume velocity q, which is given by the mechanical properties of the loudspeaker unit where an example is given in section 2.8.3 for the electro-dynamic loudspeaker. The volume velocity is in this case inversely proportional to frequency within the operational range so the sound pressure from the point source becomes (approximately) independent upon frequency.

4.4 Diffracted sound

A line array of infinitesimal point sources will be used modelling the baffle. The baffle shape will be defined through distance b, which is the path from the point source to the edge. The distance is a function of φ, which is used to describe the points on the edge as shown in the figure below and is running from 0 to 2π.
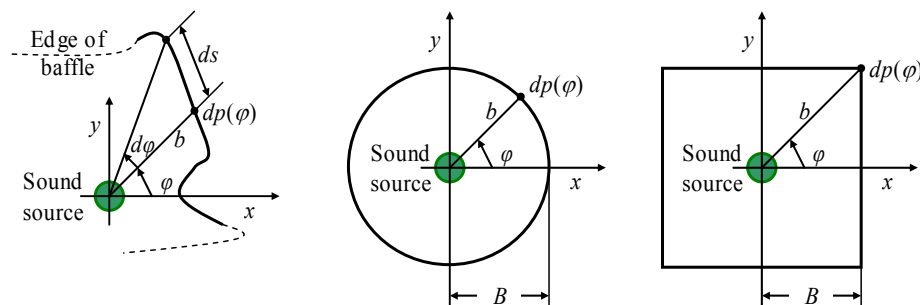
Figure 56 – Left: Definition of the infinitesimal sound pressure dp. Right: Examples of distance b for two different baffle shapes.

The infinitesimal sources are assumed radiating into half-planes thus assuming presence of an infinite baffle separating the front and rear sides. The distributed sources are placed where the boundary of the physical baffle would be located. The sound pressure from each of the infinitesimal sources is an attenuated and delayed copy of the direct sound due to the additional distance through the path $b + r_1$ from the monopole sound source to the edge. The attenuation caused by the increased distance can be ignored when the baffle dimensions are small compared to the distance to the observation point but the change in phase is crucial since 50 mm corresponds to one-half of the wave length at 3.5 kHz, i.e. change of sign.

The infinitesimal sound pressure dp_1 from each of the line segments ds is defined by the expression for the sound pressure from a point source above a reference plane with distance r_1 to the observation point and an additional delay due to b. Each infinitesimal line segment is described by the angle φ and the length of each infinitesimal line segment is proportional to $d\varphi$. Since the circumference of the unit circle is 2π must each line segment be occupying $d\varphi/2\pi$ of the unit circle and the sound pressure from each of the infinitesimal line segments becomes:

$$dp_1 = \frac{ik\rho cq}{2\pi(b + r_1)}\exp(-ik(b + r_1))\frac{d\varphi}{2\pi}$$

<div align="right">52</div>

Distance r_1 is function of observation angle θ and of φ, and the relation of b to φ is defined by the shape of the baffle, which is known when the mechanical details of the cabinet are defined. The resulting sound pressure from the diffracted wave is estimated by integration of the sources along the edge of the baffle, which corresponds to integration through one revolution of φ through the unit circle. Hence the expression for the delayed signal:

$$p_1 = \int_0^{2\pi}\frac{i\omega\rho q}{2\pi(b + r_1)}\exp(-ik(b + r_1))\frac{d\varphi}{2\pi}$$

At large distance to the observation point can b be assumed small compared to r_1 within the amplitude term and this distance is itself approaching r_0, so the expression of the diffracted sound pressure can be simplified into:

$$p_1 = \frac{i\omega\rho q}{2\pi r_0}\exp(-ikr_0)\frac{1}{2\pi}\int_0^{2\pi}\exp(-ikb)d\varphi$$

Identifying the factor in front of the integral as the sound pressure from the monopole sound source, p_0, the expression for computation of the delayed signal is reduced to a scaling function for the sound pressure originating from an undisturbed point source.

$$p_1 = \frac{p_0}{2\pi}\int_0^{2\pi}\exp(-ikb)d\varphi$$

<div align="right">53</div>

The core of the edge diffraction model is the determination of this integral.

This derivation differs from Vanderkooy, who uses the wavelet model (see the next chapter) to determine the sound pressure from the edge sources. He argues that the sound field at the edge is proportional to $1/b$ (using the variable names from this document) and that the sound field at the observation point is proportional to $1/r_1$ and concludes that the resulting sound pressure is proportional to $1/br_1$. He further argues that the signal is delayed due to the sum of

distances and arrives at the infinitesimal sound pressure $dp = \exp(-ik(b + r_1))dz/(r_1c)$ for the line sources along the edge where dz is an infinitesimal section of the edge. Vanderkooy assumes that br_1 is independent upon z, although his figure 2 shows that this is not the case, and he uses this assumption to simplify the derivation. The assumption of $br_1 = $ constant corresponds to the above simplification with $b + r_1 = r_0$ so the representations are equivalent.

4.5 Error level

The simplification that leads to the above result was based upon the assumption that the additional distance through b and r_1 could be considered small compared to r_0. In order to quantify the error due to the approximation, the acceptable error level e will be introduced. The largest distance through the diffraction path will be written as $b_{MAX} + r_1$ and can be represented as factor $1 + e$ times the direct path:

$$b_{MAX} + r_1 = (1 + e)r_0, \quad 0 < e < 1$$

For on-axis monitoring is distance r_1 defined by r_0 and b using the Pythagorean rule for the rectangular triangle. The approximation below is using the two first terms of the Taylor series expansion of the square root.

$$r_1 = \sqrt{r_0^2 + b_{MAX}^2} = r_0\sqrt{1 + \frac{b_{MAX}^2}{r_0^2}} \approx r_0\left[1 + \frac{b_{MAX}^2}{2r_0^2}\right]$$

Hence, by insertion:

$$b_{MAX} + r_0\left[1 + \frac{b_{MAX}^2}{2r_0^2}\right] = (1 + e)r_0 \quad \Rightarrow \quad r_0 + \left[\frac{b_{MAX}}{2r_0} + 1\right]b_{MAX} = (1 + e)r_0$$

Assuming that b_{MAX} is much smaller than r_0, the error in ignoring b_{MAX} becomes:

$$e \approx \frac{b_{MAX}}{r_0} \tag{54}$$

For a monitoring distance of $r_0 = 2$ m and 10 % of maximum error ($e = 0.1$) the largest baffle dimension must not exceed $b_{MAX} = 200$ mm.

4.5.1 Transfer function

The integral in equation 53 represents the frequency-dependency of the diffraction component so an equivalent form of the edge diffraction model is to regard the resultant sound pressure at the observation point as the output from a transfer function when it is excited by p_0:

$$\left.\begin{array}{c} p_F = (1 + RH_1)p_0 \\ p_R = (1 + R)H_1p_0 \end{array}\right\} \quad H_1 = \frac{1}{2\pi}\int_0^{2\pi} \exp(-ikb)d\varphi \tag{55}$$

H_1 is a dimension-less expression for the frequency response of the diffracted component; hence, $1 + RH_1$ is the transfer function for the front side and $(1 + R)H_1$ is the transfer function for the rear side. This representation will become attractive later in the study when higher-order diffraction components are addressed.

Two terms are to be determined to calculate the frequency response of the point source in the proximity of the baffle; the transfer function H_1 and the reflection coefficient R.

4.6 Reflection coefficient

A reflected signal is generated whenever the impedance of the medium is suddenly changed from its previous value so the *reflection coefficient* is the starting point for the model. An expression will be derived through the study of spherical waves within a conical horn, which will then be generalised into a plane disk. Derivation begins with the well-known equation for the plane wave within a tube, which was introduced within the *Acoustics* chapter and shall be augmented in this section.

Consider the conical horn shown in Figure 57, which has a source located at the top point and is characterised by an opening angle of Θ. A spherical wave is travelling through the horn toward the open end at $r = B$, where the horn is terminated by the acoustical impedance Z_{AT}, which is an unknown quantity for the moment. Some of the wave front will be reflected back into the horn and the rest will be absorbed by the acoustic impedance (or transmitted into the space outside the horn). Spherical reflection is not commonly accounted within acoustics but is anyway possible using a reflecting surface of constant radius.
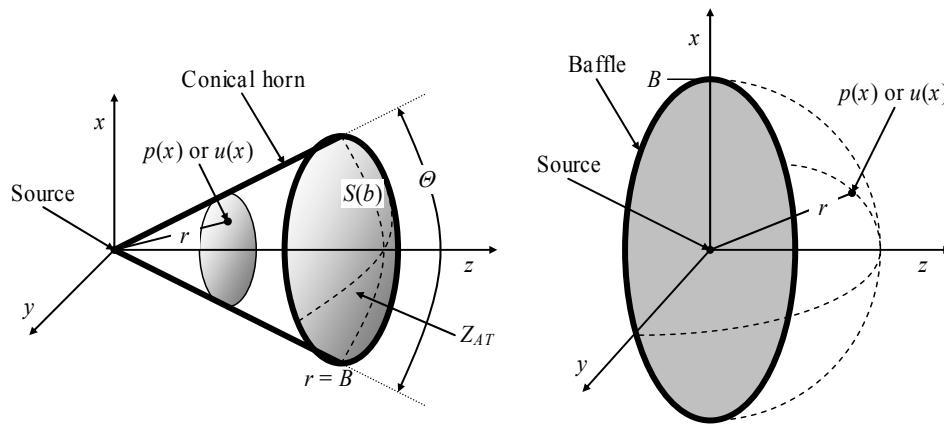
Figure 57 –A conical horn is terminated at the opening by known acoustic impedance (left) and is opened into a circular disk (right).

The wave fronts within the conical horn is characterised by the incident wave p_+ travelling outward and the reflected wave p_- travelling backward. The expressions for the sound pressure and particle velocity are reproduced below from equations 17 and 19, with the reflection factor R from equation 26 included.

$$p(r,t) = \frac{p_+}{r}\left[\exp(-ikr) + R \cdot \exp(ikr)\right]\exp(i\omega t)$$

$$u(r,t) = \frac{p_+}{r\rho c}\left[\left(\frac{1+ikr}{ikr}\right)\exp(-ikr) - \left(\frac{1-ikr}{ikr}\right)R \cdot \exp(ikr)\right]\exp(i\omega t)$$

The acoustical impedance of the spherical wave is defined as:

$$Z_{AS}(r) = \frac{p(r,t)}{S(r)u(r,t)} = \frac{\rho c}{S(r)}\frac{ikr}{1+ikr}\frac{1 + R \cdot \exp(2ikr)}{1 - \left(\frac{1-ikr}{1+ikr}\right)R \cdot \exp(2ikr)} \qquad 56$$

The differences from the previous situation with a plane wave are that the cross-sectional area is a function of radius and that the expression of the particle velocity is more complicated due to the near-field correction.

At the end of the horn where $r = B$ is the boundary condition known since the impedance must equate the terminating impedance.

$$Z_{AT} = \frac{\rho c}{S(B)} \frac{ikB}{1 + ikB} \frac{1 + R \cdot \exp(2ikB)}{1 - \left(\frac{ikB - 1}{ikB + 1}\right) R \cdot \exp(2ikB)}$$

The area $S(B)$ represents the area of the surface through which the air particles are moving, i.e. where radius is constant ($r = B$). The opening angle (Θ) is given by the conical horn and the surface area is given by (Westergren, 74):

$$S(B) = 2\pi B^2 (1 - \cos(\Theta))$$
57

For $\Theta = 0$ is the horn is closed and the cross-sectional area is zero and for $\Theta = 90°$ is the horn unfolded into a plane disk with area $2\pi B^2$. The baffle is removed for $\Theta = 180°$ where the area equals the surface of the full sphere, i.e. $4\pi B^2$.

Using this expression for the area and solving for the reflection coefficient:

$$R = \frac{1 + ikB}{1 - ikB} \frac{Z_{AT} - \frac{ikB}{1 + ikB} \frac{\rho c}{2\pi B^2 (1 - \cos(\Theta))}}{Z_{AT} + \frac{ikB}{1 - ikB} \frac{\rho c}{2\pi B^2 (1 - \cos(\Theta))}} \exp(-2ikB)$$

At $\Theta = 90°$ is the horn unfolded into a circular disk, representing the loudspeaker baffle with the loudspeaker at the centre. The exponential term represents time delay and will be ignored (see comments for equation 27). The reflection coefficient for the circular baffle becomes:

$$R = \frac{1 + ikB}{1 - ikB} \frac{Z_{AT} - \frac{ikB}{1 + ikB} \frac{\rho c}{2\pi B^2}}{Z_{AT} + \frac{ikB}{1 - ikB} \frac{\rho c}{2\pi B^2}}$$
58

This is equivalent to the expression with a plane wave with exception of the frequency-dependent terms with ikB, which are due to the particle velocity for the spherical wave.

The previously used assumption of a pressure relief at the open end; i.e. that the impedance is approaching zero, cannot be used here since the impedance of the spherical wave front is itself low at the edge of the baffle for low-frequencies. This can be seen from equation 56 using $r = B$:

$$Z_{AS}(B) \xrightarrow{kB<<0} ikB \frac{\rho c}{S(B)} \frac{1 + R}{1 - R} \xrightarrow{kB \to 0} 0$$

A more useful value for the termination impedance is given by the acoustical loading of a pulsating sphere with radius a. The current application is however not equivalent to a pulsating sphere as shown below where the baffle is seen from the edge. For radius within the range of the baffle, $r < B$, is the wave front a pulsating *half sphere* with a surface area given by $2\pi r^2$ and increasing to $2\pi B^2$ at the edge. For radius larger than the baffle radius, $r > B$, is the sphere gradually increasing its area into that of a full sphere due to the diffracted wave so the area is increasing gradually from $2\pi r^2$ to $4\pi r^2$, which is the core of the reflection idea; the increase in surface area corresponds to an impedance discontinuity.
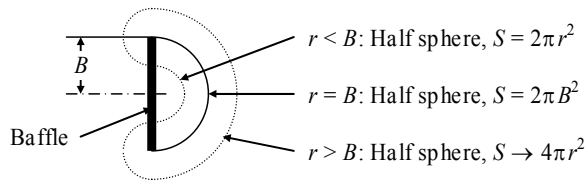
Figure 58 - The wave front is a half sphere for radius within the limit of the baffle and is gradually increasing toward the value for a full sphere for radius larger than the baffle.

The conclusion is that the wave front at the edge of the baffle is represented by a pulsating half-sphere of area $2\pi B^2$, which is one-half that of the pulsating sphere so the terminating impedance for the baffle with radius B becomes:

$$Z_{AT} = \frac{1}{2}Z_A = \frac{1}{2}\left(\frac{i\omega\rho}{4\pi B}\frac{1}{1+ikB}\right) = \frac{ikB}{1+ikB}\frac{\rho c}{8\pi B^2}$$

The radiation impedance of the sphere Z_A is given by equation 36.

Insertion into equation 58 the reflection coefficient becomes:

$$R = -\frac{3}{5}\frac{1+ikB}{1+\frac{3}{5}ikB} \rightarrow \begin{cases} -0.60 & kB \rightarrow 0 \\ -1.00 & kB \rightarrow \infty \end{cases} \qquad 59$$

It could be argued that the radiation impedance is changing from half sphere at the boundary into that of a full sphere and that the terminating impedance should represent the latter situation ($Z_{AT} = Z_A$) and using this argument the resulting reflection coefficient becomes:

$$R = -\frac{1}{3}\frac{1+ikB}{1+\frac{1}{3}ikB} \rightarrow \begin{cases} -0.33 & kB \rightarrow 0 \\ -1.00 & kB \rightarrow \infty \end{cases} \qquad 60$$

These equations are plotted below. It will later be seen that the first model applies well to measurements while the second does not. This supports the assumption that the acoustical impedance can be represented by the radiation impedance of the half-sphere.
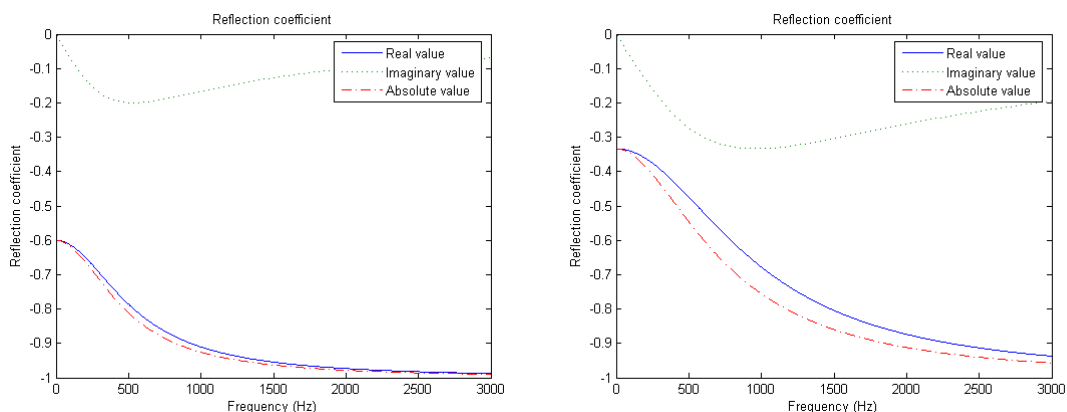
Figure 59 – The reflection coefficient showing the result of the half-sphere model (left) and the full sphere model (right).

The model is debatable:

- The derivation is based upon the simplified wave equation for spherical waves thus ignoring relation to θ and φ. The wave front may be perfectly spherical even at the highest frequency although high-order modes can exist for $kB > 1$, which corresponds to 320 Hz for $B = 170$ mm and may limit the application of the model.

- A half sphere is not physically realisable.

- It has not been proved that a conical horn can be unfolded into a circular disk although the wave equation is not invalidated and it is further assumed that the sound pressure is constant throughout the sphere, which is the same as saying that any point on the sphere is affected by the presence of an edge at the border of the sphere.

To conclude, the following value of the reflection coefficient will be used within this study.

$$R = -0.60 \qquad\qquad 61$$

The fixed values of the reflection coefficient as well as the full expressions will be compared to the measurements in the following section to support the selection.

4.7 Analytical expressions

The diffracted component p_1 is dependent upon the shape of the baffle, the location of the point source representing the loudspeaker and the observation point. The expressions will start assuming on-axis monitoring using a circular baffle with the point source at the centre of the baffle. Off-axis monitoring will be considered, the source will be moved off from the centre and the shape will be changed into elliptic and rectangular baffle shapes.

More complicated baffles become too difficult to derive and use so the section following the elementary baffle shapes introduces a numerical approach.

4.7.1 Circular baffle, on-axis

For an observation point at the axis of symmetry ($\theta = 0°$) and at large observation distance thus allowing use of the above assumption and with a circular baffle where $b = B$, the expression for the delayed sound pressure becomes:

$$p_1 = p_0 \exp(-ikB)\frac{1}{2\pi}\int_0^{2\pi} d\varphi$$

The integral is easily computed and the delayed sound becomes:

$$p_1 = p_0 \exp(-ikB) \qquad\qquad 62$$

The delay function is modifying the phase of the signal but leaves the amplitude unchanged, so strong interference must be expected at the observation point. Inserting into expression 50 gives the result for the circular baffle:

$$p_F = p_0 + R \cdot \exp(-ikB)p_0$$
$$p_R = (1+R) \cdot \exp(-ikB)p_0 \qquad\qquad 63$$

A plot is shown below using fixed values of the reflection coefficients; $R = -0.60$ is shown to the left and is seen to apply reasonably well to the measurements, while $R = -0.33$, which is shown to the right, starts above the correct level and the ripple amplitude is far too low.
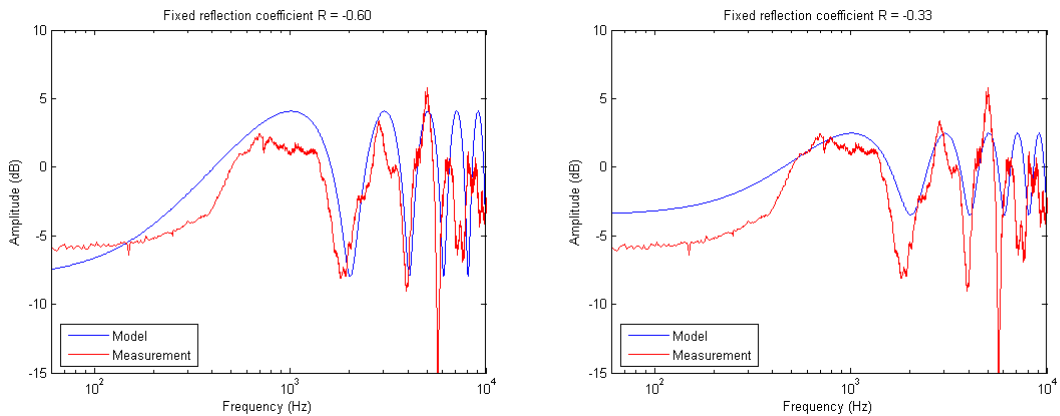
Figure 60 – On-axis response with two different values of the reflection coefficients.

The full expressions of the reflection coefficients are used for the plots below where the main difference is the high-frequency end, where the reflection coefficient is approaching −1.00 for both models thus seriously increasing the ripple amplitude. It is obvious that this behaviour cannot be used as a model thus voting in favour of a fixed value.
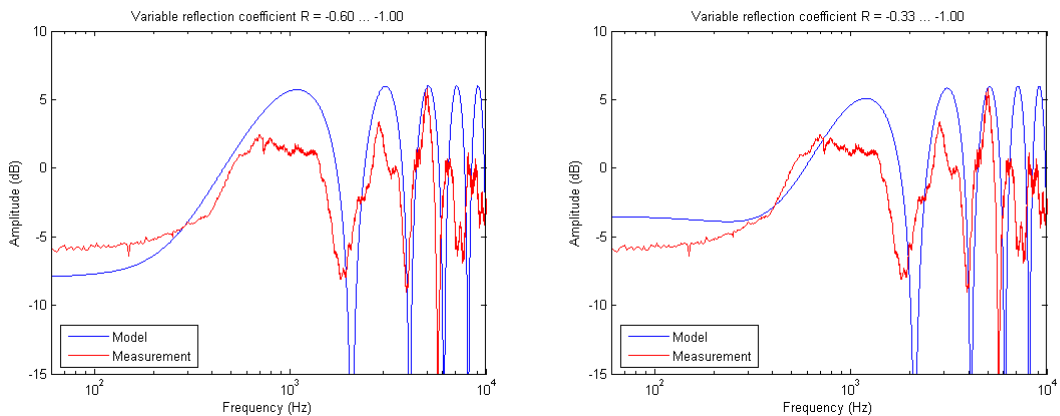
Figure 61 - On-axis response with the reflection coefficient given by equation 59 (left) and equation 60 (right) showing far too much high-frequency signal being reflected.

The model includes an estimate of the radiation into the rear side (shadow zone) and plots are shown below using the fixed values of the reflection coefficient.
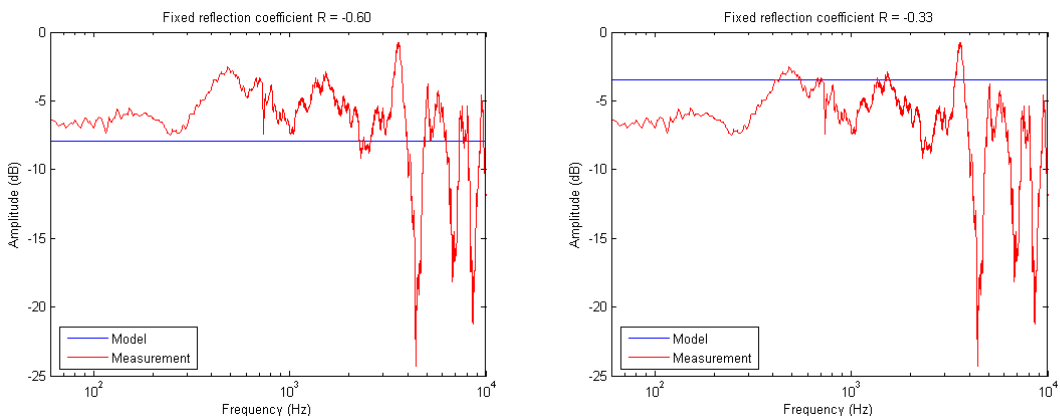
Figure 62 – Rear-side response with two different reflection coefficients.

According to equation 28 is the transmission coefficient $T = 1 + R = 0.40$ so the response for the rear side is estimated to –8 dB without dependency to frequency. The corresponding level for $R = 0.33$ is $T = 0.67$ or a level of –3.5 dB. Neither response is correct but $R = -0.60$ is close to the measured low-frequency level although the peaks around 500 Hz and 1.5 kHz are missing. The plot for $R = -0.33$ is too high in the low-frequency level but is correct at 500 Hz and 1.5 kHz, which is considered a coincidence. The first value is the most correct for an average evaluation throughout the frequency spectrum (viewed by eye).

The rear side response is shown below using the full expressions from equations 59 and 60 but neither model can correctly model the spectrum of the transmitted signal. It is obvious that the expressions are over-estimating the reflection at high frequency thus again indicating that a fixed value is to be preferred.
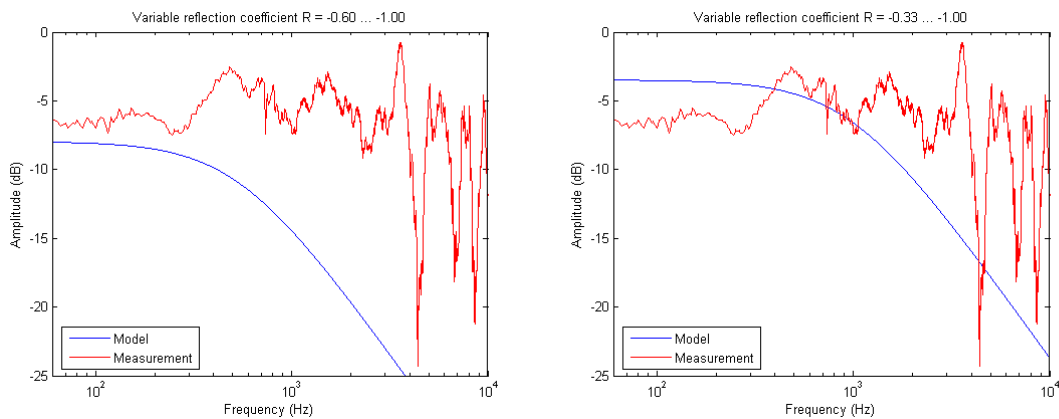
Figure 63 – Rear-side response with variable expressions for the reflection coefficient.

The difference between the calculated and measured frequency responses are shown below for the two fixed reflection coefficients (front side responses). Both curves depart from the ideal but the curve with $R = -0.60$ is close to 0 dB difference for middle frequency where the curve with a reflection coefficient $R = -0.33$ is offset 2 dB throughout the middle frequency range. The first curve oscillates around 0 dB at high frequencies where the second curve oscillates around the 2 dB offset value.
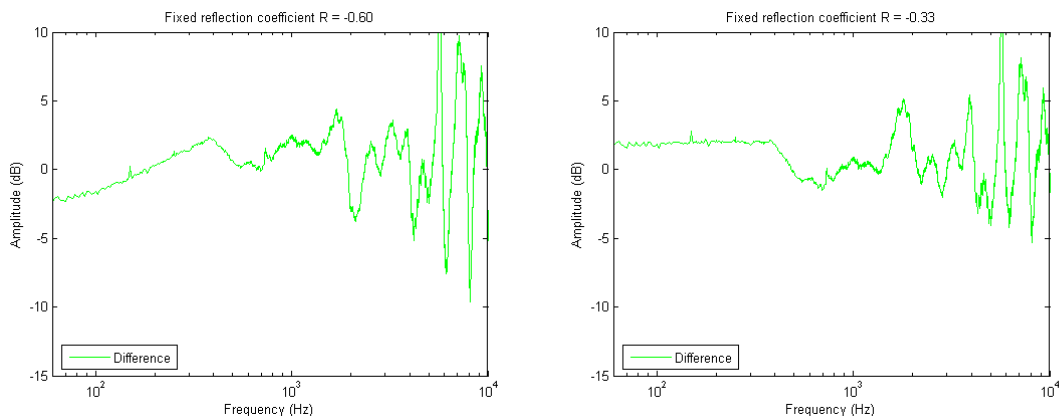
Figure 64 – Difference between calculated and measured frequency responses using the fixed values of the reflection coefficient.

All in all, the best fit is the fixed reflection coefficients of $R = -0.60$ since both the front and rear sides are most accurately modelled.

This baffle is comes into play around $kB = 1$ where the phase of the reflected signal is changed 90° from its initial value thus is defining the *cut-in frequency*; around 320 Hz for a baffle radius of $B = 170$ mm. The delay is one-half wavelength at $kB = \pi$ (some 1 kHz) where the direct signal combines with the reflected signal without loss (constructive interference) thus forming the first *peak frequency*. The delay is one wavelength at $kB = 2\pi$ (2 kHz) where the reflected signal is again in anti-phase with the direct sound resulting in destructive interference, which is the first *dip frequency*. The characteristic frequencies are:

$$f_{CUT-IN} = \frac{c}{2\pi B}, \quad f_{PEAK} = \frac{c}{2B}, \quad f_{DIP} = \frac{c}{B} \qquad 64$$

The response ripples up and down at higher frequencies.

4.7.2 Circular baffle, off-axis

Distance r_1 is constant only for on-axis monitoring with a circular baffle thus indicating the need of analysing other observation angles. The relation of r_1 to the observation angle will be calculated using the figure below, which shows a system with a circular baffle. The drawing to the right represents a projection to the *xz*-plane.

Figure 65 – Estimation of distance r₁ as function of the observation point expressed by θ.

Line segment z_0 is the projection of r_0 to the *z*-axis and line segment x_0 is determined from the Pythagorean law for the right-angled triangle formed by the line segments: z_0, $B + x_0$ and r_0.

$$r_0^2 = \left(B + x_0\right)^2 + z_0^2 \quad \Rightarrow \quad B + x_0 = \sqrt{r_0^2 - z_0^2} \quad \Rightarrow \quad x_0 = \sqrt{r_0^2 - z_0^2} - B$$

Since $z_0 = r_0 \cos(\theta_0)$ we have:

$$x_0 = r_0 \sqrt{1 - \cos^2(\theta_0)} - B = r_0 \sin(\theta_0) - B$$

Distance r_1 can now be defined for the triangle formed by the line segments: z_0, x_0 and r_1:

$$r_1 = \sqrt{x_0^2 + z_0^2}$$
$$= \sqrt{\left(r_0 \sin(\theta_0) - B\right)^2 + \left(r_0 \cos(\theta_0)\right)^2}$$
$$= \sqrt{r_0^2 \sin^2(\theta_0) + B^2 - 2r_0 b \sin(\theta_0) + r_0^2 \cos^2(\theta_0)}$$

Using the relation $\sin^2(x) + \cos^2(x) = 1$ and moving distance r_0 outside the square root, this can be simplified to:

$$r_1 = r_0\sqrt{1+\left(\frac{B}{r_0}\right)^2 - 2\frac{B}{r_0}\sin(\theta_0)}$$

r1 = sqrt[r0^2 + b^2 - 2bsin()]

Assuming that B/r_0 is small enables us to approximate the square root by the first two terms of its power series expansion (Westergreen, 196).

$$r_{1MIN}, r_{1MAX} \approx r_0\left[1 \pm \frac{B}{r_0}\sin(\theta_0)\right], \quad B \ll r_0, \quad 0 < \theta_0 < 90° \qquad 65$$

The equation applies to the front side only, i.e. for θ_0 from 0° to 90°, and does not include the effect of angle φ. Changing φ from 0 to 180° corresponds to changing θ from positive to negative, which is reflected by the plus/minus sign , so r_1 can be larger or smaller than r_0. For $\theta_0 = 90°$, i.e. at the edge of the baffle, and with $B/r_0 = 0.1$, we get the value $r_{1MIN} = 0.90\ r_0$, and $r_{1MAX} = 1.10\ r_0$, which indicates that the change in r_1 is moderate for a typical set-up.

If we – for the sake of simplicity – assume that distance r_1 is changed linearly from r_{1MIN} to r_{1MAX} for φ moving from 0 to π and that the distance is again changed linearly back to r_{1MIN} for φ moving further from π to 2π, we have the following relation:

$$r_1 = \begin{cases} r_{1MIN} + (r_{1MAX} - r_{1MIN})\dfrac{\varphi}{\pi} & 0 < \varphi < \pi \\[2mm] 2r_{1MAX} - r_{1MIN} - (r_{1MAX} - r_{1MIN})\dfrac{\varphi}{\pi} & \pi < \varphi < 2\pi \end{cases}$$

Insertion of the limiting values from equation 65 and assembling terms:

$$r_1 = \begin{cases} \left(1 + \left(\dfrac{2\varphi}{\pi} - 1\right)\dfrac{B}{r_0}\sin(\theta_0)\right)r_0 & 0 < \varphi < \pi \\[2mm] \left(1 + \left(3 - \dfrac{2\varphi}{\pi}\right)\dfrac{B}{r_0}\sin(\theta_0)\right)r_0 & \pi < \varphi < 2\pi \end{cases}$$

Using equation 53 to get an expression for the sound pressure of the reflected wave:

$$p_1 = \exp(-ikB)\frac{1}{2\pi}\left[\int_0^\pi \exp\left(-ikB\left(\frac{2\varphi}{\pi} - 1\right)\sin(\theta_0)\right)d\varphi + \int_\pi^{2\pi} \exp\left(-ikB\left(3 - \frac{2\varphi}{\pi}\right)\sin(\theta_0)\right)d\varphi\right]p_0$$

The integrations are evaluated and the terms are assembled into:

$$p_1 = \exp(-ikB)\frac{\exp(ikB\sin(\theta_0)) - \exp(-ikB\sin(\theta_0))}{2ikB\sin(\theta_0)}p_0$$

Using Euler's formula for the sine function (Westergren, 62) the equation for the reflected (or diffracted) signal can be written:

$$p_1 = \exp(-ikB)\frac{\sin(kB\sin(\theta_0))}{kB\sin(\theta_0)}$$

Hence:

$$p_1 = \exp(-ikB)\,\text{sinc}(kB\sin(\theta_0))\,p_0 \qquad\qquad 66$$

The *sinc* function is unity for zero argument, which is at low frequencies where the interference is at its maximum, and decays toward zero for increasing argument with oscillations around zero (see Figure 110). The decaying amplitude is thus reducing the interference at high frequencies.

For an observation point right at the axis of symmetry ($\theta_0 = 0$) is the sinc function unity and the result is simply a signal delayed by the size of the baffle and the result is identical to the previous result for on-axis.

The result for the front and rear sides of the baffle is plotted below for a circular baffle with radius $B = 0.17$ m radius and 30° off-angle.
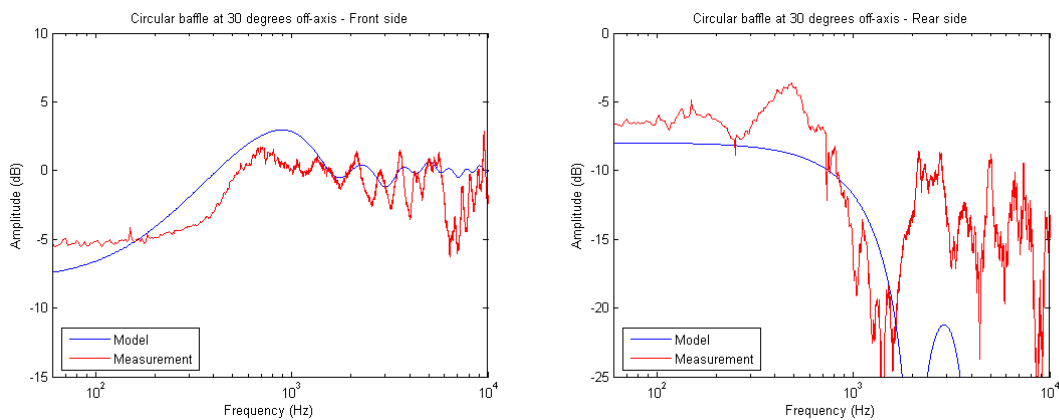
Figure 66 – Amplitude response for an observation angle of 30° for the front side (left) and the rear side where the measurement at 150° was used as reference (right).

The expression models the broad outline but misses the ripples at high frequency.

The lowest frequencies are some 2 dB higher than calculated due to the missing second-order effects and the peak around 1 kHz is 2 dB more pronounced within the calculated response than within the measurements. However, the over-all behaviour of the baffle is modelled reasonably well despite the visual differences between the calculated and measured responses especially at high frequency.

The first zero where the sinc function suppresses the diffracted signal occurs at:

$$kB\sin(\theta_0) = \pi \quad \Rightarrow \quad f_0 = \frac{c}{2B\sin(\theta_0)}$$

The zero frequency is 2 kHz at $\theta_0 = 30°$ and is reduced to 1 kHz at $\theta_0 = 90°$. The resultant front side response is unaffected by the baffle at the zero frequencies since the interference from the diffracted signal is removed at these frequencies so the amplitude crosses the 0 dB grid here. The 2 kHz zero frequency is easily seen in the rear side plot.

The rear side response is not correctly modelled but the average response is reflected although the zero frequency is around 1.5 kHz within the measurements.

4.7.3 Elliptic baffle, on-axis

The derivation of $b(\varphi)$ for the elliptic baffle follows the same route as was shown above but the derivation is not trivial and has been moved to the appendix (section 1.1) where a general approach for the determination of the effect of the baffle is developed.

It is obvious that an elliptic baffle can be regarded a projection of a circle onto a plane tilted relative to the plane of the circle and this results in the below equation for 30° of tilting (note the similarity to the above off-axis model although the parameters have been changed). The delay is reduced to 81 % of that of the off-axis model since the delay represents the average value between long and short. The sinc function is more than halved compared to the off-axis model thus increasing the zero frequency accordingly.

$$p_1 = p_0 \exp(-0.81ikB)\operatorname{sinc}(0.19kB)$$

The model is compared to measurements below using a tilted circular baffle as the reference. The left figure shows the response on-axis for the front side and the right curve represents the shadow zone, i.e. the rear side spectrum. The measurements were a circular baffle tilted 30° for front side and 120° for rear side. The agreement to measurements is not as good as for the circle, and there are two reasons for this; first of all the simplicity of the model and secondly the difference between regarding the ellipse a projection of a circle and the true expression for a tilted circle.
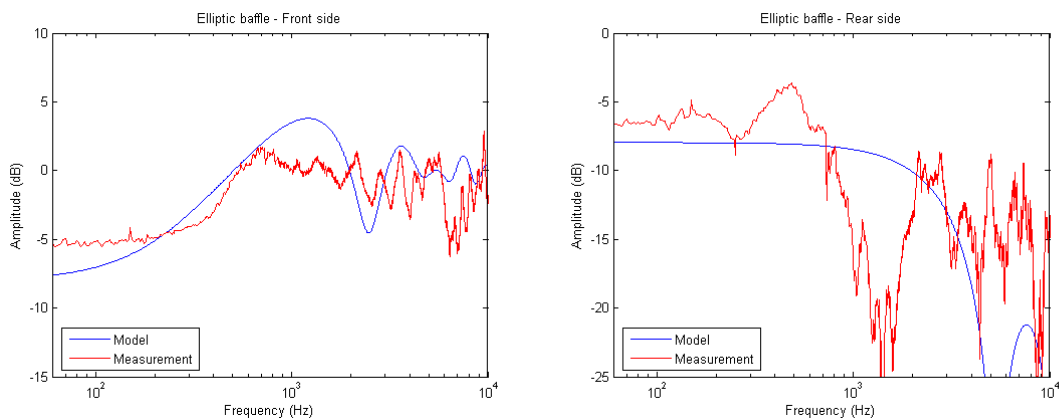
Figure 67 – Front-side and rear-side for the elliptic model using 30° projection angle.

The on-axis response is not as close to the measured frequency response as the off-axis model displayed above although the model can be used but the rear-side response is useful only up to 300 Hz with very large differences from the measured response at frequencies above 1 kHz.

An equation for the tilted circular baffle is derived in section 7.2.6 and is for 30° of tilting identical to the derived model for off-axis monitoring at 30° so the plots will not be shown but the conclusion is that the result of either the off-axis model or the tilted model is far better than the projection model; but this should not surprise since the projection model does not take the change in delay time into account.

4.7.4 Circular baffle with offset source

The equation for a baffle with an offset source is derived in the appendix for the general case of an elliptic baffle (see section 7.2.7). For the circular baffle the equation becomes:

$$p_1 = \frac{p_0}{2}\left[\exp\left(-ikB\left(1-\frac{d_B}{4}\right)\right)\text{sinc}\left(kB\frac{3d_B}{4}\right) + \exp\left(-ikB\left(1+\frac{3d_B}{4}\right)\right)\text{sinc}\left(kB\frac{d_B}{4}\right)\right], \quad d_B = \frac{D}{B}$$

The sound pressure will be calculated for $D = 50$ mm, which corresponds to 30 % of radius, and for $D = 100$ mm, which corresponds to 60 % of radius. The equations become:

$$p_1 = \frac{p_0}{2}\left[\exp\left(-0.93ikB\right)\text{sinc}\left(0.22kB\right) + \exp\left(-1.22ikB\right)\text{sinc}\left(0.07kB\right)\right], \quad \text{for} \quad D = 5\,\text{cm}$$

$$p_1 = \frac{p_0}{2}\left[\exp\left(-0.85ikB\right)\text{sinc}\left(0.44kB\right) + \exp\left(-1.44ikB\right)\text{sinc}\left(0.15kB\right)\right], \quad \text{for} \quad D = 10\,\text{cm}$$

The results are plotted below where it is interesting to see that the offset suppresses most of the high-frequency oscillation leaving only a dip at 1.5 kHz. Fairly good agreement is seen for the measured response with moderate offset (5 cm corresponding to 30 % of radius), while the larger offset of 10 cm (60 %) fails at the 1.5 kHz dip frequency.
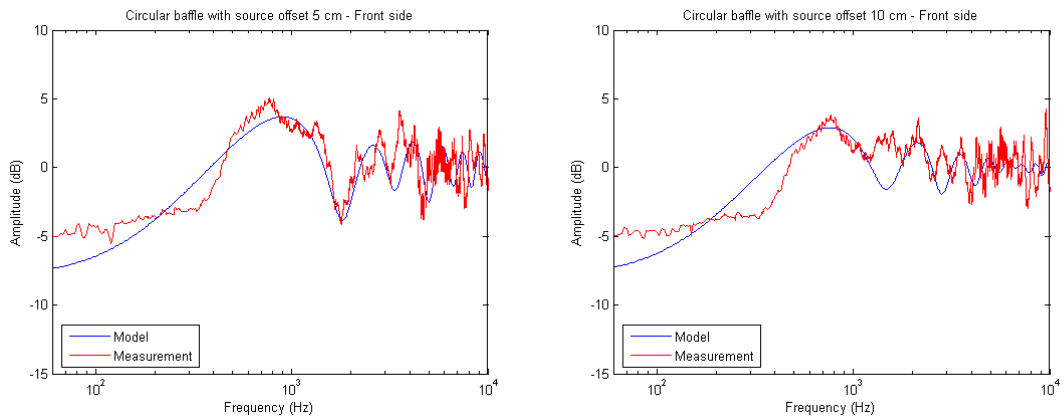
Figure 68 – On-axis response for circular baffle with source offset 5 cm or 10 cm.

The difference between the calculated and measured frequency spectrum is shown below for the offsets and the calculated responses are within ±5 dB of the measured responses.
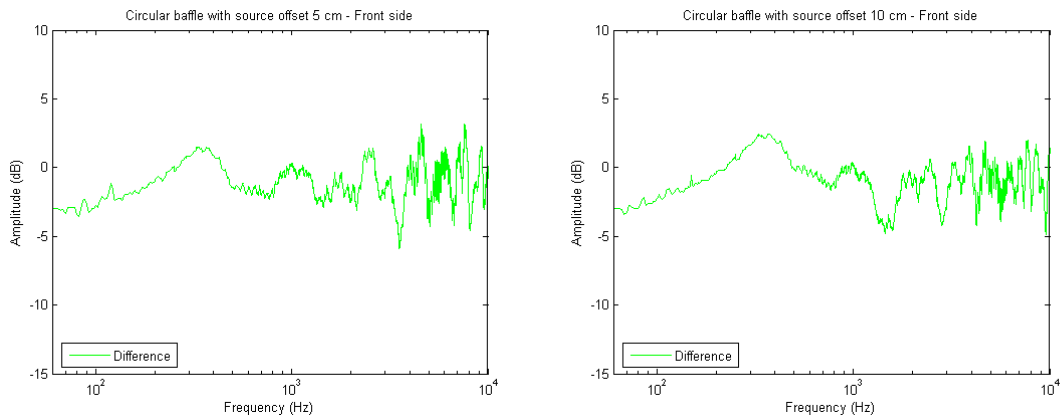
Figure 69 – Difference between calculated and measured frequency spectrum.

4.7.5 Rectangular baffle with offset source

The rectangular baffle is harder to model than the circular and elliptic baffles but the result is more useful since the vast majority of real baffles are rectangular. The modelling problems lead to the requirement of numerical calculation methods, which follow in the next section. The equation for a rectangular baffle is derived in the appendix (see section 7.2.9) using a very simple model with baffle size $1.15B$ high by $2B$. For $B = 170$ mm this corresponds to a baffle with the measure 200 mm by 340 mm.

$$p_1 = p_0 \frac{1}{3} \exp(-ikB) \left[\exp(-ikD) + 2\cos\left(\frac{kD}{2}\right) \mathrm{sinc}\left(\frac{kD}{2}\right) \right]$$

For an offset of $D = 0$ the model becomes the equation for a circular baffle, thus illustrating the lack of model complexity. For an offset one half the distance from centre to the edge along the long side we have:

$$p_1 = p_0 \frac{1}{3} \exp(-ikB) \left[\exp(-0.50ikB) + 2\cos(0.25kB)\mathrm{sinc}(0.25kB) \right], \quad \text{for} \quad D = 85\,\text{mm}$$

The resulting on-axis response is shown below together with the difference between model and measurement.
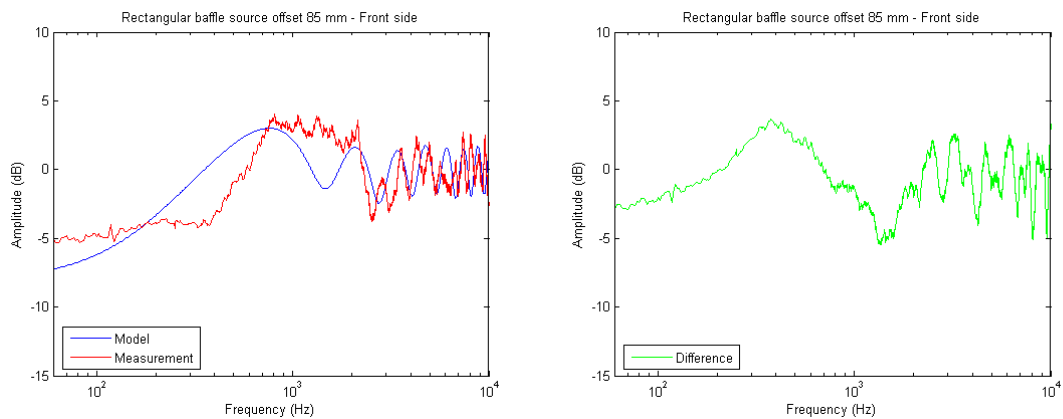
Figure 70 – Front-side response (left) and difference from measured response (right) for rectangular baffle (200 mm by 340 mm) with source offset 85 mm.

The implemented model is not sufficiently complex to represent all details of the rectangular baffle but the model is anyway around ±5 dB of the measured response. It is possible to increase the complexity as shown in the appendix, but the workload involved is not justified unless an analytical expression is indeed required.

4.7.6 Conclusion

The method presented so far results in a simple analytical function consisting of one or two delay terms and ripple functions build from the complex exponential and sinc functions. The expressions can reproduce the broad outline of the frequency spectrum such as the low-frequency 6 dB reduction in amplitude (*loss of bass*) and approximate the amplitude of the ripple at the higher frequencies; but the models are not accurate. The expressions may prove valuable for implementing into an analytic function describing the loudspeaker within a baffle but more accurate models will be required for other applications and this is the objective of the following section.

4.8 Numerical simulation

The edge diffraction model is well-suited for numerical computations allowing increased accuracy and larger freedom for selection of observation distance and observation angle. The following implementation is intended for use within MATLAB using the fast execution of vector arithmetic. The model will be enhanced gradually as the implementation is progressing and the model is including more information.

A point source is used to represent the loudspeaker thus avoiding blurring of the results due to the size and directivity of the loudspeaker. The source is assumed located inside the boundary and a number of point sources are located along the edge to represent the shape of the baffle. The observation point can be located anywhere within the half-space in front of the baffle for calculation of the front-side spectrum or behind the baffle for the rear-side spectrum. The algorithm does not produce the correct simulation at the edge of the baffle (90°).

The sound pressure at the observation point consists of the direct signal from the main sound source and a finite number of contributions from the point sources located along the edge. The model below shows the definitions used for the model using a rectangular baffle but the model can use almost any shape.
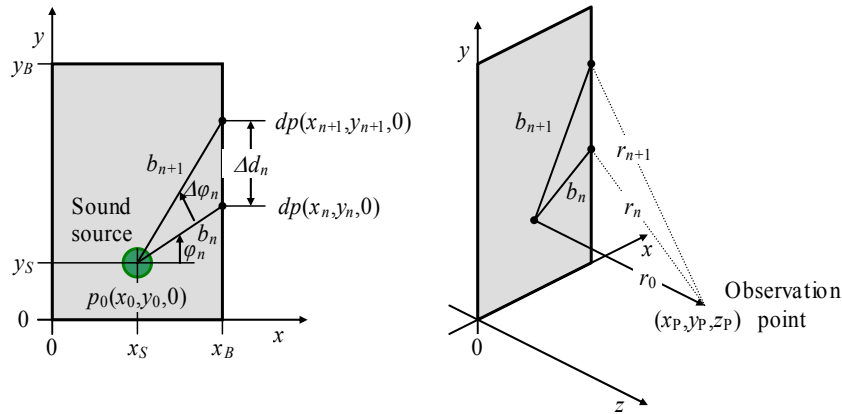
Figure 71 – Definition of the coordinate system used for the model.

The direct signal is given by equation 35 since the model assumes the loudspeaker being represented by a point source above an infinite baffle and the resulting sound pressure at the observation point at distance r_0 from the source is:

$$p_0 = p(r_0) = \frac{ik\rho c q}{2\pi r_0} \exp(-ikr_0)$$

The source will be located at $(x_0, y_0, 0)$, and the observation point is located at (x_P, y_P, z_P), so the distance between the source and observation point becomes:

$$r_0 = \sqrt{(x_P - x_0)^2 + (y_P - y_0)^2 + z_P^2} \qquad\qquad 67$$

Radiation from the edge is represented by a number of point sources called *edge sources*, each representing a line segment Δd_n as shown in Figure 71 where line segment n begins at edge source n and extends to edge source $n + 1$ with distance b_n to the starting point. The effective length of the line segment is given by the angle of the line segment viewed from the source and this angle will be called $\Delta\varphi$. All segments along the edge of the baffle are included when

the sum $\Delta\varphi_1 + \Delta\varphi_2 + ... + \Delta\varphi_N$ equals 2π so the sound pressure at the observation point from the edge source associated to segments n is proportional to $\Delta\varphi_n/2\pi$ in full analogy to the derivation of equation 52. Hence, the sound pressure from edge source n:

$$\Delta p_n = \frac{ik\rho cq}{2\pi(b_n + r_n)}\exp(-ik(b_n + r_n))\frac{\Delta\varphi_n}{2\pi}$$

68

In this equation are the parameters b_n, r_n and $\Delta\varphi_n$ to be defined.

Edge source n is located at $(x_n, y_n, 0)$ and the main source is located at $(x_0, y_0, 0)$ so the distance from the main source to the edge source is:

$$b_n = \sqrt{(x_0 - x_n)^2 + (y_0 - y_n)^2}$$

69

It is possible to include the z-coordinate in order to model baffles with curved surface.

The observation point is assumed located at (x_P, y_P, z_P) so the distance from edge source n to the observation point is:

$$r_n = \sqrt{(x_P - x_n)^2 + (y_P - y_n)^2 + z_P^2}$$

70

An expression is required for the angle occupied by the line segment and this is calculated from the length of the line segment associated with the edge source:

$$\Delta d_n = \sqrt{(x_{n+1} - x_n)^2 + (y_{n+1} - y_n)^2}$$

71

For the last point is Δd_N calculated using $x_n = x_N$ and $x_{n+1} = x_1$, which is the distance from the last point to the first thus closing the curve from x_1 to x_N back to the starting point x_1.

The angle that line segment Δd_n is occupying viewed from the source is given by the law of cosines for the triangle formed by the lines b_n and b_{n+1} (Westergren, 68):

$$\Delta d_n^2 = b_n^2 + b_{n+1}^2 - 2b_n b_{n+1}\cos(\Delta\varphi_n)$$

72

Hence the segment angle:

$$\Delta\varphi_n = \arccos\left(\frac{b_n^2 + b_{n+1}^2 - \Delta d_n^2}{2b_n b_{n+1}}\right)$$

73

Assembling the above information, the sound pressure and the corresponding transfer function at the observation point for the front side radiation p_F and similar for the rear side radiation p_R becomes given by:

$$p_F = p_0 + R\sum_{n=1}^{N}\Delta p_n \quad \Rightarrow \quad H_F(f) = 1 + R\sum_{n=1}^{N}\frac{\Delta p_n}{p_0}$$

$$p_R = p_0(1+R)\sum_{n=1}^{N}\Delta p_n \quad \Rightarrow \quad H_R(f) = (1+R)\sum_{n=1}^{N}\frac{\Delta p_n}{p_0}$$

Here is N the total number of edge sources and R is the reflection coefficient. The expression to the right have been normalised to the direct sound through division with p_0 thus defining the transfer function of the baffle. This is a frequency-dependent and position-dependent factor describing the alteration of the free-field sound pressure from an undisturbed spherical source (above a reference plane) due to the presence of the loudspeaker baffle.

Insertion of the expressions for Δp_n and p_0 gives the transfer functions for the font side H_F and for the rear side H_R:

$$H_F(f) = 1 + R\frac{1}{2\pi}\sum_{n=1}^{N}\frac{r_0}{b_n+r_n}\exp\left(ik[r_0-b_n-r_n]\right)\Delta\varphi_n$$

$$H_R(f) = (1+R)\frac{1}{2\pi}\sum_{n=1}^{N}\frac{r_0}{b_n+r_n}\exp\left(ik[r_0-b_n-r_n]\right)\Delta\varphi_n$$

74

The parameters r_0, b_n, r_n and $\Delta\varphi_n$ are defined above, the frequency is represented by $k = 2\pi f/c$, the total number of points along the edge is $N > 1$ and the reflection coefficient is $R = -0.60$.

Any selection of coordinates for the edge sources is allowed but the distance between any two points should be small compared to wavelength; so $k\Delta d_n < 1$ defines the frequency limit:

$$f < \frac{c}{2\pi\Delta d_n} \approx \frac{cN}{2\pi C}$$

75

The approximation applies to N equidistant points along the edge with circumference C. For a baffle with measure 200 mm by 340 mm the circumference is 1.08 m and using 16 points the upper frequency limit becomes 800 Hz so 200 points are required for calculation to 10 kHz. For the on-axis response are the segments at approximately the same distance from the observation point, which may reduce the required number of sources as will be shown below.

The implementation to follow calculates 6401 measurement points from 0 to 12800 Hz using steps of 2 Hz. Each step consists of complex calculations for vectors with the size given by the number of edge sources and for 200 sources is the requirement more than one million calculations so relatively long computation time was expected. However, the time required were five seconds for calculation of the full frequency spectrum including two seconds for the output plot thus showing the power of the MATLAB language. The computer was Intel Pentium 4 running at 2.4 GHz and equipped with 750 Mbyte of RAM.

4.8.1 Examples

The calculation can be performed with few segments due to the high degree of symmetry, which can be seen below where the left-hand plot is using only two edge sources but produces the same result as the right-hand plot using 200 edge sources.
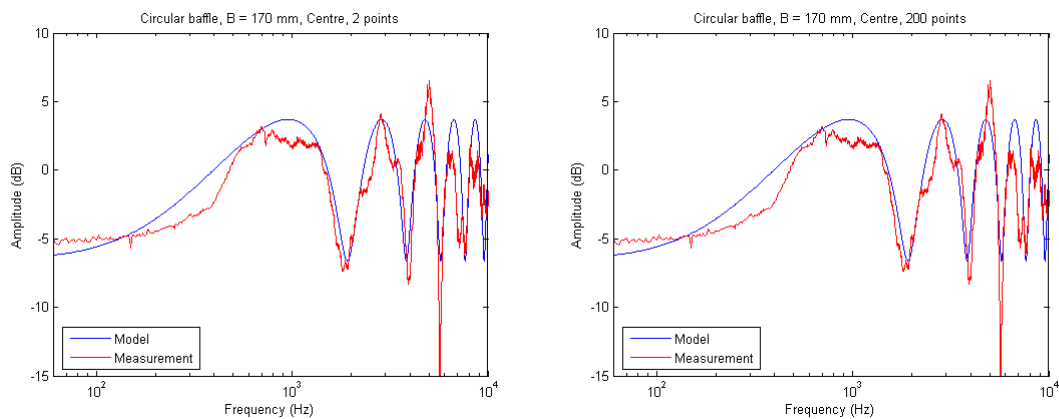
Figure 72 – On-axis frequency spectrum for the circular baffle using 2 point sources (left) and 200 point sources (right) at $r_0 = 1.41$ m distance to observer.

More edge sources are required for off-axis monitoring as can be seen from below where the 30° tilting of the baffle creates am elliptic shape thus requiring more edge sources.
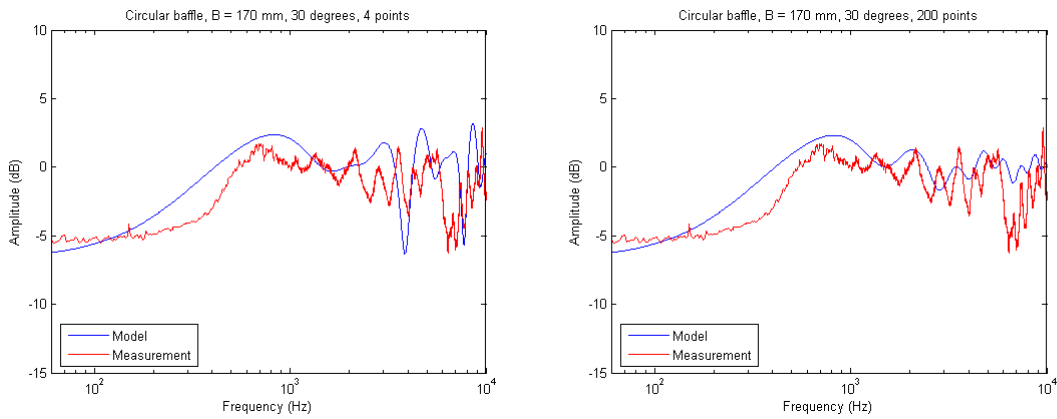
Figure 73 - Frequency spectrum at 30° for the circular baffle using 4 and 200 point sources.

The responses for 60° and 90° differ somewhat from the measurement but peaks and dips are modelled correctly. The direct signal is too loud at large observation angles.
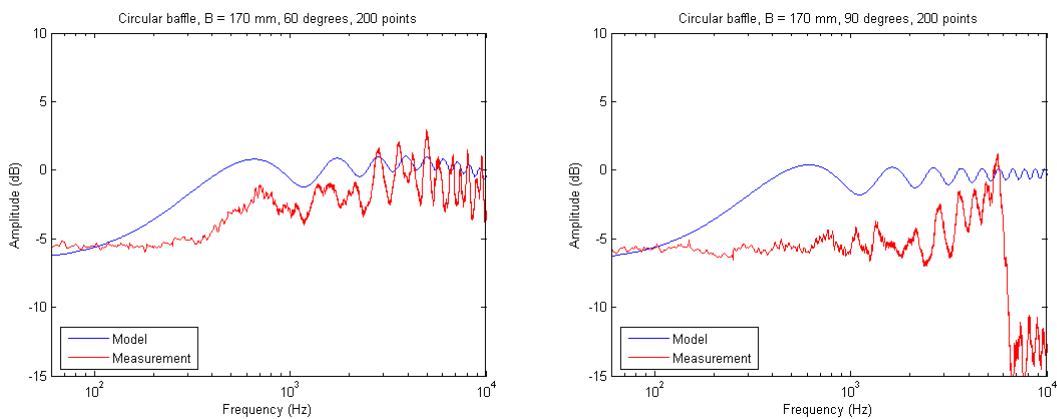
Figure 74 – Frequency spectrum at 60° (left) and 90° (right).

The rear-side spectrum is plotted below using the H_R function from equation 74 where the diffracted signal is modelled as the transmitted signal. There are large differences.
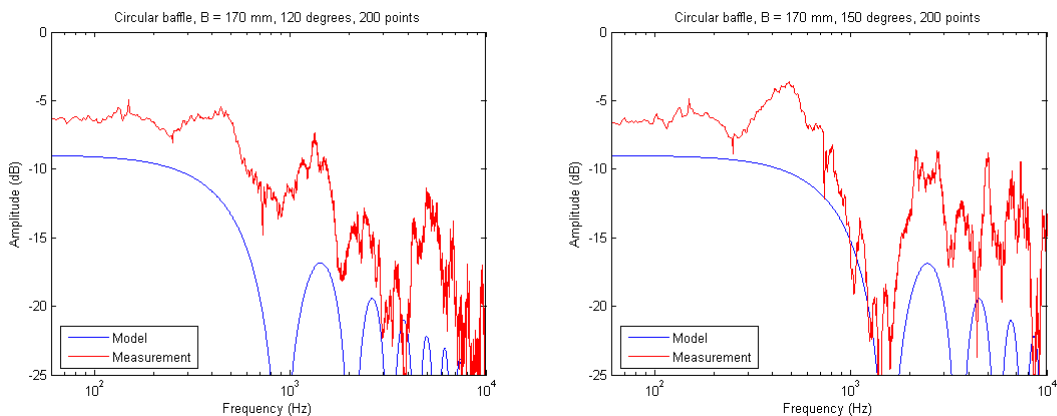
Figure 75 – Rear-side frequency spectrum at 120° and 150°.
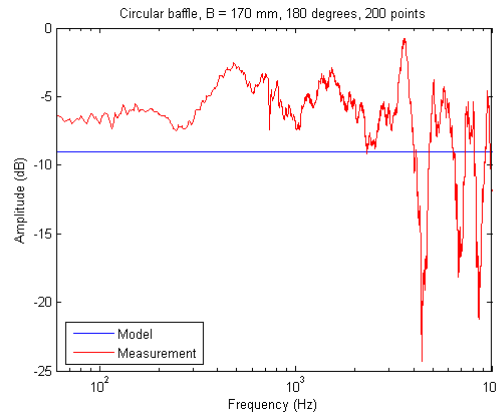
Figure 76 – Rear-side frequency spectrum at 180°.

The prediction of flat rear-side spectrum at −8 dB for 180° is far from being correct although the measured spectrum is more or less flat up to 3 kHz with an average value around −5 dB so the simulation is 3 dB low and without the details. The tilted responses at 120° and 150° are some 5 dB low for frequencies below 1 kHz but they show approximately correct cut-off and peak frequencies so the broad outline is correct.

4.9 Higher-order diffraction components

The model used so far includes only one reflection from the baffle although there are several pulses in the impulse response corresponding to second-order and higher order diffraction components (Vanderkooy, 929-931).

4.9.1 Second-order diffraction component

Below is sketched the construction of an idealised impulse response where p_0 is the direct signal from the source, which is arriving at the observation point at time t_0. The signal from the source reaches the edge after a short delay due to distance B from the source to the edge as the first-order diffraction component p_1, which is defined as follow for a circular baffle with the source at the centre:

$$p_1 = \exp(-ikB)p_0$$

This signal is at the edge divided into a reflected signal of amplitude Rp_1, which is arriving at the observation point within the front side at time t_1 and is causing the interference studied in the previous section; and also a transmitted signal of amplitude Tp_1, which is arriving at the observation point at time t_1 within the rear side (shadow zone) as the rear-side diffraction also studied previously.

The reflected or transmitted signals may travel along either side of the baffle but only the contribution from the front side will be considered here so the reflected signal Rp_1 is assumed to travel from the edge toward the opposite edge with a second delay related to distance $2B$.

Hence, this second-order diffraction component becomes:

$$p_2 = \exp(-2ikB)Rp_1$$
$$= \exp(-3ikB)Rp_0$$

This signal is at the edge divided into two contributions, a signal reflected into the front side of amplitude Rp_2 and a signal transmitted into the rear side of amplitude Tp_2.
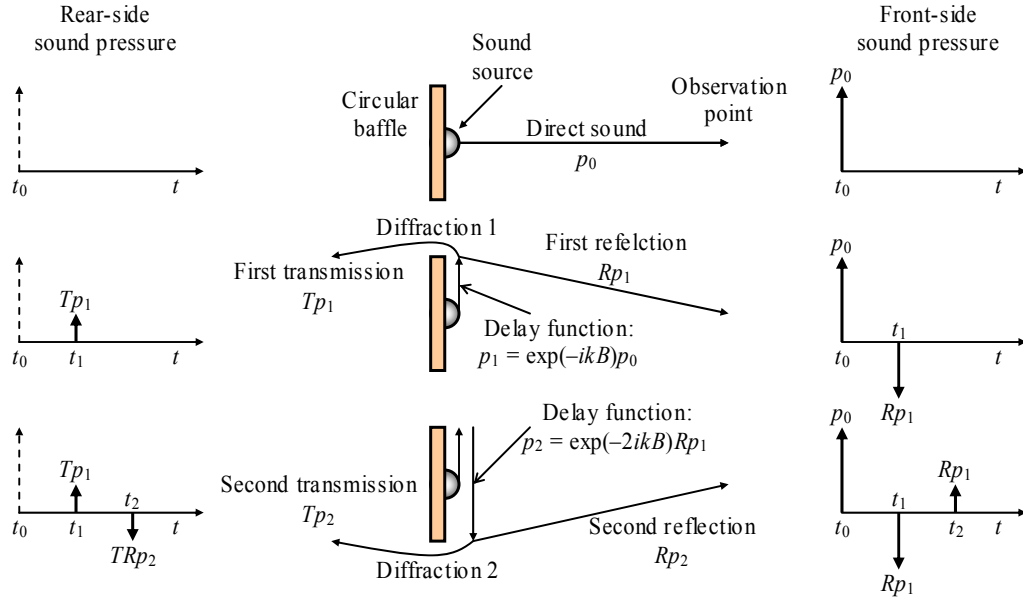
Figure 77 – Graphical construction of the resultant impulse response for a circular baffle where only the signals travelling along the front side are implemented into the theory.

Assembling the fragments we arrive at the following expressions for the two sides of the baffle:

$$p_F = p_0 + Rp_1 + Rp_2$$
$$p_R = Tp_1 + Tp_2$$

76

This is in contrast to Vanderkooy who assumes the first-order diffracted signal to be radiated in any direction from the edge and thus energising the other edge sources so the resultant radiation becomes blurred. The present model assumes that the signal is partially reflected and transmitted and as such can only move back and forth, i.e. along radius for a circular baffle. This assumption may not hold in real life but the second-order diffraction is a correction to the model and is not the core of the model.

Inserting the expressions for the circular baffle, we get:

$$p_F = \left[1 + \exp(-ikb)R + \exp(-3ikb)R^2\right]p_0$$
$$p_R = \left[1 + \exp(-2ikb)R\right]\exp(-ikb)Tp_0$$

77

A generalisation from circular baffles into any baffle shape is possible using the previous division of the edge into short sections each with distance b_n from the source and distance e_n to the opposite side of the baffle. The derivation of the second-order diffraction component begins with the first-order diffraction component, which was estimated in equation 68 and is reproduced below:

$$\Delta p_n^{(1)} = \frac{ik\rho cq}{2\pi(b_n + r_n)}\exp(-ik(b_n + r_n))\frac{\Delta\varphi_n}{2\pi}$$

The term $ik\rho cq/2\pi$ is due to the point source located at the centre of the baffle; the denominator $b_n + r_n$ is the distance from the source to the observation point, which is also observed within the exponential as a factor controlling the delay and $\Delta\varphi_n/2\pi$ is the fraction of the edge occupied by the line segment from edge source n to edge source $n + 1$.

The sound pressure from an unobstructed point source above an infinite baffle and at distance r_0 to the observer is:

$$p_0 = \frac{ik\rho c q}{2\pi r_0} \exp(-ikr_0)$$

Using this, the expression for the first-order diffraction component can be written as function of the unobstructed point source:

$$\Delta p_n^{(1)} = \frac{r_0}{b_n + r_n} \exp(ik(r_0 - b_n - r_n)) \frac{\Delta\varphi_n}{2\pi} p_0$$

The first-order diffraction component is an attenuated and delayed replica of the original sound from the main point source (the loudspeaker). The amplitude and phase are changed due to the increased distance and the amplitude is further scaled by the size of the line segment.

The model of second-order diffraction is relating the differential source to the sound pressure from the corresponding first-order diffraction component, so it is reduced in amplitude and delayed due to the added edge-to-edge distance e_n between the edge sources, into:

$$\Delta p_n^{(2)} = \frac{b_n + r_n}{b_n + r_n + e_n} \exp(-ike_n)\Delta p_n^{(1)}$$

$$= \frac{b_n + r_n}{b_n + r_n + e_n} \exp(-ike_n)\frac{r_0}{b_n + r_n} \exp(ik(r_0 - b_n - r_n))\frac{\Delta\varphi_n}{2\pi} p_0$$

$$= \frac{r_0}{b_n + r_n + e_n} \exp(ik(r_0 - b_n - r_n - e_n))\frac{\Delta\varphi_n}{2\pi} p_0$$

Using equation 76, the sound pressure for front side of the baffle becomes:

$$p_F = p_0 + \sum_{n=1}^{N}\left(R\Delta p_n^{(1)} + R^2\Delta p_n^{(2)}\right)$$

$$= p_0 + \sum_{n=1}^{N}\left(R\frac{r_0}{b_n + r_n} \exp(ik(r_0 - b_n - r_n))\frac{\Delta\varphi_n}{2\pi} p_0 \right.$$

$$\left. + R^2\frac{r_0}{b_n + r_n + e_n} \exp(ik(r_0 - b_n - r_n - e_n))\frac{\Delta\varphi_n}{2\pi} p_0 \right)$$

$$= p_0 + \sum_{n=1}^{N}\left(R\frac{r_0}{b_n + r_n} + R^2\frac{r_0}{b_n + r_n + e_n} \exp(-ike_n) \right)\exp(ik(r_0 - b_n - r_n))\frac{\Delta\varphi_n}{2\pi} p_0$$

$$= p_0 + R\sum_{n=1}^{N}\left(1 + R\frac{b_n + r_n}{b_n + r_n + e_n} \exp(-ike_n) \right)\frac{r_0}{b_n + r_n} \exp(ik(r_0 - b_n - r_n))\frac{\Delta\varphi_n}{2\pi} p_0$$

The expression to the right of the parenthesis is the first-order diffraction component and the parenthesis contains the frequency-dependent alteration due to the second-order diffraction component. The summation is thus changed from the initial form $(1 + H_1)p_0$ where H_1 represents the frequency-dependent alteration due to the first-order diffraction components to $(1 + (1 + H_2)H_1)p_0$ where H_2 represents the frequency-dependent alteration due to the second-order diffraction components.

And similarly for the rear side of the baffle:

$$p_R = \sum_{n=1}^{N}\left(T\Delta p_n^{(1)} + T^2\Delta p_n^{(2)}\right) = T\sum_{n=1}^{N}\left(1 + T\frac{b_n + r_n}{b_n + r_n + e_n}\exp(-ike_n)\right)\Delta p_n^{(1)}$$

Using equation 74, the transfer functions become:

$$H_F(f) = 1 + R\frac{1}{2\pi}\sum_{n=1}^{N}\left(1 + R\frac{b_n + r_n}{b_n + r_n + e_n}\exp(-ike_n)\right)\frac{r_0}{b_n + r_n}\exp(ik[r_0 - b_n - r_n])\Delta\varphi_n$$

$$H_R(f) = T\frac{1}{2\pi}\sum_{n=1}^{N}\left(1 + T\frac{b_n + r_n}{b_n + r_n + e_n}\exp(-ike_n)\right)\frac{r_0}{b_n + r_n}\exp(ik[r_0 - b_n - r_n])\Delta\varphi_n$$

78

The transfer coefficient is $T = 1 + R$ and the edge-to-edge distance e_n will be selected somewhat arbitrarily using "the most distant point", which is assumed to be the distance from edge source n to edge source $n + N/2$ in order to get something easy to implement. This is an acceptable assumption since the second-order diffraction is not a significant source of sound but merely a correction to an existing model.

The relation for the distance between opposite edge sources are defined as:

$$e_n = \sqrt{(x_{n+N/2} - x_n)^2 + (y_{n+N/2} - y_n)^2} \quad n = 1\text{K }N/2$$

$$e_n = \sqrt{(x_{n-N/2} - x_n)^2 + (y_{n-N/2} - y_n)^2} \quad n = N/2\text{K }N$$

The equations were programmed into the MATLAB program as *Edge diffraction model 2*.

4.9.2 Examples

The results are shown below for the circular baffle with the source at the centre and the distance $r_0 = 1.41$ m to the observation point.
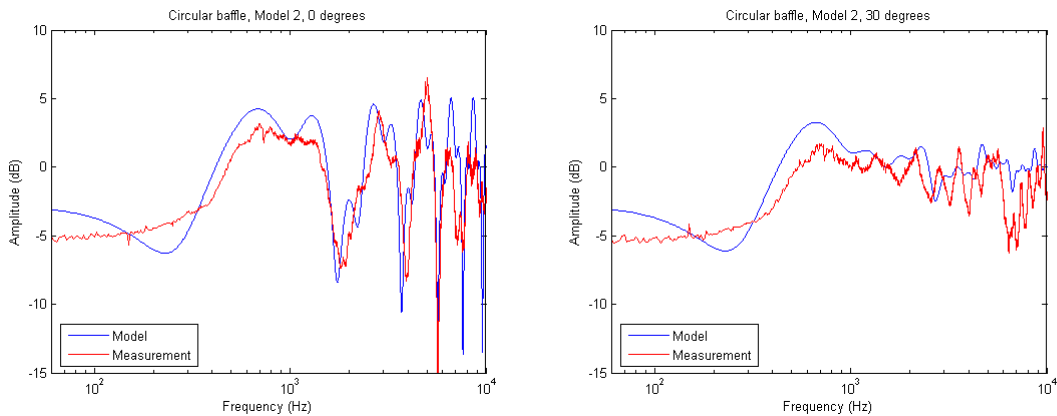
Figure 78 – Front side frequency response with two diffraction components.

The inclusion of second-order diffraction components is clearly visible. At the low-frequency end is the level increased from –8 dB to –3 dB, which is over compensating the response but this will be corrected when the third-order diffraction components are being included in the following section. The same argument applies to the low-frequency end of the simulations for 30°, 60° and 90°. The result is fair at medium and high frequencies for 0° and 30°.
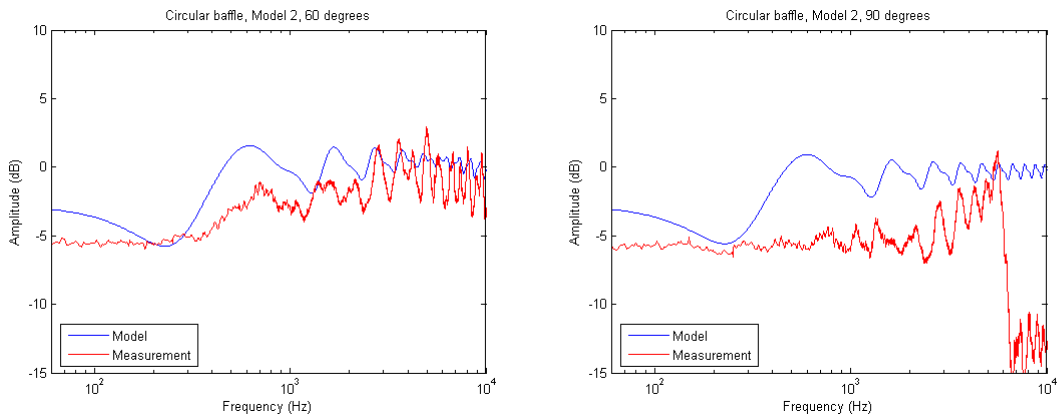
Figure 79 – Front side frequency response with two diffraction components.

Simulation at 60° and 90° are too high, which is a general statement for off-axis modelling with the model. Although the simulation for 60° is fair; the simulation for 90° is not.

The rear side model is used to model 90° by specifying 91° to trig the model selection code but using the rear-side model is far from an improvement. However, the response for 120° has much of the measured response although the level is now on the low side.
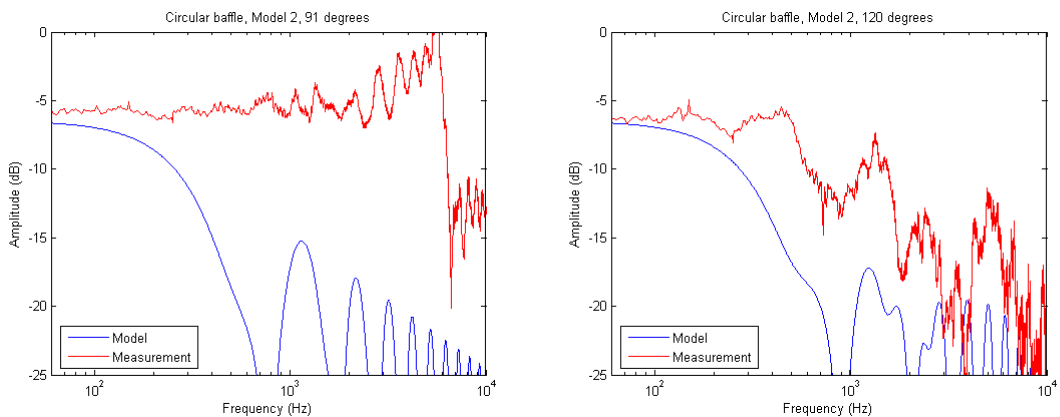
Figure 80 – Rear side frequency response with two diffraction components.

The simulation for 150° is surprisingly good when compared to the other rear-side simulations but the simulation for 180° is not of much use.
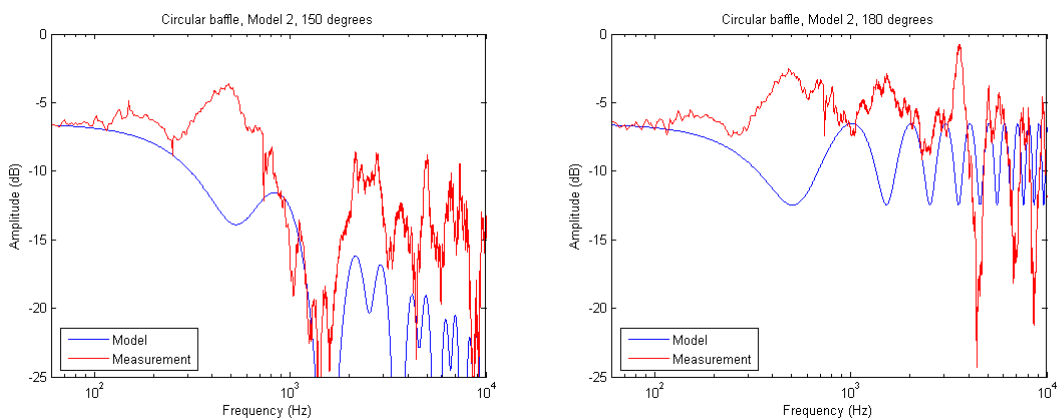
Figure 81 – Rear side frequency response with two diffraction components.

The second-order diffraction component was an improvement despite the assumptions made during the development in order to simplify the algorithm. Inspired by the progress, the third-order diffraction component will be considered.

4.9.3 Third-order diffraction component

From the previous section we have the first-order diffraction component defined as a scaled copy of the direct signal with the amplitude scaling due to the distance being increased from the direct path from source to observer (r_0) to the path via the edge source ($b_n + r_n$) and delayed relative to the direct signal ($r_0 - b_n - r_n$):

$$\Delta p_n^{(1)} = \frac{r_0}{b_n + r_n} \exp\left(ik\left(r_0 - b_n - r_n\right)\right)\frac{\Delta\varphi_n}{2\pi} p_0$$

The second-order diffraction component is attenuated due to the distance being increased from $b_n + r_n$ to $b_n + r_n + e_n$ where e_n is the additional distance from the edge source to the edge source at the opposite side of the baffle and delayed due to the same distance:

$$\Delta p_n^{(2)} = \frac{b_n + r_n}{b_n + r_n + e_n} \exp\left(-ike_n\right)\Delta p_n^{(1)}$$

Consequently, the third-order diffraction component becomes:

$$\Delta p_n^{(3)} = \frac{b_n + r_n + e_n}{b_n + r_n + 2e_n} \exp\left(-ike_n\right)\Delta p_n^{(2)}$$

$$= \frac{b_n + r_n}{b_n + r_n + 2e_n} \exp\left(-2ike_n\right)\Delta p_n^{(1)}$$

Using equation 76, the sound pressure for front side of the baffle becomes:

$$p_F = p_0 + \sum_{n=1}^{N}\left(R\Delta p_n^{(1)} + R^2\Delta p_n^{(2)} + R^3\Delta p_n^{(3)}\right)$$

Inserting the expressions for the diffraction components:

$$p_F = p_0 + \sum_{n=1}^{N}\left(R\Delta p_n^{(1)} + R^2\frac{b_n + r_n}{b_n + r_n + e_n}\exp\left(-ike_n\right)\Delta p_n^{(1)} + R^3\frac{b_n + r_n}{b_n + r_n + 2e_n}\exp\left(-2ike_n\right)\Delta p_n^{(1)}\right)$$

$$= p_0 + R\sum_{n=1}^{N}\left(1 + R\frac{b_n + r_n}{b_n + r_n + e_n}\exp\left(-ike_n\right) + R^2\frac{b_n + r_n}{b_n + r_n + 2e_n}\exp\left(-2ike_n\right)\right)\Delta p_n^{(1)}$$

$$= p_0 + R\sum_{n=1}^{N}\left(1 + R\left(\frac{b_n + r_n}{b_n + r_n + e_n} + R\frac{b_n + r_n}{b_n + r_n + 2e_n}\exp\left(-ike_n\right)\right)\exp\left(-ike_n\right)\right)\Delta p_n^{(1)}$$

The summation consists of the original terms for calculation of the first-order diffraction component with the expression $1 + R(\ldots)\exp(-ike_n)$ included as a correction due to the presence of the second-order and third-order diffraction components.

Using equation 74, the transfer functions become:

$$H_F(f) = 1 + \frac{R}{2\pi}\sum_{n=1}^{N}\left(1 + R\left(\frac{b_n + r_n}{b_n + r_n + e_n} + R\frac{b_n + r_n + e_n}{b_n + r_n + 2e_n}\exp(-ike_n)\right)\exp(-ike_n)\right)$$

$$\times \frac{r_0}{b_n + r_n}\exp(ik[r_0 - b_n - r_n])\Delta\varphi_n$$

$$H_R(f) = \frac{T}{2\pi}\sum_{n=1}^{N}\left(1 + T\left(\frac{b_n + r_n}{b_n + r_n + e_n} + T\frac{b_n + r_n + e_n}{b_n + r_n + 2e_n}\exp(-ike_n)\right)\exp(-ike_n)\right)$$

$$\times \frac{r_0}{b_n + r_n}\exp(ik[r_0 - b_n - r_n])\Delta\varphi_n$$

79

The equations were written to *Edge diffraction model 3* and the result is shown below.

4.9.4 Examples

The third-order diffraction component corrects the low-frequency level and reduces the high-frequency ripple amplitude for simulations of 0° and 30° observation angle.
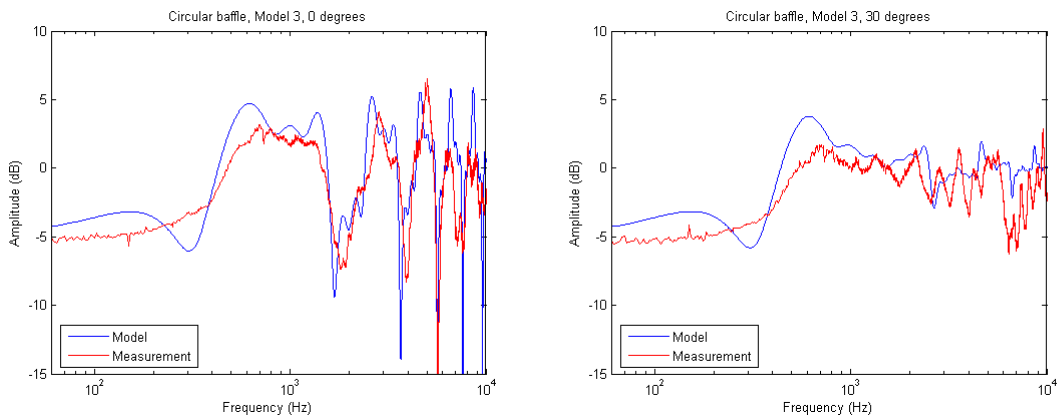
Figure 82 – Front side frequency response with three diffraction components.

Simulation of 60° and 90° are improved at the low-frequency end but the high-frequency level is too high and the asymptote for 90° toward the high frequencies is wrong.
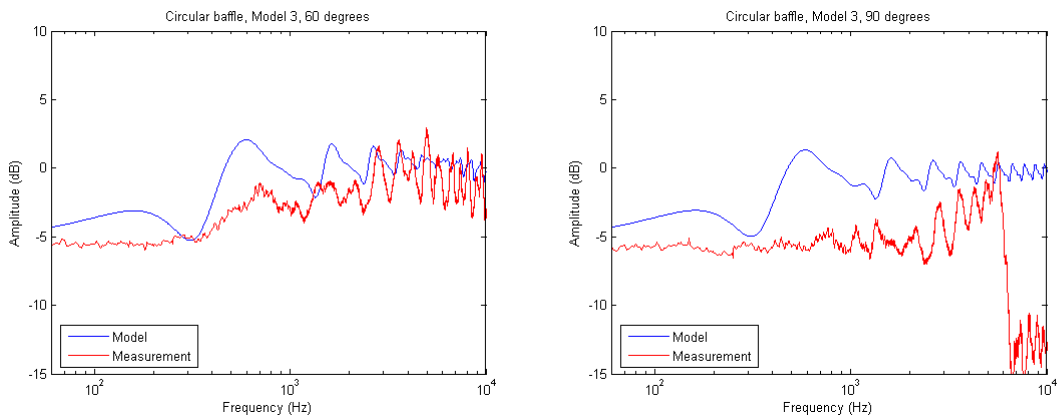
Figure 83 – Front side frequency response with three diffraction components.

The rear side is only slightly improved.
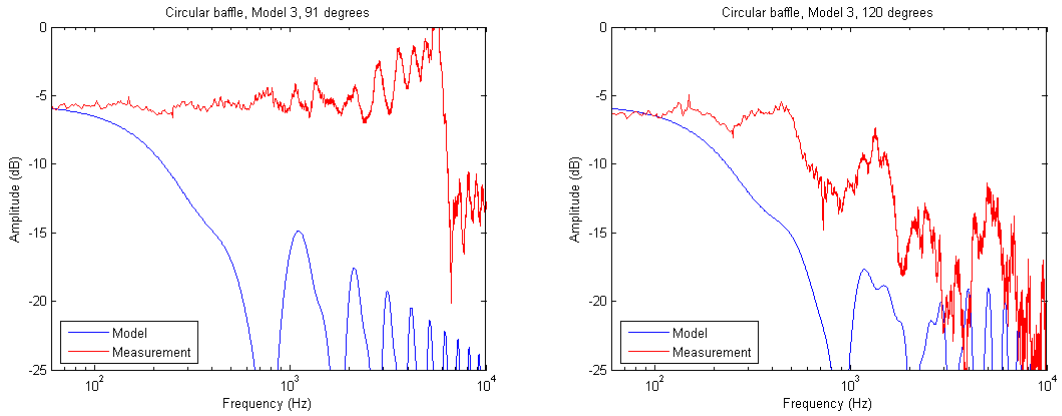
Figure 84 – Front side frequency response with three diffraction components.
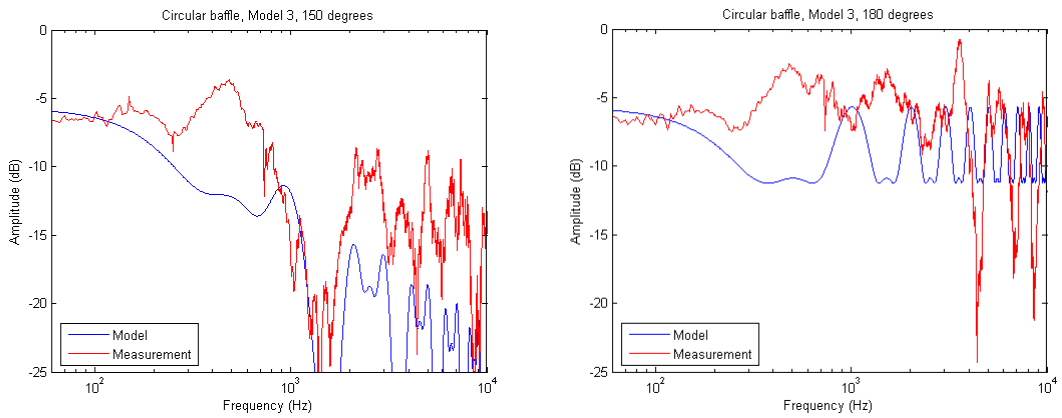
Figure 85 – Rear side frequency response with three diffraction components.

The analytical expressions proved insufficient when the source was offset significantly from the centre of the baffle so the behaviour of the numerical simulation will be investigated. The observation point for the simulation was kept fixed at 1.41 m from the centre of the circular baffle with the source being offset along the positive direction of the *y*-axis.
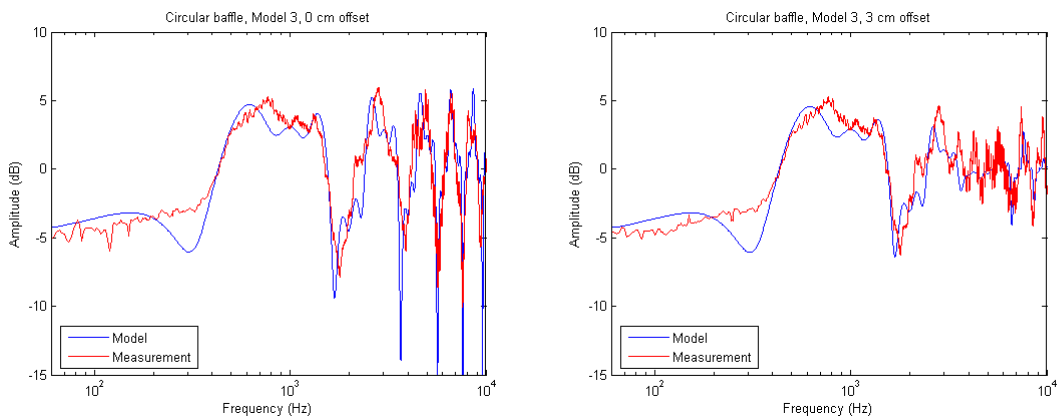
Figure 86 – Frequency response with source offset 0 and 3 cm.

Small offsets are modelled correctly, allowing for one or two decibels of uncertainty. The notch frequency is changed slightly for the first 3 cm offset and this is correctly modelled. The result below for 6 cm and 9 cm offsets corresponds to approximately 50 % of radius.
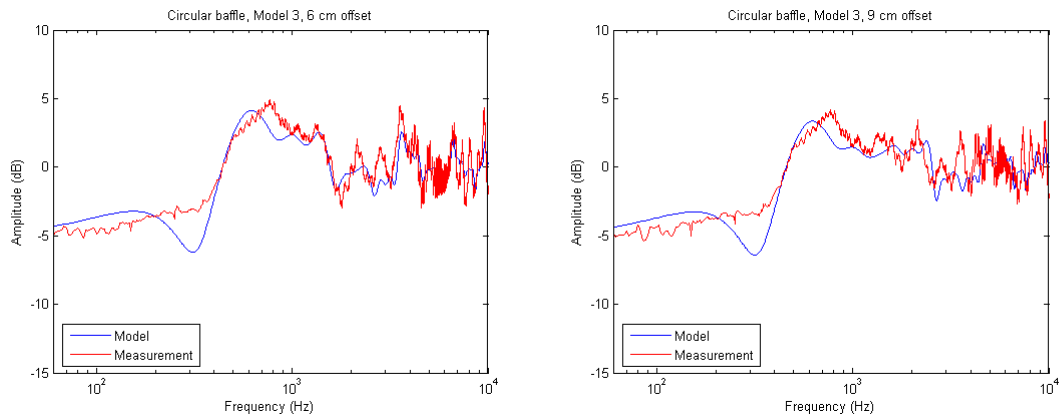
Figure 87 – Frequency response with source offset 6 cm and 9 cm.

Offsetting the source to 6 cm removes the dip at approximately 2 kHz and at 9 cm is the dip changed into a small peak and these changes are also reflected by the simulation. The high-frequency ripples of the measurement are not modelled in details but the broad outline is reproduced satisfactory.

For offsets at 12 cm and 15 cm is the slope from 500 Hz to 5 kHz slowly changing and the simulation reproduces this with peaks and dips at the right frequencies although the ripple amplitude is less than within the measurement.
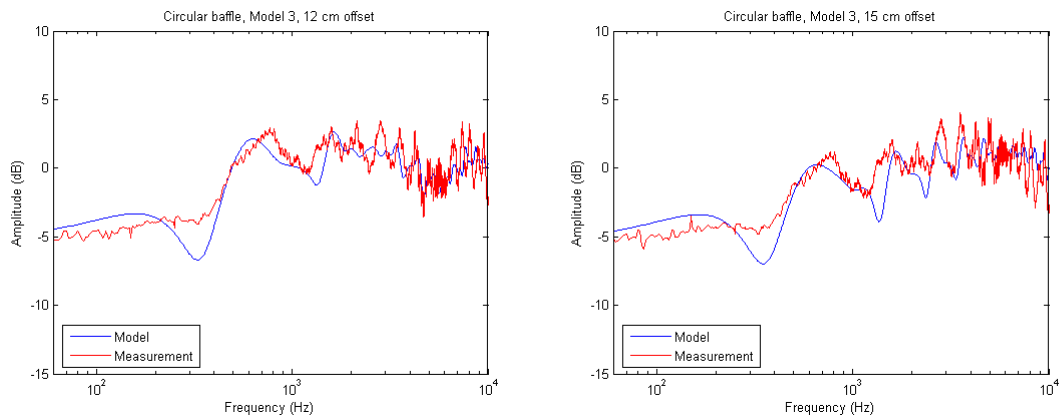
Figure 88 – Frequency response with source offset 12 cm and 15 cm.

However, increasing the offset to 18 cm and 25 cm causes problems but the simulations are related to test points *outside* the border of the baffle. Despite the simulation errors are the location of peaks and dips correct but the over-all slope is not and the simulated level is on the high side.
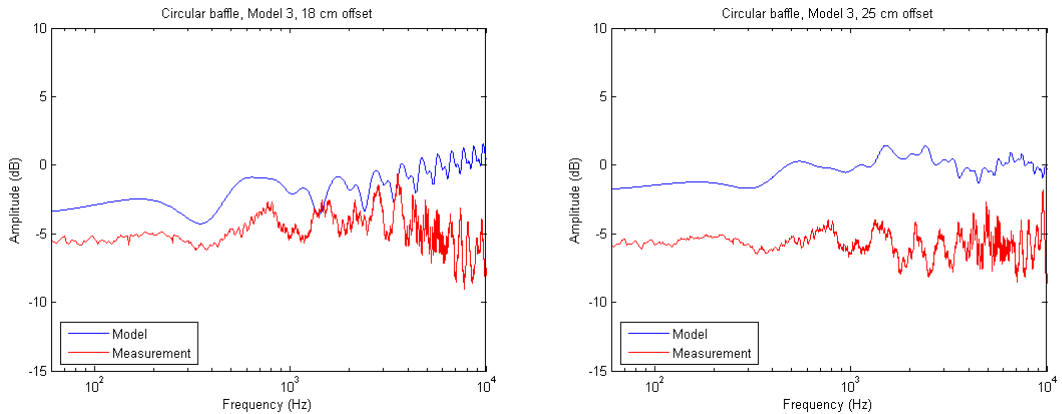
Figure 89 – Frequency response with source offset 18 cm and 25 cm.

The agreement with the measurements is quite satisfactory when the source is located within the limits of the baffle but the algorithm cannot accept a source outside the edge of the baffle.

Measurements with the rectangular baffle are comparable to the previous measurement using a circular baffle and the figures will not be reported. The simulation is generally correct for 0° and 30° observation angle and even 60° is simulated quite well although 90° is not; the level is almost 5 dB higher than the measurements. The comments to the rear-side simulations are equivalent to those of the circular baffle.

Offsetting the source on the rectangular baffle generates the following outputs where the observation point is on-axis with the centre of the baffle (x_P = 0.10 m and y_P = 0.17 m) and the observation distance was 1.41 m with the measurement corrected according to the description within the *Measurement* chapter.

For position 1 (see section 3.5.2 for the definition) was the source (loudspeaker) positioned at the centre of the baffle (x_S = 0.10 m, y_S = 0.17 m). The simulation is shown below together with the difference between simulation and measurement and this shows that the simulation is within ±3 dB up to 3 kHz and ±4 dB throughout the frequency range.
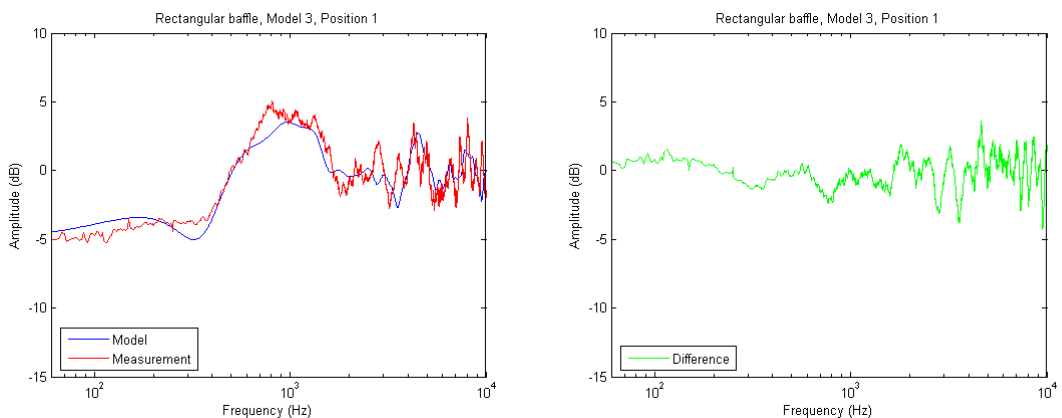
Figure 90 – Frequency response with rectangular baffle and test point at position 1.

For position 2 was the source moved 50 % down along the vertical axe thus corresponding to the typical location for small two-way loudspeaker boxes (x_S = 0.10 m, y_S = 0.085 m).
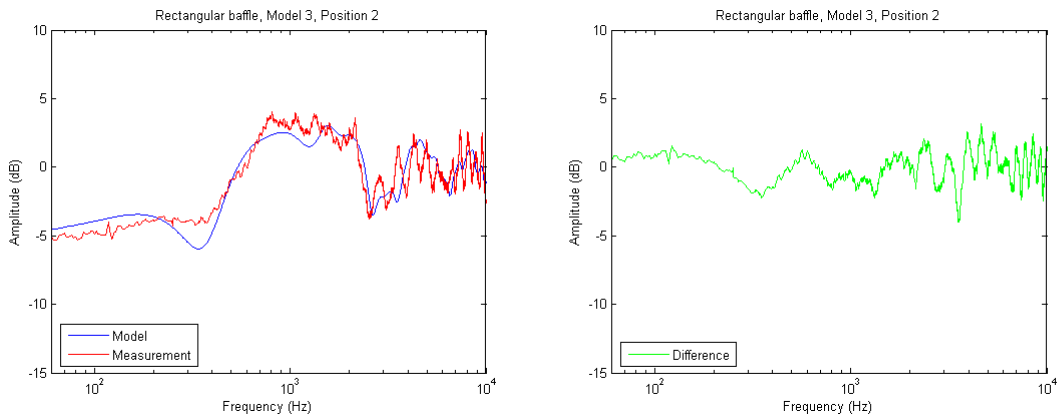
Figure 91 – Frequency response with rectangular baffle and test point at position 2.

For point 3 was the source moved 50 % along the horizontal axe to a position often seen used for the treble unit for small two-way loudspeaker boxes ($x_S = 0.15$ m, $y_S = 0.085$ m).
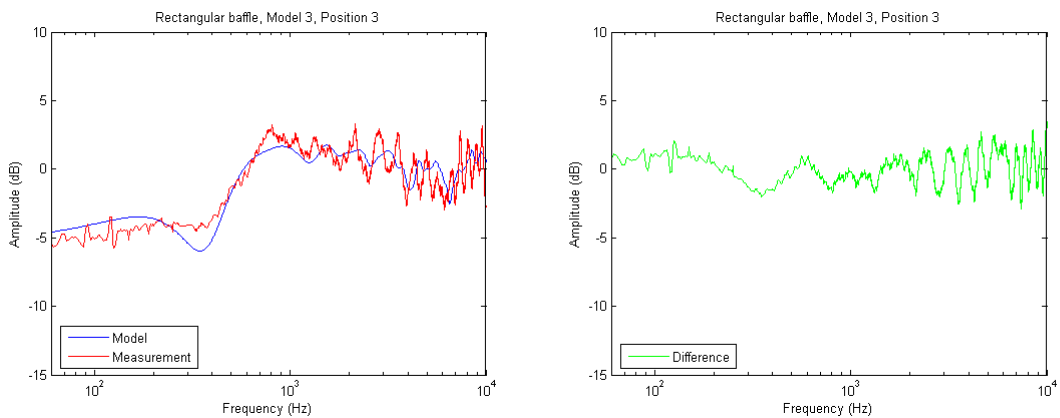
Figure 92 – Frequency response with rectangular baffle and test point at position 3.

The results are quite satisfactory with most of the simulation within ±3 dB relative to the measurements.

4.9.5 Reflection coefficient reviewed

It seems that the simulation has become slightly "wilder" so the effect of a minor change of the reflection coefficient value will be tested with the reflection coefficient changed ±15 % and the result is shown below. The curve for the low-amplitude value (–0.50) is smooth and come close to the measurements while the high-amplitude value (–0.70) is obviously wrong. For comparison is the result using the current value (–0.60) slightly on the high side (see Figure 82); however, it is the correct choose when the model is using first-order diffraction (see Figure 72).

The conclusion is that an optimal value (for thin baffles) will be within the range:

$$-0.50 \leq R \leq -0.60 \qquad\qquad 80$$

The value used by Bews & Hankford and by Urban et al. is –0.50 and Wright reports –0.58 as result from a simulation run. The value used by Vanderkooy is within the range for source to observer angle via the edge of $0 < \chi < 67°$, which dictates very short measurement distance so his typical value is higher.
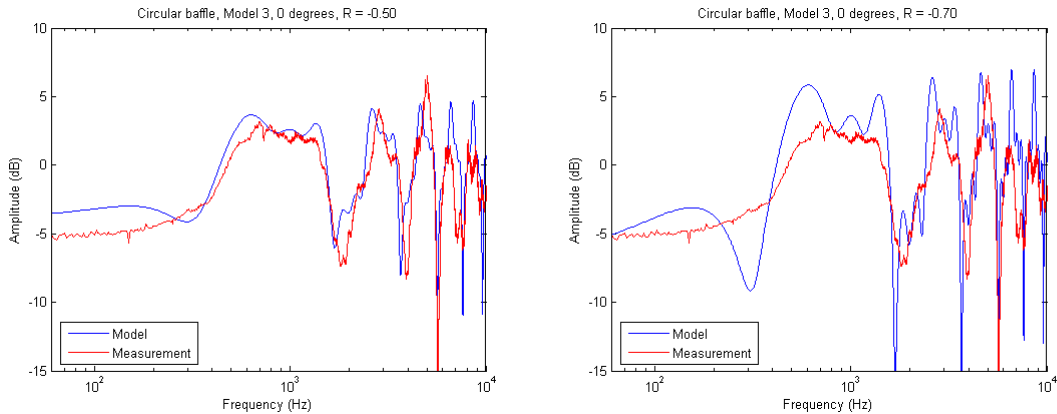
Figure 93 – Frequency response using reflection coefficient –0.50 (left) and –0.70 (right).

The Rayleigh theory used by Bews & Hankford (equation 49) can be written in a more appropriate form (Urban, 1045):

$$R = \frac{1}{2}\left(\frac{4\pi}{4\pi - \gamma} - 2 \right)$$

The interior wedge angle is $\gamma = 2\pi$ for an infinite baffle where the reflection coefficient becomes $R = 0$ so there is no reflection from the non-existent border; $\gamma = \pi$ for a boxlike cabinet where $R = -0.33$, which indicates that 67 % of the signal is transmitted around the edge to the shadow side; and $\gamma = 0$ for a thin baffle where $R = -0.50$ so 50 % of the signal is reflected back into the front side and 50 % is transmitted to the shadow side.

According to the present work should the factor ½ in front of the equation be a parameter with a value given by equation 80.

4.9.6 Loudspeaker directivity

It was the intention to model the behaviour of the baffle alone and not to include the effects related to the loudspeaker, such as its directivity and smearing. However, the model can easily be modified to include a model of the loudspeaker. The directivity can be described as the diffraction caused by plane waves travelling through a circular aperture (see section 5.1.1), which gives an analytic expression of loudspeaker directivity.

The dependency to observation angle is described through the following equation θ is the observation angle with 0° for loudspeaker on-axis:

$$F(\theta) = \frac{2J_1(ka \sin(\theta))}{ka \sin(\theta)} \qquad 81$$

This model must be included at two places. The first place is to affect the direct sound from the loudspeaker, which is described by function $F(\theta)$ for the selected observation angle and where on-axis corresponds to $F(0) = 1$ and is independent upon frequency. The second place is to affect the sound that is propagating toward the baffle edge and this is described through $F(90°)$ with strong dependency on ka since the sine function is unity.

The transfer functions used for the above plots were written into the MATLAB program as *Edge diffraction model 4* using the following algorithm:

$$H_F(f) = F(\theta) + F(0)\frac{R}{2\pi}\sum_{n=1}^{N}\left(1 + R\left(\frac{b_n + r_n}{b_n + e_n + r_n} + R\frac{b_n + r_n + e_n}{b_n + r_n + 2e_n}\right)\exp(-ike_n)\right) \times$$

$$\frac{r_0}{b_n + r_n}\exp(ik[r_0 - b_n - r_n])\Delta\varphi_n$$

$$H_R(f) = F(0)\frac{T}{2\pi}\sum_{n=1}^{N}\left(1 + T\left(\frac{b_n + r_n}{b_n + e_n + r_n} + T\frac{b_n + r_n + e_n}{b_n + r_n + 2e_n}\right)\exp(-ike_n)\right) \times$$

$$\frac{r_0}{b_n + r_n}\exp(ik[r_0 - b_n - r_n])\Delta\varphi_n$$

82

Execution time was increased to 20 seconds due to the addition of the Bessel functions.

The result for $a = 0.1$ m corresponding to an 8 inch bass loudspeaker is shown below for the on-axis (0°) and off-axis (30°) responses and compared to the existing measurements.
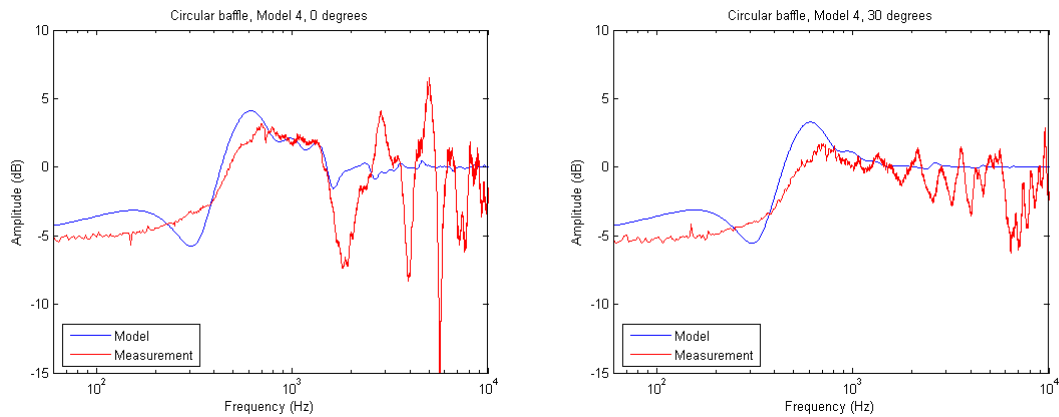
Figure 94 – Frequency response with loudspeaker directivity included within the model.

The reduction in high-frequency ripple is easily observed and indicates that the effect of the baffle is reduced at high frequencies. A loudspeaker is directive for $ka > 1$ corresponding to frequencies above 550 Hz where radiation is gradually becoming concentrated along 0°. The model can not be expected valid at the highest frequencies since a real loudspeaker will suffer from break-up for frequencies above $ka \approx 2\pi$ where the wavelength is comparable to the circumference and this corresponds to 3.5 kHz for $a = 0.10$ m.

4.9.7 Fourth-order diffraction component

There is a simple scheme for addition of fourth/order diffraction components or even higher corrections but this is not required and it will most probably not cause any improvement of the simulation. There are two reasons for this.

First of all is the level of high-order diffraction components scaled by R^n so the level becomes reduced with increasing order. The amplitude scaling is $R^1 = -0.60$ for the first-order diffraction component, $R^2 = 0.36$ for the second-order component and $R^3 = -0.22$ for the third-order component. There is no reason to include higher order diffraction components since the

next scaling factor becomes $R^4 = 0.13$ so the correction is limited to ±13 % (±1 dB) when related to the direct signal.

Secondly, the model is approximate and assumes that the diffraction components can be described through one edge source per edge source, i.e. there are no phase spreading so signal blurring is probably not modelled correctly.

4.9.8 Conclusion

The numerical edge diffraction model performs very well for observation points within approximately ±60° of on-axis but fails for angles approaching the edge at ±90° where the level departs 5 dB from the measured response. However, this is an improvement to the Vanderkooy model where the levels are approaching infinity (Vanderkooy, 926). The rear side response for more than ±90° is not modelled correctly since the difference from the measured data is too large to be accepted.

A model based upon a numerical approach must operate fast to be of interest and the implementation fulfils this requirement by providing one with a full 6400 point frequency response within 5 seconds using 200 edge sources and a standard personal computer.

The *distributed edge dipole* model of Urban et al. will now be considered. The model differs from the edge diffraction model by removing the imaginary plane between front side and rear side and the inclusion of angular form factors for both the main source and the edge sources. Apart from these changes is the model very similar to the numerical edge diffraction model and the required changes within the algorithm represents minimal workload.

4.10 Distributed Edge Dipole model

The model of Urban et al. takes its offspring from a theoretical study of the driving pressure for a source mounted in a finite baffle. The ratio of this sound pressure to the sound pressure of the source mounted on an infinite baffle was showed to be described by:

$$F_0(\theta) = \frac{1 + \cos(\theta_0)}{2}$$

Urban et al. states that the equation is derived using the Kirchhoff approximation and that this is not validated for angles above 90° but they assume that the equation can be used for all angles. The main direction for output from the source is on-axis (0°) where the expression is unity, At the edge of the baffle (90°) is the sound pressure reduced to 0.50 and at the rear side (>90°) is expression the level reduced and approaches zero at 180°.
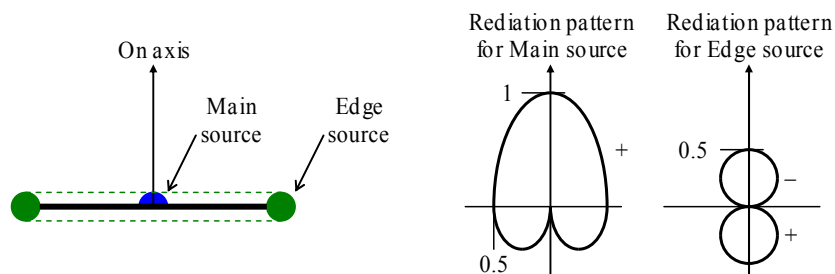
Figure 95 – Angular form factors for the main and edge sources.

An important distinction from the edge diffraction model is that the main source is active for all observation angles and that the edge sources are continuous across the boundary.

Another important difference from the edge diffraction model is the definition for the edge sources where Urban et. al. quotes Vanderkooy for an experiment with a tweeter mounted at the centre of a circular baffle:

> It was observed that the wave radiated from the edges was in phase opposition when facing the baffle (illuminated zone) and in phase when the observation point was behind the baffle (shadow zone). This experimental result prompted us to visualise the phenomenon in the following way.
>
> When the main piston compresses the air at very low frequencies, the air flows in every direction and, in particular, along the baffle surface until it reaches the edge, turns around, and goes behind. This movement of the air around the edge is like a "ring piston" moving backward in opposition to the main piston. It is thus possible to understand the "phase reversing" in the illuminating zone and the "in-phase" pressure in the shadow zone. (Urban, 1046).

The edge sources can be described as a distributed dipole source, which is the origin to the name of the model.

$$F_n(\theta) = -\frac{1}{2}\cos(\theta_n)$$

Hence, the edge sources radiates into the front side with amplitude –0.50 at on-axis and the amplitude of the radiation is gradually reduced to zero toward the edge (90°) and then increased within the rear side onto +0.50 at 180°.

The model will be implemented using the basic ideas from the edge diffraction model and the figure below defines the nomenclature for the various angles required by the angular form factors.
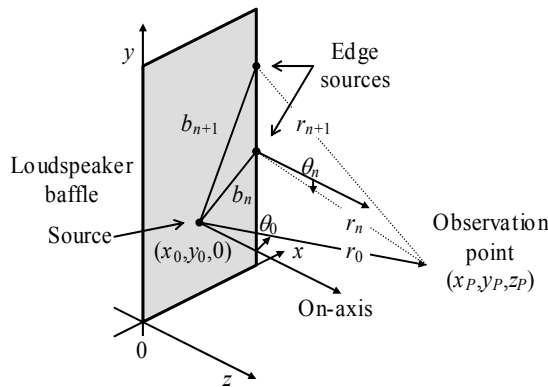
Figure 96 – Definition of the coordinate system used for the DED model. The baffle can be located arbitrarily within the coordinate system although $z_0 = 0$ is a requirement.

The observation angle θ for the main source is the angle between r_0 and the normal defining the loudspeaker on-axis and this is a vector parallel to the z-axis. For the main source is the observation angle given by a little trigonometry:

$$r_0 \sin(\theta_0) = \sqrt{(x_P - x_S)^2 + (y_P - y_S)^2} \quad \Rightarrow \quad \theta_0 = \arcsin\frac{\sqrt{(x_P - x_S)^2 + (y_P - y_S)^2}}{r_0}$$

The main source (the loudspeaker) located at $(x_0, y_0, 0)$, the edge sources at $(x_n, y_n, 0)$ and the observation point at (x_P, y_P, z_P). The variables x_P, y_P, x_n and y_n are defined in section 4.8. For the edge source is the observation angle given by an equivalent expression:

$$r_n \sin(\theta_n) = \sqrt{(x_P - x_n)^2 + (y_P - y_n)^2} \quad \Rightarrow \quad \theta_n = \arcsin \frac{\sqrt{(x_P - x_n)^2 + (y_P - y_n)^2}}{r_n}$$

The main source was unity in the previous edge diffraction model so the angular form factor F_0 is substituted for the "1" in the H_F expression of equation 74. The edge sources are "weighted" by F_n so this factor is simply multiplied onto the expression within the summation and the reflection coefficient is removed from the equation.

The DED algorithm becomes:

$$H(f) = \frac{1 + \cos(\theta_0)}{2} - \frac{1}{2}\left(\frac{1}{2\pi} \sum_{n=1}^{N} \frac{r_0}{b_n + r_n} \exp(ik[r_0 - b_n - r_n])\cos(\theta_n)\Delta\varphi_n \right) \qquad 83$$

The equations were written to the MATLAB file as the *DED model* and the result is shown below.

4.10.1 Examples

The frequency response is shown below for different observation angles. The DED model performs very well for 0° and 30° although the ripple amplitude is somewhat lesser than the measurement.
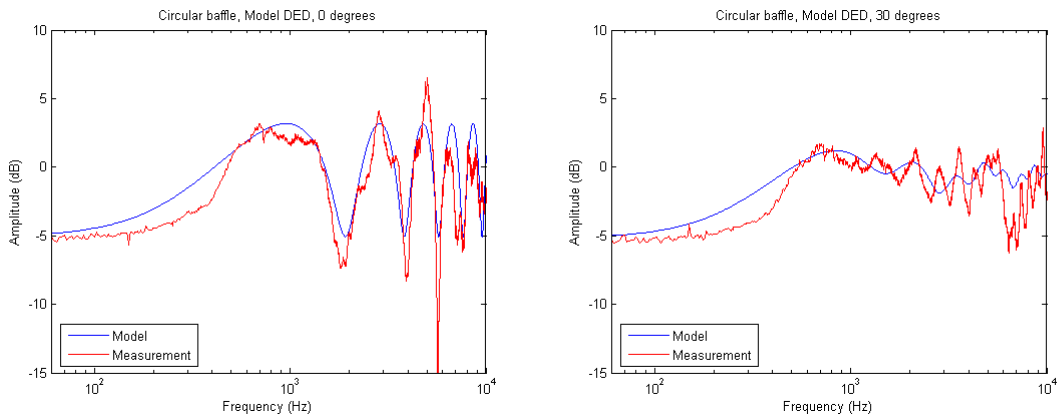
Figure 97 – Frequency response for the DED model.

For an observation angles 60° is the response better than with the Edge diffraction model although the over-all level is slightly below the measured value. Anyway, the model is robust and can accept 90° of observation angle, which is an improvement compared to the edge diffraction model.
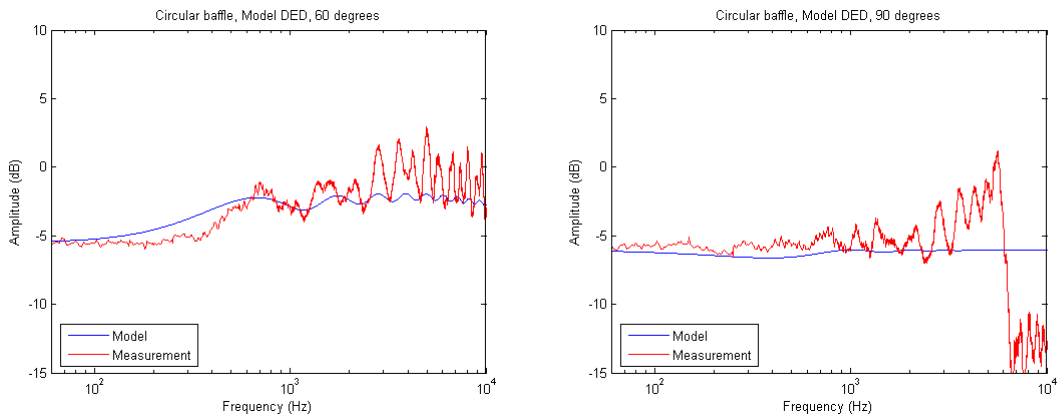
Figure 98 – Frequency response for the DED model.

For the rear side is the response less impressing and the simulated level is higher than the measurements for 120°, 150° and 180°.
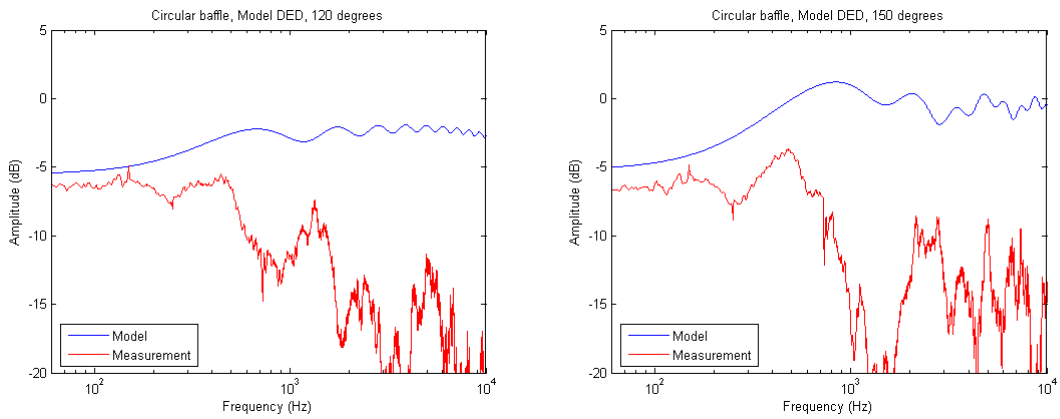
Figure 99 – Frequency response for the DED model.

The final simulation for 180° shows strong ripples.
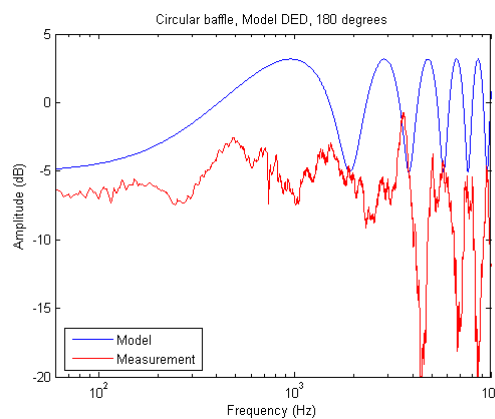
Figure 100 – Frequency response for the DED model.

The rear side is not well modelled; in this respect was the edge diffraction model a better suggestion.

4.10.2 Modification

The results are impressive but the general view is that amplitude changes on front side are modelled on the low side while the signal in the rear side is too high. It was therefore tempting to reintroduce the reflection coefficient.

The modified DED algorithm becomes:

R = -0.6

$$H(f) = \frac{1 + \cos(\theta_0)}{2} + \frac{R}{2\pi} \sum_{n=1}^{N} \frac{r_0}{b_n + r_n} \exp(ik[r_0 - b_n - r_n]) \cos(\theta_n) \Delta\varphi_n \qquad 84$$

The equations were written to the MATLAB file as the *DED model* and the result is shown below.

4.10.3 Examples

The results for 0° and 30° are generally improved by the correction although the level at the low-frequency end is slightly below the measured value.
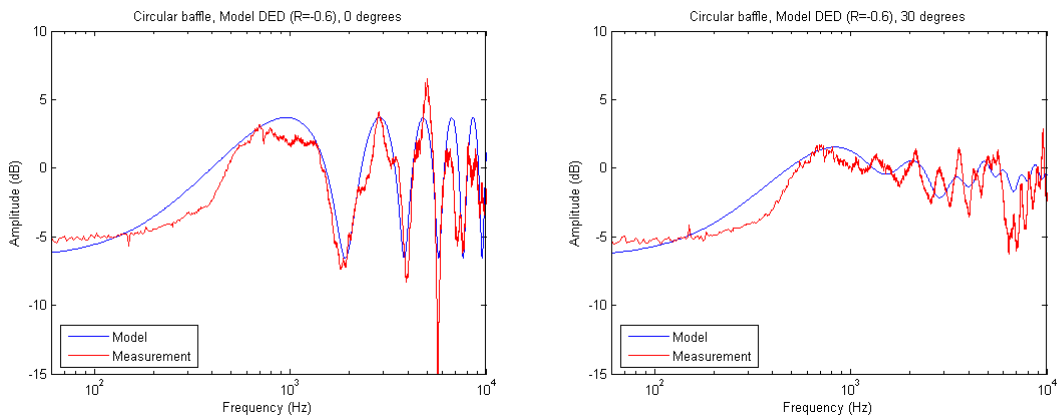
Figure 101 – Frequency response for the modified DED model.

The changes are barely visible for 60° but the responses are at least not invalidated by the modification. The 90° simulation is not changed but this is absolutely correct; the diffraction sources are silent at this angle due to the cosine function.
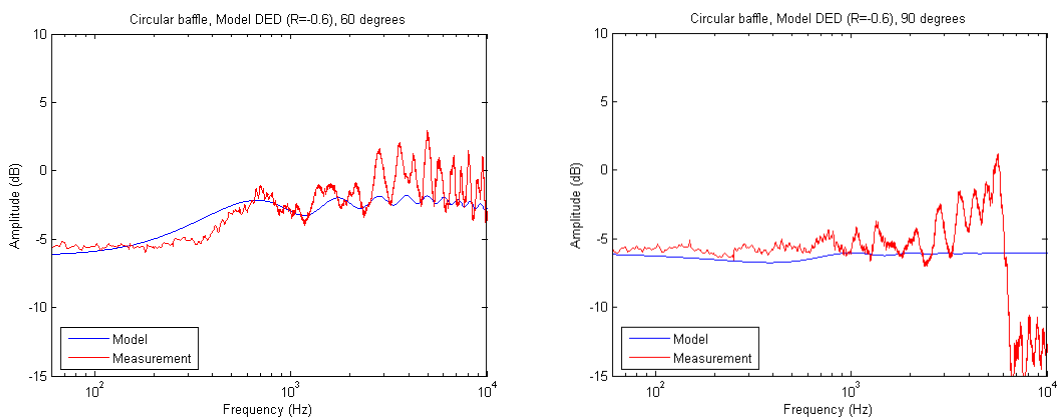
Figure 102 – Frequency response for the modified DED model.

The results for 120° and 150° are slightly improved by the approximately 1 dB lowering of the signal level within the rear side but the difference between the simulated values and the measured is still relatively large.
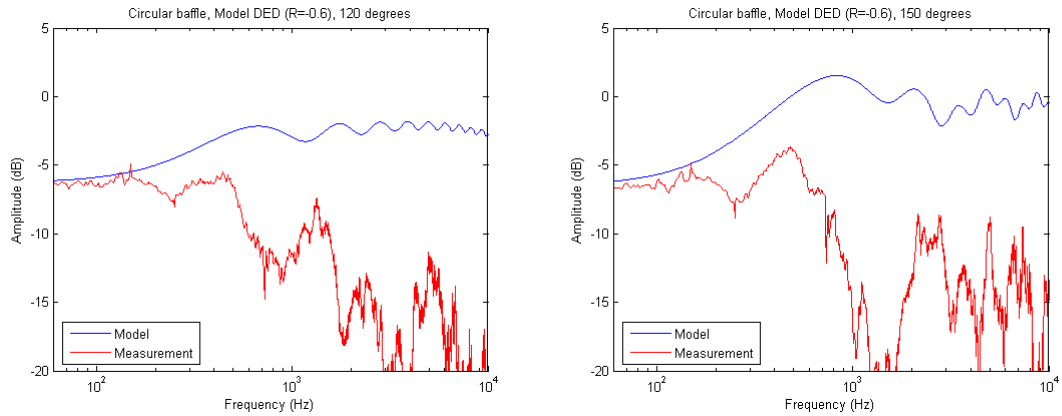
Figure 103 – Frequency response for the modified DED model.

The response for 180° is also closer to the low-frequency level but the amplitude of the high-frequency ripples is increased.
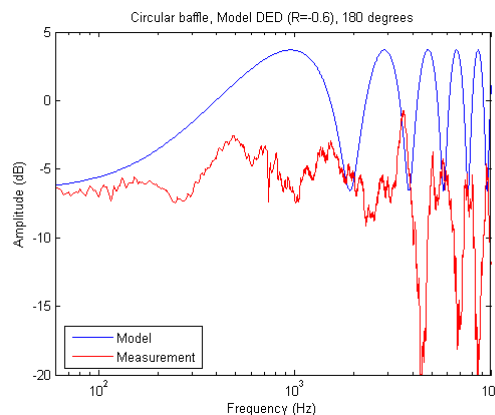
Figure 104 – Frequency response for the modified DED model.

The value –0.60 of the reflection coefficient is slightly better suited than the value –0.50 as was proposed by Urban et al. but the difference is not large.

4.11 Conclusion

The distributed edge diffraction model by Urban et al. is an excellent simulation model for the observation range up to and including the edge of the baffle at 90° where the response is very well reproduced. However, the model is incorrect for larger observation angles where the simulated level is increased and thus departing from the measurement. This range is better represented by the numerical edge diffraction model.

This concludes the diffraction models and the next chapter will address the wavelet model.

5 Wavelet models

According to the principle of Christiaan Huygens (Holland, 1629-1695) is any point of a wave front a region of disturbance, which acts as a source of secondary waves, wavelets, and the position of the wave front at a later time is the envelope of the wavelets. The method was devolved within the field of optics and describes diffraction as any deviation from geometrical optics that results from the obstruction of a wave front of light (Pedrotti, 324).
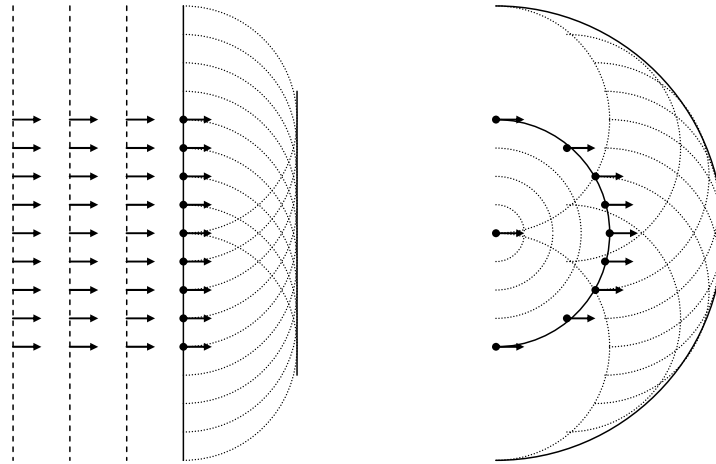
Figure 105 – Graphical representation of Huygens principle with plane waves (left) and spherical waves (right); the wave front is assumed to emit secondary waves, known as wavelets, that add up to the resulting wave front at later time.

If both the source and observation points are at large distance from the diffraction aperture, so that the wave fronts are approximating plane waves, it is *far-field diffraction* with the theory according to Joseph von Fraunhofer (Germany, 1878-1826); when this is not the case and the curvature of the wave front must be taken into account, it is *near-field diffraction* with the theory developed by Augustin Jean Fresnel (France, 1788-1827). Both theories will be addressed within this study.

Visible light is electromagnetic waves, as well as thermal radiation and radio waves for terrestrial broadcast, and the waves propagate without any medium required between the source and observer. Audible sound is pressure waves propagating through a medium, such as air or water, so the results from the field of optics cannot be assumed to apply directly to acoustics; however, both fields are described through the wave equation and therefore share the same basic solutions. Acoustical signals operate with wavelengths from 20 mm to 20 m so the far-field assumption is rarely met in real life and can only be considered fulfilled at high frequencies so the Fresnel near-field theory must be considered in most cases.

The far-field theory is used to introduce the wavelet theory by deriving expressions for the sound pressure behind an aperture, which is here limited to an opening within an infinite baffle, and the results is compared to the well-known theory of loudspeaker radiation patterns. The near-field theory leads to the Fresnel integral and Cornu spiral, which are tools for calculating the frequency response behind an infinite edge, which is used as a model of the loudspeaker edge. The models are then combined to describe the radiation from a loudspeaker with finite baffle.

5.1 The Fraunhofer far-field approximation

The resultant sound pressure at the observation point is calculated from summation of the contributions from infinitesimal sound sources, wavelets, which are described through the infinitesimal area dS and the particle velocity u of the plane wave. The sound pressure within a plane wave is $p = \rho c u$, where ρc is the specific impedance of air. Since the volume velocity is $q = Su$ and u is constant for a plane propagating wave, we have the following relation for the infinitesimal volume velocity of a plane wave:

$$\frac{dq}{dS} = \frac{dSu}{dS} = u \quad \Rightarrow \quad dq = udS \qquad 85$$

Each wavelet is represented by a point source, which is assumed radiating equally well in any direction, so the infinitesimal sound pressure at the observation point at distance r from the wavelet with particle velocity u and infinitesimal area dS becomes:

$$dp = \frac{ik\rho c}{4\pi r}\exp(-ikr)udS \qquad 86$$

A plane wave is not physically realisable but it can be assumed that the wave front is locally plane within a limited region if the distance to the source is sufficiently large.

5.1.1 Circular aperture

Plane waves hitting an infinite baffle with a circular aperture may represent a conventional loudspeaker within an infinite baffle assuming that the loudspeaker diaphragm is a plane vibrating piston. The model shows that the theory applies equally well to physical pistons as to imaginary vibrating surfaces.
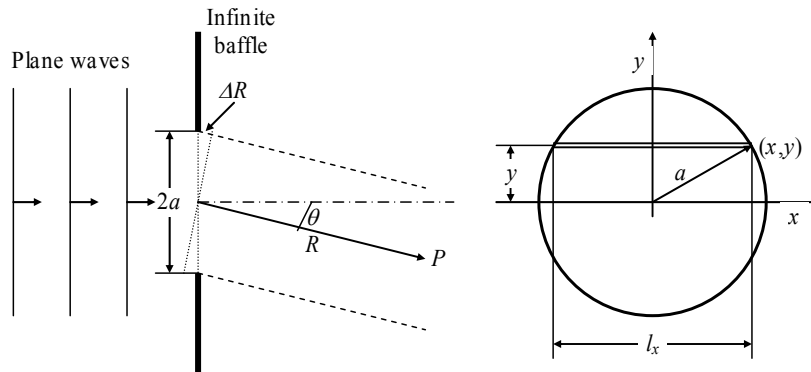
Figure 106 – *Left*: Plane waves are approaching an infinite baffle with circular aperture.
Right: Integration uses a horizontal strip of width lx and height dy to cover the aperture.

The infinitesimal area within the aperture is $dS = l_x dy$ according to Figure 106, so the infinitesimal sound pressure at the observation point becomes:

$$dp = \frac{ik\rho cu}{4\pi r}\exp(-ikr)l_x dy$$

The resultant sound pressure at the observation point is given by:

$$p = \int_{-a}^{a} \frac{ik\rho cu}{4\pi r}\exp(-ikr)l_x dy$$

Using the equation for the circle, $x^2 + y^2 = a^2$, where x and y are variables within a rectangular coordinate system and a is radius of the circle, we can solve for x as: $x^2 = a^2 - y^2$. The length of the horizontal strip l_x is 2 times the x-value since it is the distance from $-x$ to x:

$$l_x = 2\sqrt{a^2 - y^2}$$

The distance r from the wavelets within the strip to the observation point is dependent upon the y-coordinate and the observation angle:

$$r = R + y\sin(\theta)$$

The integration becomes:

$$p = \frac{ik\rho cu}{4\pi}\int_{-a}^{a}\frac{2\sqrt{a^2 - y^2}}{R + y\sin(\theta)}\exp(-ik(R + y\sin(\theta)))dy$$

Using the assumption of large distance to the observation point simplifies the denominator since the relation to y can be ignored but this is not possible with the phase term. The constant terms can be moved outside the integral.

$$p = 2\frac{ik\rho cu}{4\pi R}\exp(-ikR)\int_{-a}^{a}\sqrt{a^2 - y^2}\exp(-iky\sin(\theta))dy$$

The square root is rewritten by moving radius outside the integration.

$$p = 2a\frac{ik\rho cu}{4\pi R}\exp(-ikR)\int_{-a}^{a}\sqrt{1 - \left(\frac{y}{a}\right)^2}\exp(-iky\sin(\theta))dy$$

This integral takes the standard integral form upon making the substitutions (Pedrotti, 332):

$$v = \frac{y}{a}\quad\text{and}\quad\gamma = ka\sin(\theta)$$

Integration is through y from $-a$ to a so the corresponding range for v is from -1 to 1 and the incremental variable is substituted by $dy = adv$. Hence, the integral:

$$p = 2a^2\frac{ik\rho cu}{4\pi R}\exp(-ikR)\int_{-1}^{1}\sqrt{1 - v^2}\exp(-i\gamma v)dv$$

The definite integral is computed into (Pedrotti, 333):

$$p = 2a^2\frac{ik\rho cu}{4\pi R}\exp(-ikR)\frac{\pi J_1(\gamma)}{\gamma}$$

$J_1(\gamma)$ is the first-order Bessel function of the first kind and the ratio $J_1(\gamma)/\gamma$ approaches $\frac{1}{2}$ for γ approaching zero and it is observed that πa^2 represents the area of the circular aperture. The sound pressure at distance R and observation angle θ becomes:

$$p = \frac{ik\rho c\pi a^2 u}{4\pi R}\exp(-ikR)\frac{2J_1(ka\sin(\theta))}{ka\sin(\theta)} \qquad 87$$

The factor $\pi a^2 u$ represents the volume velocity through the aperture.

Dependency to frequency and observation angle is plotted below for *ka* values up to 20 and observation angles up to 90°. A similar expression is found in the literature for the directivity of a circular piston within an infinite baffle (Leach, 25).
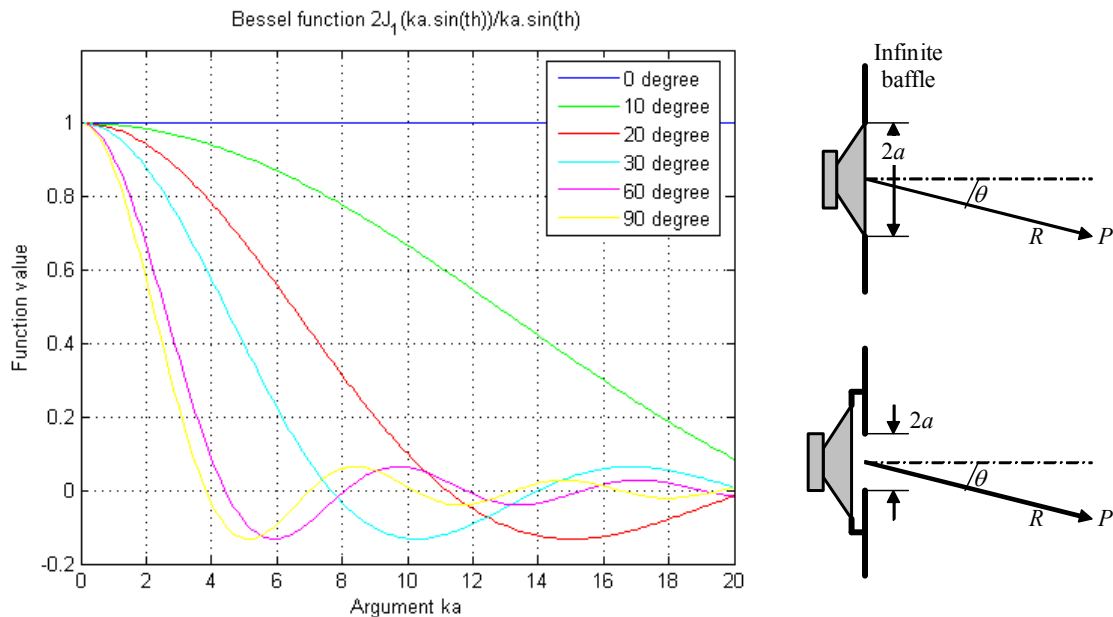
Figure 107 – Directivity pattern for circular aperture within an infinite baffle at different *ka* values and observation angles (left); definition of observation angle (top right) and an example of using an aperture to increase the beam width by lowering radius (bottom right).

At low frequencies is the expression $2J_1(ka\sin(\theta))/ka\sin(\theta)$ approaching unity so the sound output from the circular aperture is independent upon frequency and observation angle. The beam width is narrowed at higher frequencies or for large aperture radius. The beam width will in this study be defined at the first zero of the Bessel function (Asmar, 251).

$$J_1(ka\sin(\theta)) = 0 \quad \Rightarrow \quad ka\sin(\theta) = 3.832 \quad \Rightarrow \quad f = \frac{3.832c}{2\pi a \sin(\theta)} \approx 0.61\frac{c}{a\sin(\theta)} \qquad 88$$

The first zero-frequency becomes 2.1 kHz for $a = 0.1$ m and $\theta = 90°$. As can be seen from the figure above is the –3 dB point reached for an argument of approximately 1.61, which corresponds to the above formula with factor 0.61 changed to 0.26, hence, the set-up will show a –3 dB frequency around 900 Hz and a null at 2.1 kHz both at 90°.

The importance of the result is the concentration of sound within a limited region in front of the loudspeaker for increased frequency; so radiation from the loudspeaker toward the edge is becoming reduced at high frequency thus reducing the reflection from the cabinet edges.

One way of increasing the observation range for a given loudspeaker (typically a bass loudspeaker) is to mount the loudspeaker behind a circular aperture with radius less than the radius of the diaphragm thus reducing *a*. If the volume velocity from the loudspeaker remains unchanged despite the increased loading then the resulting sound pressure remains unchanged since the particle velocity at the aperture is increased by the ratio of cross-sectional areas. However, it is more likely that the volume velocity will be reduced by the increased loading. Other known problems are that the cavity in front of the loudspeaker becomes a Helmholtz resonator and that the output from the loudspeaker is delayed with respect to the output from other loudspeakers mounted on the same baffle.

The frequency response is shown below at different observation angles for a circular baffle with radius a = 0.1 m, thus representing a typical 8 inch bass loudspeaker. The curve for 0° was calculated using 1° observation angle to avoid division with zero, hence the slight drop off at the high frequency end.
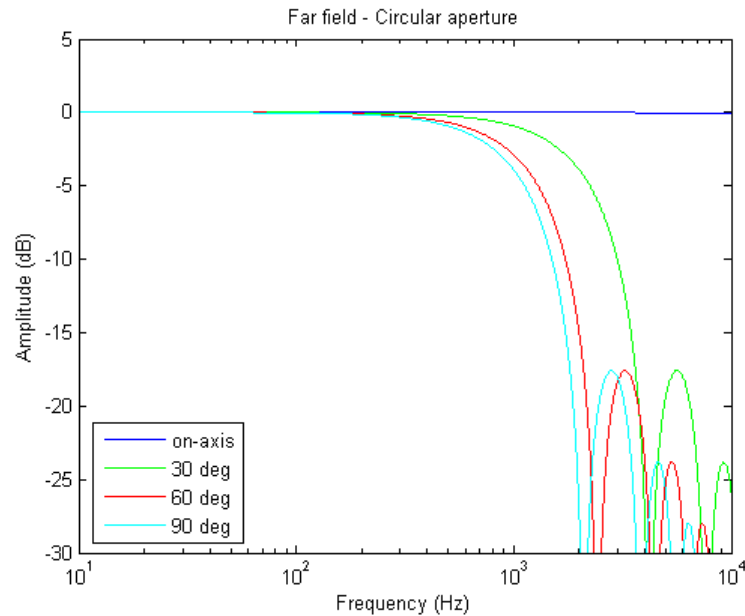
Figure 108 – Frequency response for circular aperture with radius 100 mm.

The high-frequency response is cut-off above 2 kHz for an observation angle of 30° and above 1 kHz for larger observation angles. The radiation at 90°is toward the edge so this must be taken into account for the model to represent the physical loudspeaker.

5.1.2 Rectangular aperture

Plane waves hitting an infinite baffle with a rectangular aperture may represent an array of loudspeakers mounted close together on the same baffle and oscillating in phase or an electrostatic loudspeaker mounted within an infinite baffle and assuming that the diaphragm is vibrating uniformly. Another application is sound propagation from one (large) room to the next through the door opening between the rooms or music output through a window.

The infinitesimal area of the aperture is $dS = dxdy$ so the infinitesimal sound pressure at distance r from each wavelet becomes:

$$dp = \frac{ik\rho cu}{4\pi r}\exp(-ikr)dxdy$$

The sound pressure at the observation point is found through integration over the rectangular aperture, which is through x from $-A/2$ to $A/2$ and y from $-B/2$ to $B/2$:

$$p = \int_{-B/2}^{B/2}\int_{-A/2}^{A/2}\frac{ik\rho cu}{4\pi r}\exp(-ikr)dxdy$$
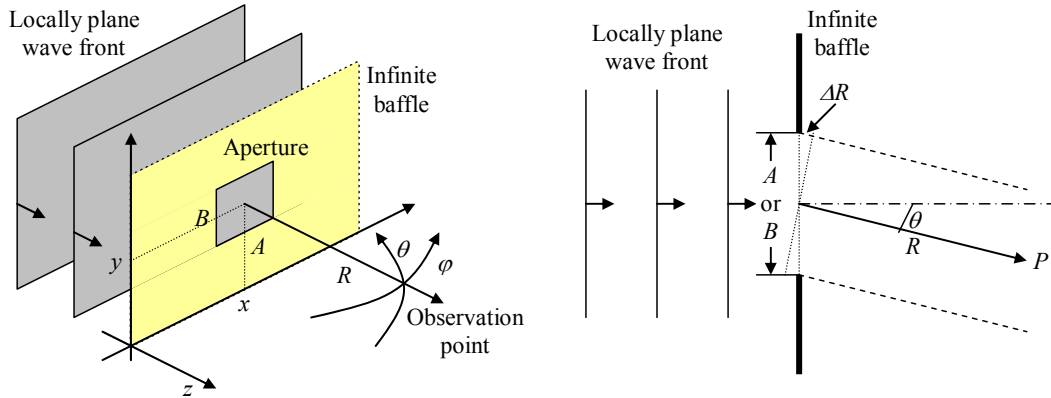
Figure 109 – Plane waves are approaching an infinite plane baffle with rectangular aperture.

For on-axis measurement is the distance from any wavelet to the observation point equal to R plus or minus a small distance ΔR, which is due to the observation angle. Using θ_H for the horizontal observation angle this distance becomes $x\sin(\theta_H)$ where x is the horizontal position within the aperture. A similar result is obtained for the vertical plane with θ_V as the vertical observation angle so the distance r between each wavelet and the observation point becomes:

$$r = R + x\sin(\theta_H) + y\sin(\theta_V)$$

The amplitude of the wavelet is given by the denominator and the variation due to the x and y terms can be assumed negligible at large distance, simplifying the integral by setting $r = R$ so the amplitude term can be moved outside:

$$p = \frac{ik\rho cu}{4\pi R}\exp(-ikR)\int_{-A/2}^{A/2}\exp(-ikx\sin(\theta_H))dx\int_{-B/2}^{B/2}\exp(-ikx\sin(\theta_V))dy$$

The error due to this assumption becomes $(A/2 + B/2)/R$ at the extremes of the aperture. Allowing for 10 % of error is the requirement $R = 5(A + B)$ so an aperture with $A = B = 1$ m, i.e. a window within a large wall, requires 10 m of distance to satisfy the far-field condition.

The integrals are equivalent so the derivation will be shown for one integral only:

$$\int_{-A/2}^{A/2}\exp(-ikx\sin(\theta_H))dx = \frac{1}{ik\sin(\theta_H)}\left[\exp(-ikx\sin(\theta_H))\right]_{-A/2}^{A/2}$$

$$= \frac{2A}{2ikA\sin(\theta_H)}\left[\exp\left(-i\frac{kA\sin(\theta_H)}{2}\right) - \exp\left(i\frac{kA\sin(\theta_H)}{2}\right)\right]$$

Using Euler's formula for the sine function (Westergren, 62):

$$\int_{-A/2}^{A/2}\exp(-ikx\sin(\theta_H))dx = -\frac{2A}{kA\sin(\theta_H)}\sin\left(\frac{kA\sin(\theta_H)}{2}\right) = -A\,\mathrm{sinc}\left(\frac{kA\sin(\theta_H)}{2}\right)$$

A similar expression is found for the *y*-coordinate. The sound pressure at the observation point within the far field from a rectangular aperture becomes:

$$p = \frac{ik\rho cABu}{4\pi R}\exp(-ikR)\,\text{sinc}\!\left(\frac{kA\sin(\theta_H)}{2}\right)\text{sinc}\!\left(\frac{kB\sin(\theta_V)}{2}\right) \qquad 89$$

Note that *ABu* is the volume velocity through the aperture and that the directivity functions for the *x* and *y* directions are independent and can be described by the same plot, which is shown below. Note the similarity to the plot for the circular aperture.

The response is shown for *kA* or *kB* up to 20.
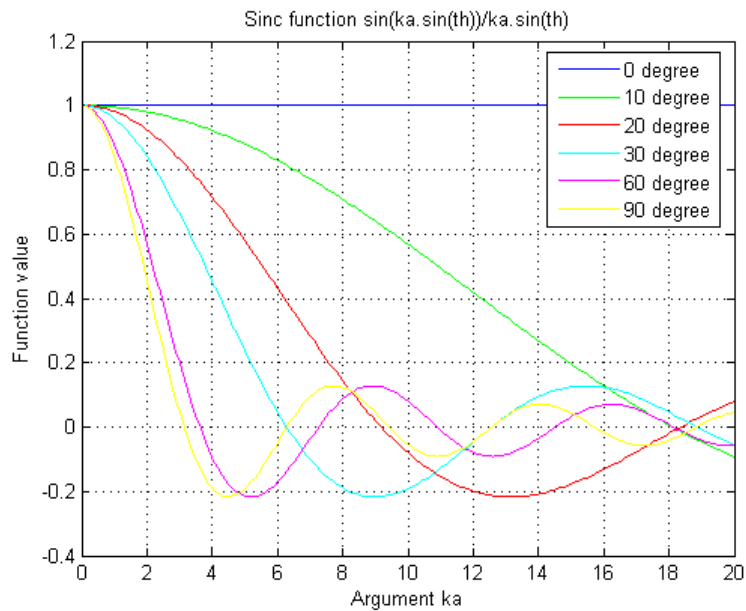
Figure 110 - Directivity pattern for rectangular aperture within an infinite baffle at different
_ka_ values (_ka = kA_ or _kB_) and observation angles.

At low frequencies where *kA* and *kB* are approaching zero is the sound pressure independent upon the observation angle and the sound is spread equally well is any direction in front of the baffle. The sinc functions come into play at higher frequencies where it is limiting the beam width thus concentrating the sound in front of the aperture.

The first zero of the sinc function will be used in this study defining the beam width:

$$\text{sinc}\!\left(\frac{kA\sin(\theta_H)}{2}\right) = 0 \quad \Rightarrow \quad \frac{kA\sin(\theta_H)}{2} = \pi \quad \Rightarrow \quad f = \frac{c}{A\sin(\theta_H)}$$

A similar equation is found for the vertical plane. The first zero is 3.5 kHz for a rectangular aperture with $A = 0.1$ m and $\theta_H = 90°$. Using the frequency for -3 dB, the argument must equate 1.38 and the frequency becomes 0.22 times the above calculated value. Hence, the set-up will show a -3 dB frequency about 770 Hz and a null at 3.5 kHz both measured at 90°. The zero is moved to 4.9 kHz for $\theta_H = 45°$.

When the area of the circular aperture is equal to that of a square aperture ($A = B$) we get the relation $A = 1.77a$ and the zero frequency of the square aperture becomes:

$$f = 0.56 \frac{c}{a \sin(\theta)}$$

This is less than 8 % below the zero frequency for the circular aperture, so the two apertures behave similar when related to area although the radiation pattern from a circular aperture is independent upon rotation around on-axis while the rectangular aperture is not.

The frequency response is shown below at different horizontal observation angles for the rectangular aperture with $A = 0.1$ m /horizontal) and $B = 0.2$ m and (vertical) corresponding to a square sound source with width 0.2 m and height 0.4 m. The curve for 0° was calculated using 1° observation angle to avoid division with zero, hence the on-axis drop off toward high frequencies. The responses are similar to that of the circular aperture.
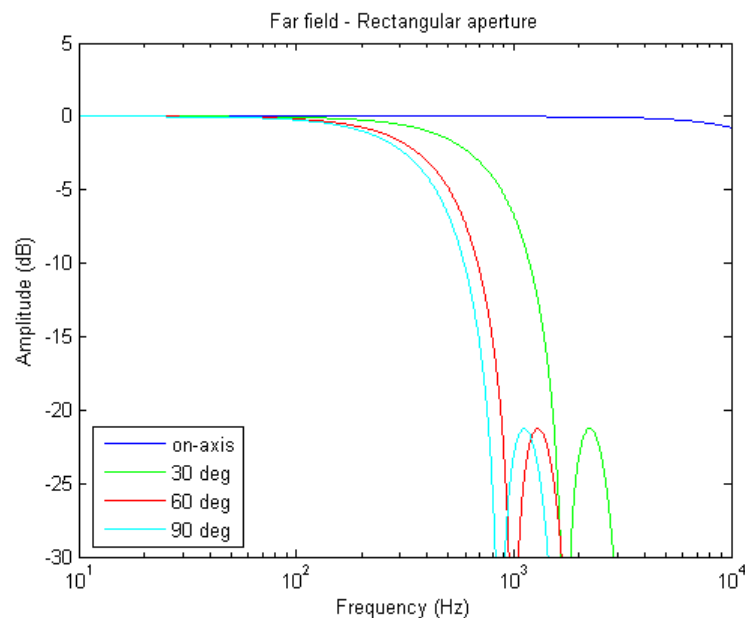
Figure 111 – Frequency response for rectangular aperture with A = 100 mm.

According to equation 24 is the sound pressure of a plane wave $p = \rho c u$ so the transfer function can be derived by dividing equation 89 with the sound pressure of the undisturbed plane wave:

$$M(f) = \frac{fAB}{2cR} \operatorname{sinc}\left(\frac{kA \sin(\theta_H)}{2} \right) \operatorname{sinc}\left(\frac{kB \sin(\theta_V)}{2} \right) \xrightarrow{k,\theta \to 0} \frac{fAB}{2cR}$$

The magnitude of the sound pressure at the observation point is proportional to the surface area of the aperture AB and inversely proportional to distance R. This corresponds to the well-known situation of a person opening a door into a building with loud music; the sound pressure outside the building is increased while the surface area of the opening is increased and becomes reduced when the observer walks away from the opening.

Assuming that the wave front is due to a spherical sound source within the building but can be assumed locally plane at the aperture, then the reference sound pressure of the undisturbed wave front becomes proportional to frequency according to equation 33 thus removing the

frequency dependency of the above equation; hence, the aperture does not in itself attenuate the sound as function of frequency.

$$M(f) = \frac{ABu}{q} \text{sinc}\left(\frac{kA\sin(\theta_H)}{2}\right)\text{sinc}\left(\frac{kB\sin(\theta_V)}{2}\right) \xrightarrow{k,\theta \to 0} \frac{AB}{S}$$

It is assumed that the relation between particle velocity u and volume velocity q of the locally plane wave front can be expressed as $q = Su$, where S is a fixed surface area defining a limit for "large area" where the sound pressure approaches that of the undisturbed wave front.

One consequence of the above relation is that a loudspeaker grill should cover but a fraction of the diaphragm area in order to avoid attenuation of the sound output.

5.1.3 Semi-infinite baffle

A numerical algorithm will be developed for calculation of the spectrum with an semi-infinite baffle, which can be regarded as a simplified model of diffraction around the corner of a loudspeaker cabinet. However, the far-field theory cannot directly cope with infinite aperture size so the integral will be modified to include a weighting function in order to converge. The following derivation is inspired by the previous sections but is not related to any references.
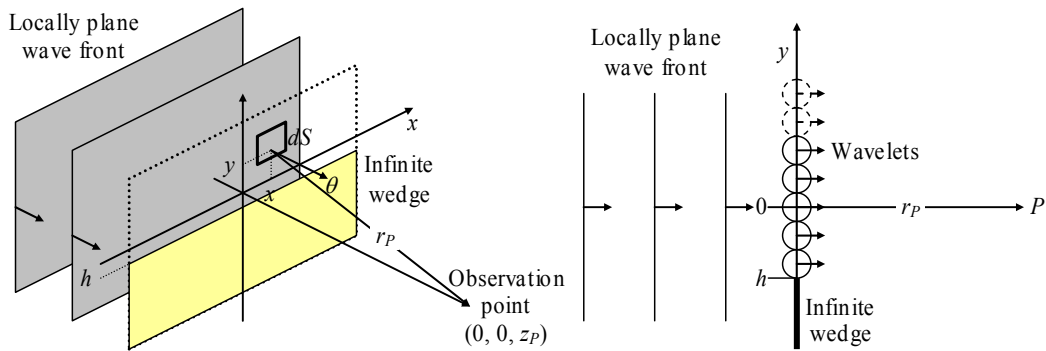
Figure 112 – Plane waves are approaching an aperture.

An infinite edge is assumed to block the plane wave from $y < h$ where h is the vertical position of the edge so $h > 0$ for a edge above the observer height. The infinitesimal area of the part of the plane wave, which is above the edge, is $dS = dxdy$ so the infinitesimal sound pressure at distance r_P from each wavelet becomes:

$$dp = \frac{ik\rho cu}{4\pi r_P}\exp(-ikr_P)dxdy$$

The sound pressure at the observation point is found through integration over the semi-infinite aperture with x from $-\infty$ to ∞ and y from the edge height h to ∞:

$$p = \int_h^\infty \int_{-\infty}^\infty \frac{ik\rho cu}{4\pi r_P}\exp(-ikr_P)dxdy$$

An observer is assumed located at $(0, 0, z_P)$ where z_P is positive. The distance between the wavelet at $(x, y, 0)$ and observer becomes:

$$r_P = \sqrt{x^2 + y^2 + z_P^2}$$

Insertion gives the integral for determination of the sound pressure:

$$p = \frac{ik\rho cu}{4\pi} \int\limits_{h}^{\infty} \int\limits_{-\infty}^{\infty} \frac{\exp\left(-ik\sqrt{x^2 + y^2 + z_P^2}\right)}{\sqrt{x^2 + y^2 + z_P^2}} dxdy \qquad 90$$

The square root is increasing from z_P toward infinity for growing x and y so the exponential is rotating at increasing speed while the amplitude decays toward zero with first-order inverse proportionality to x and y. A picture around (0, 0) is shown in Figure 113 (left) and shows that the decay is relatively slow and the oscillating exponential is expected to retard convergence.

One way to accelerate computation of the integral is to include a weighting function $w(x,y)$, which is unity around (0, 0) and decays for increasing x and y thus focussing on the wavelets within proximity of the observation point while suppressing the radiation from wavelets at large distance since distant sources are assumed less important. This is in accordance with the oblique factor introduced by Fresnel (Pedrotti, 370-372) and is discussed in section 5.2.1, although the present expression is somewhat different.
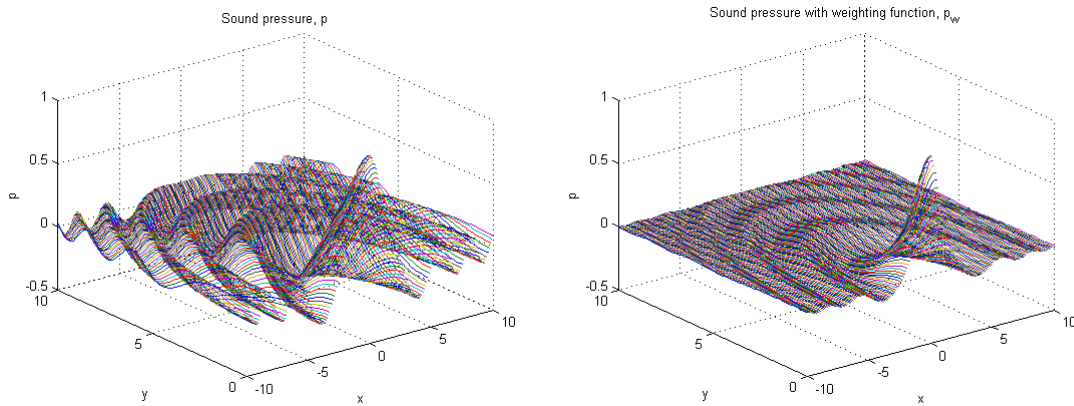
Figure 113 – The complex integrant without weighting function (left) and with the cosine weighting function (right) using $z_P = 1$ m, $f = 10$ Hz, x, y in meters and $y > 0$.

It was chosen to use a cosine function with the argument defined as the angle between the line from the wavelet to the observer and the normal to the plane wave, i.e. the z-axis, which gives 0° or $w(x,y) = 1$ for wavelets close to the observation point and 90° or $w(x,y) = 0$ for x and y approaching plus and minus infinity. Since the weighting function suppresses information we changes the summation and a correction factor C must be included to restore the integral to the correct value. Hence, the integral:

$$p_w = C \frac{ik\rho cu}{4\pi} \int\limits_{-h}^{\infty} \int\limits_{-\infty}^{\infty} \frac{\exp\left(-ik\sqrt{x^2 + y^2 + z_P^2}\right)}{\sqrt{x^2 + y^2 + z_P^2}} \cos(\theta) dxdy \qquad 91$$

Inclusion of a weighting function is somewhat controversial since the problem at hand has been changed and the solution may not present valuable information to the original problem. The new integral may converge faster but this does not guarantee that the computed value represents a useful solution. However, the plane wave is non-physical due to the unlimited energy so the theory is anyway an approximation since it assumes the presence of an infinite wave front with constant particle velocity; it is more likely that the wave front is *locally plane* with decreasing particle velocity at increased distance from the observation point.

The cosine function will be expressed from the geometry of the problem using the cosine law (Westergren, 68) for the distance d between y_P at the y-axis and the wavelet, which is defining the angle seen from the observer. Distance d is thus given by the horizontal distance x and the vertical distance y using the Pythagorean rule for the triangle, and we have:

$$x^2 + y^2 = z_P^2 + r_P^2 - 2z_P r_P \cos(\theta) \quad \Rightarrow \quad \cos(\theta) = \frac{z_P^2 + r_P^2 - x^2 - y^2}{2z_P r_P}$$

Insertion of the expression for r_P gives:

$$\cos(\theta) = \frac{z_P^2 + x^2 + y^2 + z_P^2 - x^2 - y^2}{2z_P \sqrt{x^2 + y^2 + z_P^2}} = \frac{z_P}{\sqrt{x^2 + y^2 + z_P^2}}$$

The ratio approaches zero for x or y approaching infinity thus attenuating distant wavelets and the ratio is unity for $x = y = 0$, which is at the wavelet closest to the observation point. The consequence of including the weighting function is shown graphically in Figure 113 (right). The main peak around $x = y = 0$ is narrowed and the waves are reduced significantly; we will return to the effect of this pulse narrowing later.

Insertion of the weight function gives the following integral:

$$p_w = C \frac{ikz_P \rho c u}{4\pi} \int_h^\infty \int_{-\infty}^\infty \frac{\exp\left(-ik\sqrt{x^2 + y^2 + z_P^2}\right)}{x^2 + y^2 + z_P^2} dx dy \qquad 92$$

An analytical solution to this integral is not known to the author, although a solution with Bessel functions or something of the like could be expected, so a numerical approach will be addressed for computation of the sound pressure at the observation point.

5.1.4 Numerical integration

The variables x and y and the observer to edge height h will be normalised to the variables α β and β_{MIN} using the observation distance z_P from the aperture plane as the scaling factor.

$$\alpha = \frac{x}{z_P}, \quad \beta = \frac{y}{z_P}, \quad \beta_{MIN} = \frac{h}{z_P} \qquad 93$$

The argument to the square root and the denominator becomes:

$$x^2 + y^2 + z_P^2 = \left(\alpha^2 + \beta^2 + 1\right)z_P^2$$

The derivatives of the new variables α and β become:

$$\frac{d\alpha}{dx} = \frac{1}{z_P} \quad \Rightarrow \quad dx = z_P d\alpha \quad \text{and} \quad \frac{d\beta}{dy} = \frac{1}{z_P} \quad \Rightarrow \quad dy = z_P d\beta$$

Only the lower integration limit for β is affected by the substitution and inserting into the integral gives the following expression for the integral:

$$p_w = C \frac{ikz_P \rho c u}{4\pi} \int_{\beta_{MIN}}^\infty \int_{-\infty}^\infty \frac{\exp\left(-ikz_P\sqrt{1 + \alpha^2 + \beta^2}\right)}{1 + \alpha^2 + \beta^2} d\alpha d\beta$$

Numerical integration approximates the integration using finite lower and upper integration limits since infinity is so far away so the lower and upper integration limits will be substituted

by α_{MIN} and α_{MAX} for the α-variable and β_{MIN} and β_{MAX} for the β–variable where β_{MIN} is a parameter describing the relative distance to the edge and the other three are representing infinite limits.

The range between α_{MIN} and α_{MAX} will be divided into $2M$ equidistant segments and the range between β_{MIN} and β_{MAX} will be divided into N equidistant segments. The reason for not dividing the β–range into $2N$ segments is that β_{MIN} is close to zero, say $|\beta_{MIN}| < \beta_{MAX}/10$, so the β–range is semi-infinite.

$$\Delta\alpha = \frac{\alpha_{MAX} - \alpha_{MIN}}{2M}, \quad \Delta\beta = \frac{\beta_{MAX} - \beta_{MIN}}{N} \qquad 94$$

The infinite range above the edge is now reduced to a finite surface defined through the coordinates (α_{MIN}, β_{MIN}) for the lower left corner and (α_{MAX}, β_{MAX}) for the upper right corner with $2MN$ discrete area segments. This corresponds to a rectangular aperture with the width given by $W = \alpha_{MAX} - \alpha_{MIN}$ centred at $x = 0$ and height $H = \beta_{MAX} - \beta_{MIN}$. The major differences from the previous study using a rectangular aperture are that the integration is intended approaching the value for infinite limits and also that the observation height is a parameter; we are not just monitoring on-axis.

It is now possible to substitute the infinite and semi-infinite integrations by finite summations of definite integrals covering the discrete area sections with width $\Delta\alpha$ and height $\Delta\beta$:

$$p_w = C \frac{ikz_P\rho cu}{4\pi} \sum_{n=1}^{N} \int_{\beta_n}^{\beta_{n+1}} \sum_{m=-M}^{M-1} \int_{\alpha_m}^{\alpha_{m+1}} \frac{\exp\left(-ikz_P\sqrt{1+\alpha^2+(\beta-\gamma)^2}\right)}{1+\alpha^2+(\beta-\gamma)^2} \, d\alpha \, d\beta$$

Indexing may seem rather arbitrary; the α-values are indexed from $-M$ to $M-1$ and are thus reflecting the symmetry around zero while the β-values are indexed from 1 to N, although the first β-values may be positive or negative depending upon β_{MIN}. An explanation follows.

The α-values are represented in MATLAB by a vector containing $2M$ elements with the values calculated from $-M$ to $M-1$ and this vector do not need indexing when referenced in the programme since the calculation uses the MATLAB dot-commands for multiplication and division; hence, the command A.*B is not a matrix multiplication but two vectors multiplied element by element as a_1b_1, a_2b_2 and s forth. However, the α-values are formally defined through the index m and the step size $\Delta\alpha$ as follows:

$$\alpha_m = m\Delta\alpha, \quad m = -M \text{K } 0\text{K } M-1 \qquad 95$$

A for-loop is used for stepping through the β_n values and the range is bound to be from 1 and up due to an index restriction of the language. The β_n values will thus be represented by:

$$\beta_n = (n-1)\Delta\beta + \beta_{MIN}, \quad n = 1\text{K } N \qquad 96$$

For $\beta_{MIN} < 0$ is the first β-values negative and $\Delta\beta$ is increased to reflect the larger range up to N and for $\beta_{MIN} > 0$ is all β-values positive and $\Delta\beta$ is decreased to reflect the smaller range.

Since the variables are fixed at constant values for each segment, the result of the integrations is approximated by the function value at the start of the interval multiplied by the area of the interval:

$$p_w = C \frac{ikz_P \rho c u}{4\pi} \sum_{n=1}^{N} \sum_{m=-M}^{M-1} \frac{\exp\left(-ikz_P \sqrt{1+\alpha_m^2+\beta_n^2}\right)}{1+\alpha_m^2+\beta_n^2} \Delta\alpha\Delta\beta$$

Insertion of the definition for the step sizes gives:

$$p_w = C \frac{ikz_P \rho c u}{4\pi} \frac{\alpha_{MAX}-\alpha_{MIN}}{2M} \frac{\beta_{MAX}-\beta_{MIN}}{N} \sum_{n=1}^{N} \sum_{m=-M}^{M-1} \frac{\exp\left(-ikz_P \sqrt{1+\alpha_m^2+\beta_n^2}\right)}{1+\alpha_m^2+\beta_n^2}$$

We are interested in a transfer function defining the relative amplitude of the sound pressure regardless of the sound pressure within the plane wave so the expression will be normalised to the sound pressure of the incident plane wave: $\rho c u$, which reduces the first factor after the scaling constant to the dimension-less factor $ikz_P/4\pi$, which is proportional to frequency and observation distance but otherwise independent upon system parameters.

Symmetry around $x = 0$ enforces $\alpha_{MIN} = -\alpha_{MAX}$ so the α-term can be written as α_{MAX}/M and the transfer function becomes:

$$p_w = C \frac{ikz_P}{4\pi} \frac{\alpha_{MAX}(\beta_{MAX}-\beta_{MIN})}{MN} \sum_{n=1}^{N} \sum_{m=-M}^{M-1} \frac{\exp\left(-ikz_P \sqrt{1+\alpha_m^2+\beta_n^2}\right)}{1+\alpha_m^2+\beta_n^2} \qquad 97$$

The step sizes are given by equation 94 when the integration limits and number of steps have been decided and the values of α_m and β_n are then calculated from equation 95 and 96. The plots will use kz_P as a parameter stepping through the frequency-distance range of interest and parameter γ will be changed from plot to plot thus calculating the frequency response versus the observation height.

A disturbing result in the equation is that the transfer function appears proportional to distance through the ikz_P factor but this is not the case. Since $\alpha_{MAX} = x_{MAX}/z_P$ and $\beta_{MAX} = y_{MAX}/z_P$ is scaling with $ikz_P\alpha_{MAX}\beta_{MAX}$ equivalent to $ikx_{MAX}y_{MAX}/z_P$ and thus inversely proportional to z_P, as could be expected.

The transfer function is to be used for studying relative changes in sound pressure levels, which are commonly being expressed in decibels, so the transfer function will be calculated from:

$$K_w = 20\log_{10}\left| C \frac{ikz_P}{4\pi} \frac{\alpha_{MAX}(\beta_{MAX}-\beta_{MIN})}{MN} \sum_{n=1}^{N} \sum_{m=-M}^{M-1} \frac{\exp\left(-ikz_P \sqrt{1+\alpha_m^2+\beta_n^2}\right)}{1+\alpha_m^2+\beta_n^2} \right| dB \qquad 98$$

The zero dB reference is unity transfer function value, which is equivalent to the sound pressure of the undisturbed plane wave. This is expected met for β_{MIN} approaching minus infinity and will be used to determine the constant C.

It is required determining the integration limits and number of steps sufficient in order to get the best ratio between precision and computation time. An arbitrary selected stop criterion for the summation could be to use 0.01 % of the initial amplitude thus defining "small" as 10^{-4}. Since the denominator use squared values for α and β we have the *first rule-of-thumb*:

$$\alpha_{MIN} = -100, \quad \alpha_{MAX} = 100, \quad \beta_{MAX} = 100 \qquad 99$$

An upper limit must be defined for kz_P since the complex exponential is rotating fast for high kz_P-values thus introducing the risk of "under sampling" at high frequencies. For large value of α is the phase approximately proportional to α (and similarly for β large):

$$kz_P\sqrt{1+\alpha^2+\beta^2} \xrightarrow[\alpha\to\infty]{} kz_P\alpha$$

The incremental change in phase from α to $\alpha + \Delta\alpha$ is $kz_P\Delta\alpha$ and the phase increment must not exceed π in order to avoid missing a change of sign so we get the *second rule-of-thumb*:

$$kz_P\Delta\alpha < \pi \quad \Rightarrow \quad kz_P < \frac{\pi}{\Delta\alpha} = \frac{\pi M}{\alpha_{MAX}} \quad \Rightarrow \quad f < \frac{cM}{2z_P\alpha_{MAX}} \qquad 100$$

For z_P = 1 m and $M = \alpha_{MAX}$ is $\Delta\alpha$ = 1 and the upper frequency limit becomes 170 Hz but the response extends to 1.7 kHz for $M = 10\alpha_{MAX}$, where the step size is $\Delta\alpha$ = 0.1, so small step size is recommended for good resolution at the high frequencies.

The required resolution for a given measurement set-up, is:

$$\Delta\alpha = \frac{\alpha_{MAX}}{M} < \frac{1}{2z_P f}$$

For z_P = 1 m and f = 10 kHz we get $\Delta\alpha < 50\ 10^{-6}$ and using α_{MAX} = 1000 we need a fairly high number of steps: $M = \alpha_{MAX}/\Delta\alpha = 20\cdot10^3$, so computing time is sacrificed for bandwidth.

A starting point for the design could thus be $M = N = 1000$ and $\alpha_{MAX} = \beta_{MAX} = 100$, which corresponds to 2 million computations (2MN) for one frequency point and the frequency limit is around 2 kHz for 1 m of observation distance ($kz_P < \pi/\Delta\alpha$). The computer used for calculation used the Intel Celeron processor running at 2.4 GHz and with 736 megabyte of ram. The frequency response below with 201 discrete points required 10 minutes of execution time for one curve, which corresponds to a computation time of 1.5 µs for the expression.
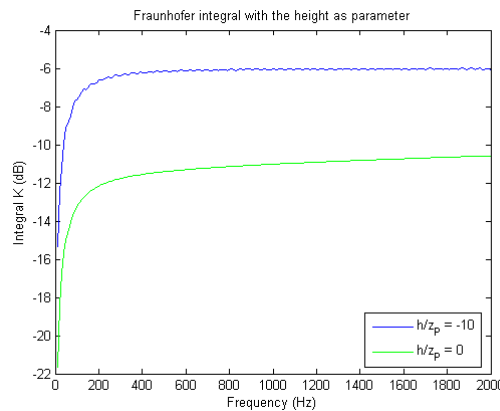
Figure 114 – Initial calculation of frequency response with almost no obstruction (top curve) and 50 % blocking (bottom curve).

There are two curves: The top curve is for $h/z_P = -10$, which represents almost no edge since the distance to the edge is ten times larger than the horizontal distance to edge so integration is almost from minus infinity to plus infinity for both coordinates. The effect of the edge can thus be expected minimal and the transfer function should output 0 dB but the result was close to –6 dB thus indicating a missing factor of two. The lower curve is for $h/z_P = 0$ where the edge blocks half the wave front so the energy is reduced to half of its initial value and the expected result was thus –6 dB but the output is between –10 to –12 dB depending upon the frequency. This is close to a factor of two but not as precisely as could be wished. It seems that the function must be multiplied by factor 2, but there might be more to it so the effect of the weighting function will be studied before deciding upon a scaling value.

A couple of test runs was performed with the weighting function where the variables α^2 and β^2 were first used as they are shown in equation 98 and then scaled with constant δ:

$$w(x, y) = \frac{z_P}{\sqrt{(\delta x)^2 + (\delta y)^2 + z_P^2}}, \quad 0 < \delta < 1$$

Scaling used $\delta = 1/3$ to produce $(\alpha/3)^2$ and $(\beta/3)^2$ as can be seen in equation 101, and $\delta = 1/10$ to produce $(\alpha/10)^2$ and $(\beta/10)^2$. The result is shown to the left below and shows that the low-frequency range is improved for the widening of the weight function. A zoom on the last scaling ($\delta = 1/10$) is shown to the right where two different integration ranges are also shown.

It is seen that the final value is reached at a lower frequency when the weighting function is widened but the asymptotical value is not changed so the weighting function is not related to the final value and is thus not responsible for the missing factor 2.
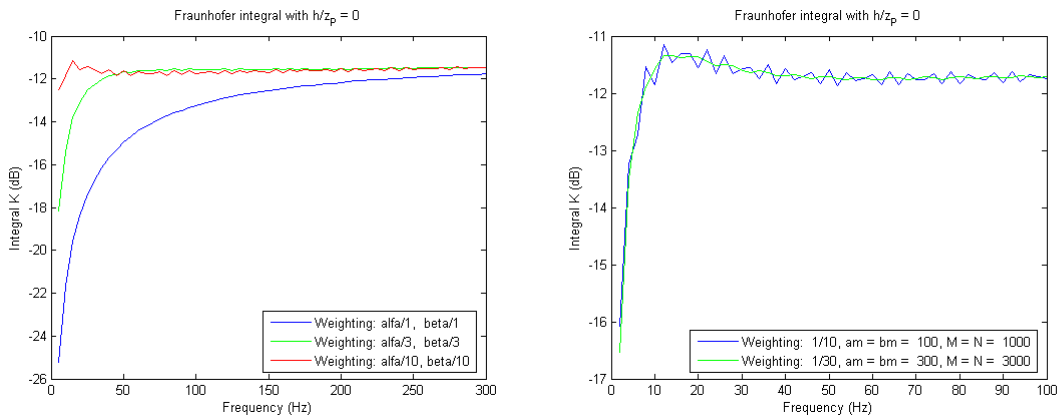
Figure 115 – The effect of widening the weighting function is to increase the low-frequency level and also to increase the ripple.

Further widening of the weight function corresponds to removal of the weight function so the effect of completely removing the weight function is shown below. The implemented integral was equation 98 with a square root in the denominator. The integral is approaching a final value but the oscillations are seriously retarding convergence so the weighting function is indeed required.
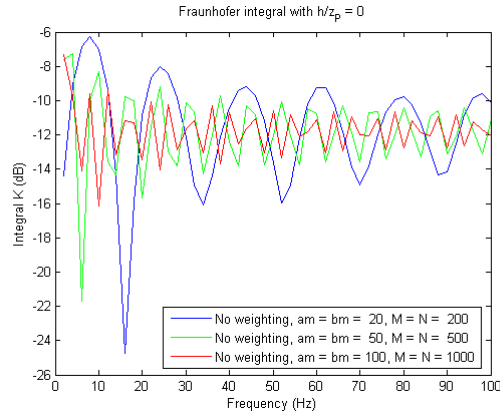
Figure 116 – Removing the weight function results in strong ripple amplitude.

In order to conclude the above discussion, the decision is to increase the level by 6 dB so the constant becomes $C = 2$ and the transfer function will also be modified to include some relaxation of the weighting function to benefit in the low-frequency region. The selection was in favour of $\delta = 1/3$, which seems a good compromise between increased level and the ripple.

The transfer function becomes:

$$L_w = 20\log_{10}\left|\frac{ikz_P}{2\pi}\frac{\alpha_{MAX}(\beta_{MAX}-\beta_{MIN})}{MN}\sum_{n=1}^{N}\sum_{m=-M}^{M-1}\frac{\exp\left(-ikz_P\sqrt{1+\alpha_m^2+\beta_n^2}\right)}{\sqrt{(1+\alpha_m^2+\beta_n^2)(1+\frac{1}{9}\alpha_m^2+\frac{1}{9}\beta_n^2)}}\right|\text{dB} \qquad 101$$

Recommended values are $M = N = 1000$ and $\alpha_{MAX} = \beta_{MAX} = 100$ for a start. The values for α_m and β_n are then calculated according to equation 95 and 96 and the lower integration limit $\beta_{MIN} = h/z_P$ is the input parameter. The upper frequency limit is 2 kHz but can be increased by decreasing the step size (see equation 94). Factor 1/9 in the denominator is due to δ-squared for moderate widening of the weighting function and can be changed, if required, to modify the low-frequency behaviour.

5.1.5 Semi-infinite baffle

An observer is assumed located at height $y = 0$ and at distance z_P from a semi-infinite baffle, which is obstructing part of the plane wave. The upper edge of the baffle is at $y = h$ so the observer is relatively unaffected for $h < 0$ and the baffle blocks more than 50 % of the observable range for $h > 0$.
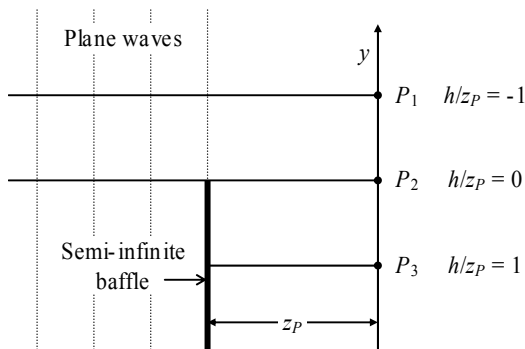
Figure 117 – An infinite edge is blocking part of the sound at the observation point.

The response is plotted below.
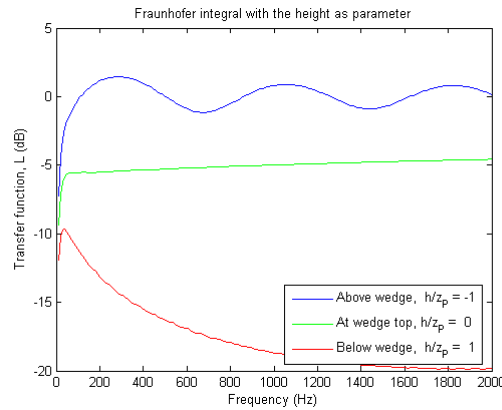
Figure 118 – Semi-infinite baffle with an observer at distance z_P from the baffle. The top curve is for the observer above the edge; the middle curve is for observer at same height as the baffle and the bottom curve is for the observer below the baffle edge.

This result will be compared to the near-field approximation to be introduced in the following section and it will be seen that the results are very comparable although not identical.

5.1.6 Loudspeaker off-axis response

The output from a loudspeaker will be modelled using the theory for the semi-infinite baffle to estimate the off-axis response of a loudspeaker. The output from a loudspeaker is far from plane but this fact will be ignored in order to test the applicability.

The set-up is shown below where the loudspeaker cabinet is tilted θ with respect to the horizontal plane thus realising an observation angle from 0° and up to 180°. For an angle below 90° is the observation point above the semi-infinite baffle ($h < 0$) while the point is below for larger values of the angle ($h > 0$).
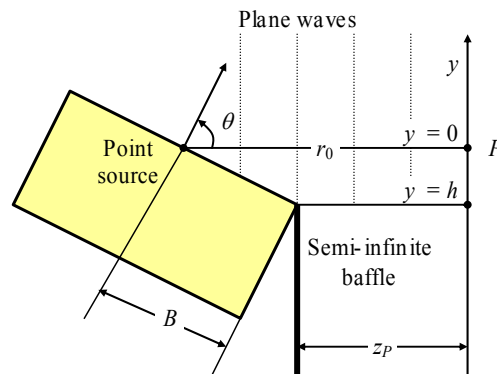
Figure 119 – An infinite edge is blocking part of the sound at the observation point.

Parameter h is given by the size of the box and the observation angle:

$$h = -B\sin\left(\frac{\pi}{2} - \theta\right)$$

The observation distance r_0 is fixed so distance z_P between the semi-infinite baffle and the observer is determined from:

$$r_0 = z_P + B\cos\left(\frac{\pi}{2} - \theta\right) \quad \Rightarrow \quad z_P = r_0 - B\cos\left(\frac{\pi}{2} - \theta\right)$$

Hence the lower integration limit, which is required for the numerical algorithm:

$$\beta_{MIN} = \frac{h}{z_P}$$

It is obvious that r_0/B must be larger than unity.

The frequency range extends to 10 kHz and this demands the following relation between the integration limit and the step size (from equation 100):

$$f < \frac{cM}{2z_P\alpha_{MAX}} \quad \Rightarrow \quad M > \frac{2fz_P}{c}\alpha_{MAX}$$

Assuming that integration to $\alpha_{MAX} = \beta_{MAX} = 20$ is sufficient, we get $M = N > 1620$ for a distance between the semi-infinite baffle and the observer of $z_P = 1.41$ m. Implementation is very time consuming with an estimated computation time of 5 hours for a complete frequency response plot with 6400 frequency points so the code was changed to skip 99 out of 100 frequency points and to interpolate the missing frequency values. This reduced the number of calculated frequencies to 65 and computation time to around 5 minutes for one plot of the frequency spectrum but at the expense of 200 Hz step size within the frequency axis.

The result is shown below (using $M = N = 1200$). The range below 200 Hz is incorrect due to interpolation between zero amplitude at 0 Hz and the result of simulation at 200 Hz.
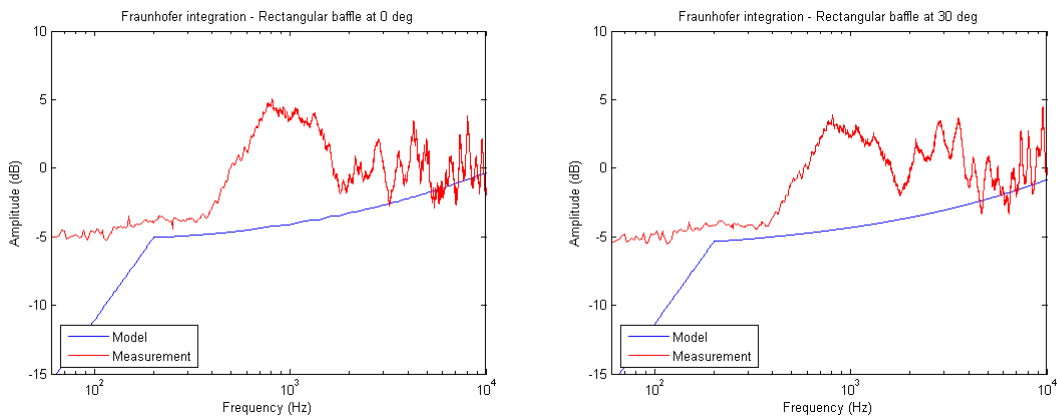
Figure 120 – Frequency response for 0° and 30° off/axis simulations.
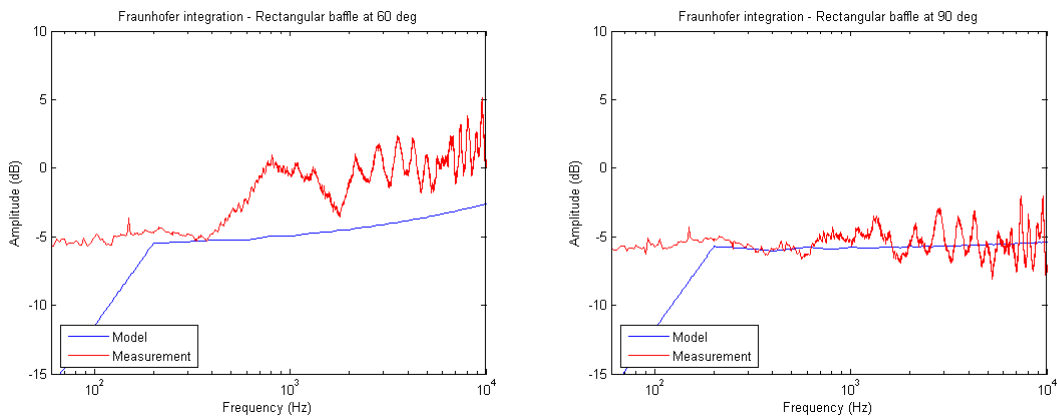
Figure 121 – Frequency response for 60° and 90° off/axis simulations.
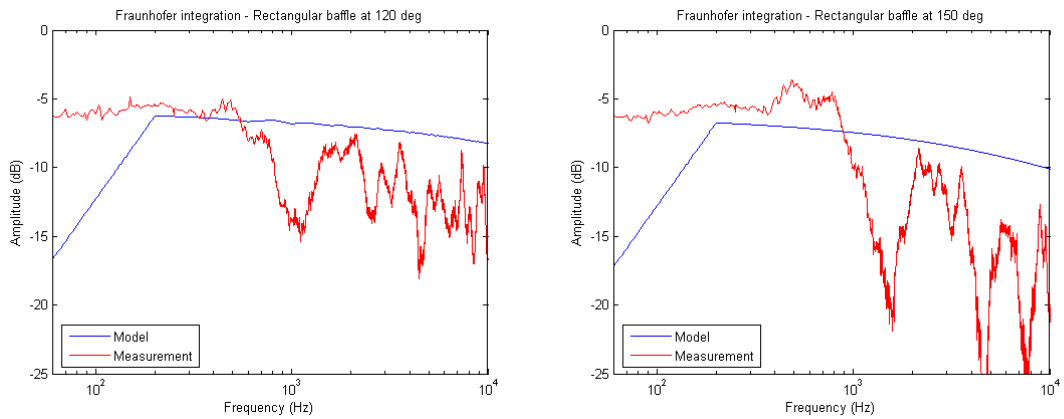
Figure 122 – Frequency response for 120° and 150° off/axis simulations.
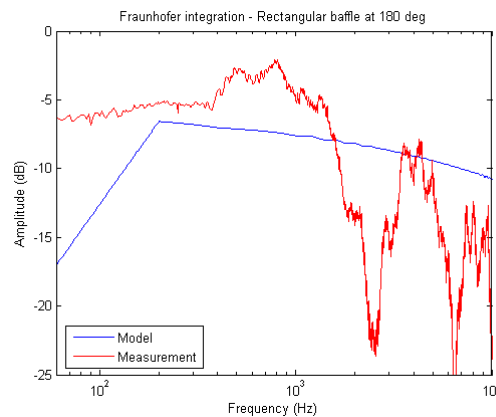
Figure 123 – Frequency response for 180° off/axis simulations.

The responses are not impressing but note that the level at 200 Hz is within 2 dB of the correct level and that the slope is correct for the simulations up to 90°. The simulated response at higher observation angles is not that worse when compared to the simulations from the previous chapter using the numerical edge diffraction model.

The main reason for the result is that the loudspeaker was assumed to output plane waves and that this is certainly not the case.

It is interesting to note that there are visible changes despite the relatively small changes in the input parameter h/z_P from –0.071 (0°) to 0.071 (180°) and that the slope of the curves changes from positive below 90° to negative above 90°. The range for h/z_P means that the simulations are performed with approximately 57 % of the plane wave being active for 0° precisely 50 % for 90° and approximately 43 % for 180°.

The results should be compared to the equivalent set-up for the application of the Fresnel approximation technique shown in section 5.1.6.

5.2 The Fresnel near-field approximation

Short distance to source and observer violates the assumptions of far-field operation so the curvature of the wave front from the source must be taken into account as well as the distance to the observer. The near-field diffraction theory becomes much more involved than far field, but the equations are hard to solve and approximations are required anyway. This study takes its onset from the field of optics and is initially using the same approximations in order to solve the equations. This leads – almost – to the Fraunhofer integral so little is gained. Within optics there seems to be a well-established route to a solution, which is however violating the initial assumptions but is leading to a simple set of equations describing the diffraction. This study will follow the "optical path" to the Fresnel equations where modelling takes over.

5.2.1 The Fresnel diffraction integral

A typical arrangement is shown Figure 124 where a spherical wave is propagating through an aperture within an infinite baffle. It is assumed that the sound pressure within the wave front at the aperture has the same value as without the aperture; that the source and observer distances are larger than the aperture dimensions and that the aperture dimensions are large compared to wavelength (Pedrotti, 368).

The sound pressure at the aperture is given by equation 33 for a point source at distance r_S:

$$p_A = \frac{ik\rho c}{4\pi r_S} \exp(-ikr_S)q$$
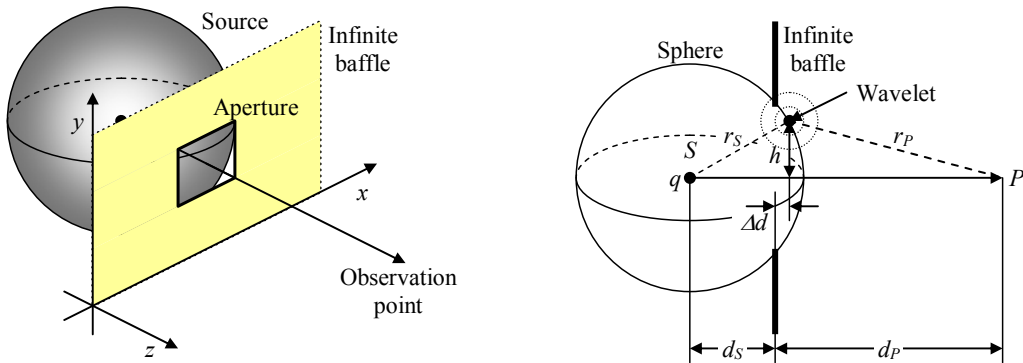
Figure 124 – A spherical wave front is propagating from a point source toward an infinite plane baffle with a rectangular aperture. It is assumed that the unobstructed part of the sphere is propagating through the hole and the wave front becomes the source of wavelets.

It is assumed that the particle velocity u_A is constant throughout the surface. The particle velocity is determined from the specific impedance of a sphere according to equation 29:

$$Z_S = \frac{p_A}{u_A} = \rho c \frac{ikr_S}{1+ikr_S} \quad \Rightarrow \quad u_A = \frac{1+ikr_S}{ikr_S}\frac{p_A}{\rho c}$$

Insertion of the expression for the sound pressure at the aperture gives the infinitesimal volume velocity dq_A for the wavelet, which is assumed radiating equally in all directions:

$$dq_A = u_A dS = \frac{1+ikr_S}{ikr_S}\frac{ik}{4\pi r_S}\exp(-ikr_S)qdS$$

The resulting sound pressure at the observation point is again using equation 33 for a point source, now with distance r_P to the observation point and integration through the aperture A.

$$dp = \frac{ik\rho c}{4\pi r_P} \exp(-ikr_P) dq_A \quad \Rightarrow \quad p = \int_A \frac{ik\rho c}{4\pi r_P} \exp(-ikr_P) dq_A$$

Insertion of the infinitesimal volume velocity dq_A gives:

$$p = \int_A \frac{ik\rho c}{4\pi r_P} \exp(-ikr_P) \frac{1+ikr_S}{ikr_S} \frac{ik}{4\pi r_S} \exp(-ikr_S) q dS$$

The constant and frequency-dependent terms will be assembled into P_1, which represents pressure (the unit is: $\mathrm{kgm^{-1}s^{-2}} = \mathrm{N/m^2} = \mathrm{Pa}$) and it should not be confused with the static air pressure P_0. Note that P_1 is frequency dependent and is approaching first-order proportionality at low frequencies and second-order proportionality at high frequencies.

$$P_1 = \frac{1+ikr_S}{ikr_S} \left(\frac{ik}{4\pi} \right)^2 \rho c q \qquad\qquad 102$$

The Fresnel diffraction integral becomes.

$$p = P_1 \int_A \frac{\exp(-ik(r_S + r_P))}{r_S r_P} dS \qquad\qquad 103$$

The factor P_1 in front of the integral differs from the reference (Pedrotti, 368), not because this concerns acoustical signals as opposed to the electromagnetic waves of the optical field, but since the reference generally ignores scaling factors and concentrates on the core of diffraction, which is the integral. This can be allowed within optics where the change in wavelength is typically limited to an octave or less; however, acoustic signals may extend through ten octaves so knowledge of the frequency dependency is required.

Fresnel introduced an oblique factor $F(\theta)$ attenuating the diffracted waves according to the direction in order to suppress the backward-travelling wave and this was later placed on more rigorous basis by Kirchhoff. The wavelet amplitude is attenuated by the below function where θ is the angle between the directions of propagation and observation:

$$F(\theta) = \frac{1+\cos(\theta)}{2} = \cos^2\left(\frac{\theta}{2} \right) \qquad\qquad 104$$

The function is unity for $\theta = 0°$, becomes ½ at $90°$ and is zero at $180°$.

The oblique factor is addressed with the Fresnel diffraction theory only and does not appear with the Fraunhofer diffraction theory. The oblique factor has been referenced within the field of audio by Vanderkooy and others. It does not simplify the problem of solving the equations although interference from mirror sources can be ignored in some circumstances. The complications introduced by the oblique factor are not easily solved so the model is ignored in the references used (Pedrotti and Heavens) – as it will be in the present study.

Radius of the spherical wave front r_S from the source is constant but distance r_P from the wavelet to the observation point is a function of the location on the sphere. The sum of r_S and r_P can be expressed as functions of the known distances d_S and d_P and position h within the aperture, which represents either x or y within the coordinate system; see Figure 124. The two

triangles formed by the lines $d_S - r_S - h$ and $d_P - r_P - h$ introduces a small distance Δd, which is added to d_S and subtracted from d_P. Using Pythagoras on the triangles and simplifying the square root using Taylor series expansion we get:

$$r_S = \sqrt{(d_S + \Delta d)^2 + h^2} = d_S\sqrt{1 + \left(\frac{\Delta d}{d_S}\right)^2 + 2\frac{\Delta d}{d_S} + \left(\frac{h}{d_S}\right)^2} \approx d_S\left[1 + \frac{1}{2}\left(\frac{\Delta d}{d_S}\right)^2 + \frac{\Delta d}{d_S} + \frac{1}{2}\left(\frac{h}{d_S}\right)^2\right]$$

$$r_P = \sqrt{(d_P - \Delta d)^2 + h^2} = d_P\sqrt{1 + \left(\frac{\Delta d}{d_P}\right)^2 - 2\frac{\Delta d}{d_P} + \left(\frac{h}{d_P}\right)^2} \approx d_P\left[1 + \frac{1}{2}\left(\frac{\Delta d}{d_P}\right)^2 - \frac{\Delta d}{d_P} + \frac{1}{2}\left(\frac{h}{d_P}\right)^2\right]$$

Taylor series expansion requires that Δd and h are sufficiently small compared to d_S and d_P. The sum removes the first-order dependency upon Δd although the squared terms survive, so the relation becomes:

$$r_S + r_P \approx d_S + d_P + \left(\frac{1}{d_S} + \frac{1}{d_P}\right)\left(\frac{h^2}{2} + \frac{\Delta d^2}{2}\right) \tag{105}$$

The dependency to Δd squares was omitted in the reference (Pedrotti, 368). The distance Δd is given by the angle between r_S and d_S, which will be called α_S and is defined as shown below. Simplifying through the use of the Taylor series expansion, and assuming α_S small, we get:

$$\Delta d = r_S[1 - \cos(\alpha_S)] \approx \frac{r_S\alpha_S^2}{2}$$

The angle is given through the following sine-relation, which will also be simplified through the use of the Taylor series expansion:

$$h = r_S\sin(\alpha_S) \approx r_S\alpha_S \quad \Rightarrow \quad \alpha_S \approx \frac{h}{r_S}$$

Combining the expressions, we get the relation between Δd and h:

$$\Delta d \approx \frac{h^2}{2r_S}$$

Since $r_S = d_S + \Delta d$, and Δd squared can be assumed small compared to $d_S\Delta d$, we get:

$$\Delta d \approx \frac{h^2}{2(d_S + \Delta d)} \quad \Rightarrow \quad d_S\Delta d + \Delta d^2 = \frac{h^2}{2} \quad \Rightarrow \quad \Delta d \approx \frac{h^2}{2d_S}$$

Insertion into equation 105 gives:

$$r_S + r_P \approx d_S + d_P + \left(\frac{1}{d_S} + \frac{1}{d_P}\right)\left(1 + \frac{h^2}{4d_S^2}\right)\frac{h^2}{2}$$

Assuming h/d_S less than one enables us to ignore the second parenthesis thus requiring that the source is at some minimum distance behind the aperture, i.e. not closer to the baffle than the size of the aperture. Hence the following relation for the sum, which is also found in the reference (Pedrotti, 378):

$$r_S + r_P \approx d_S + d_P + \left(\frac{1}{d_S} + \frac{1}{d_P} \right) \frac{h^2}{2} \tag{106}$$

The product of r_S and r_P will at a later stage in this derivation be assumed constant, so the product will be investigated; this was not considered in the reference, which assumed the product as constant without further argumentation. The product is given by the following approximate expression, where terms containing $h^2 \Delta d$ or with h^4 has been removed:

$$r_S r_P \approx d_S d_P \left[1 + \frac{\Delta d}{d_S} - \frac{\Delta d}{d_P} + \frac{1}{2} \left(\frac{h}{d_P} \right)^2 + \frac{1}{2} \left(\frac{h}{d_S} \right)^2 \right] \xrightarrow{h \to 0} d_S d_P \tag{107}$$

It is seen that the effect of Δd is counteracted and becomes completely eliminated for $d_S = d_P$ but the product is function of h, and is thus only approximately constant. It may be possible to derive an expression stating the relation between d_S and d_P for an optimum constant product, but this is overkill. The product will in the following be assumed constant.

The sum of distances d_S and d_P represents the length of the *line-of-sight* between the point source and the observer and is:

$$D = d_S + d_P \tag{108}$$

The Fresnel length L for distances d_S and d_P will be introduced. It is defined by the same rule as used within electronics for the parallel connection of impedances:

$$\frac{1}{L} = \frac{1}{d_S} + \frac{1}{d_P} \quad \Rightarrow \quad L = \frac{d_S d_P}{d_S + d_P} \tag{109}$$

For equal distances is the Fresnel length $d_S/2 = d_P/2$, while the Fresnel length is less than this for any other combination of d_S and d_P. For large ratios between the distances will the Fresnel length approximate the shortest distance; i.e. for $d_S/d_P \ll 1$ is $L \to d_S$, corresponding to a model representing a loudspeaker cabinet with large distance to the measurement microphone.

The wave front approaches plane waves for Δd approaching zero so this parameter can be used to decide between using the plane wave front approximation according to Fraunhofer or the spherical wave front according to Fresnel, where d is any of d_S or d_P:

$$\Delta d = \frac{h_{MAX}^2}{2d} < \lambda = \frac{c}{f} \quad \Rightarrow \quad f < \frac{2cd}{h_{MAX}^2}$$

For $d = h = 1$ m, the limit becomes 700 Hz so the Fresnel near-field theory is required below the limit while Fraunhofer far-field theory is sufficient above.

The required approximate relation becomes:

$$r_S + r_P \approx D + \frac{h^2}{2L} \tag{110}$$

Insertion into equation 103 gives:

$$p = P_1 \exp(-ikD) \int_A \frac{1}{r_S r_P} \exp\left(-\frac{ikh^2}{2L}\right) dS \qquad\qquad 111$$

Integration was in the reference assuming a cylindrical wave front where the problem can be reduced to an infinitesimal strip with fixed width given by the aperture and the application to both coordinates was implied (Pedrotti, 379). The present study will follow another route with surface integration through the x and y axes. Distance h will be representing the distance from the origin to a point within the aperture and with a length given by:

$$h^2 = x^2 + y^2$$

Assuming that the product $r_S r_P$ is constant, the integration becomes:

$$p = P_1 \frac{\exp(-ikD)}{r_S r_P} \int_A \exp\left(-\frac{ikx^2}{2L}\right) \exp\left(-\frac{iky^2}{2L}\right) dx dy$$

This integral can be split into two integrals with one in x and the other in y since the two exponentials are function of one coordinate each.

$$p = P_1 \frac{\exp(-ikD)}{r_S r_P} \int_{x_1}^{x_2} \exp\left(-\frac{ikx^2}{2L}\right) dx \int_{y_1}^{y_2} \exp\left(-\frac{iky^2}{2L}\right) dy \qquad\qquad 112$$

The two integrals are similar so a common method for solving them will be sought and this method is through the use of the Fresnel integrals.

5.2.2 The Fresnel integral

The Fresnel integral to consider is:

$$I_F = \int_{x_1}^{x_2} \exp\left(-\frac{ikx^2}{2L}\right) dx \qquad\qquad 113$$

It appears to be a common procedure within the field of optics to substitute the variable x into a dimension-less variable v, which is at the same time relating it to the Fresnel length and the wavelength. The argument to the exponential function can be written:

$$\frac{k}{2L} x^2 = \frac{\pi}{L\lambda} x^2 = \frac{\pi}{2} \frac{2}{L\lambda} x^2 = \frac{\pi}{2} v^2$$

The reason for including factor $\pi/2$ is unknown to the author. Hence, the substitution of:

$$v = \sqrt{\frac{2}{L\lambda}} x \qquad\qquad 114$$

For $d_S = d_P$ is $L = d_S/2$ and $L \to d_S$ for d_S small and similarly $L \to d_P$ for d_P small.

The differential dx must be substituted as well and is determined by differentiating v with respect to x:

$$\frac{dv}{dx} = \sqrt{\frac{2}{L\lambda}} \quad \Rightarrow \quad dx = \sqrt{\frac{L\lambda}{2}} dv$$

Insertion of the substitution gives the integral shown below, where v_1 and v_2 represents the new integration limits for the corresponding aperture limits x_1 and x_2:

$$I_F = \int_{v_1}^{v_2} \exp\left(-\frac{i\pi}{2}v^2\right)\sqrt{\frac{L\lambda}{2}}dv \quad \text{where} \quad v_1 = \sqrt{\frac{2}{L\lambda}}x_1, \quad v_2 = \sqrt{\frac{2}{L\lambda}}x_2$$

Moving the independent factors outside the integral and using Euler's substitution formula for the complex exponential, we get:

$$I_F = \sqrt{\frac{L\lambda}{2}}\left[\int_{v_1}^{v_2}\cos\left(\frac{\pi}{2}v^2\right)dv - i\int_{v_1}^{v_2}\sin\left(\frac{\pi}{2}v^2\right)dv\right] \qquad 115$$

Available tables and numerical software assumes integration from zero to the upper limit, so the definite integrals must be changed into integrals starting from zero, which is readily done as shown below using the cosine integral as an example:

$$\int_{v_1}^{v_2}\cos\left(\frac{\pi}{2}v^2\right)dv = \int_{0}^{v_2}\cos\left(\frac{\pi}{2}v^2\right)dv - \int_{0}^{v_1}\cos\left(\frac{\pi}{2}v^2\right)dv$$

The integrals from zero and up are the Fresnel cosine and sine integrals named $C(v)$ and $S(v)$ respectively.

$$
\left.
\begin{aligned}
C(v) &= \int_{0}^{v}\cos\left(\frac{\pi}{2}\gamma^2\right)d\gamma \\
S(v) &= \int_{0}^{v}\sin\left(\frac{\pi}{2}\gamma^2\right)d\gamma
\end{aligned}
\right\} \xrightarrow[v\to\infty]{} \frac{1}{2} \qquad 116
$$

Hence, the definite integral from v_1 to v_2 becomes:

$$I_F = \sqrt{\frac{L\lambda}{2}}\left(C(v_2) - C(v_1) - i\left[S(v_2) - S(v_1)\right]\right) \qquad 117$$

The integrals are tabulated in various text books, for instance Pedrotti on page 380, and can be calculated through the MAPLE instructions available from MATLAB[1]. The cosine and sine integrals are plotted below for v extending from -5 to 5. Both integrals are zero for $v = 0$ and approaches ± 0.5 for v approaching $\pm\infty$ with decaying oscillations. The difference is the horizontal tangent to the sine integral at the origin and orthogonal oscillations.

---

[1] The MAPLE functions are addressed through the mfun-command within MATLAB but not available within the Student Edition according to the help-menu – but the mfun-call proved functional anyway. Execution is from time to time cancelled with a cryptically error message but functionality was restored after restarting the MATLAB environment. This could be a time-out error limiting the usefulness of the Student Edition package, or it could be a software error.
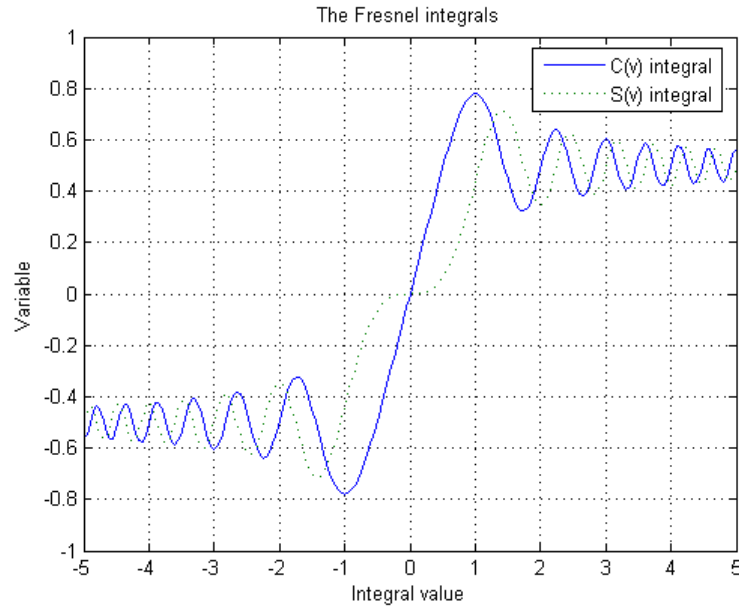
Figure 125 – Fresnel cosine and sine integrals with the argument from –4 to 4.

The dimension-less variable v is function of wavelength according to equation 114 but the relation is not common to acousticians, where it is preferred using parameter k together with a length parameter, such as source radius or observation distance. One way of realising this is the following substitution that relates x (or y) to the dimension-less variable v using k and the Fresnel length L:

$$v = \sqrt{\frac{2}{L\lambda}}x = \sqrt{\frac{2\pi}{\pi L\lambda}}x = \sqrt{\frac{k}{\pi L}}x = \sqrt{\frac{kL}{\pi L^2}}x = \sqrt{\frac{kL}{\pi}}\frac{x}{L} \qquad 118$$

Using the definition of the angular wave number, the proportionality constant can be written with frequency and Fresnel length as the parameters:

$$v = \sqrt{\frac{2f}{cL}}x \qquad 119$$

Since $L = d_S d_P/(d_S + d_P)$ is $L \rightarrow d_S$ for large distance to the observation point and $L \rightarrow d_P$ for large distance to the source (thus approximating the Fraunhofer far-field theory). For the aperture midway between source and observer is $d_S = d_P$ and $L = d_S/2 = d_P/2$.

For zero frequency is $v = 0$ so the integral is zero regardless of the Fresnel length and the input variable x and the proportionality constant is invariant for $f \propto L$, which can be used to scale one measurement to another.

5.2.3 The Cornu spiral

If the Fresnel cosine and sine integrals are plotted against variable v with $C(v)$ along the abscissa (real axis) and $S(v)$ along the ordinate (imaginary axis) then the result becomes the complex curve as shown in the figure below. At the centre of the coordinate system is $v = 0$ which corresponds to the point $0 + i0$ on the curve and the point moves to the right in quadrant 1 for positive values of v and to the left in quadrant 3 for negative values of v. The curve oscillates around two points, the *eyes*, representing minus infinity (–0.5, –0.5) and plus infinity (0.5, 0.5) for the variable v.
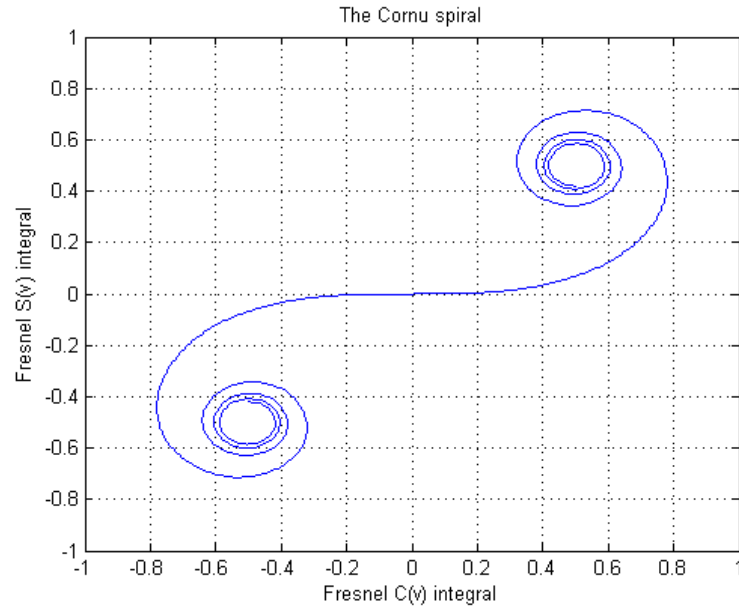
Figure 126 – The Cornu spiral for Fresnel integrals $C(v)$ and $S(v)$ with v from –4 to 4.

Integration through the range from v_1 to v_2 corresponds to the subtraction $C(v_2) - C(v_1)$, for the real component and $S(v_2) - S(v_1)$ for the imaginary component.

5.2.4 Transfer function

Returning to the problem of determining the sound pressure at the observation point, the integrals from equation 112 is rewritten into Fresnel integrals. The Fresnel integral is given by equation 113, with a solution given by equation 117, and is for the x-direction:

$$I_F = \int_{x_1}^{x_2} \exp\left(-\frac{ikx^2}{2L}\right)dx = \sqrt{\frac{L\lambda}{2}}\left(C(v_{x2}) - C(v_{x1}) - i[S(v_{x2}) - S(v_{x1})]\right) \qquad 120$$

A similar expression applies to the y-direction and the integration limits are translated from x or y into v using equation 114 or 118. A new scale factor will be introduced, P_2, carrying the extra terms of equations 112 and 120. Factor $L\lambda/2$ appears below without the square root since the calculation is a product of two I_F integrals.

$$P_2 = P_1 \frac{\exp(-ikD)}{r_S r_P}\frac{L\lambda}{2} = \frac{1 + ikr_S}{ikr_S}\left(\frac{ik}{4\pi}\right)^2 \rho c q \frac{\exp(-ikD)}{r_S r_P}\frac{L\lambda}{2}$$

The factor $L\lambda/2$ can be written as $\pi L/k$ (see equation 118); hence the definition:

$$P_2 = i\frac{1 + ikr_S}{kr_S}\frac{\exp(-ikD)}{r_S r_P}\frac{kL\rho c}{16\pi}q \qquad 121$$

The factor is a pressure (the unit is: $\mathrm{kgm^{-1}s^{-2}} = \mathrm{Nm^{-2}} = \mathrm{Pa}$).

The sound pressure at the observation point becomes:

$$p = P_2\left(C(v_{x2}) - C(v_{x1}) - i[S(v_{x2}) - S(v_{x1})]\right)\left(C(v_{y2}) - C(v_{y1}) - i[S(v_{y2}) - S(v_{y1})]\right) \qquad 122$$

A reference is required for calculation of the transfer response and it will been chosen to use the sound pressure of a sphere with radius equal to the distance between source and observer,

which is D, since this would be the sound pressure at the observation point without the obstruction due to the baffle. The sound pressure of the reference is given by equation 33:

$$p_D = \frac{ik\rho c}{4\pi D} \exp(-ikD)q$$

Combining P_2 with p_D gives:

$$\frac{P_2}{p_D} = \frac{i \dfrac{1+ikr_S}{kr_S} \dfrac{\exp(-ikD)}{r_S r_P} \dfrac{kL\rho c}{16\pi} q}{\dfrac{ik\rho c}{4\pi D}\exp(-ikD)q} = i\frac{1+ikr_S}{kr_S}\frac{kL\rho c}{16\pi r_S r_P}\frac{4\pi D}{ik\rho c} = \frac{1+ikr_S}{kr_S}\frac{LD}{4r_S r_P}$$

The last term can be simplified by substituting $r_S \approx d_S$ and $r_P \approx d_P$, which is justified for large distance compared to the size of the aperture, and representing L by the definition from equation 108, we get:

$$\frac{LD}{r_S r_P} \approx \frac{\dfrac{d_S d_P}{d_S + d_P}(d_S + d_P)}{d_S d_P} = 1$$

This means, that the ratio between P_2 and p_D approach ¼ for $kr_S > 1$, which is above 55 Hz for a source at distance $r_S = 1$ m behind the aperture.

Again using $r_S \approx d_S$, which is an approximation only affecting the low-frequency range, the transfer function becomes:

$$H = \frac{1+ikr_S}{4kr_S}\left(C(v_{x2})-C(v_{x1})-i[S(v_{x2})-S(v_{x1})]\right)\left(C(v_{y2})-C(v_{y1})-i[S(v_{y2})-S(v_{y1})]\right) \qquad 123$$

This expression applies generally to any rectangular aperture where the dimensions of the aperture are not larger than the distance to the source and observation point; a requirement, which must be satisfied, as will be shown below.

5.2.5 Transfer function problems

Using the Fresnel integrals for solving problem with large apertures invalidate several of the assumptions leading to the transfer function; the distance h is not small for apertures approaching infinity in one or more directions, so the equation for $r_S + r_P$ becomes incorrect and $r_S r_P$ cannot be assumed constant. It is anyway common practice within the field of optics to apply the Fresnel integrals for solving problems with apertures approaching infinity. The explanation must be that the result of doing so is indeed leading to useful results. However, problems are also encountered as the following analysis will show.

A simple way of checking the transfer function for large apertures is studying the result of an aperture approaching infinity; i.e. the complete removal of the baffle. This leaves the spherical wave form unobstructed and the transfer function must be unity since there is nothing to distort the wave front – but as will be shown below, this is not the case.

Inserting the coordinates for the infinite aperture $x_1 \rightarrow -\infty$, $x_2 \rightarrow \infty$, $y_1 \rightarrow -\infty$, and $y_2 \rightarrow \infty$ into the expression, the transfer function becomes:

$$H = \frac{1+ikr_S}{4kr_S}\left(C(\infty)-C(-\infty)-i[S(\infty)-S(-\infty)]\right)\left(C(\infty)-C(-\infty)-i[S(\infty)-S(-\infty)]\right)$$

$$= \frac{1+ikr_S}{4kr_S}(1-i)(1-i)$$

The terms with $1 - i$ represent the vectors of the Carnu plot for the x and the y directions; from minus infinity at (–0.5, –0.5) to plus infinity at (0.5, 0.5). Assuming large distance to the source, the magnitude of the transfer function approaches:

$$|H| = \left|\frac{1+ikr_S}{4kr_S}\sqrt{2}\sqrt{2}\right| \xrightarrow[kr_S \rightarrow \infty]{} \frac{1}{2}$$

This is obviously wrong and the error is due to assumption violations. A correction will be given in the section to follow.

Another problem is the amplitude at low frequencies, which "blows up" for kr_S approaching zero, which occur at very low frequencies or with a source approaching the aperture:

$$|H| = \left|\frac{1+ikr_S}{4kr_S}\sqrt{2}\sqrt{2}\right| \xrightarrow[kr_S \rightarrow 0]{} \infty$$

This is more troublesome to cure than the above amplitude error since the complex factor comes directly from the specific impedance of a sphere and omission of the term is violating fundamental acoustic relations. The term approaches unity at higher frequencies, where the amplitude appears to be correct with the exception of the missing factor of two, but the term is increased for low frequencies, which is in contradiction to what could be expected and it is without physical explanation. However, the term is problematic and must be removed, which corresponds to state that the impedance of a sphere is ρc regardless of the distance to the source – we have transformed the spherical wave into a plane wave!

5.2.6 Aperture ratio

Integration was performed within the xy-plane assuming that the wavelets of the spherical wave front could be projected onto the plane without distortion. This assumption holds when a surface area of the sphere is indeed approximating the surface area of the projection. When the area of the sphere is larger than the projection, the wavelets are "squeezed together" thus reducing their effective area, dS, so the strength of radiation is reduced since the wavelets are assumed described by the infinitesimal volume velocity $dq = udS$.

Assuming a circular aperture we can express the size of the aperture as the angle between radius of the sphere at the edge of the aperture and the direction to the observer (the z-axis). The distance d_S from source to the aperture is a known quantity and radius of the sphere from the source can be written using d_S and a, thus solely using known parameters:

$$d_S = r_S \cos(\alpha) = \sqrt{d_S^2 + a^2}\,\cos(\alpha) = d_S\sqrt{1+\frac{a}{d_S}}\,\cos(\alpha)$$

Hence, the definition for the angle where σ will be introduced as the *aperture ratio* defined as the ratio between aperture height (radius) and the distance to the source.

$$\cos(\alpha) = \frac{1}{\sqrt{1+\sigma^2}}, \quad \sigma = \frac{a}{d_S} \qquad\qquad 124$$

For small apertures is the aperture ratio close to zero while it approaches infinity for large apertures thus limiting the angle to the range from 0 to 90°. The result can be generalised into rectangular apertures, assuming that the aperture is not too far from the shape of a circle. For an aperture with width 2A wide and height 2B and using the geometric mean of the two directions for calculation of an average aperture size, we get:

$$\sigma_A = \frac{A}{d_S}, \quad \sigma_B = \frac{B}{d_S} \quad \Rightarrow \quad \sigma = \sqrt{\sigma_A \sigma_B} = \frac{\sqrt{AB}}{d_S} \qquad\qquad 125$$

It will be required dividing the theory into individual treatments for the two dimensions when the ratio between the dimensions A and B is large.
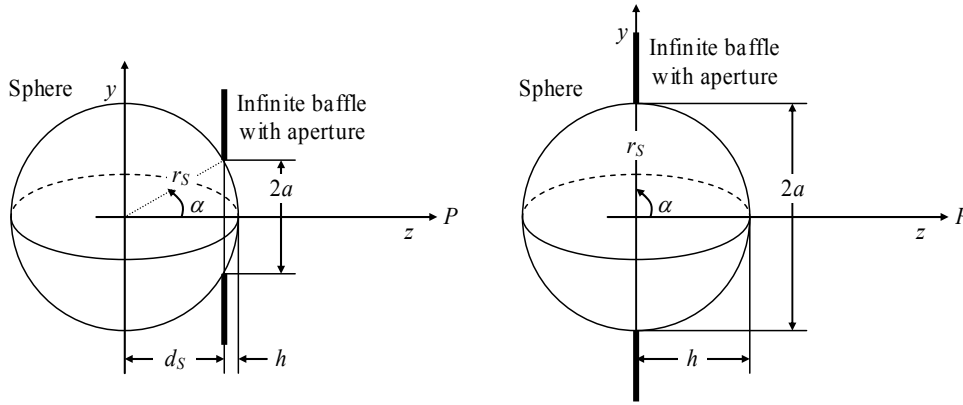
Figure 127 – Part of a spherical wave front is propagating through an aperture with two different aperture angles.

We will now derive an expression of the "wavelet distortion" due to the projection of the sphere onto the *xy*-plane of the aperture. The area of the projection of the right-hand part of the sphere onto the plane is the area of the circular aperture with radius a, which can be expressed by the sphere radius and the above aperture angle.

$$S_P = \pi a^2 = \pi r_S^2 \sin(\alpha)$$

The surface area of the sphere to be projected, i.e. the actual area of the right-hand part of the sphere, is given by the height h of the curved surface over the aperture according to the following expression (Westergren, 74) and the height can be expressed by the sphere radius and the aperture angle:

$$S_A = 2\pi r_S h = 2\pi r_S^2 (1 - \cos(\alpha))$$

Hence the ratio between the surface areas:

$$s = \frac{S_P}{S_A} = \frac{\pi r_S^2 \sin^2(\alpha)}{2\pi r_S^2 (1 - \cos(\alpha))} = \frac{\sin^2(\alpha)}{2(1 - \cos(\alpha))}$$

Using the trigonometric relation for sine squared the ratio can be expressed as:

$$s = \frac{1 - \cos^2(\alpha)}{2(1 - \cos(\alpha))} = \frac{(1 + \cos(\alpha))(1 - \cos(\alpha))}{2(1 - \cos(\alpha))} = \frac{1 + \cos(\alpha)}{2} \rightarrow \begin{cases} 1 & \alpha \rightarrow 0 \\ 1/2 & \alpha \rightarrow \pi/2 \end{cases}$$

The result for large apertures ($s = 1/2$) is exactly the result of the transfer function for the unobstructed sphere (large angle) and although not a proof of the cause of the error, it is at least a starting point for restoring the amplitude to the correct value.

Inserting the above definition of cosine, we finally get the equation for amplitude correction:

$$s = \frac{1}{2}\left(1 + \frac{1}{\sqrt{1 + \sigma^2}}\right) \qquad\qquad 126$$

For $\sigma = 0.1$ where $\alpha = 6°$ is the area ratio $s = 0.9975$ so the amplitude is corrected by 0.25 % or less, i.e. small apertures. For $\sigma = 1$ where $\alpha = 45°$ is $s = 0.85$ so the correction is 15 % and the aperture is neither small nor large. For $\sigma = 10$ where $\alpha = 84°$ is $s = 0.55$ so projection distortion is serious and the aperture is large.

Referring to the transfer function in equation 123, the previously fixed one-fourth scaling factor will be substituted by the following scaling factor:

$$H_A = \frac{1}{4s} = \frac{1}{2\left(1 + \dfrac{1}{\sqrt{1 + \sigma^2}}\right)} = \frac{1}{2}\frac{\sqrt{1 + \sigma^2}}{\sqrt{1 + \sigma^2} + 1} \qquad\qquad 127$$

Hence, $H_A = \frac{1}{4}$ for $\sigma \rightarrow 0$ (small apertures) and $H_A = \frac{1}{2}$ for $\sigma \rightarrow \infty$ (large apertures) with values within this range for "medium" apertures.

5.2.7 Modified transfer function

Removing the troublesome scaling factor due to the spherical waveform and including the aperture correction H_A we get the following modified transfer function:

$$\boxed{H = H_A\left(C(v_{x2}) - C(v_{x1}) - i[S(v_{x2}) - S(v_{x1})]\right)\left(C(v_{y2}) - C(v_{y1}) - i[S(v_{y2}) - S(v_{y1})]\right)} \qquad 128$$

The aperture correction factor H_A is calculated from equation 127 with the aperture ratio σ given by equation 124 for circular aperture or 125 for rectangular apertures and the arguments to the Fresnel integrals are calculated from equation 114, 118 or 119 and the Fresnel integrals are evaluated from equation 116.

For control, consider the infinite aperture with: $x_1 \rightarrow -\infty$, $x_2 \rightarrow \infty$, $y_1 \rightarrow -\infty$ and $y_2 \rightarrow \infty$; the aperture ratio becomes $\sigma = \infty$ and thus the aperture correction factor $H_A = \frac{1}{2}$ (large aperture). The amplitude of the transfer response becomes unity and independent upon frequency as shown below.

$$H = \left|\tfrac{1}{2}\left(\tfrac{1}{2} + \tfrac{1}{2} - i\left[\tfrac{1}{2} + \tfrac{1}{2}\right]\right)\left(\tfrac{1}{2} + \tfrac{1}{2} - i\left[\tfrac{1}{2} + \tfrac{1}{2}\right]\right)\right| = \left|\tfrac{1}{2}(1 - i)(1 - i)\right| = 1$$

This concludes the development of the transfer function according to the Fresnel near-field approximations. The following sections will use the results on different applications including the loudspeaker baffle.

5.2.8 Semi-infinite baffle

The semi-infinite baffle shown in Figure 128 may represent a noise barrier between a noisy road and domestic area but it may also be used as a model for the off-axis response of a loudspeaker baffle with the point source representing the loudspeaker unit.
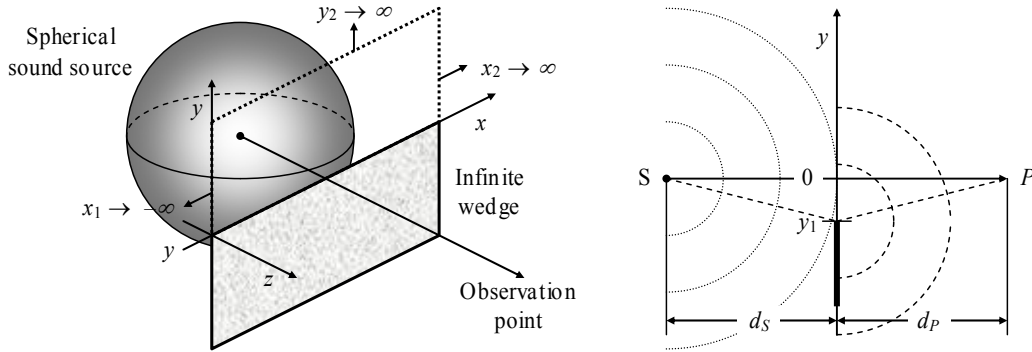
Figure 128 – An infinite edge is blocking part of the sound at the observation point.

An observer sees most of the radiation (dotted) plus the diffraction (dashed) from the edge when it is below the line-of-sight from source to observer ($y_1 < 0$). An observer sees 50 % of the wave front when the edge is just at the line-of-sight ($y_1 = 0$) and a level of –6 dB is expected since half the power within the wave front is removed. An observer sees only the diffracted signal when the edge obstructs the line-of-sight ($y_1 > 0$) so there will be no interference with the direct signal.

Assume that the coordinate system is arranged with the edge at the y-axis where zero is at the line-of-sight so that the aperture becomes semi-infinite in the y-direction and described by the following coordinates $x_1 \rightarrow -\infty$, $x_2 \rightarrow \infty$ and $y_2 \rightarrow \infty$; we get the aperture ratio $\sigma = \infty$ and the aperture correction $H_A = \frac{1}{2}$ (large aperture) so the transfer function for the sound pressure behind the obstruction (the semi-infinite baffle) becomes:

$$H = \tfrac{1}{2}\left(C(\infty) - C(-\infty) - i\left[S(\infty) - S(-\infty)\right]\right)\left(C(\infty) - C(v_{y1}) - i\left[S(\infty) - S(v_{y1})\right]\right)$$

Since $C(\infty) = S(\infty) = \frac{1}{2}$ and $C(-\infty) = S(-\infty) = -\frac{1}{2}$, the first parenthesis becomes $(1 - i)$ and the result is:

$$H = \tfrac{1}{2}(1 - i)\left(\tfrac{1}{2} - C(v_{y1}) - i\left[\tfrac{1}{2} - S(v_{y1})\right]\right)$$

Using the scaling factor for y_1 from equation 118 we get:

$$H = \tfrac{1}{2}(1 - i)\left(\tfrac{1}{2} - C(v_{y1}) - i\left[\tfrac{1}{2} - S(v_{y1})\right]\right), \quad v_{y1} = \sqrt{\frac{kL}{\pi}}\,\frac{y_1}{L} \tag{129}$$

Here is y_1 the edge height above the direct sight from the source to the observer; this means that y_1 is positive when the edge is blocking the line-of-sight between source and observer and negative when the observer can see the source.

Plots of the transfer function are shown using three different values of the distance d_S between source and edge while the distance d_P to observer is kept constant at 1 m. The response is calculated for three fixed positions of the edge specified through y_1. For the upper curve is the edge below the line-of-sight ($y_1 = -1$ m), for the middle curve is the edge positioned just at the line-of-sight ($y_1 = 0$) and for the bottom curve is the edge obstructing the direct sight between source and observer ($y_1 = 1$ m) so that only the diffracted signal is monitored.

The first plot is for $d_S = d_P = 1$ m (below, left) and the second plots keeps d_P unchanged while changing $dS = 0.1$ m (below, right).
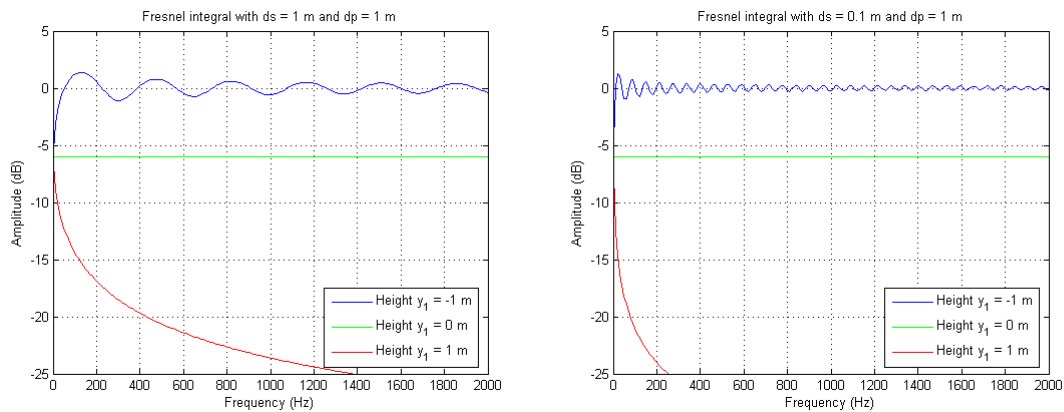
Figure 129 – Transfer function with source 1 m from baffle (left) or 0.1 m (right) and the observer 1 m from baffle measured and at three different heights.

The third plot uses $dS = 10$ m (below, left) is compared to the Fraunhofer integration from the previous section (below, right). This comparison shows that the Fresnel near-field approximation approaches the far-field theory for large distance to the source since the spherical wave front can be considered locally plane at large distance.
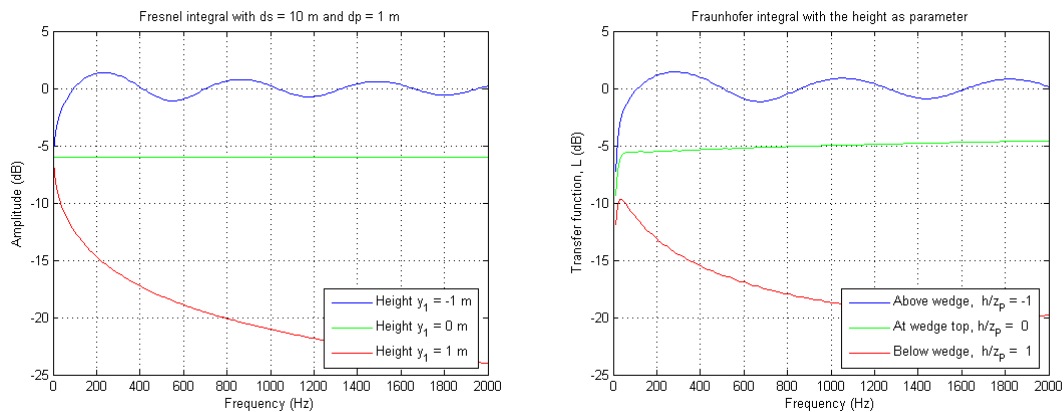
Figure 130 – Transfer function with source 10 m from baffle (left) and Fraunhofer far-field approximation (plane wave source) for an observer 1 m from the baffle (right).

The frequency response oscillates around 0 dB for an observer above the line-of-sight since the diffracted signal from the baffle is interfering with the direct signal. The ripples are suppressed for a baffle edge right at the line-of-sight since the delay between the signals is reduced to zero and the level is reduced by 6 dB since half the signal power is removed from reaching the observer (the Fresnel near-field approximation assumes that the blocked signal does not cause interference; it disappears, as if the baffle were perfectly absorbing). The frequency response for an observer below the line-of-sight is increasingly attenuated at the higher frequencies.

The Fresnel length is insensitive to interchanging d_S and d_P so the plots remains the same for a fixed distance between source and baffle of 1 m and with the distance between baffle and observer as parameter.

5.2.9 Loudspeaker off-axis response

The model for the semi-infinite baffle will be used to simulate the off-angle response of a loudspeaker cabinet. The idea is based upon a result from the *Measurement* section where it was shown that the diffraction from a narrow baffle (0.5 m wide) was almost identical to that of a three times wider baffle. This does not at all prove that a finite baffle performs as a semi-infinite baffle, but it does not harm to make an experiment and see if it fits. The finite baffle will thus be considered represented by a semi-infinite baffle, which opens the possibility of using the Fresnel near-field approximations.
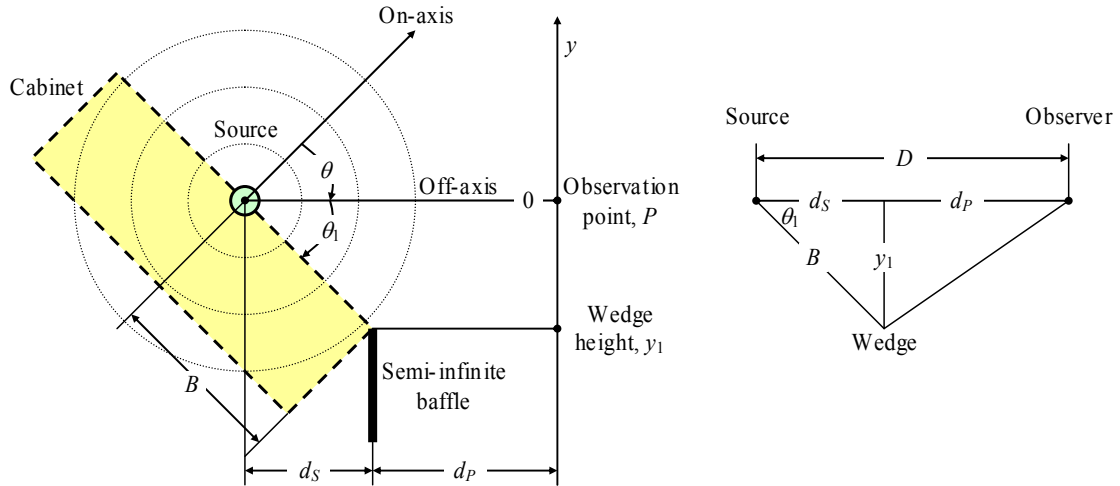
Figure 131 – An semi-infinite baffle is used as model for loudspeaker off-axis performance.

The cabinet dimension of interest is B and may represent width or height depending upon the requirement. The observation distance D and observation angle θ are specified by the requirements for the set-up. The required distances d_S and d_P are determined by:

$$d_S = B\cos(\theta_1), \quad \theta_1 = \pi/2 - \theta$$
$$d_P = D - d_S$$

The edge of the semi-infinite baffle is located at the y-coordinate of the loudspeaker baffle edge used for the simulation. The height of the semi-infinite baffle is thus:

$$y_1 = -B\sin(\theta_1)$$

The Fresnel variable v related not only to the height of the semi-infinite baffle but also to frequency and is calculated through the use of equation 109 and 119:

$$v_{y1} = \sqrt{\frac{2f}{cL}}\, y_1, \quad L = \frac{d_S d_P}{d_S + d_P}$$

The transfer function is (according to equation 129):

$$H = \tfrac{1}{2}(1-i)\left(\tfrac{1}{2} - C(v_{y1}) - i\left[\tfrac{1}{2} - S(v_{y1})\right]\right)$$

The result is shown below for a loudspeaker with $B = 0.10$ m, which corresponds to a side length of 0.20 m. The observation distance was $D = 1.30$ m (the measurements were not offset to 1.41 m as is done elsewhere) and the observation angle is the parameter.
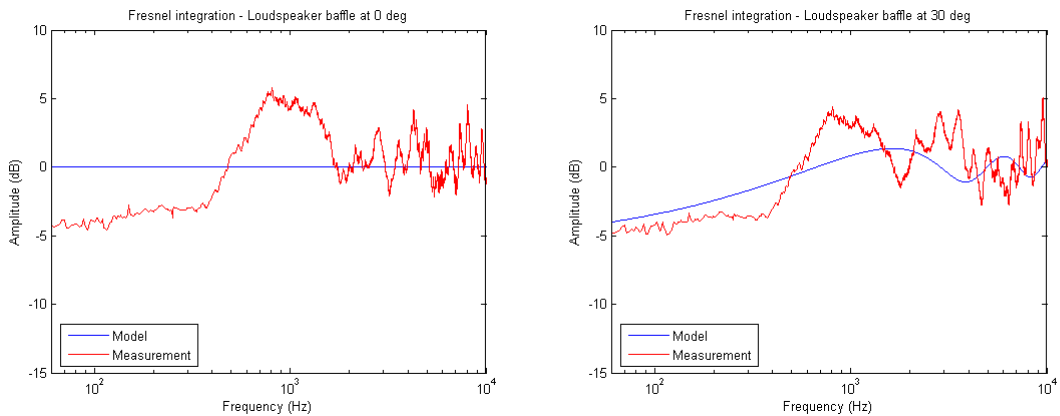
Figure 132 – Fresnel integration method used to determine the on-axis (0°) and 30° off-axis response for a loudspeaker baffle using a semi-infinite baffle as model.
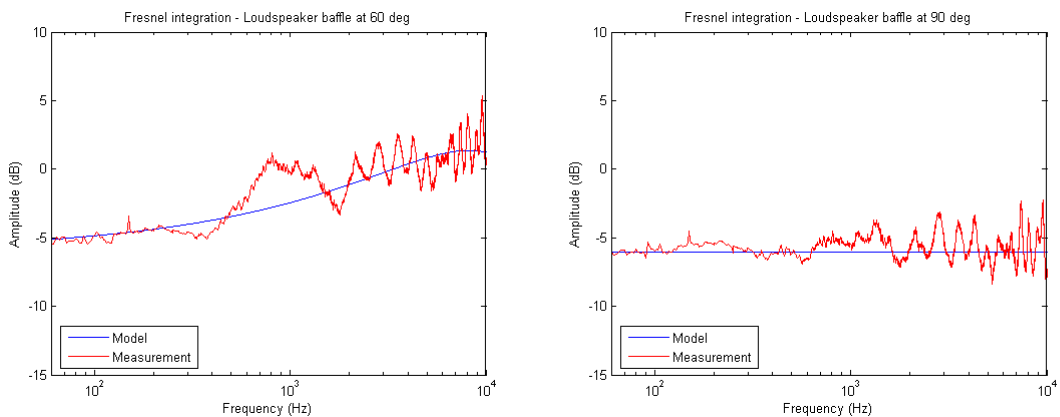
Figure 133 – Fresnel integration method used to determine the 60° and 90° off-axis response for a loudspeaker baffle using a semi-infinite baffle as model.

The responses are correct in broad outline, i.e. ignoring the finer details. The measurement are including contributions from all four edges so full accordance to measurements cannot be expected from a simulation using one edge only. The 6 dB loss of bass was correctly modelled for the 30°, 60° and 90° examples above; only the calculation at 0° failed in this respect so it was decided to run a couple of simulations to find the limit where the model starts working. The figures below show the evolution in 5° steps and with the measurement at 0° used for reference since measurements at points between 0° and 20° were not available.
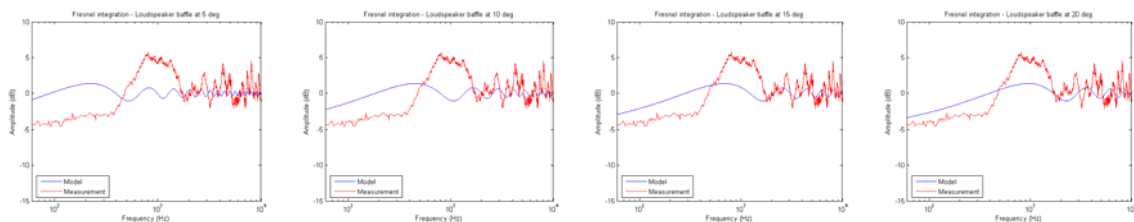
Figure 134 – Off-axis response for 5°, 10°, 15° and 20° and compared to measurement at 0°.

The low-frequency level is starting near 0 dB and is moving downward toward the correct value, which is reached around 20° with a fair approximation from 15°. The model is thus of limited value for an observation point close to on-axis.

For angles above 90° is the direct signal from source blocked and only the diffracted component is received at the observation point. The results are reported below and show good agreement at 120° and 150° although the finer details are missing.
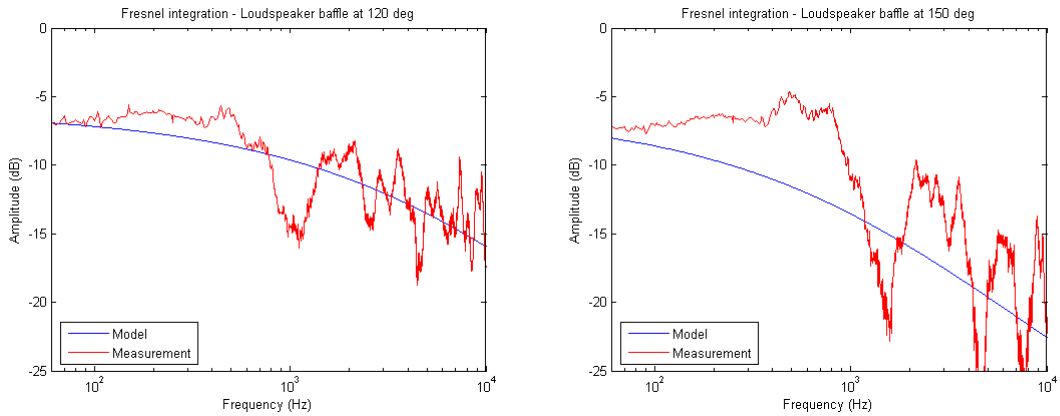
Figure 135 – Fresnel integration method used to determine the 120°, 150°, 170° and 179° off-axis response for a loudspeaker baffle.

The response at 180° can not be calculated since the Fresnel length becomes zero so the last test was performed at 179° with the measurement result shown for 180°. The result was far away from the measured response so a calculation at 170° was included.
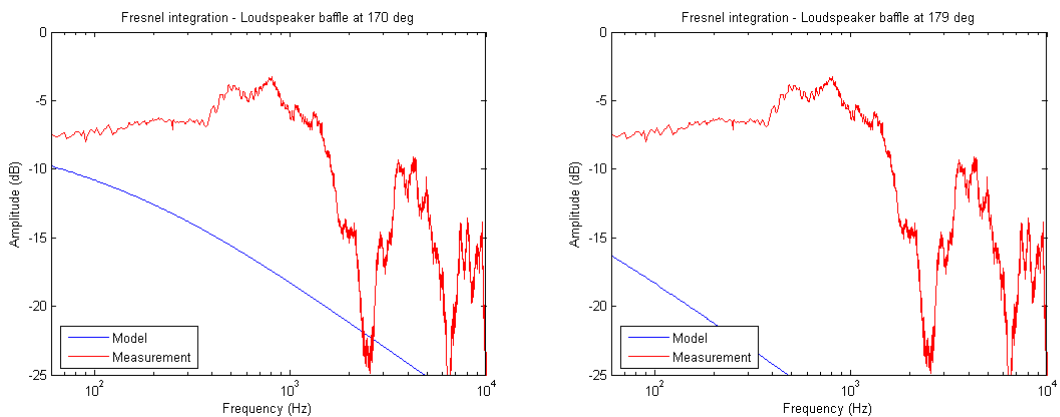
Figure 136 – Fresnel integration method used to determine the 120°, 150°, 170° and 179° off-axis response for a loudspeaker baffle.

As a conclusion, the semi-infinite baffle is useful as model for off-axis responses from 30° to 150° but it does not model all details of the loudspeaker baffle. An important feature of the method is that the transition from front side to rear side is smooth so the method can be used as a complement to the models presented in the previous chapter, they should be preferred for simulations within ±30° from on-axis.

Execution time for a frequency spectrum with 6400 points was less than 3 minutes.

5.2.10 Rectangular baffle

The transfer function for a rectangular aperture will be studied for its use as a model for the rectangular loudspeaker baffle since the radiation is assumed equivalent to the radiation from a point source behind an infinite baffle with an aperture shaped as the baffle.
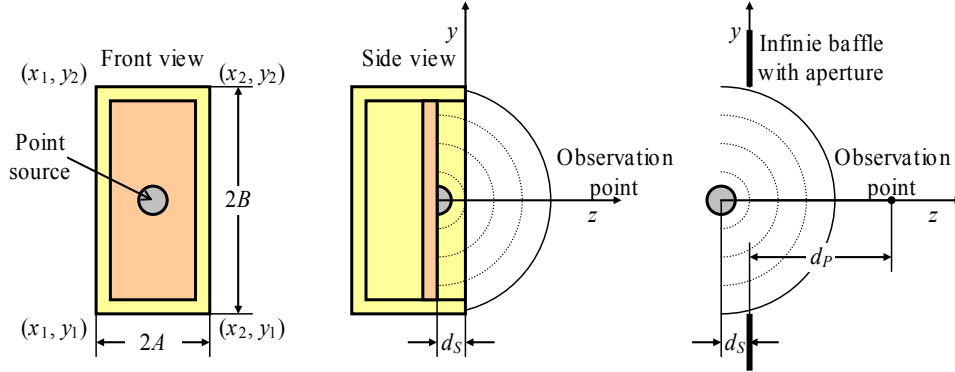
Figure 137 – Loudspeaker baffle and the spherical wave form at the rectangular aperture.

The point source should ideally be located flush with the front baffle, but this requires $d_S = 0$ so the Fresnel length becomes zero and cannot be used for scaling to the Fresnel variable. A compromise is required so a finite distance will be allowed corresponding to moving the loudspeaker baffle back from the front. This design is avoided in real loudspeaker due to problems with standing waves but must be accepted here to use the Fresnel theory.

For an observation distance of r_0 measured from the aperture, which defines the front of the box, and using horizontal off-axis simulations using the xz-plane the coordinates becomes:

$$x_P = r_0 \sin(\theta)$$
$$y_P = 0$$
$$z_P = r_0 \cos(\theta)$$

The transfer function is related to the aperture and the loudspeaker is assumed to be located at the centre; hence: $x_1 = -A$ and $x_2 = A$ for the horizontal axe and $y_1 = -B$ and $y_2 = B$ for the vertical axe. The observation point cannot be moved – but the aperture can – so we have the following aperture coordinates with θ as the observation angle:

$$x_1 = -A + R\sin(\theta) \quad x_2 = A + R\sin(\theta)$$
$$y_1 = -B \qquad\qquad y_2 = B$$

The integration limits for the Fresnel integrals is given by equation 119 where the scaling by h relates the Fresnel variables to the size and position of the aperture, the distance to the source and observation point and to frequency:

$$v_{x1} = hx_1, \quad v_{x2} = hx_2, \quad v_{y1} = hy_1, \quad v_{y2} = hy_2, \quad \text{where} \quad h = \sqrt{\frac{2f}{cL}}$$

The transfer function is given by equation 128 as:

$$H = H_A\big(C(v_{x2}) - C(v_{x1}) - i[S(v_{x2}) - S(v_{x1})]\big)\big(C(v_{y2}) - C(v_{y1}) - i[S(v_{y2}) - S(v_{y1})]\big)$$

The aperture correction is defined from equation 127 with the aperture size given by equation 125 with the current loudspeaker baffle defined by $2A = 0.20$ m and $2B = 0.34$ m:

$$H_A = \frac{1}{2}\frac{\sqrt{1+\sigma^2}}{\sqrt{1+\sigma^2}+1}, \quad \sigma = \frac{\sqrt{AB}}{d_S}$$

The result is shown below and is seen to be very dependent upon the selection of d_S and there is no clear relation between the calculated and measured responses so this method is not useful for calculation of on-axis responses.
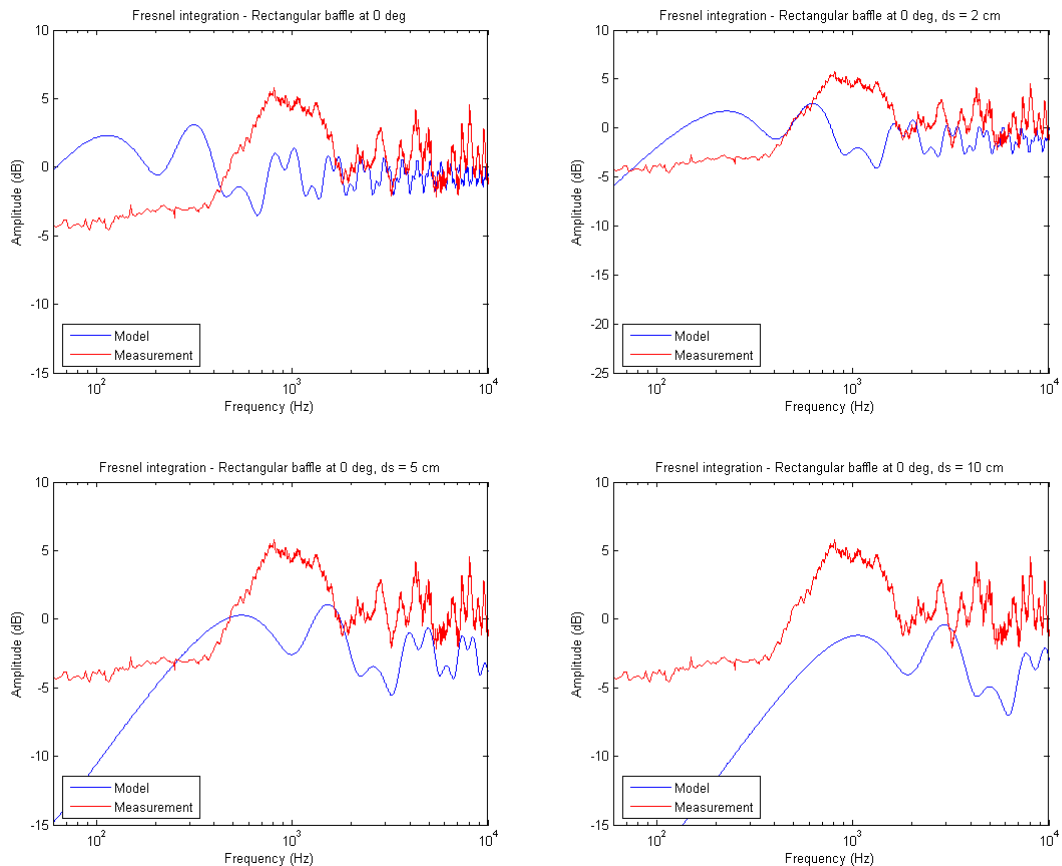
Figure 138 – Fresnel integration used with rectangular aperture as model for a rectangular baffle at 0° observation angle with d_S = 1, 2, 5 and 10 cm.

Execution time for 6400 frequency points was less than 10 minutes. This includes 8 calls to the MAPLE commands for Fresnel cosine and sine integrals so more than $50\ 10^3$ integrals have been calculated thus requiring about 10 ms for each integral.

5.3 Conclusion

The Fraunhofer far-field theory and the Fresnel near-field theory are valuable tools for determining the angular pattern of a source and diffraction around the edge of a baffle. The computational power required is relatively large so the models are not (yet) interesting for implementing within real-time computer-aided systems.

6 Software

This chapter presents the software for the models.

6.1.1 Angular response

The angular response was plotted from the seven files monitored at 0°, 30° and so on to 180°. The 0° on-axis response were used for normalisation (0 dB reference) and results were averaged through a ±5 % range around the centre frequency.

```
% =======================================================================
% ANGULAR PLOTS
% =======================================================================
% Plot the angular response for the selected source files.
%
% The file format is:   (1) Line number:   N = 1, 2, 3, ..., 6401.
%                        (2) Frequency:     F = 0, 2, 4, ..., 12800 Hz.
%                        (3) Real value.
%                        (4) Imag value.
%
% Average plot over points corresponding to 10 % frequency
% Index for the centre frequency is calculated from:    F = 2*(N-1)
% Hence the line number:                                 N = F/2+1
%
% Written by Tore Skogberg, (c) 2006.

% Files: SourceAngular Response.png

clear
format compact

% === GET FILES =========================================================
fid=fopen('5-CircularBaffle\FreqRespSource000.dat');
DF=fscanf(fid, '%e %e %e %e', [4 inf]); fclose(fid);
DF=DF'; M(1,:)=sqrt(DF(:,3).^2 + DF(:,4).^2);
fid=fopen('5-CircularBaffle\FreqRespSource030.dat');
DF=fscanf(fid, '%e %e %e %e', [4 inf]); fclose(fid);
DF=DF'; M(2,:)=sqrt(DF(:,3).^2 + DF(:,4).^2);
fid=fopen('5-CircularBaffle\FreqRespSource060.dat');
DF=fscanf(fid, '%e %e %e %e', [4 inf]); fclose(fid);
DF=DF'; M(3,:)=sqrt(DF(:,3).^2 + DF(:,4).^2);
fid=fopen('5-CircularBaffle\FreqRespSource090.dat');
DF=fscanf(fid, '%e %e %e %e', [4 inf]); fclose(fid);
DF=DF'; M(4,:)=sqrt(DF(:,3).^2 + DF(:,4).^2);
fid=fopen('5-CircularBaffle\FreqRespSource120.dat');
DF=fscanf(fid, '%e %e %e %e', [4 inf]); fclose(fid);
DF=DF'; M(5,:)=sqrt(DF(:,3).^2 + DF(:,4).^2);
fid=fopen('5-CircularBaffle\FreqRespSource150.dat');
DF=fscanf(fid, '%e %e %e %e', [4 inf]); fclose(fid);
DF=DF'; M(6,:)=sqrt(DF(:,3).^2 + DF(:,4).^2);
fid=fopen('5-CircularBaffle\FreqRespSource180.dat');
DF=fscanf(fid, '%e %e %e %e', [4 inf]); fclose(fid);
DF=DF'; M(7,:)=sqrt(DF(:,3).^2 + DF(:,4).^2);

% === DEFINE SCALES =====================================================
F = [125 250 500 1000 2000 4000 8000];      % Frequencies (Hz).
A = [0 30 60 90 120 150 180];               % Angles (degrees).
C = ['b' 'g' 'r' 'c' 'm' 'y' 'k'];          % Colours for plot.

% === PLOT CURVES =======================================================
for f=1:7                      % Step through frequencies.
    N = F(f)/2+1;              % Get index to centre frequency.
    N1 = round(0.95*N);        % Index to -5 %.
    N2 = round(1.05*N);        % Index to +5 %.
    for k=1:7                  % Step through angles.
        R(k)=20*log10(mean(M(k,N1:N2))/mean(M(1,N1:N2)));
    end
    plot(A,R,C(f));            % Plot the selected curve.
    hold on                    % Keep plot active.
end
```

```matlab
% === PLOT LABELS =======================================
axis([0 180 -30 5]);
grid on
title('Source angular response');
xlabel('Observation angle (degrees)');
ylabel('Amplitude (dB)');
legend('125 Hz','250 Hz','500 Hz','1 kHz','2 kHz','4 kHz','8 kHz', ...
       'Location','SouthWest');
```

6.1.2 Impulse response

The edge diffraction model used the calculated impulse response for a circular baffle where the measured frequency response was converted to impulse response using the MATLAB command for inverse Fourier transformation: IFFT.

The program reads the input file for the measurement and for the reference and calculates the complex transfer function in "FreqResp", which is a vector with 6401 complex elements. The impulse response is calculated directly and plotted with real, imaginary and amplitude values.

```matlab
% ====================================================================
% Calculate the transient response from measurements.
% ====================================================================
% Input is the monitored frequency response 0 ... 12800 Hz in 2 Hz step
% from the measurement of the on-axis response of the circular baffle
% normalised to the measurement of the on-axis response without baffle.
%
% Written by Tore Skogberg, (c) 2006.

clear
format compact

% --- Constants
tm = 1/2;               % Sampling time (s)
dt = 1/12800;           % Incremental time (s)
t = 0:dt:tm;            % Time axis (s)

% --- Get source and reference files
s='5-CircularBaffle/FreqRespBaffle000.dat';        % Source file
fid=fopen(s);
d=fscanf(fid, '%e %e %e %e', [4 inf]);
fclose(fid);
d=d';
s='5-CircularBaffle/FreqRespInitial4.dat';         % Reference file
fid=fopen(s);
r=fscanf(fid, '%e %e %e %e', [4 inf]);
fclose(fid);
r=r';

% --- Plot normalised frequency response
figure(1);
FreqResp = (d(:,3)+i*d(:,4)) ./ (r(:,3)+i*r(:,4));  % Response Re+i*Im

semilogx(r(:,2), 20*log10(abs(FreqResp)),'-');
axis([100 10000 -15 25]);
title('Impulse response - Frequency spectrum');
xlabel('Frequency (Hz)');
ylabel('Amplitude (dB)');

% --- Plot impulse response
figure(2);
TimeResp = ifft(FreqResp);
plot(t,real(TimeResp),'-.',t,imag(TimeResp),':',t,abs(TimeResp),'-');
axis([0 2e-3 -1 1]);
title('Impulse response - Time response');
xlabel('Time (s)');
ylabel('Amplitude');
legend('Real','Imag','Amplitude');
```

6.1.3 Comparing models to measurements

This software was used for the majority of plots. The software is basically divided into three sections; first, an introduction with definition of constants used; second, a selection of models to analyse and third, an output block for plotting. Most models are deactivated by "commenting" the lines within the software list or through **UseModel**, which is a software selector used to enable or disenable code segments through **if** and **elseif** commands. Most models include algorithms for calculation of both front-side and rear-side spectra and the software listing includes reference to the PNG-file used internally for this documentation.
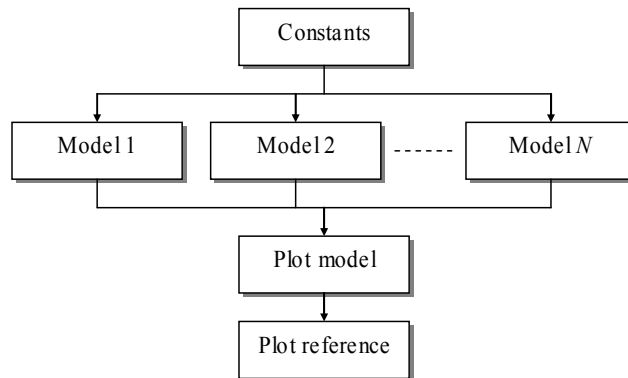
Figure 139 – Software layout with a common block for the definition of constants followed by the individual models and finally the common block for plotting of the results.

All plots consist of two inputs: the result from the model (plotted in blue colour) and the input from the file selected for comparison (plotted in red colour). The selected file is plotted as the difference between the measurement and the average of the four measurements selected as the free-field reference.

```
% ===================================================================
% COMPARE RESPONSE TO MEASUREMENT
% ===================================================================
% Plot the calculated frequency response and compare to measurement.
%
% Written by Tore Skogberg, 2006.
% -------------------------------------------------------------------

clear
format compact
disp('Executing ...');

% -------------------------------------------------------------------
% DEFINITIONS
% -------------------------------------------------------------------
% Constants, parameters and variables used throughout the program.
% The "CONSTANTS" can be changed at will, "Parameters" affects the
% calculated plot and "Output control" affects plot layout. The
% "VECTORS" are internal variables and should not be changed since
% the size should match the 6401 lines of the Data files (xxx.DAT).
% -------------------------------------------------------------------

% === CONSTANTS =====================================================

% --- Parameters
B    =     0.17;        % Radius of circular baffle (m).
R    =    -0.60;        % Reflection coefficient.
c    =    345;          % Speed of sound (m/s).

% --- Output control
fmin =     60;          % Start frequency (Hz).
fmax = 10000;          % Stop frequency (Hz).
pmax =     10;          % Maximum pressure within plot (dB).
pmin =    -15;          % Minimum pressure within plot (dB).
```

```
% offs =     0;           % No free-field correction (dB).
offs =    -6.02;          % Free-field correction (dB).
corr =     0.00;          % Distance correction (dB).

% === VECTORS ========================================================

f = 0:2:12800;            % Frequency axis (Hz) - DO NOT CHANGE.
g = 1:6401;               % Dummy index counter.
p0(g) = 1;                % Initialise p0 for 0 dB in meas. report.
k  = (2*pi/c)*f;          % Angular wavenumber (1/m).
kB = k*B;                 % Normalised frequency and range.

% ====================================================================
% MEASUREMENT REPORT - CIRCULAR BAFFLE
% ====================================================================

% Files: PlotCircularBaffleCentre000.png    (Observation angle)
%        PlotCircularBaffleCentre030.png
%        PlotCircularBaffleCentre060.png
%        PlotCircularBaffleCentre090.png
%        PlotCircularBaffleCentre120.png
%        PlotCircularBaffleCentre150.png
%        PlotCircularBaffleCentre180.png
%
%        PlotCircularBaffleOfset00cm.png    (Source offset)
%        PlotCircularBaffleOfset03cm.png
%        PlotCircularBaffleOfset06cm.png
%        PlotCircularBaffleOfset09cm.png
%        PlotCircularBaffleOfset12cm.png
%        PlotCircularBaffleOfset15cm.png
%        PlotCircularBaffleOfset18cm.png
%        PlotCircularBaffleOfset25cm.png

% === PLOT OBSERVATION ANGLE =========================================

% MainTitle='Circular baffle, 0 degrees';
% DataFile='5-CircularBaffle\FreqRespBaffle000.dat';

% === PLOT SOURCE OFFSET =============================================

% MainTitle='Circular baffle, Offset 25 cm';
% DataFile='3-CircularBaffle\FreqRespFront25cm.dat';
% corr = -0.71;

% ====================================================================
% MEASUREMENT REPORT - RECTANGULAR BAFFLE
% ====================================================================

% Files: PlotRectangularBaffleCentre000.png
%        PlotRectangularBaffleCentre030.png
%        PlotRectangularBaffleCentre060.png
%        PlotRectangularBaffleCentre090.png
%        PlotRectangularBaffleCentre120.png
%        PlotRectangularBaffleCentre150.png
%        PlotRectangularBaffleCentre180.png
%        PlotRectangularBafflePoint1.png
%        PlotRectangularBafflePoint2.png
%        PlotRectangularBafflePoint3.png

% === PLOT OBSERVATION ANGLE =========================================

% MainTitle='Rectangular baffle, 180 degrees';
% DataFile='4-RectangularBaffle\FreqRespCentre180.dat';

% === PLOT SOURCE OFTSET =============================================

% MainTitle='Rectangular baffle, Point 3';
% DataFile='4-RectangularBaffle\FreqRespCentre000.dat';   % Point 1
% DataFile='4-RectangularBaffle\FreqRespOffset.dat   ';   % Point 2
% DataFile='4-RectangularBaffle\FreqRespAsym.dat     ';   % Point 3

% ====================================================================
% EDGE DIFFRACTION MODEL - REFLECTION COEFFICIENT
% ====================================================================
```

```
% Files: PlotFixedReflectionCoefficient1.png    (R = -0.60 Front)
%        PlotFixedReflectionCoefficient2.png    (R = -0.33 Front)
%        PlotFixedReflectionCoefficient3.png    (R = -0.60 Rear)
%        PlotFixedReflectionCoefficient4.png    (R = -0.33 Rear)
%        PlotFixedReflectionCoefficient5.png    (R = -0.60 Dif Front)
%        PlotFixedReflectionCoefficient6.png    (R = -0.33 Dif Front)
%        PlotVariableReflectionCoefficient1.png (R = -0.60 Front)
%        PlotVariableReflectionCoefficient2.png (R = -0.33 Front)
%        PlotVariableReflectionCoefficient3.png (R = -0.60 Rear)
%        PlotVariableReflectionCoefficient4.png (R = -0.33 Rear)

% === FIXED REFLECTION COEFFICIENT ===================================

% R  = -0.60;
% p1 = exp(-i*kB);
% MainTitle = 'Fixed reflection coefficient R = -0.60';
% DataFile='5-CircularBaffle\FreqRespBaffle000.dat';
% p0 = 1 + R.*p1;          % Front side sound pressure.
% DataFile='5-CircularBaffle\FreqRespBaffle180.dat';
% p0 = (1 + R).*p1;        % Rear side sound pressure.

% === VARIABLE REFLECTION COEFFICIENT ===============================

% R  = -0.60*((1+i*kB)./(1+0.60*i*kB));
% p1 = exp(-i*kB);
% MainTitle = 'Variable reflection coefficient R = -0.60 ... -1.00';
% DataFile='5-CircularBaffle\FreqRespBaffle000.dat';
% p0 = 1 + R.*p1;          % Front side sound pressure.
% DataFile='5-CircularBaffle\FreqRespBaffle180.dat';
% p0 = (1 + R).*p1;        % Front side sound pressure.


% =====================================================================
% EDGE DIFFRACTION MODEL - ANALYTICAL EXPRESSIONS
% =====================================================================

% Files: PlotCircularBaffleOffsetSource5cm.png  (Offset source)
%        PlotCircularBaffleOffsetSource10cm.png (-"-)
%        PlotCircularBaffleOffsetDif5cm.png     (Offset source, dif)
%        PlotCircularBaffleOffsetDif10cm.png    (-"-)
%        PlotEllipticProjectionFront.png        (Elliptic Projection)
%        PlotEllipticProjectionRear.png         (-"-)
%        PlotEllipticProjectionFrontDif.png     (Elliptic Difference)
%        PlotEllipticProjectionRearDif.png      (-"-)
%        PlotTiltedBaffleFront.png              (Elliptic Tilted)
%        PlotTiltedBaffleRear.png               (-"-)
%        PlotTiltedBaffleFrontDif.png           (Elliptic Difference)
%        PlotTiltedBaffleRearDif.png            (-"-)
%        PlotRectangularBaffleFront85.png       (Rectangular 1)
%        PlotRectangularBaffleFront85Dif.png    (Rectangular 1 Dif)
%        PlotSquareBaffleFront2.png             (Rectangular 2)
%        PlotSquareBaffleRear2.png              (-"-)


% === CIRCULAR BAFFLE ===============================================

% --- Observation angle (off-axis monitoring)
% MainTitle = 'Circular baffle at 30 degrees off-axis - Front side';
% DataFile='5-CircularBaffle\FreqRespBaffle030.dat';
% p1  = exp(-i*kB).*sin(0.50*kB)./(0.50*kB);
% p0 = 1 + R*p1;            % Front side sound pressure.
% MainTitle = 'Circular baffle at 30 degrees off-axis - Rear side';
% DataFile='5-CircularBaffle\FreqRespBaffle120.dat';
% p0 = (1 + R)*p1;          % Front side sound pressure.

% === CIRCULAR BAFFLE ===============================================

% --- Offset source
% MainTitle = 'Circular baffle with source offset 5 cm - Front side';
% DataFile='3-CircularBaffle\FreqRespFront05cm.dat';
% p1  = (1/2)*(exp(-0.93*i*kB).*sin(0.22*kB)./(0.22*kB) + ...
%              exp(-1.22*i*kB).*sin(0.07*kB)./(0.07*kB));
% MainTitle = 'Circular baffle with source offset 10 cm - Front side';
% DataFile='3-CircularBaffle\FreqRespFront10cm.dat';
```

```
%  p1 = (1/2)*(exp(-0.85*i*kB).*sin(0.44*kB)./(0.44*kB) + ...
%            exp(-1.44*i*kB).*sin(0.15*kB)./(0.15*kB));
%  p0 = 1 + R.*p1;        % Front side sound pressure.


%  === ELLIPTIC BAFFLE ==========================================

%  --- 30 degree projection of circle
%  p1 = exp(-0.81*i*kB).*sin(0.19*kB)./(0.19*kB);
%  MainTitle = 'Elliptic baffle - Front side';
%  DataFile='5-CircularBaffle\FreqRespBaffle030.dat';
%  p0 = 1 + R.*p1;        % Front side sound pressure.
%  MainTitle = 'Elliptic baffle - Rear side';
%  DataFile='5-CircularBaffle\FreqRespBaffle120.dat';
%  p0 = (1 + R).*p1;       % Rear side sound pressure.


%  --- 30 degree tilted baffle
%  p1  = exp(-i*kB).*sin(0.5*kB)./(0.5*kB);
%  MainTitle = 'Tilted baffle - Front side';
%  DataFile='5-CircularBaffle\FreqRespBaffle030.dat';
%  p0 = 1 + R.*p1;        % Front side sound pressure.
%  MainTitle = 'Tilted baffle - Rear side';
%  DataFile='5-CircularBaffle\FreqRespBaffle120.dat';
%  p0 = (1 + R).*p1;       % Rear side sound pressure.


%  === RECTANGULAR BAFFLE ==========================================

%  --- Model 1
%  p1  = (1/3)*exp(-i*kB).*(exp(-0.5*i*kB) + ...
%       2*cos(0.25*kB).*sin(0.25*kB)./(0.25*kB));
%  MainTitle = 'Rectangular baffle source offset 85 mm - Front side';
%  DataFile='4-RectangularBaffle\FreqRespOffset.dat    ';
%  p0 = 1 + R.*p1;        % Front side sound pressure.


%  --- Model 2
%  p1  = (1/2)*(exp(-1.25*i*kB).*sin(0.33*kB)./(0.33*kB) + ...
%             exp(-1.04*i*kB).*sin(0.04*kB)./(0.04*kB));
%  MainTitle = 'Square baffle - Front side';
%  DataFile='4-RectangularBaffle\FreqRespCentre000.dat';
%  p0 = 1 + R.*p1;        % Front side sound pressure.
%  MainTitle = 'Square baffle - Rear side';
%  DataFile='4-RectangularBaffle\FreqRespCentre120.dat';
%  p0 = (1 + R).*p1;       % Rear side sound pressure.

%  ========================================================================
%  EDGE DIFFRACTION MODEL - NUMERICAL CALCULATION
%  ========================================================================

%  Files: PlotNumericalCircularBaffle1.png      (  0 deg,   2 points)
%        PlotNumericalCircularBaffle2.png      (  0 deg, 200 points)
%        PlotNumericalCircularBaffle3.png      ( 30 deg,   4 points)
%        PlotNumericalCircularBaffle4.png      ( 30 deg, 200 points)
%        PlotNumericalCircularBaffle5.png      ( 60 deg, 200 points)
%        PlotNumericalCircularBaffle6.png      ( 90 deg, 200 points)
%        PlotNumericalCircularBaffle7.png      (120 deg, 200 points)
%        PlotNumericalCircularBaffle8.png      (150 deg, 200 points)
%        PlotNumericalCircularBaffle9.png      (180 deg, 200 points)
%        PlotNumericalCircularBaffle10.png     ( 30 deg, Corr #1)
%        PlotNumericalCircularBaffle11.png     ( 60 deg, Corr #1)
%        PlotNumericalCircularBaffle12.png     ( 30 deg, Corr #2)
%        PlotNumericalCircularBaffle13.png     ( 60 deg, Corr #2)
%        PlotNumericalCircularBaffle14.png     (  0 deg,  0 cm)
%        PlotNumericalCircularBaffle15.png     (  0 deg,  3 cm)
%        PlotNumericalCircularBaffle16.png     (  0 deg,  6 cm)
%        PlotNumericalCircularBaffle17.png     (  0 deg,  9 cm)
%        PlotNumericalCircularBaffle18.png     (  0 deg, 12 cm)
%        PlotNumericalCircularBaffle19.png     (  0 deg, 15 cm)
%        PlotNumericalCircularBaffle20.png     (  0 deg, 18 cm)
%        PlotNumericalCircularBaffle21.png     (  0 deg, 25 cm)
%        PlotNumericalRectangularBaffle1.png   (  0 deg,   4 points)
%        PlotNumericalRectangularBaffle2.png   (  0 deg,   8 points)
%        PlotNumericalRectangularBaffle3.png   (  0 deg,  16 points)
%        PlotNumericalRectangularBaffle4.png   (  0 deg, 200 points)
%        PlotNumericalRectangularBaffle5.png   ( 30 deg, 200 points)
%        PlotNumericalRectangularBaffle6.png   ( 60 deg, 200 points)
```

```
%           PlotNumericalRectangularBaffle7.png    ( 90 deg,   200 points)
%           PlotNumericalRectangularBaffle8.png    (120 deg,   200 points)
%           PlotNumericalRectangularBaffle9.png    (150 deg,   200 points)
%           PlotNumericalRectangularBaffle10.png   (180 deg,   200 points)
%           PlotNumericalRectangularBaffle11.png   (  0 deg, Offset #2)
%           PlotNumericalRectangularBaffle12.png   (  0 deg, Offset #3)
%           PlotNumericalVersion2Circular1.png     (  0 deg, 200 points)
%           PlotNumericalVersion2Circular2.png     ( 30 deg, 200 points)
%           PlotNumericalVersion2Circular3.png     ( 60 deg, 200 points)
%           PlotNumericalVersion2Circular4.png     ( 90 deg, 200 points)
%           PlotNumericalVers1Corr1Centre000.png   (  0 deg, V=1, C=1)
%           PlotNumericalVers1Corr1Centre030.png   ( 30 deg, V=1, C=1)
%           PlotNumericalVers1Corr1Centre060.png   ( 60 deg, V=1, C=1)
%           PlotNumericalVers1Corr1Centre090.png   ( 90 deg, V=1, C=1)
%
%           PlotNumericalCircularBaffle1.png           0 deg Model 1
%           PlotNumericalCircularBaffle2.png          30 deg
%           PlotNumericalCircularBaffle3.png          60 deg
%           PlotNumericalCircularBaffle4.png          90 deg
%           PlotNumericalModel2CircularBaffle1.png     0 deg Model 2
%           PlotNumericalModel2CircularBaffle2.png    30 deg
%           PlotNumericalModel2CircularBaffle3.png    60 deg
%           PlotNumericalModel2CircularBaffle4.png    90 deg
%           PlotNumericalModel2CircularBaffle5.png    91 deg
%           PlotNumericalModel2CircularBaffle6.png   120 deg
%           PlotNumericalModel2CircularBaffle7.png   150 deg
%           PlotNumericalModel2CircularBaffle8.png   180 deg
%
%           PlotNumericalModel3Circular000.png         0 deg Model 3
%           PlotNumericalModel3Circular030.png        30 deg
%           PlotNumericalModel3Circular060.png        60 deg
%           PlotNumericalModel3Circular090.png        90 deg
%           PlotNumericalModel3Circular091.png        91 deg
%           PlotNumericalModel3Circular120.png       120 deg
%           PlotNumericalModel3Circular150.png       150 deg
%           PlotNumericalModel3Circular180.png       180 deg
%
%           PlotNumericalModel3CircularOffset00.png    0 cm  Model 3
%           PlotNumericalModel3CircularOffset03.png    3 cm
%           PlotNumericalModel3CircularOffset06.png    6 cm
%           PlotNumericalModel3CircularOffset09.png    9 cm
%           PlotNumericalModel3CircularOffset12.png   12 cm
%           PlotNumericalModel3CircularOffset15.png   15 cm
%           PlotNumericalModel3CircularOffset18.png   18 cm
%           PlotNumericalModel3CircularOffset25.png   25 cm
%
%           PlotNumericalModel3Rectangular000.png      0 deg  Model 3
%           PlotNumericalModel3Rectangular030.png     30 deg
%           PlotNumericalModel3Rectangular060.png     60 deg
%           PlotNumericalModel3Rectangular090.png     90 deg
%           PlotNumericalModel3Rectangular091.png     91 deg
%           PlotNumericalModel3Rectangular120.png    120 deg
%           PlotNumericalModel3Rectangular150.png    150 deg
%           PlotNumericalModel3Rectangular180.png    180 deg
%
%           PlotNumericalModel3RectangularP1.png      Pos 1     Model 3
%           PlotNumericalModel3RectangularP2.png      Pos 2
%           PlotNumericalModel3RectangularP3.png      Pos 3

% === MODEL SELECTION ==================================================

UseModel = 5;          % UseModel = 0 to discard the model.
                       % UseModel = 1 for model 1 First diffraction.
                       % UseModel = 2 for model 2 Second diffraction.
                       % UseModel = 3 for model 3 Third diffraction.
                       % UseModel = 4 for model 3 Diretivity.
                       % UseModel = 5 for model DED, Urban et al.

UseBaffle = 1;         % UseBaffle = 1 for circular disk radius B.
                       % UseBaffle = 2 for rectangular baffle AxB.
if (UseModel > 0)
    if (UseBaffle == 1)

        % === (BAFFLE 1) CIRCULAR BAFFLE ===============================
```

```
          %
          % The circle is specified by the number of edge sources input
          % through EdgeSources, with a nominal value of 200 sources.
          % The sources are located on a circle with radius B.
          %
          % Source location is specified through (x0, y0, z0).
          % Sbservation point is specified through (xP, yP, zP).
          % -----------------------------------------------------------
%          MainTitle = 'Circular baffle, Model DED (R=-0.6), 120 degrees';
          MainTitle = 'Circular baffle, Model DED, 150 degrees';
          DataFile='5-CircularBaffle\FreqRespBaffle150.dat   ';
%          MainTitle = 'Circular baffle, Model 3, 25 cm offset';
%          DataFile='3-CircularBaffle\FreqRespFront25cm.dat   ';
          % --- OBSERVATION POINT
          OA = 150;                        % Observation angle (deg).
          OD =   1.41;                     % Observation distance (m).

          xP = OD*sin(OA*pi/180);          % Observation point.
          yP = 0;
          zP = OD*cos(OA*pi/180);
          x0 = 0.00;                       % Source (loudspeaker).
          y0 = 0.00;
          z0 = 0.00;
          EdgeSources=200;                 % Number of edge sources.
          EdgePoint=1:EdgeSources;
          x  = B*cos(2*pi*(EdgePoint-1)/EdgeSources);
          y  = B*sin(2*pi*(EdgePoint-1)/EdgeSources);

      else

          % === (BAFFLE 2) RECTANGULAR BAFFLE ==========================
          %
          % The rectangle is specified through width (W) and height (H)
          % and the number of edge sources to use. The number is divided
          % by 4 and rounded to the nearest integer. The edge sources
          % are thenplaced equidistantly along each side.
          %
          % Source location is specified through (x0, y0, z0).
          % Sbservation point is specified through (xP, yP, zP).
          % -----------------------------------------------------------

          MainTitle = 'Rectangular baffle, Model 3, Position 3';
%          DataFile='4-RectangularBaffle\FreqRespCentre000.dat'; % Pos 1
%          DataFile='4-RectangularBaffle\FreqRespOffset.dat   '; % Pos 2
          DataFile='4-RectangularBaffle\FreqRespAsym.dat     ';  % Pos 3

          OA = 000;                        % Observation angle (deg).
          OD =   1.41;                     % Observation distance (m).

          xP = 0.10 + OD*sin(OA*pi/180);   % Observation point.
          yP = 0.17;
          zP = OD*cos(OA*pi/180);
          x0 = 0.15;                       % Source (loudspeaker).
          y0 = 0.085;
          z0 = 0.00;
          EdgeSources=200;                 % Number of edge dources (>1).
          E = round(EdgeSources/4);
          W = 0.20;                        % Baffle width (m),  W = 2A.
          H = 0.34;                        % Baffle height (m), H = 2B.
          for n = 1:E
              x(n)     = W*(n-1)/E;        % Lower edge (0,0) to (W,0).
              y(n)     = 0;
              x(n+E)   = W;                % Right edge (W,0) to (W,H).
              y(n+E)   = H*(n-1)/E;
              x(n+2*E) = W*(E-n+1)/E;      % Top edge   (W,H) to (0,H).
              y(n+2*E) = H;
              x(n+3*E) = 0;                % Left edge  (0,H) to (0,0).
              y(n+3*E) = H*(E-n+1)/E;
          end
      end

      % === PREPARE VECTORS =========================================
```

```
    r0  = sqrt((xP-x0)^2+(yP-y0)^2+(zP-z0)^2);  % Source to observer.
    b   = sqrt((x0-x).^2+(y0-y).^2);            % Source to edge.
    r   = sqrt((xP-x).^2+(yP-y).^2+zP^2);       % Edge to observer.
    th0 = asin(sqrt((xP-x0)^2+(yP-y0)^2)/r0);   % Observation angle.
    N   = length(x);                % Half number for pointer to the
    N2  = N/2;                      % second-order diffraction source.
    for n=1:N-1
        d(n)   = sqrt((x(n+1)-x(n))^2+(y(n+1)-y(n))^2);
        phi(n) = acos((b(n)^2+b(n+1)^2-d(n)^2)/(2*b(n)*b(n+1)));
        th(n)  = asin((sqrt(xP-x(n))^2+(yP-y(n))^2)/r(n));
        if (n<N2+1)
            e(n) = sqrt((x(n+N2)-x(n))^2+(y(n+N2)-y(n))^2);
        else
            e(n) = sqrt((x(n-N2)-x(n))^2+(y(n-N2)-y(n))^2);
        end
    end
    d(N)   = sqrt((x(N)-x(1))^2+(y(N)-y(1))^2);
    phi(N) = acos((b(N)^2+b(1)^2-d(N)^2)/(2*b(N)*b(1)));
    th(N)  = asin((sqrt(xP-x(N))^2+(yP-y(N))^2)/r(N));
    e(N)   = sqrt((x(N2)-x(N))^2+(y(N2)-y(N))^2);
end

% === MODEL 1 ============================================================
% Basic implementation using one diffraction component.
% Front or rear side is determined from the sign of the z-variable.
% ------------------------------------------------------------------------

if (UseModel == 1)
    disp('ED model 1');
    for g = 1:1:6401       % Index counter.
        f(g) = 2*(g-1);    % Frequency: 0, 2, 4, ..., 12800 Hz
        ik = i*2*pi*f(g)/c; % Angular frequency (1/m).
        if (zP-z0>=0)      % Front side radiation.
            p0(g) = 1 + (R/(2*pi))* ...
                    sum((r0./(b+r)).*exp(ik*(r0-b-r)).*phi);
        else               % Rear side radiation.
            p0(g) = ((1 + R)/(2*pi))* ...
                     sum((r0./(b+r)).*exp(ik*(r0-b-r)).*phi);
        end
    end

% === MODEL 2 ============================================================
% Extended model using two diffraction components.
% Front or rear side is determined from the sign of the z-variable.
% ------------------------------------------------------------------------

elseif (UseModel == 2)
    disp('ED model 2');
    for g = 1:1:6401       % Index counter.
        f(g) = 2*(g-1);    % Frequency: 0, 2, 4, ..., 12800 Hz
        ik = i*2*pi*f(g)/c; % Angular frequency (1/m).
        if (zP-z0>=0)      % Front side radiation.
            p0(g) = 1 + (R/(2*pi))* ...
                    sum((1+R*(b+r).*exp(-ik*e)./(b+e+r)).* ...
                        (r0./(b+r)).*exp(ik*(r0-b-r)).*phi);
        else               % Rear side radiation.
            p0(g) = ((1+R)/(2*pi))* ...
                     sum((1+(1+R)*(b+r).*exp(-ik*e)./(b+e+r)).* ...
                         (r0./(b+r)).*exp(ik*(r0-b-r)).*phi);
        end
    end

% === MODEL 3 ============================================================
% Extended model using three diffraction components.
% Front or rear side is determined from the sign of the z-variable.
% ------------------------------------------------------------------------

elseif (UseModel == 3)
    disp('ED model 3');
    for g = 1:1:6401       % Index counter.
        f(g) = 2*(g-1);    % Frequency: 0, 2, 4, ..., 12800 Hz
        ik = i*2*pi*f(g)/c; % Angular frequency (1/m).
        if (zP-z0>=0)      % Front side radiation.
            p0(g) = 1 + (R/(2*pi))* ...
```

```
                    sum((1+R*exp(-ik*e).*((b+r)./(b+r+e)+ ...
                        R*(b+r+e).*exp(-ik*e)./(b+r+2*e)))).* ...
                        (r0./(b+r)).*exp(ik*(r0-b-r)).*phi);
            else            % Rear side radiation.
               p0(g) = ((1+R)/(2*pi))* ...
                        sum((1+(1+R)*exp(-ik*e).*((b+r)./(b+r+e)+ ...
                            (1+R)*((b+r+e).*exp(-ik*e)./(b+r+2*e)))).* ...
                            (r0./(b+r)).*exp(ik*(r0-b-r)).*phi);
            end
        end

    % === MODEL 4 ==========================================================
    % Extended model using three diffraction components.
    % Includes model of loudspeaker directivity.
    % Front or rear side is determined from the sign of the z-variable.
    % ----------------------------------------------------------------------

    elseif (UseModel == 4)
        disp('ED model 4');
        a = 0.10;                 % Loudspeaker radius (m).
        for g = 1:1:6401          % Index counter.
            f(g) = 2*(g-1);       % Frequency: 0, 2, 4, ..., 12800 Hz
            ik = i*2*pi*f(g)/c;
            ka = ik*a/i;
            F0 = 2*besselj(1,ka*sin(th*pi/180))/(ka*sin(th*pi/180));
            F1 = 2*besselj(1,ka)/ka;
            if (zP-z0>=0)         % Front side radiation.
                p0(g) = F0 + (R*F1/(2*pi))* ...
                        sum((1+R*exp(-ik*e).*((b+r)./(b+r+e)+ ...
                            R*(b+r+e).*exp(-ik*e)./(b+r+2*e)))).* ...
                            (r0./(b+r)).*exp(ik*(r0-b-r)).*phi);
            else                  % Rear side radiation.
                p0(g) = ((1+R)*F1/(2*pi))* ...
                        sum((1+(1+R)*exp(-ik*e).*((b+r)./(b+r+e)+ ...
                            (1+R)*((b+r+e).*exp(-ik*e)./(b+r+2*e)))).* ...
                            (r0./(b+r)).*exp(ik*(r0-b-r)).*phi);
            end
        end

    % === MODEL 5 ==========================================================
    % Urban: DED model.
    % ----------------------------------------------------------------------

    elseif (UseModel == 5)
        disp('DED model');
        for g = 1:1:6401          % Index counter.
            f(g) = 2*(g-1);       % Frequency: 0, 2, 4, ..., 12800 Hz
            ik = i*2*pi*f(g)/c;   % Angular frequency (1/m).
            p0(g) = (1+cos(th0))/2 - (1/(4*pi))* ...
                    sum((r0./(b+r)).*exp(ik*(r0-b-r)).*cos(th).*phi);
        end
    end

    % ======================================================================
    % FRESNEL INTEGRATION
    % ======================================================================
    % Files: PlotFresnelInfiniteWedgeRectangular001.png     1 deg data 000
    %        PlotFresnelInfiniteWedgeRectangular005.png     5 deg data 000
    %        PlotFresnelInfiniteWedgeRectangular010.png    10 deg data 000
    %        PlotFresnelInfiniteWedgeRectangular015.png    15 deg data 000
    %        PlotFresnelInfiniteWedgeRectangular020.png    20 deg data 000
    %        PlotFresnelInfiniteWedgeRectangular030.png    30 deg data 030
    %        PlotFresnelInfiniteWedgeRectangular060.png    60 deg data 060
    %        PlotFresnelInfiniteWedgeRectangular089.png    89 deg data 090
    %        PlotFresnelInfiniteWedgeRectangular120.png   120 deg data 120
    %        PlotFresnelInfiniteWedgeRectangular150.png   150 deg data 150
    %        PlotFresnelInfiniteWedgeRectangular170.png   170 deg data 180
    %        PlotFresnelInfiniteWedgeRectangular179.png   179 deg data 180
    %        PlotFresnelInfiniteWedgeRectangular180.png   180 deg data 180
    %
    %        PlotFresnelRectangularBaffle1cm000.png         0 deg ds = 1 cm
    %        PlotFresnelRectangularBaffle2cm000.png         0 deg ds = 2 cm
    %
    %        PlotFraunhoferRectangularBafflem000.png        0 deg
```

```
%           PlotFraunhoferRectangularBafflem030.png       30 deg
%           PlotFraunhoferRectangularBafflem060.png       60 deg
%           PlotFraunhoferRectangularBafflem090.png       90 deg
%           PlotFraunhoferRectangularBafflem120.png      120 deg
%           PlotFraunhoferRectangularBafflem150.png      150 deg
%           PlotFraunhoferRectangularBafflem180.png      180 deg
%
% Execution time: max 3 min.

UseModel = 0;          % UseModel = 0 Discard models.
                       % UseModel = 1 Fresnel semi-infinite baffle.
                       % UseModel = 2 Fresnel rectanfular baffle.
                       % UseModel = 3 Fraunhofer semi-infinite baffle.
if (UseModel ==1)
    % === FRESNEL - SEMI-INFINITE BAFFLE ==============================
    MainTitle = 'Fresnel integration - Loudspeaker baffle at 0 deg';
    DataFile='4-RectangularBaffle\FreqRespCentre000.dat';
    A  =   0.10;            % Horisontal dimension (m); Width  = 2A
    D  =   1.30;            % Observation distance (m).
    th =   0;              % Observation angle (degrees).
    % --- PARAMETERS
    ds = A*cos(pi/2-pi*th/180);    % Distance to source (m).
    dp = D-ds;                     % Distance to observer (m).
    y1 = -A*sin(pi/2-pi*th/180);   % Wedge height (m).
    % --- MODEL
    HA = 0.5;              % Aperture constant (large aperture).
    L  = ds*dp/(ds+dp);    % Fresnel length (m).
    h  = sqrt(2*f/(c*L));  % Scaling factor (1/m).
    disp('...1/2');
    Cy = mfun('FresnelC',h*y1);
    disp('...2/2');
    Sy = mfun('FresnelS',h*y1);
    p0 = HA*(1-i)*(0.5-Cy-i*(0.5-Sy));

elseif (UseModel == 2)
    % === FRESNEL - RECTANGULAR BAFFLE ===============================
    MainTitle = 'Fresnel integration - Rectangular baffle at 0 deg, ds = 20 cm';
    DataFile='4-RectangularBaffle\FreqRespCentre000.dat';
    A  =   0.10;            % Horisontal dimension (m); Width  = 2A
    B  =   0.17;            % Vertical dimension (m):   height = 2B.
    r0 =   1.30;            % Observation distance (m).
    th =      0;            % Observation angle (degrees).
    % --- PARAMETERS
    ds =   0.20;                   % Source to aperture (m).
    dp =    r0*cos(pi*th/180);     % Distance to observer (m).
    x1 = -A+r0*sin(pi*th/180);     % Aperture coordinates (m).
    x2 =  A+r0*sin(pi*th/180);
    y1 = -B;
    y2 =  B;
    % --- MODEL
    s  = sqrt(A*B)/ds;                      % Aperture size.
    HA = (1/2)*sqrt(1+s^2)/(sqrt(1+s^2)+1); % Aperture correction.
    L  = ds*dp/(ds+dp);                     % Fresnel length (m).
    h  = sqrt(2*f/(c*L));                   % Scaling factor (1/m).
    disp('...1/8');                         % Display step number.
    Cx1 = mfun('FresnelC',h*x1);
    disp('...2/8');
    Cx2 = mfun('FresnelC',h*x2);
    disp('...3/8');
    Sx1 = mfun('FresnelS',h*x1);
    disp('...4/8');
    Sx2 = mfun('FresnelS',h*x2);
    disp('...5/8');
    Cy1 = mfun('FresnelC',h*y1);
    disp('...6/8');
    Cy2 = mfun('FresnelC',h*y2);
    disp('...7/8');
    Sy1 = mfun('FresnelS',h*y1);
    disp('...8/8');
    Sy2 = mfun('FresnelS',h*y2);
    p0 = HA*(Cx1-Cx2-i*(Sx1-Sx2)).*(Cy1-Cy2-i*(Sy1-Sy2));

elseif (UseModel == 3)
    % === FRAUNHOFER - RECTANGULAR BAFFLE ============================
```

```
    MainTitle = 'Fraunhofer integration - Rectangular baffle at 30 deg';
    DataFile='4-RectangularBaffle\FreqRespCentre030.dat';

    % --- INPUT PARAMETERS
    th =  030;                % Observation angle (deg).
    r0 =    0.41;             % Obsevation distance (m).
    B  =    0.10;             % Baffle half-width (m).

    % --- INTERNAL PARAMETERS
    h  = -B*sin(pi/2-th*pi/180)    % Edge height (observer = 0).
    zP = r0-B*cos(pi/2-th*pi/180)  % Edge to observer distance.

    amax =   20;              % Horisontal lintegration limits.
    bmax =   20;              % Vertical upper integration limit.
    bmin = h/zP               % Vertical lower integration limit.
    M    = 1200;              % Number points for alfa.
    N    = 1200;              % Number points for beta.
    da   = amax/M;            % Increment in alfa (note: amin = -amax).
    db   = (bmax-bmin)/N;     % Increment in beta (note: asymmetric).
    FP   = 100;               % Number of frequency points calculated.

    % --- INTEGRAL
    alfa = -amax:da:(amax*(M-1)/M); % Vector containing alfa-values.
    % --- Frequency loop
    for g=1:6401                    % Index for the frequency vector.
        f(g)=2*(g-1);               % Frequency (Hz).
        if (mod(g,FP) == 1)         % Calculate for 1, FP+1, 2FP+1, ...
            disp(g);                % Output the loop-counter value.
            ikz = i*2*pi*f(g)*zP/c; % Frequency-distance.
            % --- Summation loop
            for n=1:N               % Index for beta with N elements.
                beta = (n-1)*db+bmin;                 % Beta-value.
                abv  = sqrt(1+alfa.^2+beta^2);        % Vector.
                wf   = sqrt(1+(alfa/3).^2+(beta/3)^2);  % Weight.
                % --- ALFA summation (2M elements)
                alfasum(n) = sum(exp(-ikz*abv)./(abv.*wf));
            end
            % --- BETA summation (N elements)
            p0(g) = abs(ikz*amax*(bmax-bmin)*sum(alfasum)/(M*N*2*pi));
            if (g > FP)
                for h=(g-FP+1):(g-1)
                    p0(h) = ((g-h)*p0(g-FP) + (h+FP-g)*p0(g))/FP;
                end
            end
        end
    end
end

% ======================================================================
% PLOT THE MODEL
% ======================================================================
% Model data is stored in "p0" as amplitude values from 0 Hz to the
% upper limit at 12.8 kHz with 2 Hz spacing. Data is output with a
% logarithmic frequency axis showing the range from 60 Hz to 10 kHz,
% set through the parameters fmin and fmax, and with max and min
% sound pressure levels set through the parameters pmin and pmax.
% ----------------------------------------------------------------

disp('Plotting ...');
FreqSpec = 20*log10(abs(p0'));  % Change format and make decibel.
figure(1);                      % Prepare output picture #1.
semilogx(f,FreqSpec,'b-');      % Plot versus frequency.
axis([fmin, fmax, pmin, pmax]); % Set freq-axis and decibel-axis.
title(MainTitle);               % Set selected title.
xlabel('Frequency (Hz)');       % Set freq-axis label.
ylabel('Amplitude (dB)');       % Set decibel-axis.
hold on;                        % Keep figure ready for more plots.

% ======================================================================
% PLOT THE MEASUREMENT
% ======================================================================
% The average of four files are defined as the refference for output.
% The files are read, data is converted from real and imaginary to
% magnitude and the average is computed.
```

```
% The "fopen" command assume data files containing:
% (1) Line number, (2) Frequency, (3) Real value, (4) Imag value.
% DataFile is converted to format 6401 rows with the above 4 columns.
% Variable "MeasRefX" contains 6401 rows with the amplitude value.
% Variable "MeasRef" contains the resulting reference spectrum.
% ------------------------------------------------------------------

% --- Get measurements source file.
fid=fopen(DataFile); d=fscanf(fid, '%e %e %e %e', [4 inf]); fclose(fid);
d=d'; MeasSource=sqrt(d(:,3).^2 + d(:,4).^2);

% --- Offset measurement for rectangular baffle to 1.41 m distance.
if     (DataFile == '4-RectangularBaffle\FreqRespCentre000.dat')
    corr = -0.71;
elseif (DataFile == '4-RectangularBaffle\FreqRespCentre030.dat')
    corr = -0.57;
elseif (DataFile == '4-RectangularBaffle\FreqRespCentre060.dat')
    corr = -0.22;
elseif (DataFile == '4-RectangularBaffle\FreqRespCentre090.dat')
    corr =  0.24;
elseif (DataFile == '4-RectangularBaffle\FreqRespCentre120.dat')
    corr =  0.68;
elseif (DataFile == '4-RectangularBaffle\FreqRespCentre150.dat')
    corr =  0.99;
elseif (DataFile == '4-RectangularBaffle\FreqRespCentre180.dat')
    corr =  1.19;
elseif (DataFile == '4-RectangularBaffle\FreqRespOffset.dat    ')
    corr = -0.71;
elseif (DataFile == '4-RectangularBaffle\FreqRespAsym.dat      ')
    corr = -0.71;
elseif (DataFile == '3-CircularBaffle\FreqRespFront00cm.dat    ')
    corr = -0.71;
elseif (DataFile == '3-CircularBaffle\FreqRespFront03cm.dat    ')
    corr = -0.71;
elseif (DataFile == '3-CircularBaffle\FreqRespFront06cm.dat    ')
    corr = -0.71;
elseif (DataFile == '3-CircularBaffle\FreqRespFront09cm.dat    ')
    corr = -0.71;
elseif (DataFile == '3-CircularBaffle\FreqRespFront12cm.dat    ')
    corr = -0.71;
elseif (DataFile == '3-CircularBaffle\FreqRespFront15cm.dat    ')
    corr = -0.71;
elseif (DataFile == '3-CircularBaffle\FreqRespFront18cm.dat    ')
    corr = -0.71;
elseif (DataFile == '3-CircularBaffle\FreqRespFront25cm.dat    ')
    corr = -0.71;
else
    corr =  0.00;
end
corr

% --- Get measurements reference files.
ref1='5-CircularBaffle\FreqRespInitial3.dat';
ref2='5-CircularBaffle\FreqRespInitial4.dat';
ref3='5-CircularBaffle\FreqRespSource000.dat';
ref4='5-CircularBaffle\FreqRespSource360.dat';
fid=fopen(ref1); r1=fscanf(fid, '%e %e %e %e', [4 inf]); fclose(fid);
r1=r1'; MeasRef1=sqrt(r1(:,3).^2 + r1(:,4).^2);
fid=fopen(ref1); r2=fscanf(fid, '%e %e %e %e', [4 inf]); fclose(fid);
r2=r2'; MeasRef2=sqrt(r2(:,3).^2 + r2(:,4).^2);
fid=fopen(ref1); r3=fscanf(fid, '%e %e %e %e', [4 inf]); fclose(fid);
r3=r3'; MeasRef3=sqrt(r3(:,3).^2 + r3(:,4).^2);
fid=fopen(ref1); r4=fscanf(fid, '%e %e %e %e', [4 inf]); fclose(fid);
r4=r4'; MeasRef4=sqrt(r4(:,3).^2 + r4(:,4).^2);
MeasRef=(MeasRef1+MeasRef2+MeasRef3+MeasRef4)/4;

% --- Calculate and plot magnitude of the measured spectrum.
MeasSpec=20*log10(MeasSource)-20*log10(MeasRef)+offs+corr;
semilogx(f,MeasSpec,'r-');
legend('Model','Measurement','Location','SouthWest');
hold off;

% ===================================================================
% PLOT THE DIFFERENCE
```

```
% ================================================================
% The difference between data and reference is computed and output.
% ----------------------------------------------------------------

UseDif = 1;      % Set UseDif = 0 to discard the plot.
                 % Set UseFif = 1 to use the plot option.
if (UseDif == 1)
    figure(2);                      % Prepare output picture #2.
    Dif = FreqSpec-MeasSpec;        % Calculate difference.
    semilogx(f,Dif,'g-');
    axis([fmin, fmax, pmin, pmax]); % Set freq-axis and decibel-axis.
    title(MainTitle);               % Set selected title.
    xlabel('Frequency (Hz)');       % Set freq-axis label.
    ylabel('Amplitude (dB)');       % Set decibel-axis.
    legend('Difference','Location','SouthWest');
    hold off;
end
```

6.1.4 Fraunhofer far-field model

This section presents the implementation of the algorithm for calculating the transfer function using the assumption of plane waves approaching an infinite edge. The input is edge height h above the origin of the coordinate system. Top of the edge is at $y = h$ with the edge along the x-axis and the observer located at $y = 0$. The height h is negative for a edge obstructing less than 50 % of the plane wave. The observer is located at $x = y = 0$ and $z = z_P$. See Figure 112 for details. The implementation includes a weight function for improved convergence and a correction factor for 0 dB when the edge is removed ($h \ll -1$).

The main equation is:

$$L_w = 20\log_{10}\left| \frac{ikz_P}{2\pi} \frac{\alpha_{MAX}(\beta_{MAX}-\beta_{MIN})}{MN} \sum_{n=1}^{N} \sum_{m=-M}^{M-1} \frac{\exp\left(-ikz_P\sqrt{1+\alpha_m^2+\beta_n^2}\right)}{\sqrt{\left(1+\alpha_m^2+\beta_n^2\right)\left(1+\frac{1}{9}\alpha_m^2+\frac{1}{9}\beta_n^2\right)}} \right| \mathrm{dB}$$

The normalised variables are defined by:

$$\alpha = \frac{x}{z_P}, \quad \beta = \frac{y}{z_P}, \quad \beta_{MIN} = \frac{h}{z_P}$$

$$\alpha_m = m\Delta\alpha, \quad m = -M\,\mathrm{K}\,0\mathrm{K}\,M-1$$

$$\beta_n = (n-1)\Delta\beta + \beta_{MIN}, \quad n = 1\mathrm{K}\,N$$

The increments (step sizes) are defined by:

$$\Delta\alpha = \frac{\alpha_{MAX}-\alpha_{MIN}}{2M}, \quad \Delta\beta = \frac{\beta_{MAX}-\beta_{MIN}}{N}$$

Integration limits α_{MIN}, α_{MAX}, and β_{MAX} and number of steps M and N are input parameters.

The MATLAB dot-operators for efficient multiplication and division of vector elements are used to build a vector containing the α-elements. The vector size is $2M$. A for-loop is build for controlling the frequency axe and another for-loop is used to step through the β-elements. The counter must start from 1 due to the rule for indexing within MATLAB so the current β-value is calculated as shown above. The *abv*-vector contains the calculations over all α-elements for the current β-value corresponding to the first square root in the denominator above and the *wf*-vector contains the calculations for the weight function corresponding to the second square root. The weight function values are scaled by 1/3 before squaring to widen the

weight function according to the previous discussion. The complex calculation is stored in *alfasum*(*n*) where *n* is the current index for the β-element. After the for-loop are all elements within the vector summed and scaled with the frequency, integration range and number of steps. The output is expressed in decibels. A warning is output from MATLAB since the value is zero for the first frequency point.

```matlab
% -------------------------------------------------------------------
% FRAUNHOFER INEGRATION - INFINITE WEDGE
% -------------------------------------------------------------------
% Compute the calculated frequency response.
%
% Written by Tore Skogberg, 2006.
% -------------------------------------------------------------------
% Infinite wedge at far-field conditions.
% Includes weight function and scaling for 0 dB at no wedge.

clear
format compact

% Files: PlotInfiniteWedge1.png    Height 0 and -10.
%        PlotInfiniteWedge2.png    Weight 1, 1/3 and 1/10.
%        PlotInfiniteWedge3.png    Weight 1/10 and 1/30.
%        PlotInfiniteWedge4.png    No weighting.
%        PlotInfiniteWedge5.png    H = -1, 0 and 1.
%        PlotInfiniteWedge6.png    H = -1, 0 and 1 with grid.

% --- CONSTANTS
c    = 345;    % Speed of sound (m/s).

% --- INPUT PARAMETERS
zP   =    1;   % Observer horizontal distance from wedge (m).
h    =    1;   % Observer vertical distance above wedge (m).
f0   =   10;   % Frequency increment (Hz).

% --- INTERNAL PARAMETERS
amax =  100;   % Horisontal limits, alfa maximum.
bmax =  100;   % Vertical limit, beta maximum.
bmin = h/zP;   % Vertical limit, beta minimum.
M    = 1000;   % Number of horizontal points for alfa.
N    = 1000;   % Number of vertical points for beta.
da   = amax/M;            % Increment in alfa (note: amin = -amax).
db   = (bmax-bmin)/N;   % Increment in beta (note: asymmetric).

% --- INTEGRAL
alfa = -amax:da:(amax*(M-1)/M); % Vector containing alfa-values.
% --- Frequency loop
for g=1:201                   % Index for the frequency vector.
    g                         % Output step number to screen.
    f(g)=(g-1)*f0;            % Frequency (Hz).
    ikz = i*2*pi*f(g)*zP/c;   % Frequency-distance.
    % --- Summation loop
    for n=1:N                 % Index for beta with N elements.
        beta = (n-1)*db+bmin;                   % Beta-value.
        abv  = sqrt(1+alfa.^2+beta^2);          % Alfa-beta vector.
        wf   = sqrt(1+(alfa/3).^2+(beta/3)^2);  % Weight function.
        % --- ALFA summation (2M elements)
        alfasum(n) = sum(exp(-ikz*abv)./(abv.*wf));
    end
    % --- BETA summation (N elements)
    H(g) = abs(ikz*amax*(bmax-bmin)*sum(alfasum)/(M*N*2*pi));
end

% --- PLOT RESULT
plot(f,20*log10(H),'r-');
title('Fraunhofer integral with the height as parameter');
axis([0 2000 -25 5]);
xlabel('Frequency (Hz)');
ylabel('Transfer function, L (dB)');
legend ('Above wedge,  h/z_P = -1', ... % b
        'At wedge top, h/z_P =  0', ... % g
        'Below wedge,  h/z_P =  1', ... % r
```

```
         'Location','SouthEast');
grid on
hold on
```

7 Appendix

This chapter presents the mathematics required for derivations within the document.

7.1 Mathematical definitions

This section contains miscellaneous derivations used within this document.

7.1.1 Partial integration

Partial integration (integration by terms) is defined as follows for definite integrals, which is used here, but the procedure applies to indefinite integrals as well (Westergren, 141):

$$\int_a^b f(x)g(x)dx = \left[F(x)g(x)\right]_a^b - \int_a^b F(x)g'(x)dx$$

$$F(x) = \int f(x)dx$$

This relation will be used to transform p_r and p_{rr}.

7.1.2 First-order differentiation

First-order differentiation of a product is defined as follows (Westergren, 137), where $f'(x)$ and $g'(x)$ denotes the first-order derivatives of $f(x)$ and $g(x)$ respectively:

$$\frac{d}{dx}\{f(x)g(x)\} = f'(x)g(x) + f(x)g'(x)$$

7.1.3 Second-order differentiation

Second-order differentiation of a product is defined as follows, where $f''(x)$ and $g''(x)$ denotes the second-order derivatives of $f(x)$ and $g(x)$ respectively:

$$\frac{d^2}{dx^2}\{f(x)g(x)\} = \frac{d}{dx}\left\{\frac{d}{dx}\{f(x)g(x)\}\right\}$$

$$= \frac{d}{dx}\{f'(x)g(x) + f(x)g'(x)\}$$

$$= \frac{d}{dx}\{f'(x)\}g(x) + f'(x)\frac{d}{dx}\{g(x)\} + \frac{d}{dx}\{f(x)\}g'(x) + f(x)\frac{d}{dx}\{g'(x)\}$$

$$= f''(x)g(x) + f'(x)g'(x) + f'(x)g'(x) + f(x)g''(x)$$

Hence the rule for second-order differentiation:

$$\frac{d^2}{dx^2}\{f(x)g(x)\} = f''(x)g(x) + 2f'(x)g'(x) + f(x)g''(x)$$

7.2 Blurring

A circular baffle delays the diffracted signal by a fixed amount of time while any other baffle shape distributes the delay over time, thus blurring the diffracted signal, which has the important consequence of reducing the over-all amplitude of the ripples. The baffle shape is thus an important parameter and it is the purpose of this section to derive a method for computing the degree of blurring of the diffracted signal. The model is suited for analytical work using the expressions as well as numerical simulations using a computer.

7.2.1 Overview

Expression will be derived for the below baffle shapes. All expressions are approximations based upon the method to be presented.
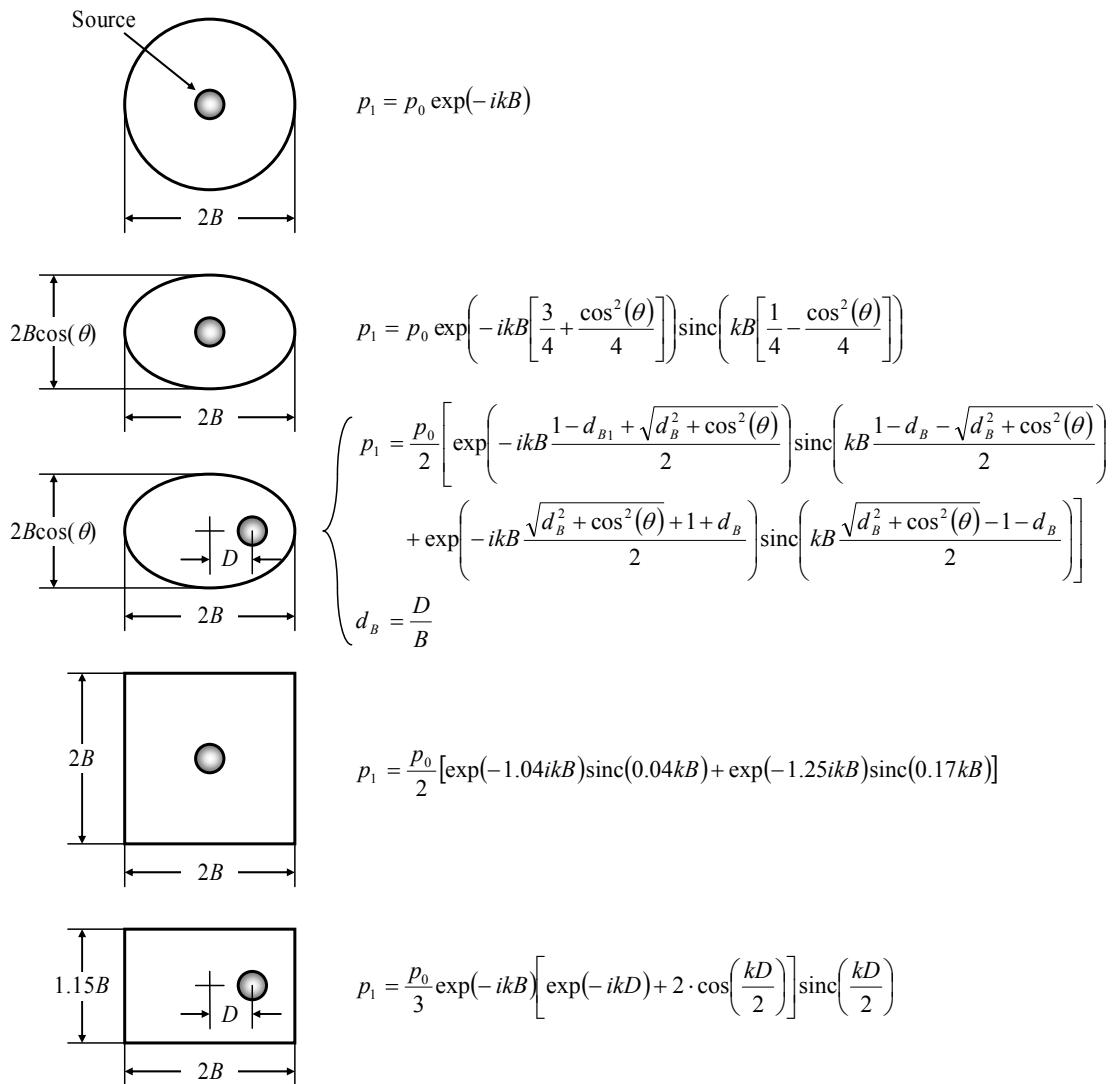
$$p_1 = p_0 \exp(-ikB)$$

$$p_1 = p_0 \exp\!\left(-ikB\left[\frac{3}{4}+\frac{\cos^2(\theta)}{4}\right]\right)\text{sinc}\!\left(kB\left[\frac{1}{4}-\frac{\cos^2(\theta)}{4}\right]\right)$$

$$\begin{cases} p_1 = \dfrac{p_0}{2}\left[\exp\!\left(-ikB\dfrac{1-d_{B1}+\sqrt{d_B^2+\cos^2(\theta)}}{2}\right)\text{sinc}\!\left(kB\dfrac{1-d_B-\sqrt{d_B^2+\cos^2(\theta)}}{2}\right)\right. \\[2mm] \left.\quad +\exp\!\left(-ikB\dfrac{\sqrt{d_B^2+\cos^2(\theta)}+1+d_B}{2}\right)\text{sinc}\!\left(kB\dfrac{\sqrt{d_B^2+\cos^2(\theta)}-1-d_B}{2}\right)\right] \\[2mm] d_B = \dfrac{D}{B} \end{cases}$$

$$p_1 = \frac{p_0}{2}\left[\exp(-1.04ikB)\text{sinc}(0.04kB)+\exp(-1.25ikB)\text{sinc}(0.17kB)\right]$$

$$p_1 = \frac{p_0}{3}\exp(-ikB)\left[\exp(-ikD)+2\cdot\cos\!\left(\frac{kD}{2}\right)\right]\text{sinc}\!\left(\frac{kD}{2}\right)$$

Figure 140 – Sound pressure of diffraction (first reflection) for different baffle shapes.

Dimension B represents the size of the baffle and D an offset from the centre along one of the axes. All baffles are assumed rigid and the loudspeaker is represented by a point source.

7.2.2 Theory

The sound pressure generated by the diffracted sound at the edge of the baffle is calculated from integration of infinitesimal sound sources located on an infinite plane at positions corresponding to the edges of the baffle. The assumption of large observation distance and on-axis listening generates the below expression (from equation 53), which describes the sound pressure of the diffracted sound at the observation point as a transfer function (the integral) multiplied by the direct signal (p_0).

$$p_1 = \frac{p_0}{2\pi} \int_0^{2\pi} \exp(-ikb)\,d\varphi$$

Distance b is function of angle φ and will be written as $b = Bf(\varphi)$, where B is a fixed length, characterising the baffle size, and $f(\varphi)$ is a dimensionless function, characterising the baffle shape and where $f(\varphi) > 0$ for all φ since the distance between source and edge must be positive. Thus, we have:

$$p_1 = \frac{p_0}{2\pi} \int_0^{2\pi} \exp(-ikBf(\varphi))\,d\varphi$$

The function $f(\varphi)$ will be approximated by linear sections of fixed length. The shape will thus be described by a straight line from $f(\varphi_0)$ to $f(\varphi_1)$, another straight line from $f(\varphi_1)$ to $f(\varphi_2)$ and so forth, with each section being defined by the starting point $f(\varphi_n)$ and the slope s_n, where n is the section number (0 to $N-1$) and the total number of sections is $N = 2\pi/\Delta\varphi$.

Two examples are shown in the picture below with the angle φ ranging from 0 to 2π, but the starting and ending points can be at any angle as long as the total range is 2π. Since the range is closed by one full revolution of φ, the starting function value $f(\varphi_0)$ must equal the limiting function value $f(\varphi_N)$ since they describes the same point. The first drawing represents a baffle with circular shape whose radius is constant so $b = B$ and $f(\varphi) = 1$. The second drawing represents a square baffle where b is at the maximum value at the cornet points.
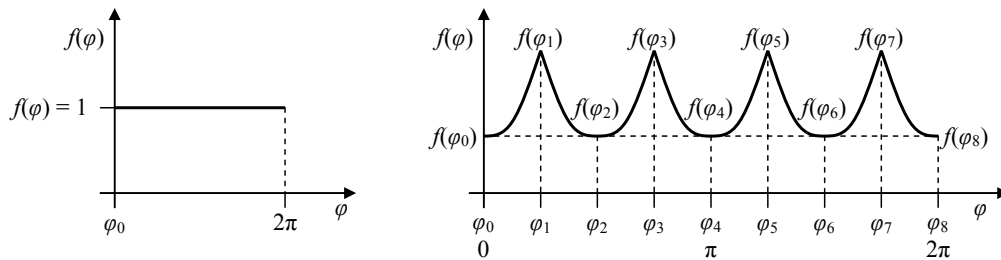
Figure 141 – The shape function for two baffle shapes, circular (left) and square (right) both assuming that the loudspeaker is placed symmetrically at the centre.

Assuming that the sections are of identical length, each with the step size $\Delta\varphi$, and that the number of line segments is N, the function can be approximated by:

$$f(\varphi) = s_n \cdot (\varphi - \varphi_n) + f(\varphi_n), \quad \varphi_n < \varphi < \varphi_n + \Delta\varphi, \quad n = 1,2,3,\mathrm{K}, N-1$$

$$s_n = \frac{f(\varphi_n + \Delta\varphi) - f(\varphi_n)}{\Delta\varphi}, \quad \Delta\varphi = \frac{2\pi}{N}$$

Insertion of this definition into the integral produces:

$$p_1 = p_0 \frac{1}{2\pi} \sum_{n=0}^{N-1} \int_{\varphi_n}^{\varphi_n+\Delta\varphi} \exp\left(-ikB\left[s_n \cdot (\varphi - \varphi_n) + f(\varphi_n)\right]\right) d\varphi$$

$$= p_0 \frac{1}{2\pi} \sum_{n=0}^{N-1} \exp\left(-ikBf(\varphi_n)\right) \int_{\varphi_n}^{\varphi_n+\Delta\varphi} \exp\left(-ikBs_n \cdot (\varphi - \varphi_n)\right) d\varphi$$

The first exponential corresponds to a delay defined by baffle size $Bf(\varphi_n)$ at the considered point while the second exponential represents the effect of blurring. Computing the integral generates the following expression:

$$p_1 = p_0 \frac{1}{2\pi} \sum_{n=0}^{N-1} \exp\left(-ikBf(\varphi_n)\right) \left[\frac{\exp\left(-ikBs_n \cdot (\varphi - \varphi_n)\right)}{-ikBs_n}\right]_{\varphi_n}^{\varphi_n+\Delta\varphi}$$

$$= p_0 \frac{1}{2\pi} \sum_{n=0}^{N-1} \exp\left(-ikBf(\varphi_n)\right) \frac{\exp\left(-ikBs_n\Delta\varphi\right) - 1}{-ikBs_n}$$

The last term represents a sine function, which can be seen by moving half the value of the exponential function outside the brackets and using Euler's formula for the sine function on the brackets (Westergren, 62). Introducing the step size $\Delta\varphi$ shows that the sine function is divided by its argument, and it is thus recognised as the sinc function.

$$p_1 = p_0 \frac{1}{2\pi} \sum_{n=0}^{N-1} \exp\left(-ikBf(\varphi_n)\right) \exp\left(-\frac{ikBs_n\Delta\varphi}{2}\right) \frac{2}{kBs_n} \frac{\exp\left(\frac{ikBs_n\Delta\varphi}{2}\right) - \exp\left(-\frac{ikBs_n\Delta\varphi}{2}\right)}{2i}$$

$$= p_0 \frac{1}{2\pi} \sum_{n=0}^{N-1} \exp\left(-ikB\left(f(\varphi_n) + \frac{s_n\Delta\varphi}{2}\right)\right) \frac{2\Delta\varphi}{kBs_n\Delta\varphi} \sin\left(\frac{kBs_n\Delta\varphi}{2}\right)$$

$$= p_0 \frac{\Delta\varphi}{2\pi} \sum_{n=0}^{N-1} \exp\left(-ikB\left(f(\varphi_n) + \frac{s_n\Delta\varphi}{2}\right)\right) \mathrm{sinc}\left(\frac{kBs_n\Delta\varphi}{2}\right)$$

Using the definition of s_n enables the delay function being expressed by the average function value for both ends of the current segment and the same relation can be used to express the sinc function as the change in function value. The constant in front of the sum is equal to $1/N$ and the result is the required expression:

$$p_1 = p_0 \frac{1}{N} \sum_{n=1}^{N-1} \exp\left(-ikB \frac{f(\varphi_n + \Delta\varphi) + f(\varphi_n)}{2}\right) \mathrm{sinc}\left(kB \frac{f(\varphi_n + \Delta\varphi) - f(\varphi_n)}{2}\right) \qquad 130$$

This equation will be addressed in the following sections but before generating a library of baffle shapes, a method shall be introduced for calculating the expression using the least possible number of segments.

7.2.3 Optimisation

A quite large number of points are required for description of a typical baffle but the number of segments required for calculation can be reduced for most baffles using symmetry of the baffle as well as mathematical properties of the expression. Using the square baffle as an example, the below drawing shows that although the shape function is defined within the

closed range from 0 to 2π, the function itself is periodic within the range from 0 to $\pi/2$, so only this range needs consideration. This reduces the number of segments to one-fourth.
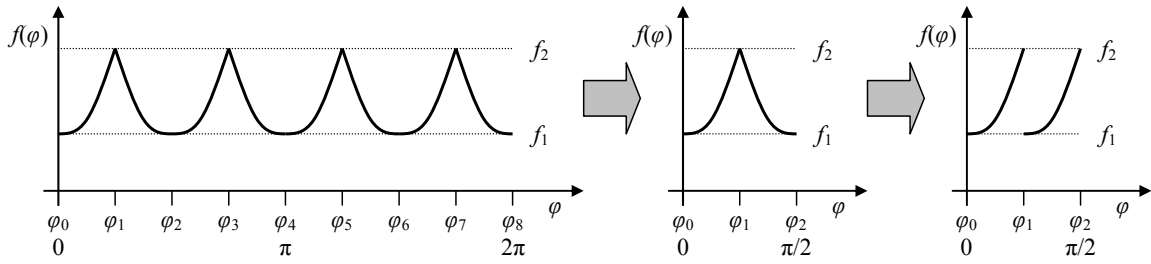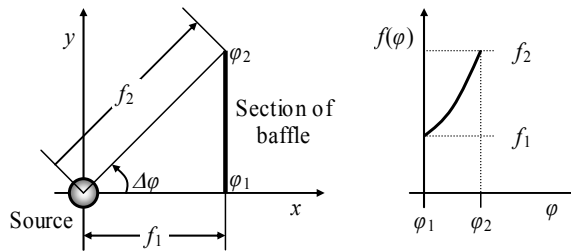

Figure 142 – The shape function for a square baffle shape oscillates between function values f_1 and f_2 (left). The periodicity of the shape function can be used to remove most of the calculation (middle) and the symmetry of the exponential and sinc functions can be used to swap the sign of the linear sections (right).

The exponential function within equation 130 is defined by the average value of two consecutive points, $f(\varphi_n)$ and $f(\varphi_{n+1})$, from now on written as f_1 and f_2, but the actual order of the points is unimportant; the function values can be interchanged without affecting the result. A similar conclusion applies to the sinc function due to the symmetry of the function to negative arguments: $\text{sinc}(-x) = \text{sinc}(x)$. As a consequence, one can swap the sign of the slope to the sections, thus calculating the remaining two sections as one section. The physical explanation is that the effective delay is calculated at the midpoint of each linear section.

The above problem can be calculated from the function values f_1 and f_2 as:

$$p_1 = p_0 \exp\left(-ikB\frac{f_1 + f_2}{2}\right)\text{sinc}\left(kB\frac{f_1 - f_2}{2}\right)$$

131

One possible implementation for this equation is an elliptic baffle where the radius is increased gradually between the minimum value and the maximum value. The shape function may not exactly model the elliptic baffle but it is at least an approximation.
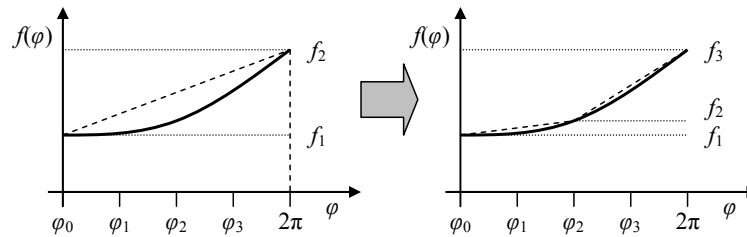

Figure 143 – The shape function for one section of the baffle.

This can be generalised, approximating the baffle by a finite number of sections with the delay defined by the mean distance and the ripple defined by the difference between the distances to the endpoints of the section. The baffle is thus described by the sum of the above contributions and divided by the number of segments. Using N segments to describe the baffle we have $N + 1$ endpoints and the following equation approximates the diffracted signal.

$$p_1 = \frac{p_0}{N}\sum_{n=1}^{N}\exp\left(-ikB\frac{f_n + f_{n+1}}{2}\right)\text{sinc}\left(kB\frac{f_n - f_{n+1}}{2}\right), \quad f_{n+1} = f_1$$

132

With two segments ($N = 2$) we have f_1, f_2 and f_3, with $f_3 = f_1$ since the loop is closed.

The sections do not need to be of the same size; φ can step with different values for each section. The simplification of the problem opens the possibility of improving the precision of the approximation by increasing the number of segments.

Figure 144 – The shape function for a square baffle shape can be reduced from eight segments to one segment as shown previously (left) thus allowing an improvement in the accuracy by using two segments to represent the shape function (right).

Using two straight lines for each segment, one for function values f_1 and f_2, and another segment for function values f_2 and f_3, results in the following expression:

$$p_1 = \frac{p_0}{2}\left[\exp\left(-ikB\frac{f_1+f_2}{2}\right)\text{sinc}\left(kB\frac{f_1-f_2}{2}\right)+\exp\left(-ikB\frac{f_2+f_3}{2}\right)\text{sinc}\left(kB\frac{f_2-f_3}{2}\right)\right] \qquad 133$$

The function values f_1 and f_2 are closer together than the function values f_2 and f_3, so the first sinc function will attenuate the signal at a higher frequency than the second sinc function.

7.2.4 Circular baffle

Radius of the circular baffle is B, which is constant so the shape function $f(\varphi)$ is unity for all φ and it is thus not required dividing the function into sections, one section from φ_0 to φ_1 using a step size of $\Delta\varphi = 2\pi$ will do. The result for the circular baffle becomes a delay function without the sinc function.

$$p_1 = p_0 \exp(-ikB) \qquad\qquad 134$$

The circular baffle does not affect the amplitude of the diffracted signal; only the phase is changed, so the circular baffle causes serious interference throughout the frequency range.
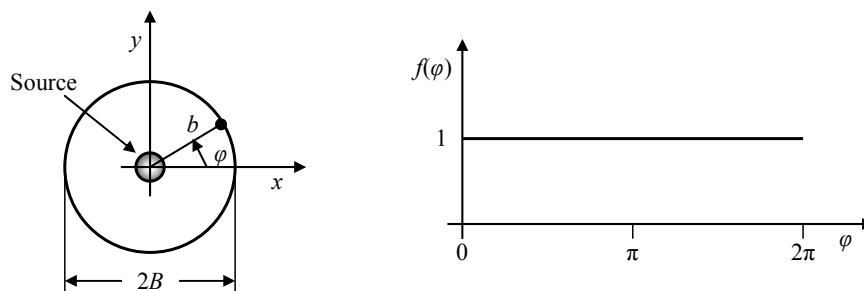
Figure 145 – Derivation of function f(φ) for an elliptic baffle.

7.2.5 Elliptic baffle

An ellipse is defined similarly to the circle as $x = B_x\cos(\varphi)$ and $y = B_y\cos(\varphi)$, where the shape is specified through the coefficients B_x and B_y and becomes a circle for $B_x = B_y$. With the major axis of the ellipse along the x-axis, the equation for the ellipse can be written:

$$x = B\cos(\varphi), \quad y = B\cos(\theta)\sin(\varphi), \quad 0 < \varphi < 2\pi, \quad 0 < \theta < \frac{\pi}{2}$$

This represents a circle for the projection angle $\theta = 0°$, and the ellipse collapses to a straight line for $\theta = 90°$, with the elliptic shapes within this range. The ellipse may alternatively be constructed as the projection of a circle onto an angled plane, which can be considered as a circular baffle observed at angle θ, so the following theory applies equally well to a circle observed off-axis at observation angle θ. The elliptic baffle and its shape function is shown below.
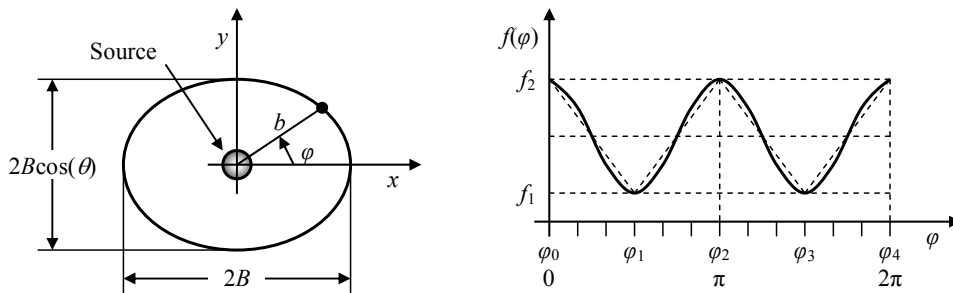

Figure 146 – Derivation of function f(φ) for an elliptic baffle.

The distance from the sound source to the edge is:

$$b = \sqrt{x^2 + y^2} = B\sqrt{\cos^2(\varphi) + \cos^2(\theta)\sin^2(\varphi)}$$

The shape function, i.e. the function describing b, becomes:

$$b = Bf(\varphi) \quad \Rightarrow \quad f(\varphi) = \sqrt{\cos^2(\varphi) + \cos^2(\theta)\sin^2(\varphi)}$$

Using the trigonometric identity for the sum of squared sine and cosine functions, the cosine can be rewritten as a squared sine.

$$f(\varphi) = \sqrt{1 - \sin^2(\varphi) + \cos^2(\theta)\sin^2(\varphi)}$$
$$= \sqrt{1 + (\cos^2(\theta) - 1)\sin^2(\varphi)}$$

A Taylor series expansion will be used to simplify the expression by removing the square root (Westergren, 196). Only the two first terms of the series expansion are used, which results in an error around 6 % for an argument approaching ±1.

$$\sqrt{1 + x} \approx 1 + \frac{x}{2} \quad \Rightarrow \quad f(\varphi) \approx 1 + \frac{\cos^2(\theta) - 1}{2}\sin^2(\varphi)$$

The function is π-periodic, so only the range from 0 to π is needed for calculation. The function will be approximated by two sections within this range, so $\Delta\varphi = \pi/2$. The maximum and minimum values are:

$$
\begin{aligned}
f_1 &= 1 & \varphi &= 0 \\
f_2 &= \left[\frac{1}{2} + \frac{\cos^2(\theta)}{2}\right] & \varphi &= \frac{\pi}{2}
\end{aligned}
$$

The expression for the sound pressure from the diffracted signal will use equation 131:

$$
p_1 = p_0 \exp\left(-ikB\frac{f_1+f_2}{2}\right)\operatorname{sinc}\left(kB\frac{f_1-f_2}{2}\right)
$$

Inserting the function values into the exponential results in the following expression:

$$
\exp\left(-\frac{ikB}{2}[f_1+f_2]\right) = \exp\left(-\frac{ikB}{2}\left[1+\frac{1}{2}+\frac{\cos^2(\theta)}{2}\right]\right)
$$

$$
= \exp\left(-ikB\left[\frac{3}{4}+\frac{\cos^2(\theta)}{4}\right]\right)
$$

The delay becomes identical to the circular baffle for $\theta = 0°$, as it should. The sinc function can be written as:

$$
\operatorname{sinc}\left(kB\frac{f_1-f_2}{2}\right) = \operatorname{sinc}\left(\frac{kB}{2}\left[1-\left[\frac{1}{2}+\frac{\cos^2(\theta)}{2}\right]\right]\right)
$$

$$
= \operatorname{sinc}\left(kB\left[\frac{1}{4}-\frac{\cos^2(\theta)}{4}\right]\right)
$$

The sound pressure of the diffracted signal for the elliptic baffle becomes:

$$
p_1 = p_0 \exp\left(-ikB\left[\frac{3}{4}+\frac{\cos^2(\theta)}{4}\right]\right)\operatorname{sinc}\left(kB\left[\frac{1}{4}-\frac{\cos^2(\theta)}{4}\right]\right) \tag{135}
$$

The delay changes from the maximum value kB obtained for $\theta = 0°$, where the elliptic baffle has become a circle, and to the minimum value of $0.75kB$ obtained at $\theta = 90°$, where the baffle is a straight line. The latter value is obviously too large but this is a result of the approximation. The sinc function changes from unity at $\theta = 0°$ to $kB/4$ at the projection angle of $\theta = 90°$.

For an elliptic baffle with height equal to 50 % of the width, the projection angle is $\theta = 60°$, for a cosine of 0.50, and the equation becomes:

$$
p_1 = p_0 \exp(-0.81ikB)\operatorname{sinc}(0.19kB) \tag{136}
$$

The elliptic baffle introduces the sinc function into the diffracted signal thus attenuating the level of the diffracted signal at the high-frequency end.

The baffle cut-off frequency can be defined as the first zero in the frequency response, which is determined from equation 135 as:

$$\text{sinc}\left(kB\left[\frac{1}{4} - \frac{\cos^2(\theta)}{4}\right]\right) = 0 \quad \Rightarrow \quad \frac{kB}{4}\left[1 - \cos^2(\theta)\right] = \pi \quad \Rightarrow \quad f_{CUT} = \frac{2}{\left(1 - \cos^2(\theta)\right)}\frac{c}{B}$$

For $B = 170$ mm and $\theta = 60°$ will the first zero occur at 5.4 kHz so the elliptic baffle is an improvement to the circular baffle only at high frequencies.

7.2.6 Off-axis correction

A circular baffle looks like an elliptic baffle when it is viewed from an angle different from on-axis and similar for a square baffle, which looks like a rectangle when it is tilted. This is shown below for the circular baffle.
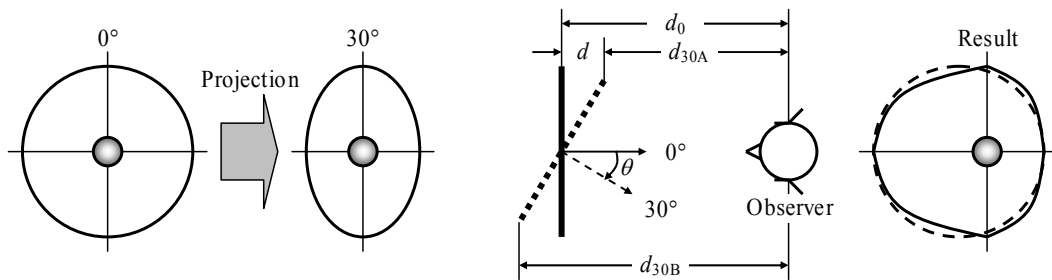
Figure 147 – The observer may see the circle turned into an ellipse but the sound must travel through a distance, which is increased for one side and decreased for the other side.

It is possible modelling the tilt using the above tools if the change in distance to the observer is taken into account; distance d_{30A} is shorter than the nominal distance d_0 while distance d_{30B} is larger. Hence, the model approximates a circle with offset source. Similar applies to a tilted square, which is turned into a rectangle, and a rectangle is turned into another rectangle.

The change in distance for a tilted baffle is:

$$d = B\sin(\theta) \tag{137}$$

The change in distance is reflected within the shape function, which becomes:

$$f_1 = 1 + \sin(\theta), \quad f_2 = 1 - \sin(\theta)$$

Insertion into equation 130 gives:

$$p_1 = p_0 \exp(-ikB)\text{sinc}(kB\sin(\theta)) \tag{138}$$

For $\theta = 30°$ the equation becomes:

$$p_1 = p_0 \exp(-ikB)\text{sinc}\left(\frac{kB}{2}\right) \tag{139}$$

7.2.7 Elliptic baffle with offset source

A model will be derived for an elliptic baffle with offset source.
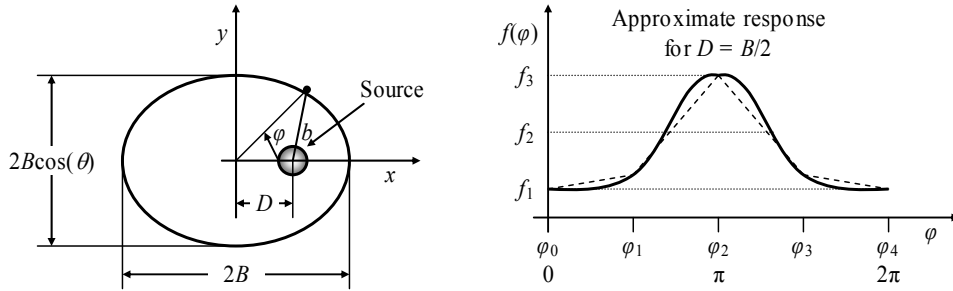

Figure 148 – Derivation of function f(φ) for an elliptic baffle with offset source.

Offsetting the source to $x = D$ does not affect the definition of the ellipse but it changes the distance from the sound source to the edge.

$$b = \sqrt{(x-D)^2 + y^2}$$
$$= B\sqrt{(\cos(\varphi)-D)^2 + (\cos(\theta)\sin(\varphi))^2}$$

The offset distance will be normalised to $d_B = D/B$ and the shape function becomes:

$$f(\varphi) = \sqrt{(\cos(\varphi)-d_B)^2 + \cos^2(\theta)\sin^2(\varphi)}$$

The function is 2π-periodic, but symmetry can halve the range needed for calculation to π. The function will be approximated by two sections within this range, so $\Delta\varphi = \pi/2$ and the function values must be calculated at $\varphi = 0$, $\pi/2$ and $\varphi = \pi$. The function values are:

$$f_1 = f(0) = \sqrt{(1-d_B)^2} = 1-d_B$$
$$f_2 = f(\pi/2) = \sqrt{d_B^2 + \cos^2(\theta)}$$
$$f_3 = f(\pi) = \sqrt{(1+d_B)^2} = 1+d_B$$

Insertion into equation 133 generates the following expression:

$$p_1 = \frac{p_0}{2}\left[\exp\left(-ikB\frac{1-d_B+\sqrt{d_B^2+\cos^2(\theta)}}{2}\right)\text{sinc}\left(kB\frac{1-d_B-\sqrt{d_B^2+\cos^2(\theta)}}{2}\right)\right.$$
$$\left. + \exp\left(-ikB\frac{\sqrt{d_B^2+\cos^2(\theta)}+1+d_B}{2}\right)\text{sinc}\left(kB\frac{\sqrt{d_B^2+\cos^2(\theta)}-1-d_B}{2}\right)\right] \qquad d_B = \frac{D}{B} \qquad 140$$

It is seen, that the model reduces to the simple exponential for a projection angle of $\theta = 0°$ and an offset of $D = 0$; as it is expected to do.

For an offset different from zero the cosine functions become unity and we have an equation for a circular baffle with offset source:

$$p_1 = \frac{p_0}{2}\left[\exp\left(-ikB\frac{1-d_B+\sqrt{d_B^2+1}}{2}\right)\mathrm{sinc}\left(kB\frac{1-d_B-\sqrt{d_B^2+1}}{2}\right) \right.$$
$$\left. + \exp\left(-ikB\frac{\sqrt{d_B^2+1}+1+d_B}{2}\right)\mathrm{sinc}\left(kB\frac{\sqrt{d_B^2+1}-1-d_B}{2}\right) \right]$$

Approximating the square roots by the Taylor series-expansion and ignoring the squaring of the d_B term within the square root we get the approximation:

$$p_1 = \frac{p_0}{2}\left[\exp\left(-ikB\left(1-\frac{d_B}{4}\right)\right)\mathrm{sinc}\left(kB\frac{3d_B}{4}\right) + \exp\left(-ikB\left(1+\frac{3d_B}{4}\right)\right)\mathrm{sinc}\left(kB\frac{d_B}{4}\right) \right] \qquad 141$$

The errors introduced by the approximations are negligible; the model is an approximation anyway. For $D = B/2$ we get $d_B = \frac{1}{2}$ and the equation becomes:

$$p_1 = \frac{p_0}{2}\left[\exp\left(-\frac{7}{8}ikB\right)\mathrm{sinc}\left(\frac{3}{8}kB\right) + \exp\left(-\frac{11}{8}ikB\right)\mathrm{sinc}\left(\frac{1}{8}kB\right) \right]$$

Using a projection angle of $\theta = 60°$ and an offset of $D = B/2$, the result becomes:

$$p_1 = \frac{p_0}{2}\left[\exp(-0.60 \cdot ikB)\mathrm{sinc}(0.10 \cdot kB) + \exp(-1.10 \cdot ikB)\mathrm{sinc}(0.79 \cdot kB)\right] \qquad 142$$

The elliptic baffle with offset source attenuates the diffracted signal above a frequency defined by the baffle dimension B and the offset. The attenuation starts where the first of the sinc function has its zero and accelerates where the second sinc function has its zero. The two zero frequencies are:

$$\mathrm{sinc}(0.10 \cdot kB) = 0, \quad \mathrm{sinc}(0.79 \cdot kB) = 0$$

The frequencies are located at different frequencies so the cut-off frequency is defined here as the geometrical midpoint of the two frequencies:

$$\left.\begin{array}{l} 0.10 \cdot kB = \pi \quad \Rightarrow \quad f_{CUT1} = 5\dfrac{c}{B} \\[2mm] 0.79 \cdot kB = \pi \quad \Rightarrow \quad f_{CUT2} = 0.63\dfrac{c}{B} \end{array}\right\} \quad \Rightarrow \quad f_{CUT} = \sqrt{f_{CUT1}f_{CUT2}} = 1.8\dfrac{c}{B}$$

The cut-off frequency becomes 3.6 kHz with $B = 170$ mm, which is in reasonable agreement with the plot.

7.2.8 Square baffle

Using a square baffle with the loudspeaker located symmetrically at the centre produces the following relation exists for the x and y coordinates of the vertical right-hand side:

$$x = B, \quad y = B\tan(\varphi), \quad -\frac{\pi}{4} < \varphi < \frac{\pi}{4}$$

Similar expressions can be stated for the other sides, but this is not required due to symmetry, as explained in section 7.2.3.
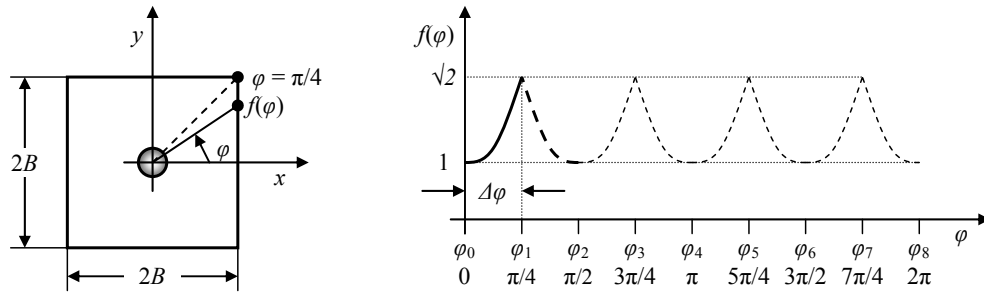
Figure 149 – Derivation of function f(φ) for a square baffle. Only the first quarter of the range is of interest due to periodicity and even this range can be halved due to symmetry.

The relation for determination of the shape function for the range from 0 to $\pi/4$ is:

$$b_B f(\varphi) = \sqrt{x^2 + y^2} = B\sqrt{1 + \tan^2(\varphi)} \quad \Rightarrow \quad f(\varphi) = \frac{B}{b_B}\sqrt{1 + \tan^2(\varphi)}$$

One of the possible definitions is shown in the figure above where $b_B = B$, for which $f(\varphi)$ becomes equal to the square root and this definition will be used below, but any other definition is equally valid. Using the symmetry, the method needs only two function values, $f(\varphi_0) = 1.00$ and $f(\varphi_1) = 1.41$, for computation of the expression.

$$p_1 = p_0 \exp\left(-ikB\frac{1+1.41}{2}\right)\mathrm{sinc}\left(kB\frac{1.41-1}{2}\right)$$

The expression becomes:

$$p_1 = p_0 \exp(-1.21ikB)\mathrm{sinc}(0.21kB) \qquad\qquad 143$$

This is almost identical to the expression of an elliptic baffle; the main difference is the delay, which 1.5 times larger thus corresponding to the larger baffle. The expression can be improved by using four two linear sections with $\varphi = 0$, $\pi/8$ and $\pi/4$. The function values are: $f(\varphi_0) = 1.00$, $f(\varphi_1) = 1.08$ and $f(\varphi_3) = 1.41$ and insertion into equation 133 generates the following expression:

$$p_1 = p_0 \frac{1}{2}\left[\exp(-1.04ikB)\mathrm{sinc}(0.04kB) + \exp(-1.25ikB)\mathrm{sinc}(0.17kB)\right] \qquad\qquad 144$$

The expression can be re-arranged by moving the first term of the sum outside the brackets:

$$p_1 = p_0 \frac{1}{2}\exp(-1.04ikB)\mathrm{sinc}(0.04kB)\left[1 + \exp(-0.21ikB)\frac{0.04}{0.17}\frac{\sin(0.17kB)}{\sin(0.04kB)}\right]$$

The term in front of the brackets is – almost – the expression of a circular baffle; the decay is close to $\exp(-ikB)$ and the sinc function is almost independent upon frequency, the first zero is located around 50 kHz. The term inside the bracket represents the change due to the four corners of the square.

The right-hand term includes division with a sine function but the equation does not blow up when the function approaches zero since the sinc function in front of the brackets approaches

zero at the same frequency. The net result at the limit becomes equal to the scaling factor within the brackets, i.e. the peak will be 0.04/0.17 or around −8 dB.

The cut-off frequency will here be defined as the zero frequency of the sinc function within the square brackets, since the sinc function in front of the brackets has limited influence within the audible range.

$$\text{sinc}(0.17kB) = 0 \;\Rightarrow\; 0.17kB = \pi \;\Rightarrow\; f_{CUT} = 2.9\frac{c}{B}$$

The cut-off frequency becomes 5.9 kHz with B = 170 mm, which is in reasonable agreement with the plot although it is close to the local peak. Interference due to diffraction is reduced above the cut-off frequency but serious rippling within the useful frequency range can be expected since the cut-off is relatively high.

7.2.9 Rectangular baffle

A rectangular baffle is not easily modelled within the polar coordinate system, so the baffle to be analysed will be fixed in the high to width ratio in order to survive the calculation. The description will use twelve segments ($\Delta\varphi$ = 30°), fixing the baffle size at $1.15B$ high by $2B$ wide (1 high by 1.73 wide), which is intended to represent a typical rectangular baffle.

The shape function will be approximated by three segments from 0 to π using the symmetry, and ignoring the minor variations within the function, which corresponds to rounding the corners of the baffle, as shown dashed in the figure below.
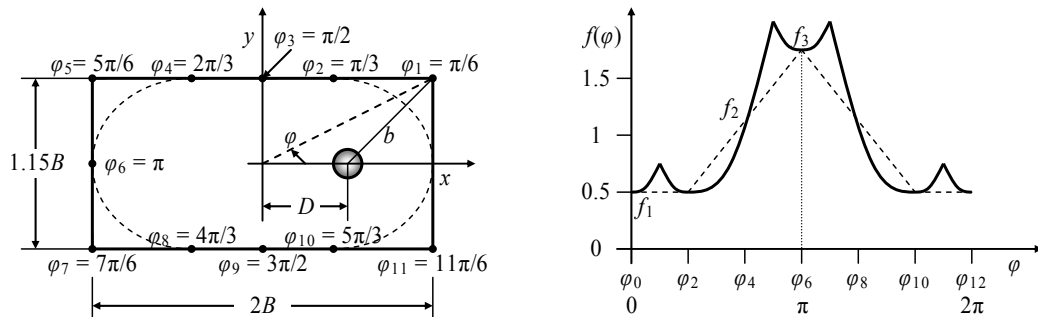
Figure 150 – Derivation of function f(φ) for a rectangular baffle with offset sound source. The shape function is shown for d = B/2 as the offset and the effect of the simplification is shown as dotted lines; the edges are rounded.

Key values of the shape function are shown below.

$$f_1 = \frac{B-D}{B} = 1 - \frac{D}{B}, \quad f_2 = \frac{f_1 + f_3}{2} = 1, \quad f_3 = \frac{B+D}{B} = 1 + \frac{D}{B}$$

Insertion into expression 130 (with $N = 3$) the equation becomes:

$$p_1 = \frac{p_0}{3}\left[\exp\left(-\frac{ikB}{2}\left(1-\frac{D}{B}+1\right)\right)\operatorname{sinc}\left(\frac{kB}{2}\left(\left(1+\frac{D}{B}-1\right)\right)\right)\right.$$

$$+\exp\left(-\frac{ikB}{2}\left(1+1+\frac{D}{B}\right)\right)\operatorname{sinc}\left(\frac{kB}{2}\left(1-1-\frac{D}{B}\right)\right)$$

$$\left.+\exp\left(-\frac{ikB}{2}\left(1+\frac{D}{B}+1\right)\right)\operatorname{sinc}\left(\frac{kB}{2}\left(1+\frac{D}{B}-1\right)\right)\right]$$

The sinc functions are identical despite the different signs and reduction of the exponentials results in:

$$p_1 = \frac{p_0}{3}\left[2\cdot\exp\left(-ikB\left(1+\frac{D}{2B}\right)\right)+\exp\left(-ikB\left(1-\frac{D}{2B}\right)\right)\right]\operatorname{sinc}\left(kB\frac{D}{2B}\right)$$

$$= \frac{p_0}{3}\exp(-ikB)\left[\exp\left(-\frac{ikD}{2}\right)+\exp\left(-\frac{ikD}{2}\right)+\exp\left(\frac{ikD}{2}\right)\right]\operatorname{sinc}\left(\frac{kD}{2}\right)$$

The square bracket is recognised as the sum of a delay and a cosine function according to the Euler formula for the cosine function (Westergren, 62). Hence:

$$p_1 = \frac{p_0}{3}\exp(-ikB)\left[\exp(-ikD)+2\cdot\cos\left(\frac{kD}{2}\right)\right]\operatorname{sinc}\left(\frac{kD}{2}\right) \qquad 145$$

For offset $D = B/2$ the expression becomes:

$$p_1 = \frac{p_0}{3}\exp(-ikB)\left[\exp\left(-\frac{ikB}{2}\right)+2\cdot\cos\left(\frac{kB}{4}\right)\right]\operatorname{sinc}\left(\frac{kB}{4}\right) \qquad 146$$

Two zero-frequencies are possible; the first is due to the terms within the square bracket and the second is generated by the sinc function. The expression can be solved analytically but MATLAB is better suited for this purpose so a file was generated representing the terms within the square bracket and the amplitude is plotted below.
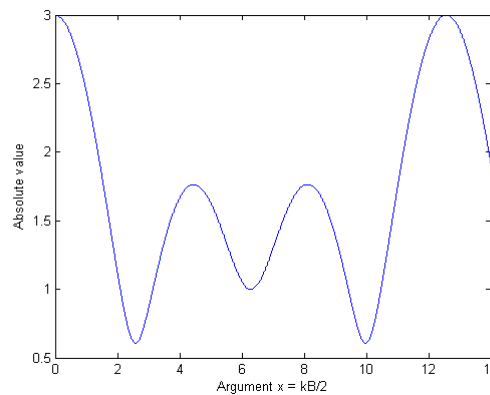
The first minimum is found for $kB/2 = 2.58$ so the cut-off frequency becomes $f_{CUT} = 0.82c/B$, which is at 1.7 kHz for $B = 170$ mm. The sinc function generates a null at $kB/4 = \pi$, so the

next cut-off is at $f_{CUT} = 2c/B = 4.1$ kHz for $B = 170$ mm. The geometric mean of the two values is 2.6 kHz, which is approximately at the peak before the level finally drops off.

7.3 Blurring of the second reflection

It is the purpose of this section to derive an equation for the blurring of the diffracted signal due to the second reflection. The reflected signal is assumed to propagate as spherical waves within the 2π solid angle in front of or behind the baffle generating new reflections whenever an edge is reached. This is illustrated below where reflection is represented by a monopole sound source located at the edge. Hence, the model may also be used to calculate the amplitude response of a loudspeaker mounted at the edge of a circular baffle.
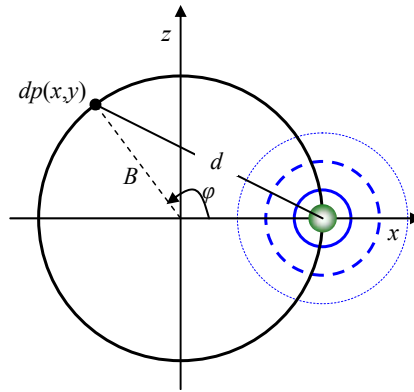

Figure 151 – Estimation of distance d as function of the observation point expressed by φ for a circular baffle with radius b. The monopole sound source of the figure represents each of the infinitesimal sound sources along the periphery of the circle.

The model will be presented for the circular baffle only, due to the complexity of the problem.

7.3.1 Theory

An infinitesimal sound source is defined on the circle periphery with the x and y coordinates determined by:

$$x = B\cos(\varphi), \quad y = B\sin(\varphi)$$

The source is assumed located at $(B,0)$ so the length of distance d to a point on the circle is changing from zero to $2B$ according to the following relation:

$$d = \sqrt{(B-x)^2 + y^2}$$
$$= B\sqrt{(1-\cos(\varphi))^2 + \sin^2(\varphi)}$$
$$= B\sqrt{2(1-\cos(\varphi))}$$

The square root can be removed using a trigonometric identity (Westergren, 127):

$$\sin^2\left(\frac{\varphi}{2}\right) = \frac{1-\cos(\varphi)}{2} \quad \Rightarrow \quad d = 2B\sin\left(\frac{\varphi}{2}\right)$$

The sound pressure at distance r_1 from each of the infinitesimal sound sources, located at the periphery of the circle and assuming an infinite plane, is:

$$dp_2 = \frac{i\omega\rho q}{2\pi(r_1 + B + d)} \exp(i\omega t - ikr_1 - ikB - ikd)\frac{d\varphi}{2\pi}$$

Ignoring the change in amplitude due to B and d, but not the change in phase, simplifies the expression by removing B and d from the dominator and setting r_1 equal to r_0. This requires the dimension $B + d$ being less than er_0, where e is the accepted error and r_0 is the distance to the observation point. Using this information the equation simplifies to:

$$dp_2 = \frac{i\omega\rho q}{2\pi r_0} \exp(i\omega t - ikr_1)\exp(-ikB)\exp(-ikd)\frac{d\varphi}{2\pi}$$

The first two terms are recognised as the original monopole sound source p_0 and the third term is recognised as the delay of a circular baffle, p_1/p_0, so the equation can be written:

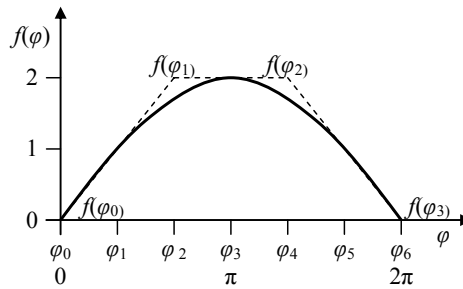$$dp_2 = p_0 \frac{p_1}{p_0}\frac{d\varphi}{2\pi} = p_1 \frac{d\varphi}{2\pi}$$

The resultant sound pressure from the sound source becomes:

$$p_2 = p_1 \frac{1}{2\pi} \int_0^{2\pi} \exp(-ikd)d\varphi$$

The expression for d is inserted:

$$p_2 = p_1 \frac{1}{2\pi} \int_0^{2\pi} \exp\left(-2ikB\sin\left(\frac{\varphi}{2}\right)\right)d\varphi$$

This is a half-sine for φ varying from π to 2π and will be approximated by three segments as shown below.

**Figure 152 – Shape function for the blurring due to a circular disk.**

The function values are $f(0) = f(2\pi) = 0$ and $f(2\pi/3) = f(4\pi/3) = 2$ and insertion these values directly into expression 130 (with $N = 3$) yields:

$$p_1 = \frac{p_0}{3}\left[\exp(-ikB)\text{sinc}(kB) + \exp(-2ikB) + \exp(-ikB)\text{sinc}(kB)\right]$$

After reduction the expression for the source at the edge of the baffle becomes:

$$p_1 = \frac{p_0}{3}\exp(-ikB)[2\cdot\mathrm{sinc}(kB)+\exp(-2ikB)]$$ 147

A plot of the transfer function is shown below with a monopole sound source at the edge of the baffle.
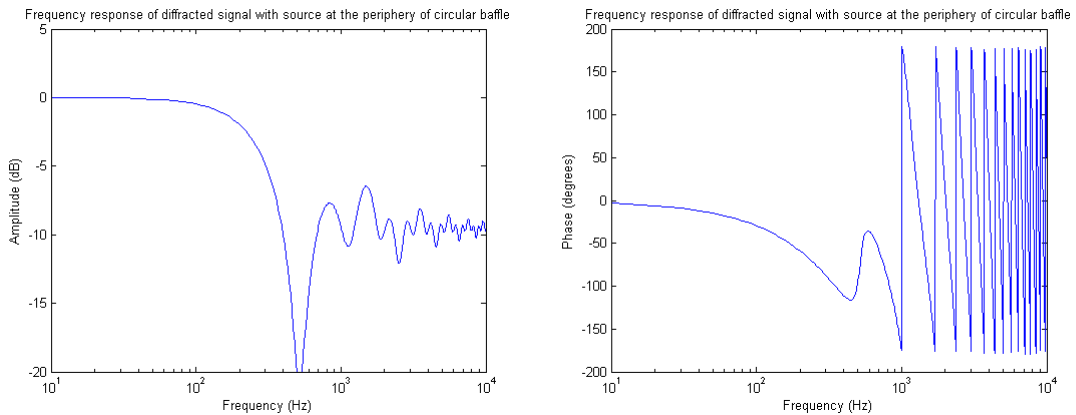

Figure 153 – Frequency response with a circular baffle and the source located at the edge of the baffle.

The effect of blurring is to attenuate the high-frequencies.

7.4 Wave equation

It was the objective modelling the wave front through solving the wave equation for a circular baffle with the sound source at the centre of the baffle. The problem was considered spherical due to the point source and the circular baffle but the wave front on the rear side of the baffle is not spherical (it is like an inflating bicycle tube) so I decided after some work to ignore the rear side radiation and concentrate on the front side only. The model is thus assuming that the propagating wave front is propagating as a spherical wave within the half-space at the front side and it was the idea to model the baffle through the boundary conditions.
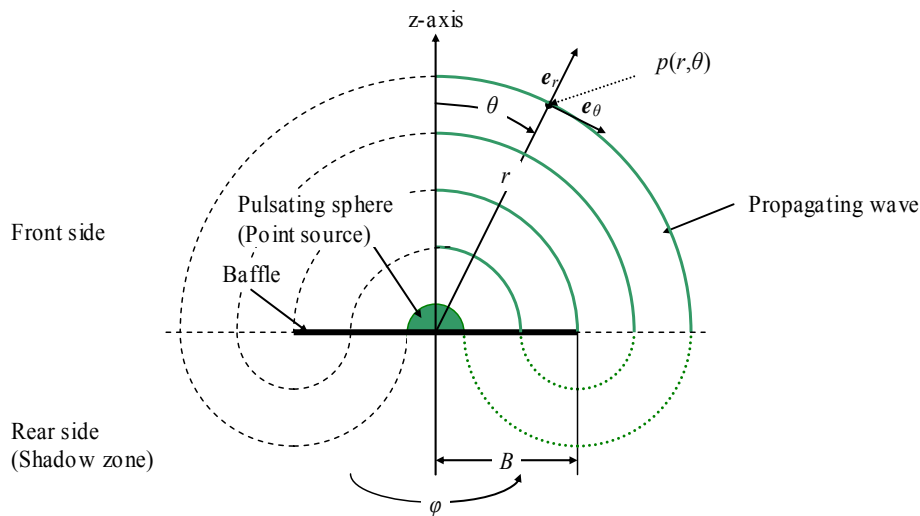
Figure 154 – Graphical representation of the diffraction model using a point source and a concentric circular baffle.

The wave equation was expected solvable using integral transformation since this method can cope with the discontinuity at the boundary of the disk. The discontinuity is at radius $r = B$, so radius was planned to be the transformed variable and radius is semi-infinite, which indicates use of the Laplace transformation.

The spherical wave equation uses the independent variables radius r and observation angle θ assuming rotation symmetry around the z-axis. The spherical wave equation is, according to equation 14:

$$\frac{\partial^2 p}{\partial r^2} + \frac{2}{r}\frac{\partial p}{\partial r} + \frac{1}{r^2}\left[\frac{\partial^2 p}{\partial \theta^2} + \cot(\theta)\frac{\partial p}{\partial \theta}\right] + k^2 p = 0, \quad p = p(r,\theta)\exp(i\omega t)$$

Multiplying by r^2 the equation becomes:

$$r^2\frac{\partial^2 p}{\partial r^2} + 2r\frac{\partial p}{\partial r} + \frac{\partial^2 p}{\partial \theta^2} + \cot(\theta)\frac{\partial p}{\partial \theta} + k^2 r^2 p = 0$$

The system is singular for $r = 0$ so a variable substitution was used to avoid problems during the Laplace transformation. The new variable will be called σ and is offsetting the start from the origin to begin at a sphere around the origin with radius a, which is small but non-zero. This is effectively a spherical source with known radius and volume velocity and should thus fit well into the model. The substitution becomes:

$$r = \sigma + a \quad \Rightarrow \quad \sigma = r - a, \quad a > 0$$

The differential $d\sigma$ is identical to dr and insertion gives the following wave equation to be Laplace transformed.

$$(\sigma + a)^2\frac{\partial^2 p}{\partial \sigma^2} + 2(\sigma + a)\frac{\partial p}{\partial \sigma} + \frac{\partial^2 p}{\partial \theta^2} + \cot(\theta)\frac{\partial p}{\partial \theta} + k^2(\sigma + a)^2 p = 0 \qquad 148$$

Laplace transforming the terms is somewhat tedious and will not be detailed here as (see section 7.4). Assembling the Laplace-transformed terms and re-substituting $\sigma + a$ back into r, we finally arrive at:

$$a^2\exp(-sa)\left(sp(a,\theta) + \frac{\partial p(a,\theta)}{\partial r}\right)$$

$$+ \left(s^2 + k^2\right)\frac{\partial^2 \hat{p}(s,\theta)}{\partial s^2} + 2s\frac{\partial \hat{p}(s,\theta)}{\partial s} + \frac{\partial^2 \hat{p}(s,\theta)}{\partial \theta^2} + \cot(\theta)\frac{\partial \hat{p}(s,\theta)}{\partial \theta} - \hat{p}(s,\theta) = 0$$

The first line represents the terms due to the spherical excitation source with radius a. Assuming that radius is small then $a^2 \rightarrow 0$ and the first line can be ignored so the transformed wave equation can be simplified into:

$$\left(s^2 + k^2\right)\frac{\partial^2 \hat{p}(s,\theta)}{\partial s^2} + 2s\frac{\partial \hat{p}(s,\theta)}{\partial s} + \frac{\partial^2 \hat{p}(s,\theta)}{\partial \theta^2} + \cot(\theta)\frac{\partial \hat{p}(s,\theta)}{\partial \theta} - \hat{p}(s,\theta) = 0 \qquad 149$$

The negative sign for the last term was surprising and was expected due to an error but the source of the error was not found.

7.4.1 Comments

Several attempts have been initiated to solve this equation – or similar equations from earlier trials – but they have not been successful. In the first trial was the terms in θ interpreted as an inhomogeneous Legendre equation (the inhomogeneous part being the Laplace-transformed terms), which was solved but proved to be a dead end; the solution forced the sound pressure to be proportional to $\cos(\theta)$ and this is obviously too limiting to be valuable. It all boils down to the problem of understanding the derivatives in s. I am used to Laplace-transformed electrical networks but this equation is quite different from the linear network theory known to me.

The books *Partial Differential Equations* by Nakhle H. Asmar (Pretience Hall, 2nd Ed 2005) and *Green's Functions with Applications* by Dean G. Duffy (Chapmann & Hall, 2001) were carefully studied but the problem remained unsolved although the last book was probably on the right track since Urban et al. solved a similar problem using the Green's function and the Kirchhoff approximation. However, I am not accustomed to Green's function and the more advanced physics and mathematics so I did not dare to follow this path.

Finn Agerkvist suggested consulting the book *Sædvanlige differentialligninger fra fysikken* by Erik Hansen (Polyteknisk forlag, 1976), which solved several minor problems but I did not find a route to a solution to the problem at hand.

Ove Skoggaard offered me two sessions of assistance where the problem was reviewed and my attempts to solve the wave equation were commented. The problem of singularity was addressed and he suggested a route to solve the problem but the Laplace transformed wave equation remained unsolvable to me.

Finn Jacobsen provided me with a reference to Vicente Cutanda, who mailed me the article *On the modelling of narrow gaps using the standard boundary element method* (J. Acoust. Soc. Am., 2001). The article included a very short appendix (20 lines), where the problem of solving the wave equation for a thin circular disk were addressed; it should be expressed in the oblate spheroidal coordinate system to become separable. A solution was shown using spheroidal angular and radial functions; however, his application used a plane circular disk excited by a plane wave, which is not representative of the model used here, and the suggested coordinate system was unknown to me so I decided not to follow the track – I had already used sufficient time on the subject.

Time has not been wasted since I have learned a lot from this study, but the time could have been used improving the remaining two models. It's a pity, but that's how it is.

"Don't worry; be happy" (Bobby McFarrin).

7.5 Laplace transformation

The transformation was developed by Pierre Simon Laplace (France, 1749-1827) for solving differential equations of the initial-value type. It is closely related to the Fourier transform but the definition range of the independent variable is semi-infinite, which is the reason for considering the transformation within this study.

7.5.1 One variable

The Laplace transform of function $f(t)$ is defined by the following integral (Asmar, 480). Variable t is commonly associated by time since the transformation was developed for solving transient problems with electrical networks, but it is a general-purpose variable and there are no restrictions on its use for other coordinate systems:

$$L\{f(t)\} = \hat{f}(s) = \int_0^\infty f(t)\exp(-st)dt \qquad 150$$

The function must be exponentially limited within the range $0 \leq t < \infty$, in order for the integral to exist. The transform exists for sufficiently large s, provided such the function satisfies the following conditions: $f(t) = 0$ for $t < 0$; $f(t)$ is continuous or piece-wise continuous in every interval; $t^n|f(t)| < \infty$ as $t \to 0$ for $n > 1$; and $\exp(-s_0 t)|f(t)| < \infty$ as $t \to \infty$ for some number s_0.

The unit of the transformed variable s is reciprocal distance (m^{-1}) and represents revolutions per length so the transformed variable represents an "oscillation domain" where s is low for slow variations with r and s is high for fast variations with r.

The Laplace transform is linear, so the sum of functions $f(t)$ and $g(t)$ with scaling constants a and b can be transformed term by term:

$$L\{af(t) + bg(t)\} = a\hat{f}(s) + b\hat{g}(s) \qquad 151$$

Other features of the Laplace transform will be quoted whenever required.

An inverse Laplace transformation exists, but will not be considered within this study.

7.5.2 Two variables

The Laplace transformation and is defined for functions of one variable but the present study require transformation of $p(r,\theta)$, which is a function of two variables so the basic definition must be changed to include a second variable. This is done by "renaming" the second variable into a *parameter* in stead of *variable*. The parameter remains fixed during the transformation but can be changed at will after the transformation. Laplace transforming a function of two parameters will use the following definition, where r is the transformed variable and θ is a fixed parameter.

$$L\{f(r,\theta)\} = \hat{f}(s,\theta) = \int_0^\infty f(r,\theta)\exp(-sr)dr \qquad 152$$

The unit is changed by the Laplace transformation so a sound pressure is changed from force per length squared (N/m^2 = Pa) to force per length (N/m).

7.6 Laplace transformed wave equation

The wave equation to be transformed is (see equation 148):

$$(\sigma+a)^2 \frac{\partial^2 p}{\partial \sigma^2} + 2(\sigma+a)\frac{\partial p}{\partial \sigma} + \frac{\partial^2 p}{\partial \theta^2} + \cot(\theta)\frac{\partial p}{\partial \theta} + k^2(\sigma+a)^2 p = 0$$

The variable has been substituted using $r = \sigma + a$, where a is a non-zero positive real number, in order to avoid a singularity at $r = 0$. The new variable σ may equal zero without singularity problems during the Laplace transformation. The derivative is not hanged: $dr = d\sigma$.

Using the linearity of the Laplace transform, the terms can be transformed individually.

7.6.1 Laplace transform of $r^2 d^2 p/dr^2$

We start by quoting the definition of the Laplace transform using the new variable.

$$L\left\{r^2 \frac{\partial^2 p(r,\theta)}{\partial r^2}\right\} = L\left\{(\sigma+a)^2 \frac{\partial^2 p(\sigma+a,\theta)}{\partial \sigma^2}\right\} = \int_0^\infty (\sigma+a)^2 \frac{\partial^2 p(\sigma+a,\theta)}{\partial \sigma^2}\exp(-s(\sigma+a))d\sigma$$

The second-order derivative of the exponential will be used to remove the squared term.

$$\frac{\partial^2}{\partial s^2}\{\exp(-s(\sigma+a))\} = (\sigma+a)^2\exp(-s(\sigma+a))$$

Differentiation can be moved outside the integration since the exponential is the only term with s-dependency.

$$L\left\{r^2 \frac{\partial^2 p(r,\theta)}{\partial r^2}\right\} = \frac{\partial^2}{\partial s^2}\int_0^\infty \frac{\partial^2 p(\sigma+a,\theta)}{\partial \sigma^2}\exp(-s(\sigma+a))d\sigma$$

Partial integration (see section 7.1.1) will be used to remove the differentiation of the sound pressure and two partial integrations will be required since differentiation is of second order. The first partial integration of the integral gives:

$$\int_0^\infty \frac{\partial^2 p(\sigma+a,\theta)}{\partial \sigma^2}\exp(-s(\sigma+a))d\sigma = \left[\frac{\partial p(\sigma+a,\theta)}{\partial \sigma}\exp(-s(\sigma+a))\right]_{\sigma=0}^{\sigma=\infty}$$
$$-(-s)\int_0^\infty \frac{\partial p(\sigma+a,\theta)}{\partial \sigma}\exp(-s(\sigma+a))d\sigma$$

The derivative of the sound pressure is bounded for σ approaching infinity since the sound pressure decays gradually toward zero for radius approaching infinity, so the only output from the square brackets is the derivative of an initial term.

$$L\left\{r^2 \frac{\partial^2 p(r,\theta)}{\partial r^2}\right\} = \frac{\partial^2}{\partial s^2}\left\{-\frac{\partial p(a,\theta)}{\partial \sigma}\exp(-sa) + s\int_0^\infty \frac{\partial p(\sigma+a,\theta)}{\partial \sigma}\exp(-s(\sigma+a))d\sigma\right\}$$

Partial integration will again be used to integrate the derivative of the sound pressure.

$$\int_0^\infty \frac{\partial p(\sigma + a, \theta)}{\partial \sigma} \exp(-s\sigma) d\sigma = \left[p(\sigma + a, \theta) \exp(-s(\sigma + a)) \right]_{\sigma=0}^{\sigma=\infty}$$

$$-(-s)\int_0^\infty p(\sigma + a, \theta) \exp(-s(\sigma + a)) d\sigma$$

The sound pressure is bounded for σ approaching infinity so the only output from the square brackets is an initial term for $\sigma = 0$ and the last term is recognised as the definition of the Laplace transform of the sound pressure when the integration variable is changed from $d\sigma$ to $d(\sigma + a)$.

$$L\left\{ r^2 \frac{\partial^2 p(r, \theta)}{\partial r^2} \right\} = \frac{\partial^2}{\partial s^2} \left\{ -\frac{\partial p(a, \theta)}{\partial \sigma} \exp(-sa) + s\left[-p(a, \theta) \exp(-sa) + sL\{p(\sigma + a, \theta)\} \right] \right\}$$

$$= \frac{\partial^2}{\partial s^2} \left\{ -\frac{\partial p(a, \theta)}{\partial \sigma} \exp(-sa) - sp(a, \theta) \exp(-sa) + s^2 \hat{p}(s, \theta) \right\}$$

The second-order derivative of the first term is:

$$\frac{\partial^2}{\partial s^2} \left\{ \frac{\partial p(a, \theta)}{\partial \sigma} \exp(-sa) \right\} = a^2 \frac{\partial p(a, \theta)}{\partial \sigma} \exp(-sa) = a^2 \frac{\partial p(a, \theta)}{\partial r} \exp(-sa)$$

The second-order derivative of the second term is calculated using the rule for differentiation of a product of two functions (see section 7.1.3):

$$\frac{\partial^2}{\partial s^2} \left\{ sp(a, \theta) \exp(-sa) \right\} = p(a, \theta) \frac{\partial^2}{\partial s^2} \left\{ s \exp(-sa) \right\}$$

$$= p(a, \theta) \left\{ \frac{\partial^2 s}{\partial s^2} \exp(-sa) + 2 \frac{\partial s}{\partial s} \frac{\partial \exp(-sa)}{\partial s} + s \frac{\partial^2 \exp(-sa)}{\partial s^2} \right\}$$

$$= p(a, \theta) \left[-2a \exp(-sa) + sa^2 \exp(-sa) \right]$$

The second-order derivative of the third term is:

$$\frac{\partial^2}{\partial s^2} \left\{ s^2 \hat{p}(s, \theta) \right\} = \frac{\partial^2 s^2}{\partial s^2} \hat{p}(s, \theta) + 2 \frac{\partial s^2}{\partial s} \frac{\partial \hat{p}(s, \theta)}{\partial s} + s^2 \frac{\partial^2 \hat{p}(s, \theta)}{\partial s^2}$$

$$= \hat{p}(s, \theta) + 4s \frac{\partial \hat{p}(s, \theta)}{\partial s} + s^2 \frac{\partial^2 \hat{p}(s, \theta)}{\partial s^2}$$

Assembling:

$$-\frac{\partial^2}{\partial s^2} \frac{\partial p(a, \theta)}{\partial \sigma} \exp(-sa) = -a^2 \frac{\partial p(a, \theta)}{\partial r} \exp(-sa)$$

$$-\frac{\partial^2}{\partial s^2} sp(a, \theta) \exp(-sa) = -p(a, \theta) \left[-2a \exp(-sa) + sa^2 \exp(-sa) \right]$$

$$+\frac{\partial^2}{\partial s^2} s^2 \hat{p}(s, \theta) = \hat{p}(s, \theta) + 4s \frac{\partial \hat{p}(s, \theta)}{\partial s} + s^2 \frac{\partial^2 \hat{p}(s, \theta)}{\partial s^2}$$

Hence, the Laplace transform of the first term of the wave equation:

$$L\left\{r^2\frac{\partial^2 p(r,\theta)}{\partial r^2}\right\} = a\exp(-sa)\left([sa-2]p(a,\theta)-a\frac{\partial p(a,\theta)}{\partial r}\right)$$
$$+\hat{p}(s,\theta)+4s\frac{\partial\hat{p}(s,\theta)}{\partial s}+s^2\frac{\partial^2\hat{p}(s,\theta)}{\partial s^2}$$

153

Note that the first part of the transform disappears for $a \to 0$ (although $a > 0$ is required).

7.6.2 Laplace transform of rdp/dr

We start by quoting the definition of the Laplace transform with the term to Laplace transform and using the new variable.

$$L\left\{r\frac{\partial p(r,\theta)}{\partial r}\right\} = L\left\{(\sigma+a)\frac{\partial p(\sigma+a,\theta)}{\partial\sigma}\right\} = \int_0^\infty (\sigma+a)\frac{\partial p(\sigma+a,\theta)}{\partial\sigma}\exp(-s(\sigma+a))d\sigma$$

The derivative of the exponential can be used to eliminate the $\sigma + a$ term:

$$\frac{\partial}{\partial s}\{\exp(-s(\sigma+a))\} = -(\sigma+a)\exp(-s(\sigma+a))$$

Differentiation can be moved outside the integration since the exponential is the only term with s-dependency and a negative sign balances the sign from the differentiation:

$$L\left\{r\frac{\partial p(r,\theta)}{\partial r}\right\} = -\frac{\partial}{\partial s}\int_0^\infty \frac{\partial p(\sigma+a,\theta)}{\partial\sigma}\exp(-s(\sigma+a))d\sigma$$

Partial integration will be used to remove the differentiation of the sound pressure.

$$\int_0^\infty \frac{\partial p(\sigma+a,\theta)}{\partial\sigma}\exp(-s(\sigma+a))d\sigma = \left[p(\sigma+a,\theta)\exp(-s(\sigma+a))\right]_{\sigma=0}^{\sigma=\infty}$$
$$-(-s)\int_0^\infty p(\sigma+a,\theta)\exp(-s(\sigma+a))d\sigma$$

The sound pressure is bounded for σ approaching infinity so the only output from the square brackets is an initial term for $\sigma = 0$ and the last term is recognised as the definition of the Laplace transform of the sound pressure.

$$L\left\{r\frac{\partial p(r,\theta)}{\partial r}\right\} = -\frac{\partial}{\partial s}\{p(a,\theta)\exp(-sa)+s\hat{p}(s,\theta)\}$$

The derivative of the first term is:

$$\frac{\partial}{\partial s}\{p(a,\theta)\exp(-sa)\} = -ap(a,\theta)\exp(-sa)$$

The derivative of the second term is:

$$\frac{\partial}{\partial s}\{s\hat{p}(s,\theta)\} = \frac{\partial s}{\partial s}\hat{p}(s,\theta)+s\frac{\partial\hat{p}(s,\theta)}{\partial s} = \hat{p}(s,\theta)+s\frac{\partial\hat{p}(s,\theta)}{\partial s}$$

Hence, the Laplace transform of the second term of the wave equation.

$$L\left\{r\frac{\partial p(r,\theta)}{\partial r}\right\}=a\exp(-sa)p(a,\theta)-\hat{p}(s,\theta)-s\frac{\partial\hat{p}(s,\theta)}{\partial s} \qquad 154$$

7.6.3 Laplace transform of $dp/d\theta$ and $d^2p/d\theta^2$

We start by quoting the definition of the Laplace transform using the new variable.

$$L\left\{\frac{\partial p(r,\theta)}{\partial\theta}\right\}=L\left\{\frac{\partial p(\sigma+a,\theta)}{\partial\theta}\right\}=\int_0^\infty\frac{\partial p(\sigma+a,\theta)}{\partial\theta}\exp(-s(\sigma+a))d\sigma$$

The differentiation can be moved to the front of the integration since the sound pressure is the only term with θ-dependency.

$$L\left\{\frac{\partial p(r,\theta)}{\partial\theta}\right\}=\frac{\partial}{\partial\theta}\int_0^\infty p(\sigma+a,\theta)\exp(-s(\sigma+a))d\sigma$$

A substitution of the integration variable from $d\sigma$ to $d(\sigma+a)$ shows that the integral is the definition of the Laplace transformation; hence, the Laplace transform of the third term of the wave equation.

$$L\left\{\frac{\partial p(r,\theta)}{\partial\theta}\right\}=\frac{\partial\hat{p}(s,\theta)}{\partial\theta} \qquad 155$$

Similar arguments leads to the Laplace transform of the second-order derivative with respect to the angle; hence, the Laplace transform of the fourth term of the wave equation.

$$L\left\{\frac{\partial^2 p(r,\theta)}{\partial\theta^2}\right\}=\frac{\partial^2\hat{p}(s,\theta)}{\partial\theta^2} \qquad 156$$

This is not surprising since the angle is a fixed variable during the transformation (parameter).

7.6.4 Laplace transform of r^2p

We start by quoting the definition of the Laplace transform using the new variable.

$$L\{r^2 p(r,\theta)\}=L\{(\sigma+a)^2 p(\sigma+a,\theta)\}=\int_0^\infty(\sigma+a)^2 p(\sigma+a,\theta)\exp(-s(\sigma+a))d\sigma$$

Second-order differentiation of the exponential is used to remove the squared factor.

$$\frac{\partial^2}{\partial s^2}\{\exp(-s(\sigma+a))\}=(\sigma+a)^2\exp(-s(\sigma+a))$$

The differentiation can be moved to the front of the integration since the exponential is the only term with s-dependency.

$$L\{r^2 p(r,\theta)\}=\frac{\partial^2}{\partial s^2}\int_0^\infty p(\sigma+a,\theta)\exp(-s(\sigma+a))d\sigma$$

The integral is recognised as the Laplace transform of the sound pressure; hence, the Laplace transform of the fifth term of the wave equation.

$$L\{r^2 p(r,\theta)\} = \frac{\partial^2 \hat{p}(s,\theta)}{\partial s^2} \qquad\qquad 157$$

8 References

8.1 Books

Leo. L. Beranek: *Acoustics*. 1993 Edition, Massachusetts Institute of Technology, 1996.

Dean G. Duffy: *Green's Functions with Applications*, Chapman & Hall/CRC, 2001.

O. S. Heavens and R. W. Ditchburn: *Insight into Optics*. Wiley, 1991.

Finn Jacobsen: *Propagation of Sound Waves in Ducts*, Note 31260, Ørsted•DTU.

Franklin F. Kuo: *Network Analysis and Synthesis*. Wiley, 1966.

W. Marshall Leach: *Introduction to Electroacoustics & Audio Amplifier Design*. Kendall/Hunt Publishing Company, 2003.

Brian C. J. Moore: *An Introduction to the Psychology of Hearing*, 5th Edition, Elsevier, 2004.

Frank L. Pedrotti and Leno S. Pedrotti: *Introduction to Optics*, 2nd Ed, Prentice Hall, 1987.

Lennart Råde & Bertil Westergren: *Mathematics Handbook for Science and Engineering*. Studentlitteratur, 5th Ed, 2004.

8.2 Journal of the Audio Engineering Society

Finn Agerkvist: *A Study of Simple Diffraction Models*, 1997.

R. M. Bews & M. J. Hawksford: *Application of the Geometric Theory of Diffraction (GTD) to Diffraction at the Edges of Loudspeaker Baffles*, 1986.

M. Urban, et al,: *The Distributed Edge Dipole (DED) Model for Cabinet Diffraction Effects*, 2004.

John Vanderkooy: *A Simple Theory of Cabinet Edge Diffraction*, 1991.

J. R. Wright: Fundamentals of Diffraction, 1996.